A theoretical and computational study of heterogeneous spatio-temporal distributions arising from density-dependent animal movement with applications to slugs in arable fields

by

John Rhys Ellis

Supervised by Natalia Petrovskaya

A thesis submitted to
The University of Birmingham
for the degree of
Doctor of Philosophy (PhD)

School of Mathematics
College of Engineering and Physical Sciences
The University of Birmingham
December 2020

Abstract

Understanding the dynamics of pest populations is essential for pest management in agriculture. Slugs alone can cause large amounts of economic damage if their population is not controlled, usually by the application of chemical pesticides. However, there is pressure to reduce the amount of pesticide used because of the potential effects on human health and the environment. One solution to this problem is to target the application of pesticide only on areas of high population density.

This thesis thoroughly investigates the mechanisms in individual movement that can lead to the formation of heterogeneous spatial distributions in a population. Using an individual based model, we show that when an animal's direction of movement is dependent on the population density in its immediate surroundings, the population can form several clusters of high density. We show that the characteristics of the clusters and their temporal stability are dependent on how individual animals move, with Brownian motion producing dense stable clusters and Lévy flight producing dynamic clusters that are highly volatile. We confirm the existence of density dependent movement behaviour through an analysis of spatial tracking data from a field experiment where slugs were released in either a group or individually. Differences in individual movement seen in the data are shown to produce a heterogeneous population distribution through another individual based model. Finally, we analyse data of slug trap counts and discuss methods that can be used for identifying high density patches that should be targeted by pesticide.

Acknowledgements

I would like to thank Dr Natalia Petrovskaya for her excellent supervision and support throughout my studies. I would also like to give my thanks to Prof Sergei Petrovskii for his guidance and also to Emily Forbes and Keith Walters for their collaboration. I learned a lot through our discussions.

I thank the School of Mathematics at the University of Birmingham for a Research Associateship that enabled me to carry out this work. I extend my thanks to my friends and all those in the department for making the experience so enjoyable.

Finally, I would particularly like to thank my family and my partner Imogen for their constant support and encouragement.

List of publications

Below is a list of publications which have been produced using work presented in this thesis.

- J. Ellis, N. Petrovskaya, E. Forbes and K.F. Walters and S. Petrovskii. Patterns of Individual Movement of the Grey Field Slug (*Deroceras reticulatum*) in an Arable Field. *Scientific Reports*, 10:17970, 2020.
- J. Ellis and N. Petrovskaya . A computational study of density-dependent individual movement and the formation of population clusters in two-dimensional spatial domains. *Journal of Theoretical Biology,* 505:110421, 2020.
- N.B. Petrovskaya, J.R. Ellis, E. Forbes and K.F. Walters. Modelling a targeted use of pesticide procedure for pest populations with heterogeneous spatial distributions. *Ecological Modelling*, 427:109059, 2020.
- J. Ellis, N. Petrovskaya and S. Petrovskii. Effect of density-dependent individual movement on emerging spatial population distribution: Brownian motion vs Levy flights. *Journal of Theoretical Biology*, 464:159-178, 2019.

Contents

List of Figures

List of Tables

Nomenclature

Unless otherwise stated, the following notation is used throughout this thesis.

List of Acronyms

Acronym	Description
1D	One-dimensional
2D	Two-dimensional
CRW	Correlated random walk
IBM	Individual based model
IPM	Integrated pest management
MSD	Mean squared displacement
RFID	Radio frequency identification
SSD	Scaled squared displacement

List of Latin Symbols

Symbol	Description
A_c	2D spatial area of a cluster
b_l	Lower threshold when defining a cluster
b_u	Upper threshold when defining a cluster
B	Number of bins in the domain
C_i	Individual trap count
d	Density threshold for movement behaviour
F	Number of fluctuations in the number of clusters
I_M	Morisita Index
k	Parameter of the power law distribution
L	Length of the domain in the IBM
M	Mass units of pesticide
N	Total size of a population
N_c	Number of clusters
n_c	Population of a cluster
n_f	Number of free animals (not in a cluster)
P	Probability of directed movement

P_m	Probability of movement
R	Perception radius
R^2	Coefficient of determination
S	The number of segments within an animal's perception radius in 2D
S	Mean trap count
S_{th}	Single trap count threshold
S_l	Trap count lower threshold
S_u	Trap count upper threshold
s	Straightness index
t	Time
T	Number of time steps
v	Slug velocity
x_n	Position of animal n along the horizontal axis
y_n	Position of animal n along the vertical axis

List of Greek Symbols

Symbol	**Description**
Δr	Radial size of a movement step in 2D
Δt	Size of time step
Δx	Size of a movement step in the horizontal direction
Δy	Size of a movement step in the vertical direction
γ	Parameter of the power law distribution
μ	Mean
ρ	Describes a given probability density function
σ	Standard deviation
θ	Angular direction of movement in 2D
θ_T	Turning angle

Chapter 1

Introduction

1.1 The importance of pest management

Slugs and other pest species are a significant problem within agriculture across the world. A pest can be defined as any species that cause damage to a crop to an unacceptable extent and can include weeds and pathogens as well as slugs and other animal species [123, 166, 192]. Slug species cause significant damage to crops with important economic consequences and therefore require careful monitoring and control via a number of different methods. Slugs are most active at night, seeking out refuge under stones and plants or moving down through the soil when it becomes light [77]. They tend to feed 1-2 hours after becoming and dark and mate during the middle period of darkness. Activity is also influenced by moisture and temperature, with cool ($\sim 14°C$), moist conditions being optimal [77].

The crops affected include cereals, oilseed rape, potatoes, asparagus, brussel sprouts, carrots and lettuce. The damage caused depends on the crop and can either reduce the yield or cause cosmetic damage, making the crop unmarketable. For example, cereals are susceptible to seed hollowing caused by slugs which can result in poor germination and poor crop establishment [77]. It is estimated that without effective control measures, damage to crop yield and quality due to slugs could cost the industry £100 million per

year for wheat, oilseed rape and potato crops in the UK alone [78, 166, 237].

A single action to reduce the damage caused by pests is rarely sufficient, meaning that a combination of methods are used cooperatively to protect crops from pest attack. The use of a range of techniques is known as integrated pest management (IPM), the aim of which is to utilize all suitable methods in a compatible way to maintain the pest population at levels below those causing economic injury [123, 213]. IPM consists of three phases: preventative measures, pest monitoring and pest control. Preventative pest management includes crop rotation and intercropping, which involve growing different crops, either sequentially or at the same time. Introducing crop variety can destabilise the life cycle of a pest, helping to keep the population at a low level [134]. A similar method, known as trap cropping, involves using plants that are favourable to the pest. This can divert the pest species from the crop to the decoy plants [214]. Another option is to grow crops that are resistant to pest attack. Recently, this has been achieved through genetic modification. Although the risks are not fully understood, it has been the focus of much research and has the potential to be a key pest management strategy [19].

The next phase of IPM, monitoring, is necessary to determine when the pest abundance has reached a level such that pest control action is necessary. This threshold level of abundance is decided by a number of factors, however economic factors are often the most common concerns for farmers and thus pest control is only used when the cost of damage caused by pests will be greater than the cost of the control action [99]. A common method for approximating the abundance of slugs and other pest species is to use animal traps and periodically take trap counts. When the average trap count reaches the chosen threshold then a control action will be taken. While this method usually only approximates total pest abundance, if sufficient traps are used it may also approximate the spatial distribution of a population, offering the potential for pest control to be targeted to areas of high density.

Biological actions such as the release of a natural enemy of the pest are options for

pest control [226], however the most widely used means of pest control is the application of pesticide. It has been estimated that around 3×10^9 kg of pesticides are used across the globe per year [188]. However, the indiscriminate use of pesticides can have serious negative consequences. The application of pesticides is costly and can risk damage to the environment [111]. Pesticides are known to contribute to air, soil and water pollution [60, 104] and there is also some evidence linking their use to human illnesses [4, 189]. The overuse of pesticides can lead to resistance in pest species making future management a more difficult task [6, 228]. Finally, lethal or sub-lethal effects on non-target organisms such as natural enemies [220] can result in resurgence in the pest population or a secondary pest to emerge. Such risks are addressed by legislation governing the development and subsequent use of pesticide products, and by technology that improves targeting and reduces drift, but there is a widespread recognition of the requirement to reduce and optimise the quantities used [146, 147].

Increased pressure to reduce the use of pesticides in agricultural crops results in an urgent need for new approaches to pest control that both reduce the quantity of any given pesticide applied to commercial agricultural fields and make those applications more precise. The concept of spatially targeted pesticide application to control pest populations has already received the attention of researchers; e.g. see [12, 32, 187, 221]. Among other examples, the study in [30] has been focused on the probability of the presence of the pest in a spatial environment, allowing for the targeted use of pesticide in spatial areas where there is a high probability of pest presence. Probability mapping has also been done at larger scales in agriculture [76] where sampling has been used to generate a probability threshold map, a contour map showing the probability of the number of pests within a known area exceeding a defined threshold. There have also been discussions on weed detection and targeted spraying of herbicide [151] as well as efforts to produce a system of automated robotic pesticide spraying over target areas for use in greenhouses [209]. Such studies, however, have not related targeted use of pesticides with the need to develop

a monitoring and control protocol that takes account of the locations of spatial patches where the population density is high. Most recently the concept of targeting molluscicide treatments at the spatially and temporally stable patches of high slug densities that have been shown to occur in arable crops have been investigated in the field [78].

1.2 The phenomenon of heterogeneous population distributions

The potential use of targeted pest control methods relies on the assumption that the population distribution of a pest species is not uniformly distributed within a field. The distribution of any population is rarely, if ever, homogeneous. In fact, distinctly heterogeneous or even 'patchy' distributions are ubiquitous in different ecosystems and are seen across many different species at different spatial and temporal scales [130, 132]. Because of its widespread appearance, the phenomenon of heterogeneous spatial distributions of a population is known to have importance in many fields of ecology outside of IPM. Understanding animal movement on different spatial and temporal scales is a major focus in biology [49, 164, 171] and it is informative for us to understand how heterogeneous populations may form in all areas of ecology.

On large scales, animal movement in response to environmental conditions such as habitat loss or seasonal changes through dispersal and migration is an important component of species survival, fitness and geographical distribution [33, 46, 105, 141]. On small scales, the reproductive success and population growth depend on the efficiency of searching for food, shelter and mating partners [195, 215, 223]. For these reasons, patterns of animal foraging have attracted considerable attention during the last few decades [115, 116, 171, 196, 201, 217, 235]. Other areas of research where spatial patterns are studied include nature conservation and renewable resource management [62, 256, 258], agriculture and forestry [5, 119, 210, 227, 248] and population dynamics [158, 182, 241].

While this thesis is presented in the context of IPM, it can also be relevant to other areas of research, particularly the theoretical work we present in Chapters 2 and 3.

Patterns that appear over large spatial scales often occur over large time scales too and can be formed over multiple generations from the dynamics of population growth. These often involve inter-species interaction such as predator-prey dynamics that can be seen in the dynamics of phytoplankton and zooplankton [143] among others [150, 158]. Another example is the competition for resources such as water in the case of vegetation patterns [122, 128], or the behavioural interaction between competing animal species [193]. Alternatively, large scale patterns can arise from the effect of spatially-correlated external factors [140] that may result in synchronization between disconnected habitats [108, 133, 206]. In a more general case, large scale patterns emerge as a result of a combined effect of the population growth, dispersal and environmental noise [21].

Meanwhile, heterogeneous distributions are also found in small spatial and small 'within generational' timescales where population reproduction is not directly involved. The area in which patterns are formed can often be on a much smaller spatial scale, confined within a single forest, lake, meadow or farm field. Here, animals of a given species can aggregate or group together to create flocks of birds [41, 71], shoals of fish [50, 191], swarms of insects [70, 153], herds of larger animals such as sheep [120, 242] or simply well-defined patches of the population density [5, 160, 177]. Unless it can be attributed to a distinct environmental heterogeneity (e.g. animal grouping at a better feeding ground), this phenomenon is thought to be either a consequence of animal 'sociality' [89, 90, 168, 234] or the effect of the density-dependence of the movement [136, 238].

In the former case, the animal adjusts its movement velocity to those of the animals around, hence resulting in a collective movement as is often seen in swarms, flocks and herds [90, 125]. In the latter case, the animal's movement direction correlates with the direction of the population density gradient. Although the movement speed of different animals is not necessarily correlated in this case, the movement direction of a given animal

tends to be towards areas with higher population density; the phenomenon that is known as taxis [118, 153, 238, 239]. These two types are not exhaustive and more complicated types of density dependence can happen too [58]. In either of the cases, the small-scale, within-generation patterns in the spatial population distribution emerge as a result of a response of individual animals to the presence of their conspecifics; hence, the properties of individual animal movement are at the core of it [235]. However, the specific mechanisms linking the formation of population patches to individual animal movement often remain obscure.

There have been many examples of studies that have identified patch formation in the distribution of an animal species. These include species of beetles [5], flatworms [160, 177] and slugs [78]. Another example is the various clustering patterns that are seen in populations of mussels that emerge from a simple interaction between individuals where the speed of their movement is dependent on the population density [135, 241]. It has been found that this clustering leads to a lower rate of mortality as the mussels have a reduced dislodgement and predation. This has also been shown in the case of a group of tadpoles, where aggregation meant that each individual had a lower rate of predation [255]. However, often the reason for patch formation is not understood and may be a combination of many different factors.

1.3 Estimating animal movement and the emergence of patterns in the spatial distribution of a population.

Although it is known that various pest populations form into simply well-defined patches of the population density or 'clusters', knowledge of the location of those clusters and an understanding of their temporal dynamics are necessary to allow for targeted application of pest control methods. As discussed above, an essential part of an IPM protocol is

pest monitoring. However, as well as knowledge of pest abundance, it is also important to know how a pest population is distributed around the field. This information can be used to inform what action is necessary to control the pest population. Monitoring data may also be input into models that can then be used to help make decisions regarding pest management techniques. A common method for approximating the distribution of a pest population, slugs in particular, is to use animal traps and after some interval of time, count how many animals have been found within each trap to approximate the local population density [15, 78, 81, 85, 177, 180]. The data can be interpolated to approximate the distribution of pests as well as the total abundance and will indicate to farmers when and where they need to apply control measures.

Traps are also useful in academic study in increasing our understanding of pest species and how they move and interact. The experimental work undertaken by Harper Adams University [78, 80] consisted of laying out a grid of slug traps in different arable fields across England and periodically returning to take trap counts. An example of a population distribution approximated from trap counts is shown in Fig. 1.1. It can be clearly seen that the distribution is patchy which suggests targeted use of molluscicide could be possible if the patches are temporally stable or the location where patches form can be predicted. The concept of a patch in regards to the data collected is discussed in more detail in Chapter 6.

In addition to understanding how a population is distributed, technology has allowed ecologists to closely follow individuals in a population to understand their movement patterns. Tracking tags allow us to monitor the GPS position of an animal and follow it over time and have been applied to assess the movements of turtles [148, 212], birds [91, 246], antelope [171] and have recently been inserted into slugs [80], the data of which will be discussed in Chapter 4. The availability of substantial data can give valuable insights into the way individual animals move and can be incorporated into mathematical models to simulate realistic movement in a population.

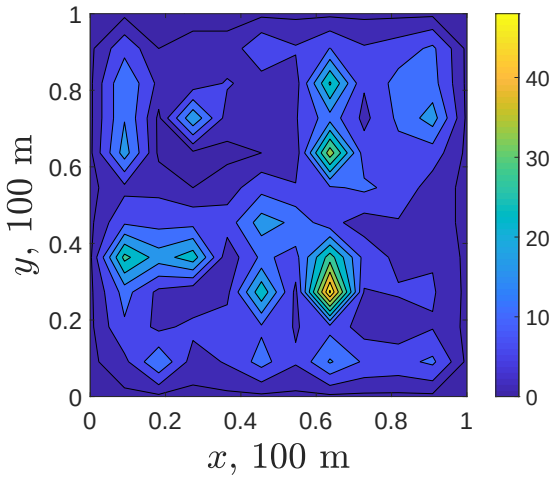

Figure 1.1: The distribution of a slug population in a field in Stoney Lawn, Shropshire, on 18.02.2016. A continuous density distribution is approximated from 100 trap counts where traps are arranged in a uniform square grid of 100 m×100 m. The density is measured in number of slugs per 10 m^2.

The knowledge of the pest population's spatial distribution is important when developing more sustainable control measures [178, 185]. An understanding is also required of the mechanisms of animal movement that lead to heterogeneous pattern formation and the temporal dynamics of the spatial distribution to make targeted application of pesticide on high density patches viable. There is theoretical and empirical evidence that the pattern of individual movement is a factor influencing population abundance over space and time [97, 127, 202] and this will be a key focus of study in this thesis.

Mathematical modelling is a vital tool for approaching such problems and has long been used in ecological studies. Models of single populations showing exponential growth were explored as early as 1202 with the Fibonacci sequence and later with the introduction of a carrying capacity, models of logistic growth were considered [16, 162]. In more recent times models have been applied to interactions between different species and with their environment, including the Lotka-Volterra model of predator-prey interactions and competition models [139, 162]. Models have also been developed to describe spatial

patterns using diffusion, such as the Fisher-Kolmogorov equation [75, 124] which is an example of a reaction-diffusion system. Other processes such as advection-diffusion [169] and chemo-taxis, seen in the famous model of slime mould [118], have also been used to show pattern formation in biology [235]. In recent times, with access to increasing computational power, computational models and numerical methods have become powerful research tools in ecology [184]. In particular, this has allowed the use of individual based models (IBMs) to simulate the interactions between discrete animals [88, 90, 235].

Individual based modelling is a useful tool for studying the processes of individuals within a system and how they interact. This can then reveal patterns in the overall system which are often non-trivial. When modelling animal movement, the IBM takes the form of a random walk, where the position of an individual is tracked through time [2, 49, 113, 116, 181, 235], although it can also be used to incorporate multiple other characteristics such as size and age [59, 87, 190, 233, 254].

There are many forms of random walk that can be used in an IBM. These include a simple random walk on a lattice where space and time are discrete or spatially continuous models where the step an individual takes at each time step is generated from a dispersal kernel [49]. Models will also vary in how the direction of movement is generated. In a basic random walk, each individual will have a uniform probability of moving in any direction, however it is often more biologically appropriate for the direction an animal moves to be related to the direction it moved previously resulting in a correlated random walk. Similarly, the direction an animal moves may be dependent on external factors such as chemical gradients, resulting in a biased random walk. Often it is appropriate to combine these factors to generate a biased and correlated random walk [49].

IBMs are also useful as a first step in deriving a mean field model, which is done by expanding terms in the random walk equation in a Taylor series and taking limits to zero to produce a diffusion-type equation [43, 49, 235]. This is a common method for producing partial differential equation (PDE) models for constructing the theories of

animal movement [49, 73, 130]. In this thesis we only look at the results from the IBM to understand the features of density-dependent movement. We expect that a mean field approach to modelling density-dependent movement would require a non-linear PDE, as in [92, 186], although we do not understand exactly how to formulate such a model. We therefore focus on an IBM to understand the features of movement that arise, enabling the development of a PDE model in the future. The potential use of PDEs in future work is discussed in more detail in Chapter 7.

In most cases, IBMs use a normal distribution as a dispersal kernel to simulate Brownian motion, which is often considered to be the most accurate approximation of animal movement [115, 218]. In this case, the dispersal kernel decays with the distance very fast (exponential or faster) and hence the probability of long-distance travel is suppressed. However, over the last two decades, there has been an intense debate on the issue of individual animal movement. More recently, there has been a trend to associate animal movement with Lévy flights [201, 217, 244]: a movement type with a much higher probability of long-distance travel described by a 'fat-tailed' dispersal kernel such as a power law distribution [245]. This type of movement is thought to be an optimal strategy when foraging for a patchy food source under certain conditions [18, 106, 194, 243] and has been observed in many different species, including honey bees, marine predators and even humans [199, 201, 217]. The study of Lévy flight is controversial however, as some of the experimental evidence from the original studies has been questioned and the suitability of Lévy flight as a description of an optimal foraging method has been disputed [24, 66, 107, 196]. It has been shown that differences in movement behaviour can affect spatio-temporal patterns in a population [97, 202]. In this thesis, we consider Lévy flight as an alternative to Brownian motion to determine the ecological consequences of different movement behaviours on a population that undergoes density-dependent movement. This will be investigated in Chapters 2 and 3 as part of the development of an IBM.

1.4 Research Objectives

The aim of this thesis is to study how density-dependent animal movement leads to the formation of heterogeneous population distributions and use the results for the development of a targeted pesticide application procedure that is applicable to real world scenarios. We will show that the introduction of density-dependent movement to a population of random walkers will result in clustering within the domain. The choice of parameters that control density dependence will be varied to analyse their effect on the properties of the clusters that emerge. This work will be shown to have implications in pest management through the analysis of real field data on the grey field slug *(Deroceras reticulatum)*. The grey field slug is an important pest of a wide range of agricultural and horticultural crops, resulting in significant economic losses in most years [167, 237]. It is widespread in Europe and in particular in the UK where the data we use in our study have been collected. We will demonstrate that this species moves with density-dependent movement and produces patchy population distributions. All modelling, data analysis and data visualisation presented in this thesis has been produced using MATLAB [145].

In Chapters 2 and 3 we introduce an IBM of a population of animals that undergo density dependent movement. At each time step, each individual is more likely to move towards an area where it can perceive a higher density of its conspecifics. Two types of movement are considered, Brownian and non-Brownian motion, and determine the effects of the type of movement and the parameter choices on the formation of clusters. This is initially explored in a simple 1D model, which is useful to understand how the parameters effect the distribution. We then extend this model into 2D to enable a more realistic simulation of a population. We compare the results produced by the 1D and 2D models and study closely the similarities and differences between clusters produced by Brownian and non-Brownian walkers.

The models discussed in the first two chapters are generic and the ideas could be

applied to any species that undergoes density dependent movement. To make the ideas applicable in the case of slugs, analysis of real life data is needed. In Chapter 4 we analyse tracking data of slugs released in an arable field. Two sets of slugs were released overnight, when they are most active. This comprised of a 'dense' set, where all slugs were released together in one location, and a 'sparse' set, where the slugs were released independently with no other slugs nearby. The differences in the movement between the two sets of slugs is analysed and in Chapter 5 we use the results to formulate an IBM that can more accurately simulate slug movement. The results indicate that patches of high density population density can form from the changes in movement.

Finally, in Chapter 6 we analyse data of slug trap counts that approximate the population distribution across a field and discuss the implications of the emergence of patches for targeted application of pesticide. Counts were taken between late autumn and early spring, when there was increased slug activity, peaking once in December and again between late February and May [78]. The method of defining a slug patch for targeting is not straightforward and can depend on the biological characteristics of the species and the priorities of the farmer. Some possible options are discussed and the reduction in total pesticide use and the effect on the slug population is calculated. Conclusions of the entire study are provided in Chapter 7.

Chapter 2

A One-Dimensional Model of Density-Dependent Individual Movement

2.1 Introduction

This chapter follows the work we presented in [68]. We consider a one-dimensional mechanistic individual-based model that relates the formation of a patchy spatial distribution of the population to density-dependent individual animal movement. We use a variation of a random walk model which is a well established technique for simulating animal movement [49, 235]. The most simple form of 1D random walk is on a lattice, where an individual has a probability of moving either one step to the left or the right at each time step. However, for a more realistic approach, a variable step size is often needed. The step size is then a random variable that is generated from a given probability density function, known as the dispersal kernel. This method is commonly used for simulating animal movement and has been used for a variety of species [2, 113, 116, 181]. Animal movement can alternatively be modelled as moving with a fixed speed for a randomly generated time interval, after which the individual reorientates and moves in a different

direction [47, 170]. This approach can be useful if the turning rate of animals is known. However, in the data we examine in Chapter 4, animal locations are recorded at fixed time intervals and therefore the use of discrete time steps and variable step sizes can allow comparisons to be made between simulations and empirical results.

We therefore develop a random walk model that is discrete in time and continuous in space. To introduce behaviour that will lead to pattern formation in the spatial distribution of the population, we expand on the simple random walk and incorporate density-dependent movement. We define this in our model as an individual having a predetermined probability of moving towards an area of high population density. We refer to movement in this way as 'directed movement' and all other movement we label as random movement. In previous studies, changes in the direction of movement have been simulated using a varying dispersal kernel or turning angle distribution that is dependent on the surrounding population [50, 73]. We introduce a 'perception radius' [190, 211] in which an individual can detect where its conspecifics are. Biologically, this perception can take the form of chemical gradients, visual or olfactory cues and sound [31, 35, 47, 247]. For example, some species of slug respond to chemical cues and are known to follow the trails of others, which can lead to aggregation [52, 55, 252]. Studies that involve herd or flocks have 'zones' around each individual that determine different types of behaviour. For example, in addition to a zone in which individuals are attracted towards each other, there may be zones around an individual in which it will reorientate to match the direction of movement of its conspecifics or move away to avoid being too close [48, 54, 90, 130, 154]. We use a method similar to those used previously, discussed in detail in Section 2.2.1, which is a more simple variation to the random walk whereby an individual will either move directly towards the area of highest density in its neighbouring area or will continue to move randomly. We believe this is a suitable approximation to the biological behaviour; we make the assumption that if an animal prefers to move towards an area of high density, it will move exactly in that direction. A single zone of attraction and

one perception radius is therefore sufficient in this model, as we only include attraction between conspecifics.

In this chapter we consider the random walk in 1D to establish the mechanisms that lead to aggregation of a population through individual movement. The 1D model is relatively computationally cheap and allows us to make an initial examination of the effect of model parameters and movement characteristics on the emergence of a heterogeneous distribution. The 1D domain is not entirely abstract however, and can be thought of as a thin transect across a movement area. We do not expect the results to greatly differ when modelling in higher dimensions and this is discussed further in Section 2.4. In Chapter 3 we expand the model to 2D and show that the results do indeed hold from the 1D model, we are then able to examine the formation of clusters in more detail and note any variations between the models.

We first consider the case where the animals perform Brownian motion (i.e. are described by a Gaussian dispersal kernel) and show that the density dependence of the movement leads to formation of distinct animals groups or clusters. We then consider the case of animals performing non-Brownian motion (described by a power law kernel) to show that, in combination with the density dependence, it leads to pattern formation with different properties. For a power law kernel, the population tends to be less aggregated than for an equivalent Gaussian kernel and the clusters (patches) appear to be less stable, in particular allowing for dynamical transition between different states.

2.2 Model description

In order to simulate animal movement with different properties and their effect on the emerging spatial population distribution, we use the individual-based modelling approach [36, 88, 113, 235]. Consequently, the position of each individual animal is described explicitly at some designated moments of time, $t_k,\ k = 0, 1, \ldots,\ t_{k+1} = t_k + \Delta t$, where Δt is the time increment. In a general case, Δt can vary with time. In this chapter, we

consider it to be constant, $\Delta t = 1$; therefore, $\{t_k\}$ is a set of positive integers.

Let us consider a population of N animals, as this model is 1D we are only concerned with their x coordinates. Given the location of the nth animal is known at time t, its position at the next moment $(t + 1)$ is simulated as

$$x_n(t + 1) = x_n(t) + \Delta x, \tag{2.2.1}$$

where the increment Δx thus gives the size of a 'step' made by the animal along its movement path during the time increment $\Delta t = 1$. The movement starts from some initial location, $x_n(0) = x_{n,0}$.

Once sufficient information about Δx is available, the movement process is fully defined. Following [49, 113, 235], we consider Δx to be a random variable distributed according to a certain probability density function $\rho(\Delta x)$. We refer to function $\rho(\Delta x)$ as the dispersal kernel. For the sake of simplicity, we assume that all animals have identical movement behaviour so that ρ is the same for all animals.

The randomness of the movement step is a subtle and somewhat controversial issue. It is more likely to reflect the incompleteness of the available information about the complex process of animal's decision-making rather than the randomness in the strict sense (for a detailed discussion of the "bugbear of randomness", see [235]). However, the theoretical framework describing individual animal movement as a random walk, at least on certain spatial and temporal scales, has been shown to be in a very good agreement with empirical studies and is widely accepted as an adequate research set-up [20, 49, 116, 235, 245].

Since the main purpose of this study is to reveal possible population-level consequences of different patterns of individual movement (in particular, Brownian and non-Brownian motion), we consider two qualitatively different cases. In the first case, the dispersal

kernel is a normal distribution with a zero mean and variance σ^2:

$$\rho\left(\Delta x\right) = \rho_G\left(\Delta x|0,\sigma^2\right) = \frac{1}{\sqrt{2\pi\sigma^2}}\exp\left(-\frac{\left(\Delta x\right)^2}{2\sigma^2}\right). \tag{2.2.2}$$

We will refer to animals performing the movement described by (2.2.2) as Brownian walkers.

In the second case, the dispersal kernel is described by a power law using the following parametrization [97]:

$$\rho\left(\Delta x\right) = \rho_P\left(\Delta x|k,\gamma\right) = \frac{C}{\left(k+\Delta x\right)^{\gamma}}, \tag{2.2.3}$$

where $k > 0$ and $\gamma > 1$ are parameters of the distribution and $C = (\gamma-1)k^{\gamma-1}$ is the normalizing coefficient so that the total probability is one, i.e. $\int_{-\infty}^{\infty}\rho(\xi)d\xi = 1$. Note that the parameter k has the dimension of length, hence it represents a characteristic distance of the movement process (see Section 3 in [117]). For $\gamma \leq 3$, the distribution is fat-tailed and the variance of the power law distribution is infinite, meaning that we cannot use this to equate the two dispersal kernels. Instead we equate survival probabilities [20], which is discussed in Section 2.3.2. In this case, the stochastic movement described by Eq. (2.2.3) is often referred to as Lévy flight. When $\gamma \leq 3$, When $\gamma > 3$, the variance is finite and therefore Eq. (2.2.3) is known to converge to the normal distribution after a large number of time steps by the Central Limit Theorem [185].

For convenience, we will refer to animals performing the movement described by dispersal kernel (2.2.3) as non-Brownian walkers, and in the particular case where $1 < \gamma \leq 3$ they may also be described as moving with Lévy flight. Asymptotically, i.e. for large Δx, the dispersal kernel (2.2.3) coincides with the Lomax distribution [138] which is a special case of Pareto distribution Type II [13]. Although originally introduced as a model to describe the distribution of wealth in the society [172], Pareto distributions were later used

to describe a broad range of phenomena in natural sciences, including animal movement [245].

We consider the movement in a closed domain so that, for any n, $0 < x_n(t) < L$ at any t. The closed boundaries at $x = 0$ and $x = L$ are modelled by introducing an additional rule. If the value of Δx generated for the $(n+1)$th step is such that either $x_n(t+1) < 0$ or $x_n(t+1) > L$ then this value of Δx is aborted. This is effectively changing the animal's decision to leave, and a new Δx is generated to make sure that the animal remains inside the domain, i.e. $0 < x_n(t+1) < L$.

2.2.1 Density-dependent movement

In the simulation procedure described above, all animals move independently, i.e. the presence of their conspecifics in a vicinity of their location does not have any effect on their choice of the next movement step. As is mentioned in the introduction, this is not always true. A moving animal often reacts to the presence of other animals by correlating the direction of its movement with the population density gradient, so that the individual movement becomes density-dependent.

In order to account for the taxis-type density dependence, we need to modify the individual-based modelling approach. Firstly, we introduce the perception radius $R \geq 0$. This is the distance in each direction (in the 1D case, left or right along the horizontal line) over which an animal can detect the presence of other animals. At any moment t, only those animals that are within the region $[x_n(t) - R, x_n(t) + R]$ are taken into account and hence can affect the movement. Note that if $R = 0$, then there is no density dependence and the animals will perform unbiased random movement, see Eqs. (2.2.1–2.2.2).

Secondly, we introduce a parameter P to quantify the strength of the directional bias, $0 \leq P \leq 1$. Let n_l and n_r be the total number of animals that are counted (within the perception radius), respectively, to the left and right of the given animal. Let u be an auxiliary random variable uniformly distributed over interval Ω where Ω is defined as

follows:

$$\Omega = [P-1, P] \text{ if } n_l < n_r, \qquad \Omega = [-P, 1-P] \text{ if } n_l > n_r, \tag{2.2.4}$$

$$\Omega = [-0.5, 0.5] \text{ if } n_l = n_r.$$

In general, the absolute value of the movement step of the density-dependent movement and its direction are affected by different factors; hence, we consider them to be uncorrelated. Thus, they can be regarded as mutually independent random variables. The probability density of having the movement step of a given value, say Δx_d, is then given by a product of the probability density of making a step of a given length $|\Delta x|$ and the probability of moving left or right. Therefore, any realization of this random variable can be written as

$$\Delta x_d \;=\; \text{sign}(u) \cdot |\Delta x|, \tag{2.2.5}$$

where Δx is the movement step of the unbiased (density-independent) movement, e.g. as given by (2.2.2) or (2.2.3).

We note here that, when taking the absolute value we are effectively using a half-normal distribution instead of the normal distribution in (2.2.2) to generate the step size in our computer simulations:

$$\rho(\Delta r) = \rho_G(\Delta r|0,\sigma^2) = \begin{cases} \frac{2}{\sqrt{2\pi\sigma^2}} \exp\left(-\frac{(\Delta r)^2}{2\sigma^2}\right) & \text{if } \Delta r \geqslant 0, \\ 0 & \text{if } \Delta r < 0, \end{cases} \tag{2.2.6}$$

where σ is the standard deviation of the original normal distribution. The distribution (2.2.6) is a special case of the folded normal distribution and has a mean μ_f and standard

deviation σ_f given by

$$\mu_f = \sigma\sqrt{\frac{2}{\pi}}, \quad \sigma_f = \sigma\sqrt{1-\frac{2}{\pi}}. \tag{2.2.7}$$

Therefore, when we refer to the parameter σ in our simulation, this is the standard deviation of the original normal distribution (Eq. (2.2.2)) and not the standard deviation of the non-negative step size. The power law distribution given by Eq. (2.2.3) is unaffected as the function is already non-negative.

If $P = 1$, then the animal always moves along the gradient of the population density. For $P = 0.5$, the probability of u being positive or negative is exactly 0.5, so that the movement becomes unbiased (effectively, density-independent). Values of $P < 0.5$ correspond to a negative density-dependence where the animal is more likely to move against the gradient (towards the area with lower population density); we do not consider this case here. In the simulations below, we consider $0.5 < P < 1$. Note that, in this case, a given animal does not move deterministically left or right simply depending on whether $n_l > n_r$ or $n_l < n_r$. In order to account for the complexity of movement decisions, we therefore have assumed that a certain degree of randomness is always present, i.e. the animal can with some probability move against the gradient of the population density, not necessarily along the gradient (as is expected on average).

In order to make the model complete, we need to specify what happens if a given animal meets another animal during its movement step, i.e. if its final position after the step is behind another animal. In this thesis, we consider the rule that the moving animal does not stop until it reaches its final destination, i.e. its movement step is not terminated if it comes close to another animal. (Alternatives to this rule will be discussed in Section 2.4 and Chapter 7.) Note that it does not mean that the animal has to jump other each other: here we recall that our 1D model corresponds to a narrow stripe rather than a line, so passing-by is possible.

Sample trajectories generated by the above rules are shown in Fig. 2.1 (obtained for

$P = 0.75$ and $R = L = 10$, i.e. in the case of a global coupling where each animal can see all other animals). It is readily seen that, as a result of the density-dependent movement, the animals tend to group together to form a 'cluster'. This observation agrees with intuitive expectations and, by itself, is hardly surprising. What is not intuitive is the properties of the arising spatial pattern (e.g. how many clusters can emerge) and how they depend on the movement parameters P, R and σ (or γ and k). We address this question in the next section.

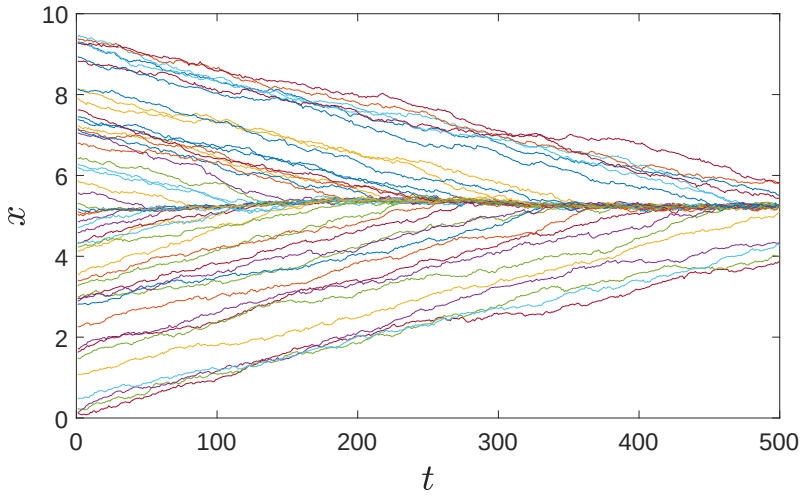

Figure 2.1: Individual movement paths of 50 animals over 500 time steps in the case of density-dependent movement with P=0.75 and $R = 10$ generated by the density-dependent random walk model using Gaussian dispersal kernel (2.2.2) with $\sigma = 0.02$. Each animal is represented by a different colour. At time $t = 0$, the population is randomly distributed over the domain $0 \leq x \leq 10$ with constant probability density.

Since our focus is on the dispersal of the population rather than individuals, it is more convenient to describe the population distribution over space by the population density rather than by an array of the coordinates for all individuals. In order to calculate the population density, we split the domain to a number of 'bins'; the number of animals inside a given bin divided by the length of the bin will approximate the population density at the location of the bin. The distribution of the population density over space then takes the form of a histogram.

Now, since the purpose of this study is to analyse the dynamics of the population clusters (patches) as a function of the movement parameters, we need a formal definition of a cluster. We say that a group of adjacent bins forms a cluster if:

1. For a given parameter b_u, where $0 < b_u < 1$, there is a bin (a 'major bin') that contains a proportion of the total population that is larger than b_u.

2. Any bin adjacent to a bin that forms part of a cluster also belongs to the cluster if it is greater than or equal to a second parameter b_l, where $0 < b_l < b_u$.

2.3 Simulation results

Our goal is to reveal typical properties of the emerging spatial distribution in the population of animals performing density-dependent individual random movement (as described in the previous section) subject to the properties of the dispersal kernel (Gaussian or power law, see Eqs. (2.2.2–2.2.3)) and the strength of the density-dependence as given by parameters P and R. For the initial condition, we consider that the population is distributed uniformly (in the statistical sense) over the domain. Mathematically, it means

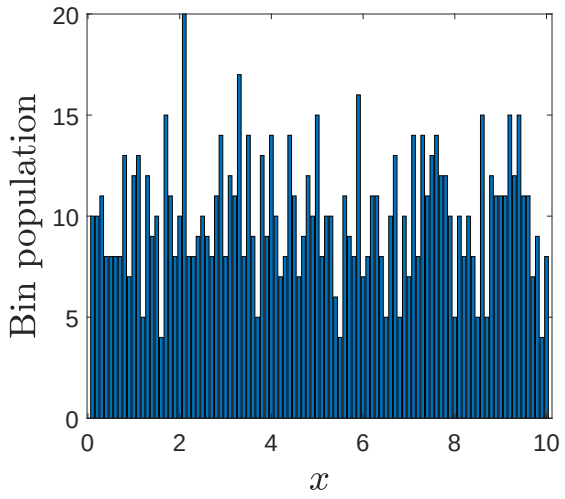

Figure 2.2: Example of the initial distribution. The total number of $N = 1000$ animals is distributed uniformly (in the statistical sense, i.e. with constant probability density) over the domain of length $L = 10$. Each column shows the number of animals in a given bin.

that the initial location of each individual is generated using the probability density function $\rho_0(x)$ that does not depend on space; for a 1D domain of length L, $\rho_0 = 1/L = const$. An example of the initial population distribution is shown in Fig. 2.2. Note that, due to the random nature of the initial distribution, the exact profile changes with each new simulation run. In this chapter (unless explicitly stated otherwise), we consider the population of $N = 1000$ animals moving in the domain of length $L = 10$ (in abstract units). The domain is split into one hundred bins, so that the spatial width of each domain is 0.1. For the proportion defining the boundaries of the cluster, the values $b_u = 0.02,\ b_l = 0.002$ are used (i.e. 2% and 0.2% of the total population respectively).

We mention here that our choice of parameters here and below is largely hypothetical. The goal of this study is to make an insight into some generic properties of the population dynamics rather than to analyse the dynamics of a specific population. The purpose of this chapter and that of Chapter 3 is not to compare the simulation results to real field or laboratory data obtained for a real animal species. Looking for 'true' parameter values is therefore not necessary given the schematic nature of our model. Instead, our purpose is to reveal the difference between the spatio-temporal patterns emerging for the two different movement types and between the system properties arising in different parameter ranges with a particular focus on understanding the effect of the directional bias as quantified by the parameter P.

2.3.1 Normal distribution: Brownian walkers

We begin with the case where the dispersal kernel is given by a normal distribution; see Eq. (2.2.2). We consider animal movement in a large spatial domain, so that the characteristic movement step is much less than the domain size, $\sigma/L \ll 1$ (this condition will be relaxed in Section 2.3.3). Typical simulation results are shown in Fig. 2.3. It is readily seen that the evolution of the initial population distribution due to individual density-dependent movement results in the aggregation of the population into several

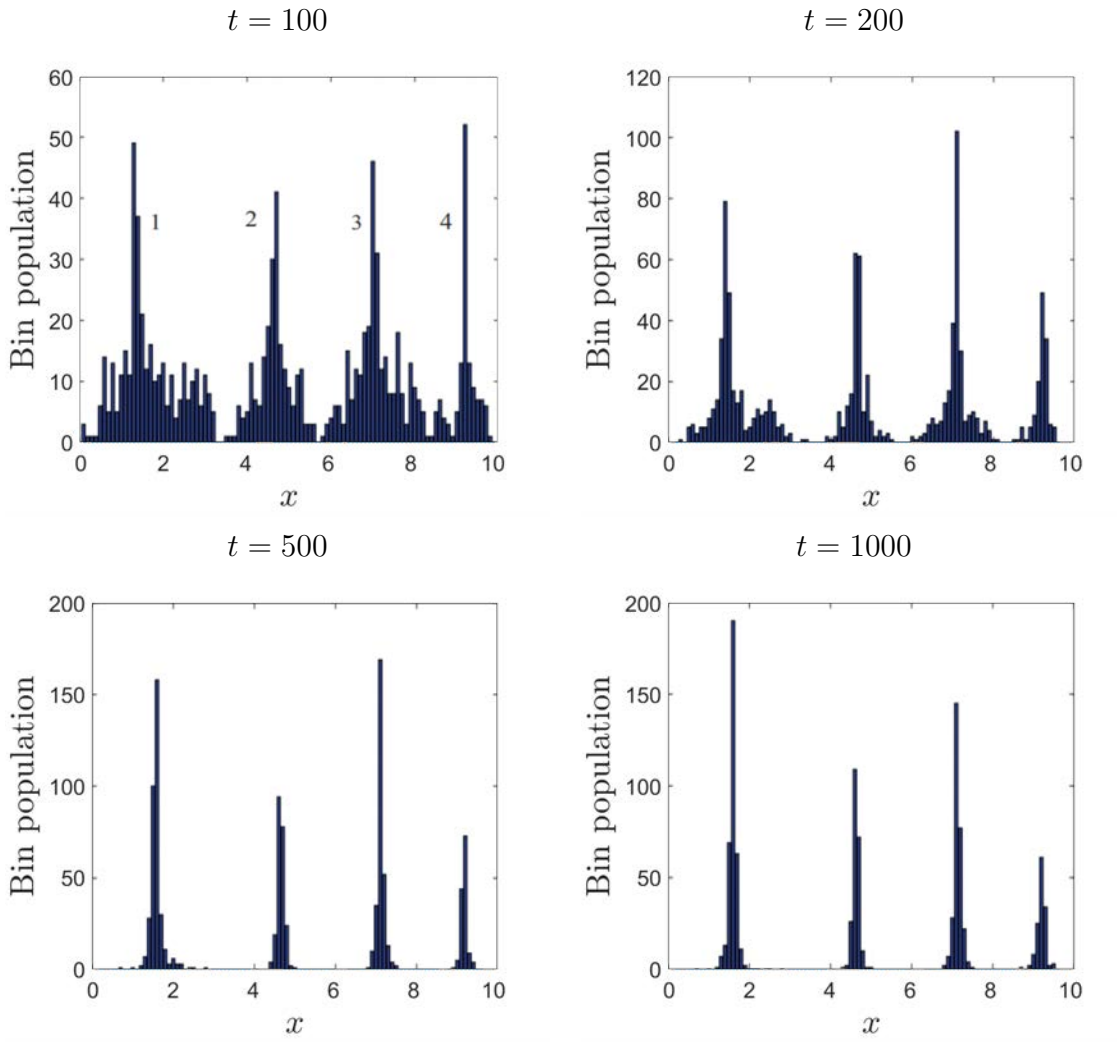

Figure 2.3: The population distribution at different moments of time emerging from a random-uniform initial distribution, see Fig. 2.2. Each column shows the number of animals in a given bin. Movement parameters are $\sigma = 0.02, P = 0.6$ and $R = 1$, other parameters are the same as in Fig. 2.2. For the convenience of a further discussion, clusters are numbered, 1 to 4, left to right; see the top left panel.

clusters or patches. The population density (i.e. the number of animals per bin) is high in the center of the cluster but close to zero between the clusters.

It is clear that there is not much difference between the population distributions shown in the left and right panels of the last row of Fig. 2.3, which corresponds to a large elapsed time. This suggests the question of whether or not the system evolves to a stationary spatial distribution and, if yes, what is the characteristic time scale for the convergence

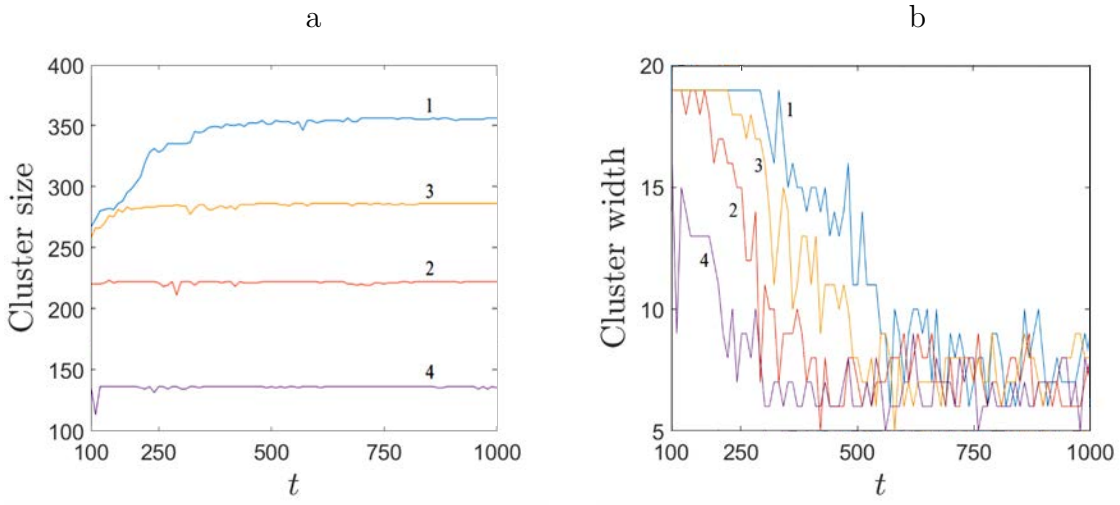

Figure 2.4: The cluster size and width over time, (a) and (b) respectively, for the population dynamics shown in Fig. 2.3. The parameters are the same as in Fig. 2.3. The curve numbering in panel (a) corresponds to cluster numbering in Fig. 2.3; note that the relative order of the curves is different from Fig. 2.3.

to the steady state. In order to make an insight into these matters, for each cluster we calculate its size (the total number of animals in the cluster) and its width (the distance between the left-most and right-most bins in the cluster). Fig. 2.4 shows the size and

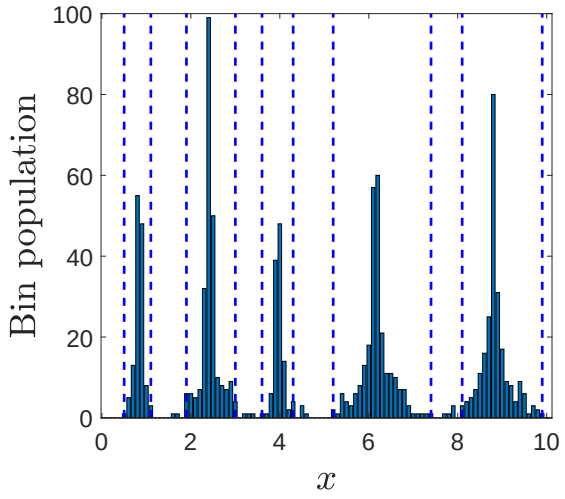

Figure 2.5: The population distribution obtained at $t = 200$ at a different realization (i.e. a different simulation run) of the system. Parameters are the same as in Fig. 2.3. The dashed vertical lines show the clusters' boundaries. The different number of clusters, i.e. five instead of four, is the result of the inherent stochasticity of the dynamics.

width of the four clusters shown in Fig. 2.3 vs time. It can be seen that the system never reaches the steady state in a strict sense as some random fluctuations around the steady state persist at all times, albeit being relatively small. The time required for the convergence to the quasi-steady state dynamics appears to depend on the size of the cluster; the larger the cluster, the longer the convergence time is.

This is seen particularly well in Fig. 2.4(b). Whilst the width of the smallest cluster (cluster 4) approaches its steady state value (up to small random fluctuations) at $t \approx 300$, for the largest cluster (cluster 1) it does not happen until $t \approx 700$. Interestingly, the convergence occurs at a somewhat different rate for the size of the cluster and for its width. For the two smallest clusters, i.e. cluster 2 and cluster 4, their size stabilizes already at $t \approx 150$ (see Fig. 2.4(a)) but their width does not reach its 'final' value until $t \approx 300$ and $t \approx 400$, respectively (Fig. 2.4(b)). For the intermediate cluster 3, its size stabilizes at $t \approx 250$ and its width at $t \approx 550$.

Based on the simulation results (note that Fig. 2.3 shows only one typical example from a large number of simulations performed) we conclude that the initial random-uniform distribution in the course of time evolves to the formation of clearly defined clusters. Interestingly, for the same parameter values the number of clusters emerging in the large time limit is not always the same. This is obviously a result of the inherent randomness of the system's dynamics which is rooted in the randomness of the individual animal movement. As just one example, Fig. 2.5 shows an evolution of the initial distribution that results in five clusters instead of four, despite using the same parameters as Fig. 2.3. Thus, for a given value of the movement parameters, the pattern formation in the course of the system's dynamics is described by the probabilities (frequencies) of observing a distribution with a different number of clusters (see Tables 2.1–2.3 below).

The number of clusters (more precisely, the distribution of the probabilities for each number of clusters) is dependent on the movement parameters. Fig. 2.6 shows the population distribution over space obtained in the case where the perception radius is $R =$

2, other parameters and the initial distribution being the same as in Fig. 2.3. Obviously, in this case only two clusters are formed.

Table 2.1: The probability of different numbers of clusters obtained in simulations for different values of the perception radius R. Other parameters are $P = 0.6$ and $\sigma = 0.02$. For any given parameter set, the probabilities were calculated based on one hundred simulation runs.

No. of clusters	$R = 1$	$R = 2$	$R = 3$	$R = 4$	$R = 5$
1	0	0	0.33	1	1
2	0	0.69	0.67	0	0
3	0.03	0.31	0	0	0
4	0.53	0	0	0	0
5	0.41	0	0	0	0
6	0.03	0	0	0	0

Table 2.2: The probability of different numbers of clusters obtained in simulations for different values of the probability of directed movement, P. Other parameters are $R = 1$ and $\sigma = 0.02$. For any given parameter set, the probabilities were calculated based on one hundred simulation runs. Note that in these simulations we did not observe any population produce less than 3 clusters.

No. of clusters	$P = 0.6$	$P = 0.7$	$P = 0.8$	$P = 0.9$	$P = 1$
3	0	0.01	0.01	0.01	0.02
4	0.51	0.56	0.48	0.42	0.42
5	0.45	0.4	0.47	0.52	0.5
6	0.04	0.03	0.04	0.05	0.06

Table 2.3: The probability of different numbers of clusters obtained in simulations for a different balance between the random and directional movement as quantified by parameters σ and P, respectively. The perception radius is chosen as $R = 1$. For any given parameter set, the probabilities were calculated based on one hundred simulation runs. Note that the probabilities do not add up to one as in some simulations no stable clusters are formed (e.g. see Fig. 2.7).

	$\sigma = 0.02$				$\sigma = 0.05$				$\sigma = 0.1$		
No. of clusters	3	4	5	6	2	3	4	5	2	3	4
$P = 0.52$	0.12	0 .72	0.05	0	0.12	0.19	0	0	0	0	0
$P = 0.55$	0.05	0.61	0.31	0	0	0.55	0.38	0	0.33	0.25	0
$P = 0.6$	0.1	0.42	0.43	0.05	0	0.23	0.71	0.04	0.07	0.73	0.13

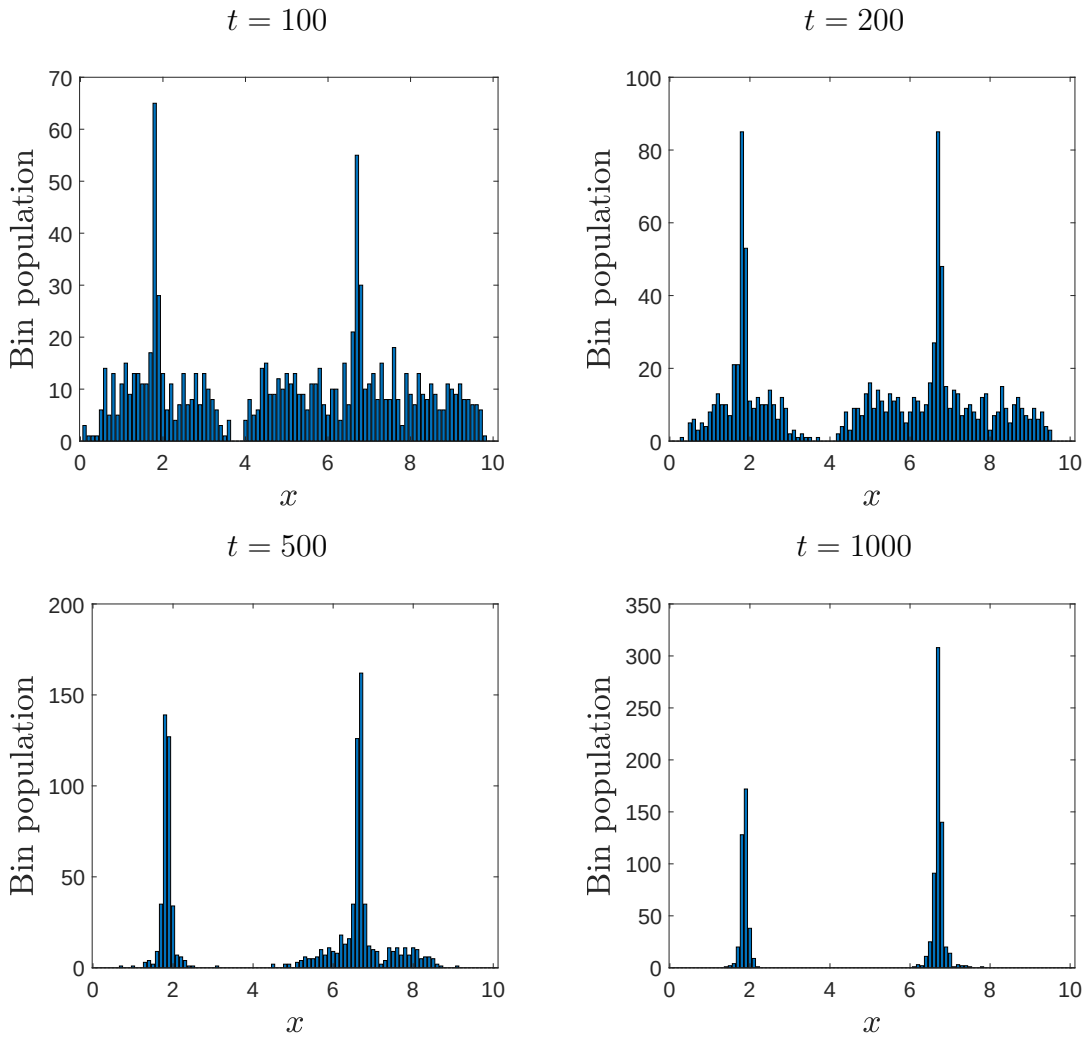

Figure 2.6: The population distribution obtained at different moments for the perception radius $R = 2$, other parameters are the same as in Fig. 2.3.

Now we investigate how the frequency of different cluster numbers depends on the movement parameters such the perception radius R, the probability of directed movement P and the standard deviation of the dispersal kernel σ. This question has been addressed through extensive numerical simulations. For a given parameter set, one hundred simulations were run, each of them until $t = 3000$. For each of the one hundred spatial population distributions obtained, the number of clusters were counted, and for each number of clusters its frequency was calculated. The results are summarized in Tables 2.1–2.3. Whilst the dependence of the results on the perception radius is intuitive,

i.e. the number of clusters tends to decrease with an increase in R (see Table 2.1, also Fig. 2.1 obtained for $R = L = 10$), the dependence on P is not. It is readily seen from Table 2.2 that, even in the case $P = 1$ when the movement becomes 'more deterministic' (the animal always move along the population density gradient), the system retains its stochastic nature as the evolution of the initial conditions can still lead to a different number of clusters. We also notice that, with an increase in σ, not only the number of clusters tends to decrease (see Table 2.3) but also their shape changes; in particular, they become less aggregated. A typical example is shown in Fig. 2.17. The effect of σ will be further investigated in Section 2.3.3.

Since parameter P quantifies the strength of the directional bias, one can expect that for the values of P close to 0.5 (where the bias disappears), the random component of the movement may be prevailing over the directional component and therefore clusters may become poorly defined or do not emerge at all. This is indeed what is observed in the simulations. Fig. 2.7 shows the spatial population distribution at a large elapsed time ($t = 9000$) obtained for $P = 0.52$. It is readily seen that the population is now distributed over the space more uniformly than it was for larger values of P. Altogether, it leads to the conclusion that the formation of clearly defined clusters is a result of the directional density-dependent individual animal movement.

A question arises here as to how stable is the number of clusters in the course of time. We have addressed it by means of long-term simulations. We have observed that the system's dynamics has two different time scales. For values of σ sufficiently small (e.g. $\sigma \leq 0.1$) and the values of P not too close to the critical value 0.5 (e.g. $P \geq 0.55$), clearly shaped clusters are formed by the time $t \sim 500$. Once emerged, this pattern can remain unchanged (subject to just small variations in the clusters size and width, see Fig. 2.4) over a considerable time, up to $t = 5000$ or even longer. However, this appears to be a transient state rather than an asymptotical one as the number of clusters then can change suddenly to another value. An example of this dynamics is shown in

Fig. 2.8: over the first stage, the number of clusters in the pattern is five (see Fig. 2.5) but it suddenly changes to four at $t \approx 5000$. Once a new pattern with a different number of clusters emerges, it then remains unchanged; we did not observe any further changes in long-term simulations.

The dynamics become essentially different in the case of either σ becoming sufficiently large or P sufficiently small. One example is shown in Fig. 2.9 where the number of clusters never stabilizes. We will call this type of spatio-temporal pattern "dynamical clusters". Similarly to the previous case (see Fig. 2.8), the dynamics have a few different time scales corresponding to different stages of the dynamics. Over the first stage, the number of clusters fluctuates wildly (for the parameters of Fig. 2.9, between zero and four). At approximately $t = 2500$, the dynamics partially stabilizes by decreasing the range of fluctuations in the number of clusters between one and three. Another change occurs at $t \approx 12000$ when the fluctuations in the number of clusters occurs predominantly between one and two (occasionally jumping up to three). No further changes in the dynamics is observed at larger time.

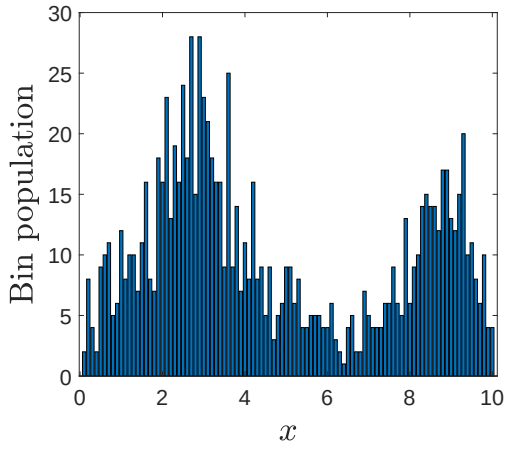

Figure 2.7: The population distribution obtained at $t = 9000$ for $P = 0.52$ and $\sigma = 0.1$, other parameters are the same as in Fig. 2.3.

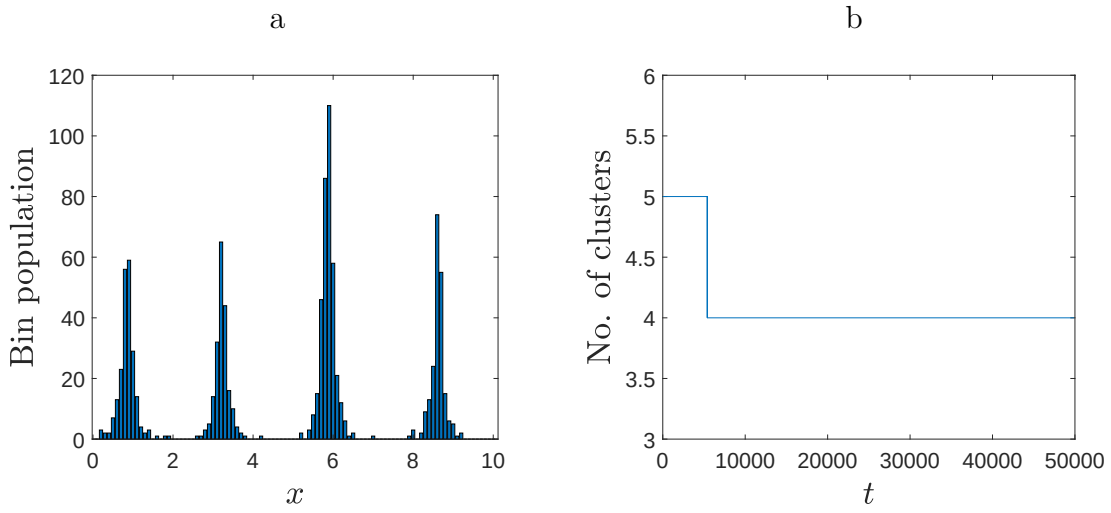

Figure 2.8: (a) The population distribution obtained at $t = 50,000$ for $\sigma = 0.02$, $R = 1$ and $P = 0.6$, other parameters are the same as above; (b) the number of the clusters in the pattern vs time. Note the abrupt transition from five to four at $t \approx 5000$.

2.3.2 Power law: non-Brownian walkers

Now we are going to consider the case where the individual movement is described by a power law as in Eq. (2.2.3). In order to make a sensible comparison between the results obtained for the dispersal kernel given by the normal distribution (see the previous section)

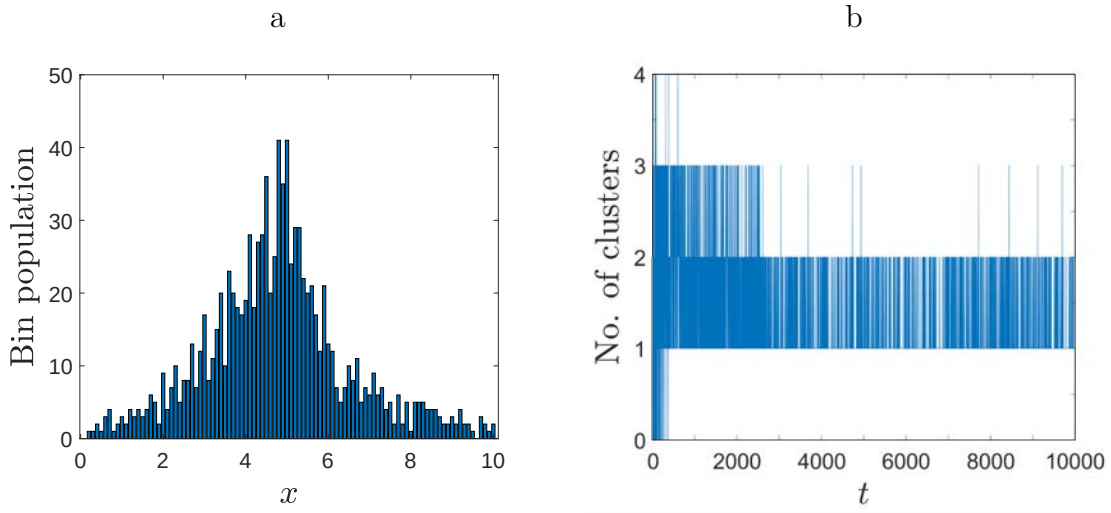

Figure 2.9: (a) The population distribution obtained at $t = 50,000$, parameters are the same as in Fig. 2.7; (b) the number of the clusters in the pattern vs time.

and those obtained for the power law (see below), a certain condition of equivalence must be established. For distributions with a finite variance, one way for doing that is to equalize the variance of different probability distributions. However, this approach does not work in the most interesting case of fat-tailed distributions, i.e. Eq. (2.2.3) with $1 < \gamma \leq 3$, because the dispersal kernel (2.2.3) does not have a finite variance. We therefore use a different approach and equalize the survival probabilities [20]. The survival probability is defined as the probability of an animal to remain within a given domain over a given interval. Let x_t be the location of a given animal at time t, then the probability that at the next observation time $(t+1)$ the animal will remain within a given distance r of its previous location, i.e. $x_t - r < x_{t+1} < x_t + r$, is calculated as follows:

$$P\left(x_t - r < x_{t+1} < x_t + r\right) \;=\; \int_{-r}^{r} \rho(\xi) d\xi. \tag{2.3.1}$$

For the two probability distributions, see Eqs. (2.2.2) and (2.2.3), we obtain, respectively:

$$P\left(x_t - r < x_{t+1} < x_t + r\right) \;=\; \mathrm{erf}\left(\frac{r}{\sqrt{2\sigma^2}}\right), \tag{2.3.2}$$

and

$$P\left(x_t - r < x_{t+1} < x_t + r\right) \;=\; 1 - \frac{k^{\gamma-1}}{(k+r)^{\gamma-1}}. \tag{2.3.3}$$

Setting the the survival probability at a hypothetical value 0.9 and taking into account that $\mathrm{erf}^{-1}(0.9) = 1.16$, we solve Eqs. (2.3.2) and (2.3.3) for r and equate the results (since r is the same), thus arriving at the following relation between the parameters:

$$k \;=\; 1.16\sqrt{2\sigma^2}\left(10^{\frac{1}{\gamma-1}} - 1\right)^{-1}. \tag{2.3.4}$$

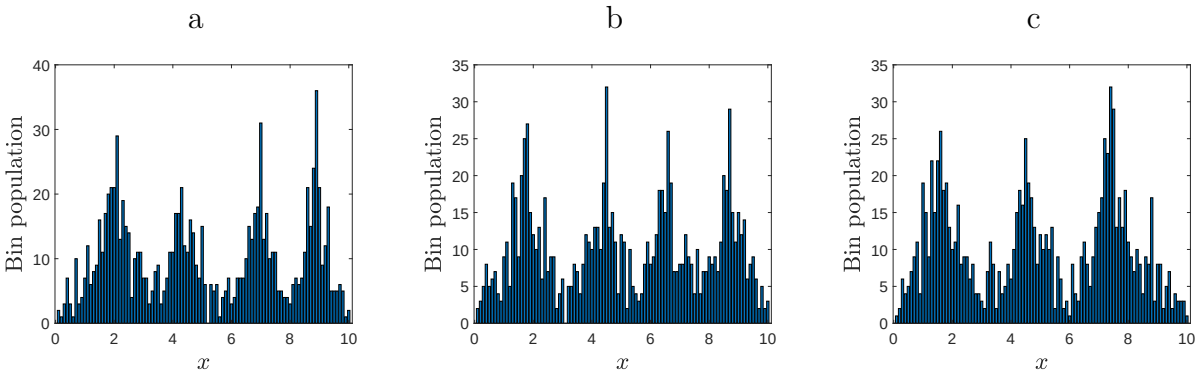

Figure 2.10: Clusters emerging in the population performing Lévy flight (2.2.3) with $\gamma = 2$. Parameter $k = 0.0036$ is calculated using the equivalence condition (2.3.4) with $\sigma = 0.02$. Other parameters are $R = 1$ and $P = 0.6$, i.e. the same as in Fig. 2.3.

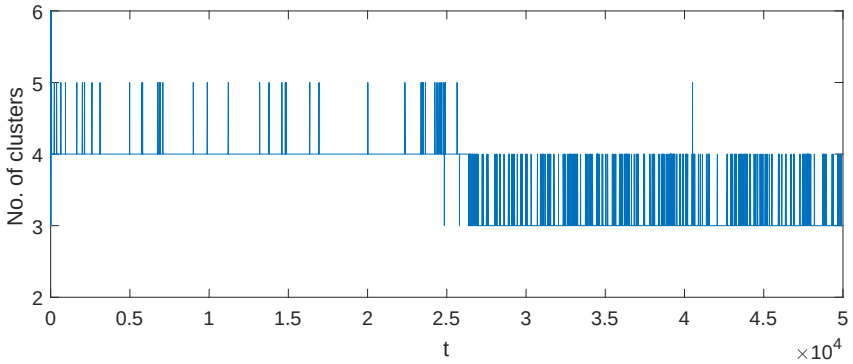

Figure 2.11: The number of clusters over time, parameters are the same as in Fig. 2.10. Over the first 25000 units of time, the number fluctuates between four and five (4/5-dynamics), at later time the number fluctuates between three and four (3/4-dynamics).

Therefore, for a given normal distribution with variance σ^2, parameter k of the 'equivalent' power law distribution (2.2.3) is given by relation (2.3.4).

Our simulations show that, in the population of non-Brownian walkers, the random-uniform initial condition evolves to an aggregated population distribution, apparently similar to the case of the normal distribution. Typical results are shown in Fig. 2.10. However, we readily observe that, apart from the generic property of the system to form spatial patterns, the population of non-Brownian walkers exhibits different properties compared to the population of the Brownian walkers with the equivalent Gaussian kernel. In particular, clusters are now much wider and less regular in shape. Moreover, the

number of clusters is not fixed any more, cf. the middle and the right panels in Fig. 2.10. A more detailed insight into the temporal dynamics (see Fig. 2.11) shows how the number of clusters fluctuates with time in an irregular manner. For the first period of $t \approx 25000$ of the system's dynamics, the number of clusters fluctuates between four and five. The system stays in the state with four clusters for most of the time (see the solid horizontal line in the left-hand side half of the figure) but makes short occasional excursion to the alternative state with five clusters. For convenience, we call this type of dynamics the "4/5-dynamics". Interestingly, the 4/5 dynamics is not sustainable and appears to be a very long transient. At $t \approx 25000$, the dynamics changes. Starting from $t \approx 25000$, the number of clusters fluctuates between three and four (being three for most of the time). We refer to this dynamics as "3/4-dynamics".

We want to emphasize that the long term transient dynamics shown in Fig. 2.11 has nothing to do with the usual transients caused by the effect of the initial conditions. In order to demonstrate that, we describe the system's dynamics by the number of transitions

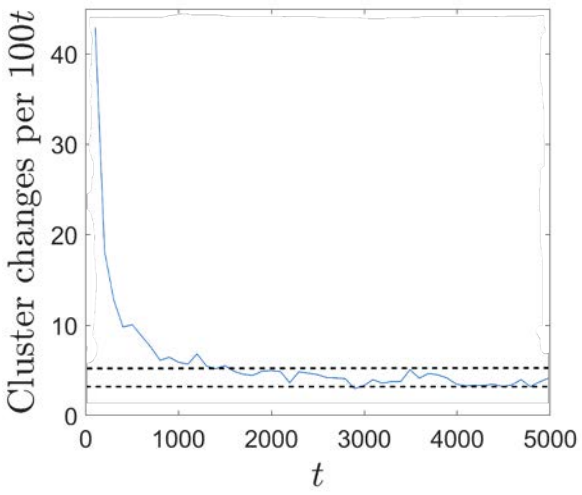

Figure 2.12: The mean number of transitions per given time between the states with different number of clusters. The mean was calculated from one hundred simulation runs. Parameters are the same as in Fig. 2.10. Convergence of the initial distribution to the quasi-steady "4/5-dynamics" is clearly seen as the number of transitions stabilizes within a certain range (as shown by the dashed horizontal lines) at $t \approx 1500$.

between the states with different number of clusters (e.g. between four and five for $0 < t < 25000$) per one hundred time units. Fig. 2.12 shows how this quantity changes with time. It is readily seen that the initial population distribution converges to the quasi-steady 4/5-dynamics by $t \approx 3000$. The system therefore exhibits two different time scales. The shorter time scale corresponds to the relaxation of the initial conditions to the 4/5 dynamics (Fig. 2.12), and the longer time-scale is the lifetime of the quasi-steady 4/5 dynamics before the system undergoes a fast transition to the asymptotical 3/4-dynamics at $t \approx 25000$.

To investigate the influence of our definition of clusters on the results, we now check

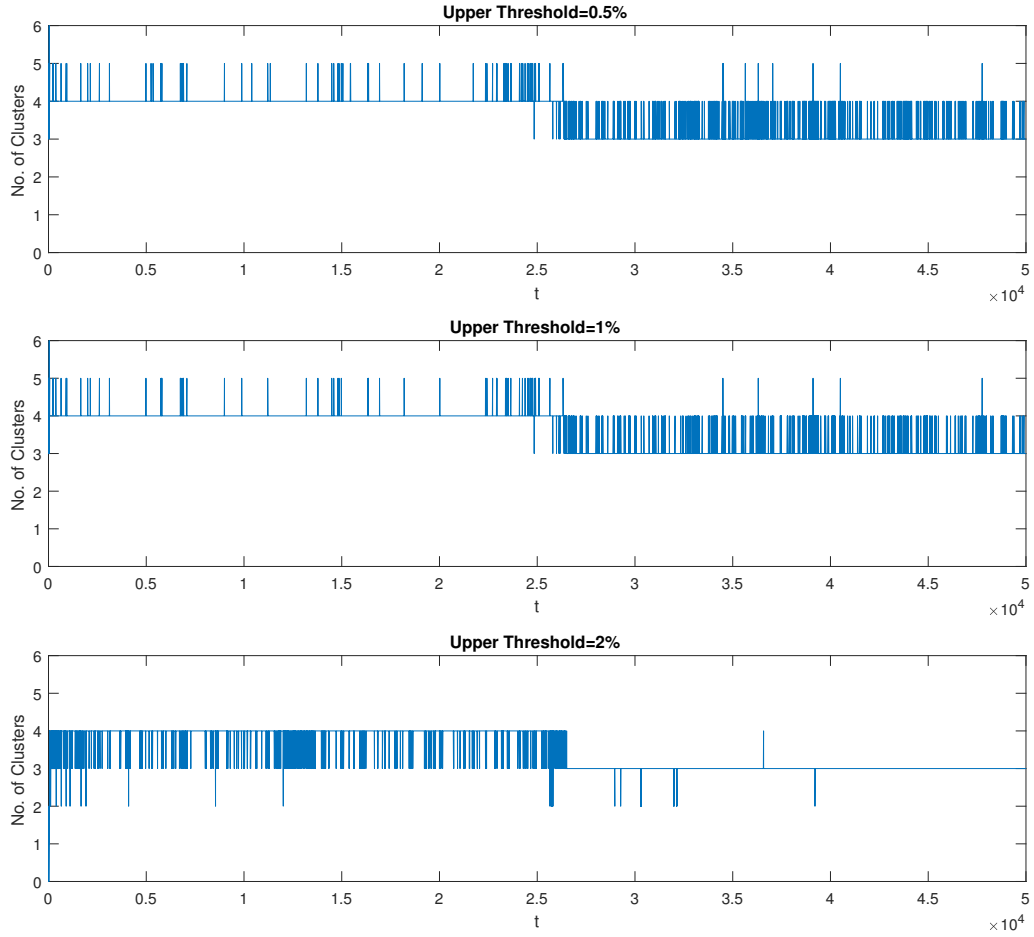

Figure 2.13: Sensitivity to the threshold density b_u defining cluster boundaries: number of clusters vs time for $b_u = 0.5\%$ (top), $b_u = 1\%$ (middle) and $b_u = 2\%$ (bottom). Parameters are the same as in Fig. 2.10.

whether our results are sensitive to the value of threshold b_u. Whilst the results obtained for the equivalent population of Brownian walkers are not sensitive to the value of the threshold as the clusters are well defined (see Fig. 2.8), in the population of non-Brownian walkers the clusters are volatile and the answer to the above question is by no means obvious. We therefore address this issue by analysing simulation results using different values of b_u. Results of the analysis are shown in Fig. 2.13. Note that here we use a simulation run different from that shown in Fig. 2.11, hence the results obtained for the same value $b_u = 0.02$ are similar but not identical, even though obtained for the same parameter values. It is readily seen that the number of clusters can become sensitive to the value of b_u when b_u becomes large. Remarkably, neither the existence of dynamical clusters nor the existence of the long-term transient is sensitive to b_u. We therefore conclude that these are genuine properties of the population dynamics of non-Brownian walkers.

Note that, due to the inherent stochasticity of the system, the duration of the long transient is essentially a random value. In our simulations, we observed that the timing of the transition to the asymptotical state can be anywhere between $t \sim 15000$ and $t \sim 45000$ (and occasionally taking smaller or larger values too). Also, in different simulations the 4/5 dynamics may include occasional excursions to the state with just three clusters, and the asymptotical state 3/4 may exhibit relatively frequent excursions to the state with five clusters.

An interesting question is how the properties of the system's dynamics may be different for different values of the exponent γ. Intuitively, one can expect that for sufficiently large values of γ the dynamics may become closer to that of Brownian walkers, because a power law distribution (2.2.3) with $\gamma > 3$ possesses a finite variance and hence converges to the normal distribution by virtue of the Central Limit Theorem. This is corroborated by simulations. Fig. 2.14 shows the results obtained for $\gamma = 4$. It is readily seen that dynamic clusters do not exist in this case; the number of clusters do not fluctuate with

time. Clusters themselves are well defined, similar to what was observed in the case of Brownian walkers, see Fig. 2.14 and the bottom panels of Fig. 2.3. Interestingly, long term transient dynamics is observed also for $\gamma = 4$: the system does not converge to its final state of three clusters until $t = 10,000$.

For large γ, it is possible to find the mean step size (for $\gamma > 2$) and the variance (for $\gamma > 3$) by calculating the first and second moment of the power law, and compare them to the half-normal distribution. The mean of the power law distribution is

$$\mu_P = \int_0^\infty x\rho_P(x)dx = \frac{k}{\gamma - 2}, \tag{2.3.5}$$

for $\gamma > 2$. When equating survival probabilities with $\sigma = 0.02$, as used in Section 2.3.1, we have $\mu_P = 0.0152$ for $\gamma = 3$ and $\mu_P = 0.0142$ for $\gamma = 4$. The mean step size of the half normal distribution (Eq. (2.2.6)) is $\mu_f = 0.016$.

The variance of the power law distribution when $\gamma > 3$ is

$$\sigma_P^2 = \int_0^\infty x^2\rho_P(x)dx - \mu_P^2 = \frac{k^2(\gamma - 1)}{(\gamma - 2)^2(\gamma - 3)}. \tag{2.3.6}$$

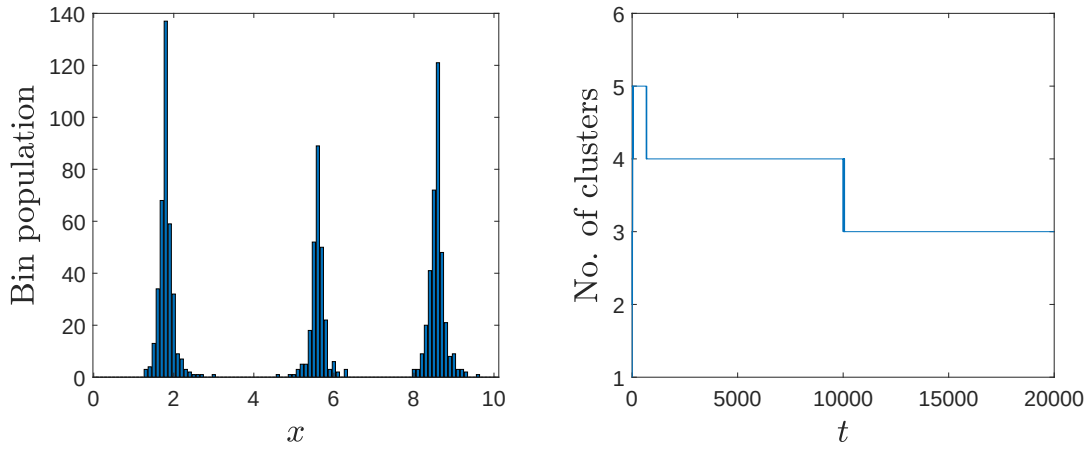

Figure 2.14: Population dynamics of non-Brownian walkers (2.2.3) with $\gamma = 4$: (left) the population distribution obtained at $t = 20,000$, (right) the number of clusters vs time. Parameters are the same as in Fig. 2.10.

Therefore the standard deviation is given by

$$\sigma_P = \frac{k\sqrt{\gamma-1}}{(\gamma-2)\sqrt{\gamma-3}}. \tag{2.3.7}$$

If we rearrange Eq. (2.3.4) for equating survival probabilities, we get

$$\sigma = \frac{k(10^{1/(\gamma-1)}-1)}{1.16\sqrt{2}}. \tag{2.3.8}$$

where σ is the standard deviation of the normal distribution that we are trying to equate the power law to. Thus the methods can be compared directly. When $\gamma = 4$, from calculating moments we get $\sigma_P = 0.866k$ and from equating survival probabilities, $\sigma = 0.704k$. Using Eq.(2.2.7), for the half normal distribution this becomes $\sigma_f = \sigma\sqrt{1-2/\pi} = 0.424k$. Therefore when k is chosen by equating survival probabilities, the standard deviation of the power law with $\gamma = 4$ is $\sigma_P = 0.0246$. This compares to $\sigma_f = 0.0121$ for the half-normal distribution.

We have also checked the opposite case, i.e. for $1 < \gamma < 2$; see the top row in Fig. 2.15. For comparison, the bottom row shows the case with $\gamma = 2$, Fig. 2.15(c), and $\gamma = 4$, Fig. 2.15(d). It is readily seen that for $\gamma = 1.1$, shown in Fig. 2.15(a), there are no clusters, so that the population is spread over the domain. As γ increases, areas of high population density becomes visible. For $\gamma = 1.5$, shown in Fig. 2.15(b), the number of clusters fluctuates in time from 0 to 3, the case of two clusters being most common (seen at approximately one half of the time steps). With a further increase in γ, clusters becomes clearly visible starting from $\gamma \approx 2$, these values are dynamic and their number fluctuates with time (see Figs. 2.11 and 2.13). For $\gamma \geq 4$, clusters are well defined and stable; the population is strongly aggregated with high population density inside the clusters and approximately zero between the clusters.

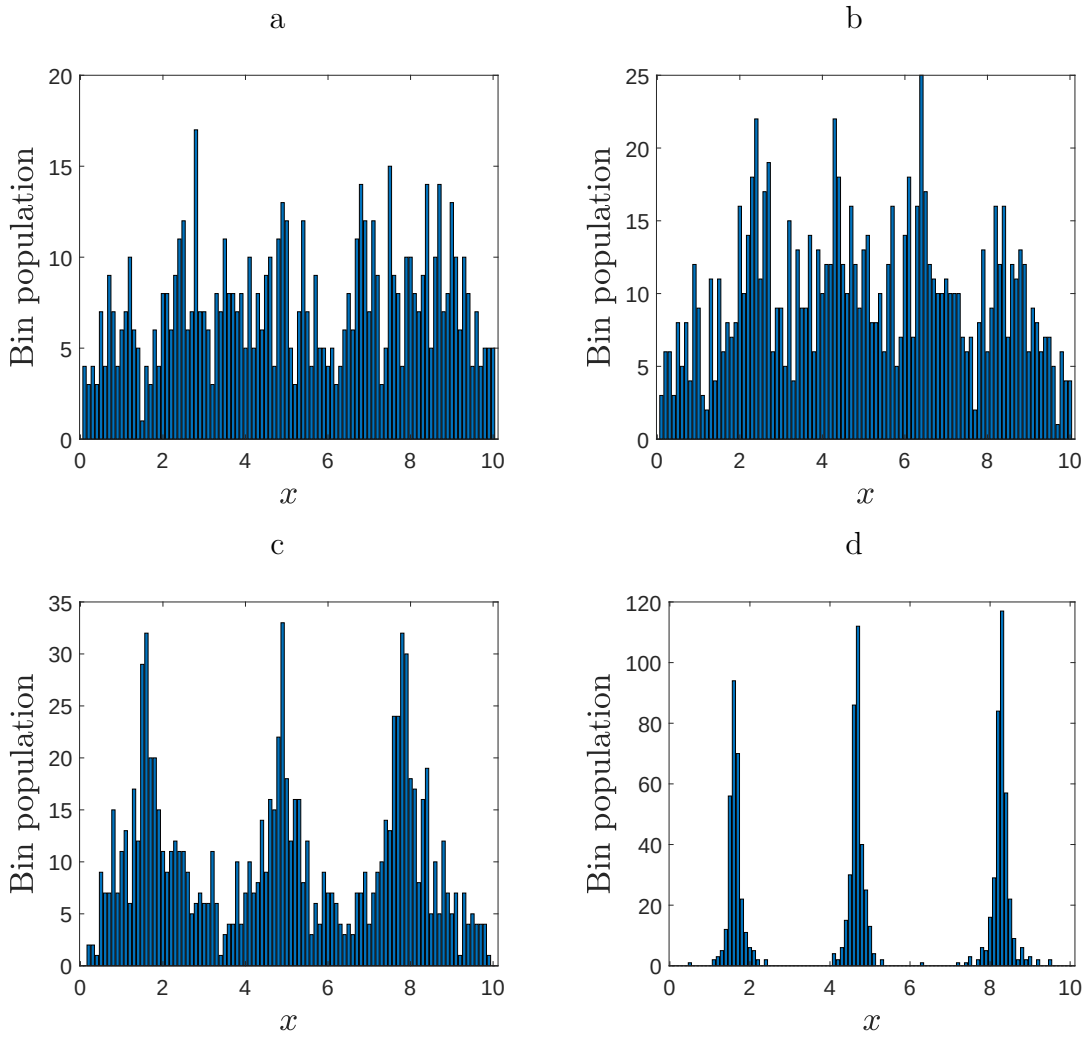

Figure 2.15: The distribution of non-Brownian walkers for different values of γ. The corresponding values of parameter k are calculated from equating survival probabilities to that of the normal distribution with $\sigma = 0.02$. (a) $\gamma = 1.1$, (b) $\gamma = 1.5$, (c) $\gamma = 2$ and (d) $\gamma = 4$. All the distributions are shown at $t = 50,000$. Parameters are the same as in Fig. 2.3.

2.3.3 Effect of the domain's finiteness

In the simulations above, we focused on the case of a large domain, i.e. where the characteristic movement step (as given by the value of the standard deviation σ of the normal distribution (2.2.2) or by the value of parameter k in the case of the power-law distribution (2.2.3)) is much smaller than the size L of the domain, i.e. $\sigma/L \ll 1$ and $k/L \ll 1$. Arguably, in this case the effect of the domain boundedness is small and the animal

movement mimics closely the corresponding movement in an unbounded space. A question arises here as to whether the significant difference that we observed above between the properties of the spatial pattern emerging in the population of Brownian walkers and the population of non-Brownian walkers would remain if the effect of the domain boundedness becomes more prominent, i.e. when σ/L or k/L are not small any more.

Recall that in our model, animals cannot leave the domain, see Section 2.2. Effectively, it means that the tail of the distribution is cut off. Although this cutoff changes the asymptotical properties of the distribution (in particular, making the variance finite), in the case where $\sigma/L \ll 1$ or $k/L \ll 1$ the remaining part of the dispersal kernel that is actually used to generate movement steps is a significantly different shape. The different shape of dispersal kernels determines the difference in the emerging patterns.

However, the situation is different in the opposite case of a small domain, i.e. $\sigma/L \gg 1$ or $k/L \gg 1$. In this case, since the maximum value of the movement step $\Delta x \leq L$, $\Delta x/\sigma \ll 1$ and $\Delta x/k \ll 1$. Therefore, both the normal distribution and the power-law distribution can be well approximated by the first two terms in their Taylor expansion, that is

$$\rho\left(\Delta x\right) \approx \frac{1}{\sqrt{2\pi\sigma^2}}\left[1 - \frac{(\Delta x)^2}{2\sigma^2}\right] \qquad \text{and} \qquad \rho\left(\Delta x\right) \approx \frac{C}{k^\gamma}\left[1 - \left(\frac{|\Delta x|}{k}\right)^\gamma\right], \tag{2.3.9}$$

respectively. The functional form of the distributions therefore becomes similar (especially, in case $\gamma = 2$) and hence one can expect that the emerging patterns, if any, should have similar properties. In fact, any stable clusters are unlikely to appear at all: in a sufficiently small domain, both distributions are approximately constant (keeping only the first terms in Eqs. (2.3.9)), which means that the position of each animal at each movement step is drawn from a uniform probability distribution. Here we recall that this is the way how we generate the initial distribution (see Fig. 2.2). Therefore, in the case of a small domain (or large characteristic movement step), the animal movement is unlikely

to result in the formation of clusters.

These heuristic arguments are confirmed by numerical simulations. Fig. 2.16(a) shows the spatial distribution of the population density across the domain of length $L = 10$ obtained at $t = 3000$ for the normal distribution (2.2.2) with $\sigma = 50$; other parameters are the same as in Fig. 2.3. It is readily seen that there are no clusters; in fact, at any time $t > 0$ the distribution is not much different from the initial distribution (not shown here for the sake of brevity). The latter observation is confirmed by statistical measures: the variance of the initial population distribution and the distribution obtained at $t = 3000$ is 9.80 and 8.95, respectively. For comparison, Fig. 2.16(b) shows the spatial population distribution obtained at $t = 3000$ in simulations with the equivalent power-law kernel, i.e. Eq. (2.2.3) with $k = 9.114$, other parameters are the same. Similarly to the above, there are no clusters. The spatial distribution remains approximately uniform; the variance calculated for $t = 1$ (not shown) and $t = 3000$ (Fig. 2.16(b)) is 9.76 and 10.79, respectively. Note that these values are not much different from the values obtained in the case of normal distribution. We therefore conclude that, in the case of a small domain, the population dynamics of Brownian walkers and non-Brownian walkers are practically indistinguishable.

We have also checked how the results may change for a larger value of the perception radius R. For that, we performed simulations with $R = 10$ and other parameters the same as in Fig. 2.16. The results that we obtained (not shown here for the sake of brevity) are very similar to the above. No clusters are formed and the population spatial distribution is approximately uniform across the domain.

We now notice that, even in the case of a large domain, e.g. for $\sigma/L \ll 1$ in the case of the normal distribution, the tail of the distribution never actually works, because the animal is not allowed to leave the domain. Similar observation obviously applies to the power law distribution, which means that its fat tail is in fact truncated. The truncated power law distribution has a finite variance, and that opens a possibility of using

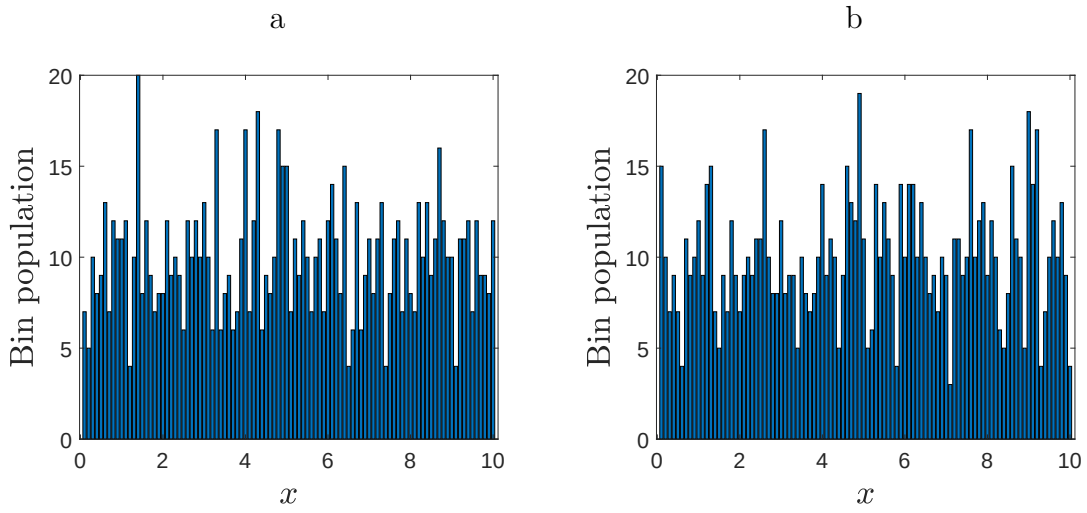

Figure 2.16: The population distributions at $t = 3000$ in the case of (a) the normal distribution of the movement steps obtained for $\sigma = 50$, other parameters are the same as in Fig. 2.3, and (b) the equivalent power law distribution. In both cases $R = 1$.

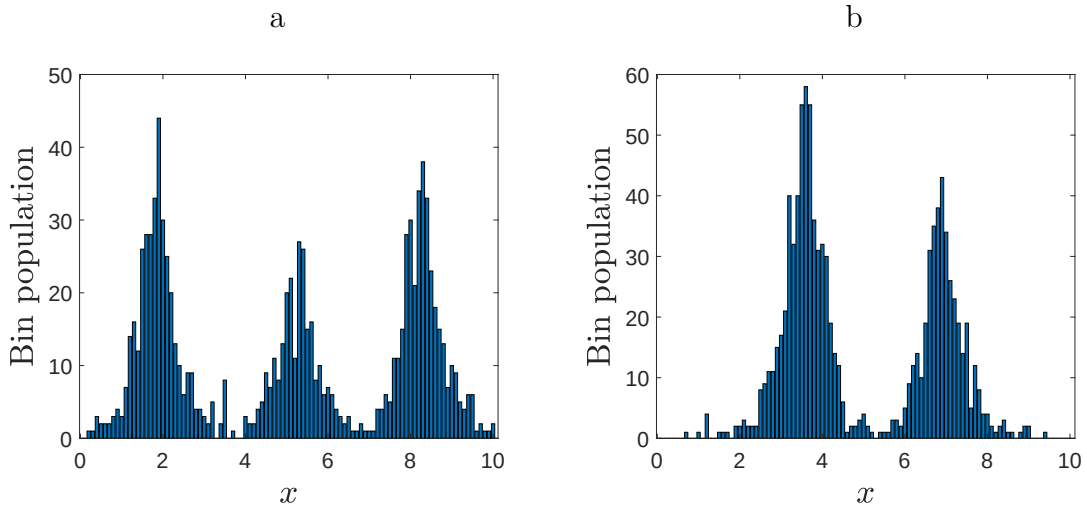

Figure 2.17: The population distributions obtained for $\sigma = 0.1414$ (other parameters are $R = 1$, $P = 0.6$, $N = 1000$ and $L = 10$, i.e. the same as in Fig. 2.3) and shown at (a) $t = 1000$ and (b) $t = 10,000$.

a different equivalence condition between the two dispersal kernels, namely by equating the variance. The question therefore arises as to how different the properties of the emerging spatiotemporal patterns obtained for the two movement types are going to be if the truncated dispersal kernels are compared.

In order to address this issue, we perform the simulations as follows. Firstly, we

consider the population dynamics of non-Brownian walkers for parameters $\gamma = 2$, $k = 0.0036$, $R = 1$ and $P = 0.6$, i.e. as in Fig. 2.10. We pool together the movement step sizes made by all animals in the population ($N = 1000$) over the first ten thousand time steps. For the resulting data set of the movement steps (altogether, 10^7 random numbers), we calculate the variance to obtain the value $\sigma^2_{PLT} \approx 0.02$, so that the corresponding standard deviation is $\sigma_{PLT} \approx 0.1414$. We then simulate the dynamics of the population of the Brownian walkers subject to the new equivalence condition:

$$\sigma \;=\; \sigma_{PLT}, \tag{2.3.10}$$

keeping all other parameters the same as above. The results are shown in Fig. 2.17. It is readily seen that now the difference between the patterns emerging in the population of non-Brownian walkers (Fig. 2.10) and in the equivalent population of Brownian walkers (as defined by (2.3.10)) is less drastic than it was previously (cf. Fig. 2.3). Yet the patterns remain clearly different; in particular, the population is much stronger aggregated and the clusters are more clearly shaped in the population of Brownian walkers. We therefore conclude that not only the large-distance asymptotics of the dispersal kernel but also its shape at intermediate distances plays an important role in shaping the population dynamics.

Alternative boundary conditions

The boundary conditions, described in Section 2.2, are modelled so that an animal will 'retake' its step if the original step were to take it outside the domain. It is important to consider how much of an effect this will have on cluster formation and whether the dynamics will change if different boundary conditions are used. Therefore, we now consider three new methods for simulating the boundary, which we label as 'periodic boundary', 'reflective boundary' and 'sticking boundary'.

For the periodic boundary, instead of retaking a step, the animal will continue the

step from the opposite boundary. The next position $x_n(t+1)$ is calculated as

$$x_n(t+1) = (x_n(t) + \Delta x) \bmod L. \tag{2.3.11}$$

At the reflective boundary, the remaining length of the step is reflected back into the domain, given by

$$x_n(t+1) = (L - (x_n(t) + \Delta x)) \bmod L. \tag{2.3.12}$$

Lastly, for the sticking boundary, the animal simply ends their step when they reach the boundary, given by

$$x_n(t+1) = \begin{cases} 0 & \text{if } x_n(t) + \Delta x < 0, \\ L & \text{if } x_n(t) + \Delta x > L \end{cases}. \tag{2.3.13}$$

To compare the results discussed so far in Section 2.3 to those when using different boundary conditions, we focus on the number of clusters that emerges from Brownian walkers and the temporal stability of clusters produced by non-Brownian walkers. In the case of Brownian walkers, we want to check the number of clusters is similar to the first column of Table 2.1. For non-Brownian walkers, we want to check if the cluster stability is visually similar to that shown in Fig. 2.11. We use the same parameters as these examples, i.e. $P = 0.6$, $R = 1$ and for Brownian walkers $\sigma = 0.02$, for non-Brownian walkers $\gamma = 2$ and $k = 0.0036$.

We note that, with this choice of parameters, the frequency that an animal hits the boundary and steps are retaken for Brownian walkers is initially (for the first 50 time steps) 0.46 retaken steps each time interval in a population of $N = 1000$. When clusters have formed this drops to 0.003 retaken steps per time interval (between $t = 100$ and $t = 1000$). For non-Brownian walkers the frequency is initially 1.98 retaken steps per time interval, dropping to 1.48 when clusters have formed. We would therefore expect that a change in the boundary conditions would not have a notable effect on cluster

Table 2.4: The probability of different numbers of clusters obtained in simulations of Brownian walkers with different boundary conditions (including the previously used method, labelled 'Retake step'). Movement parameters are $R = 1$, $P = 0.6$ and $\sigma = 0.02$. For any given parameter set, the probabilities were calculated based on one hundred simulation runs.

No. of clusters	Retake step	Periodic boundary	Reflective boundary	Sticking boundary
3	0.03	0.03	0	0.04
4	0.53	0.48	0.46	0.47
5	0.41	0.48	0.50	0.45
6	0.03	0.01	0.04	0.04

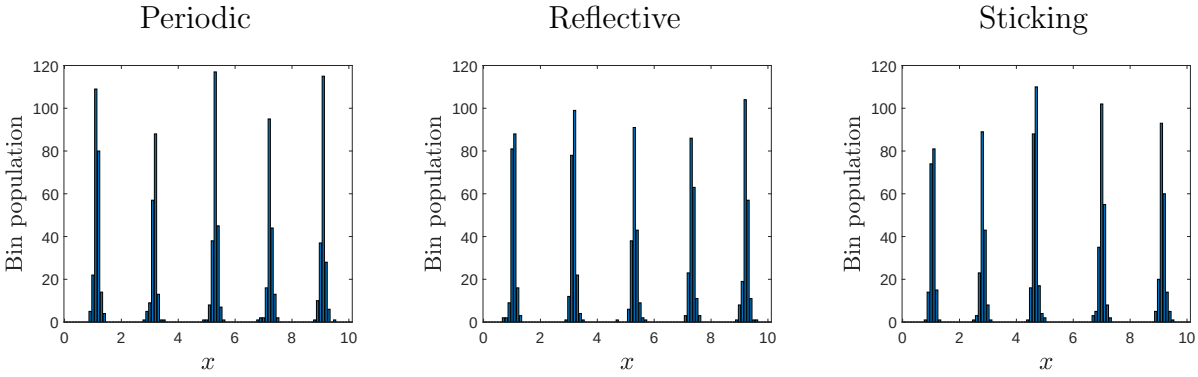

Figure 2.18: Example distributions of Brownian walkers when using periodic, reflective and sticking boundaries. The parameters are the same as Fig. 2.3.

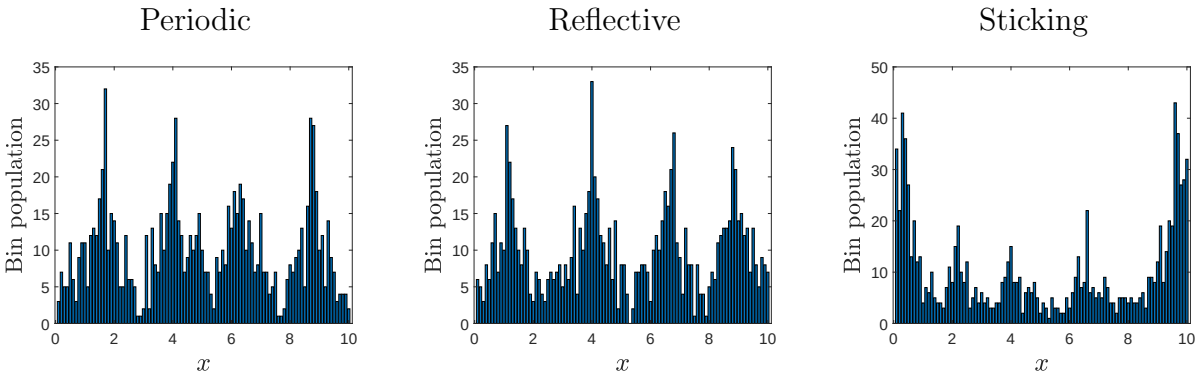

Figure 2.19: Example distributions of non-Brownian walkers when using periodic, reflective and sticking boundaries. The parameters are the same as Fig. 2.10.

formation, particularly for Brownian walkers.

Figs. 2.18 and 2.19 show example distributions that emerge from Brownian and non-Brownian walkers respectively using the alternative boundary conditions. In the case of

Brownian walkers, the distributions are visually similar to one another and to Fig. 2.5. In each distribution, five dense clusters have formed in the domain. Table 2.4 also shows that the frequency of different numbers of clusters that emerge are similar for different boundary conditions. The majority of simulations produce 4 or 5 clusters and a minority produce 3 or 6 clusters. We therefore conclude that the change in boundary conditions does not affect the formation of clusters in the case of Brownian walkers.

In Fig. 2.19, the example distributions of non-Brownian walkers when using periodic or reflective boundaries are visually similar to one another and to Fig. 2.10. This is also the case in Fig. 2.20, showing the number of clusters over time, where the fluctuations between states when using periodic or reflective boundaries is similar to that shown in Fig. 2.11. However, the sticking boundary has produced a distribution where there are two dense clusters close to each boundary and smaller clusters in the centre of the domain. This means that although the number of clusters still fluctuates, the number of clusters fluctuates mostly from zero to two, occasionally reaching 3 or 4. This is likely because when an individual sticks to the boundary, it is likely to influence the movement of other animals nearby to move towards the boundary, leading to a cluster being formed. This does not occur in the case of Brownian walkers because the number of instances of steps hitting the boundary is much smaller than for non-Brownian walkers. Though the sticking boundary may be useful in certain ecological contexts, we do not consider these dynamics in our study. The other methods do not substantially change the spatio-temporal dynamics and therefore we proceed with the closed boundary as described in Section 2.2.

Asynchronous updating

Another feature of our model is that we use synchronous updating at each time interval, where animals all make their steps based on a snapshot at the previous time step. An alternative to this is for each animal in the population to update its position sequentially,

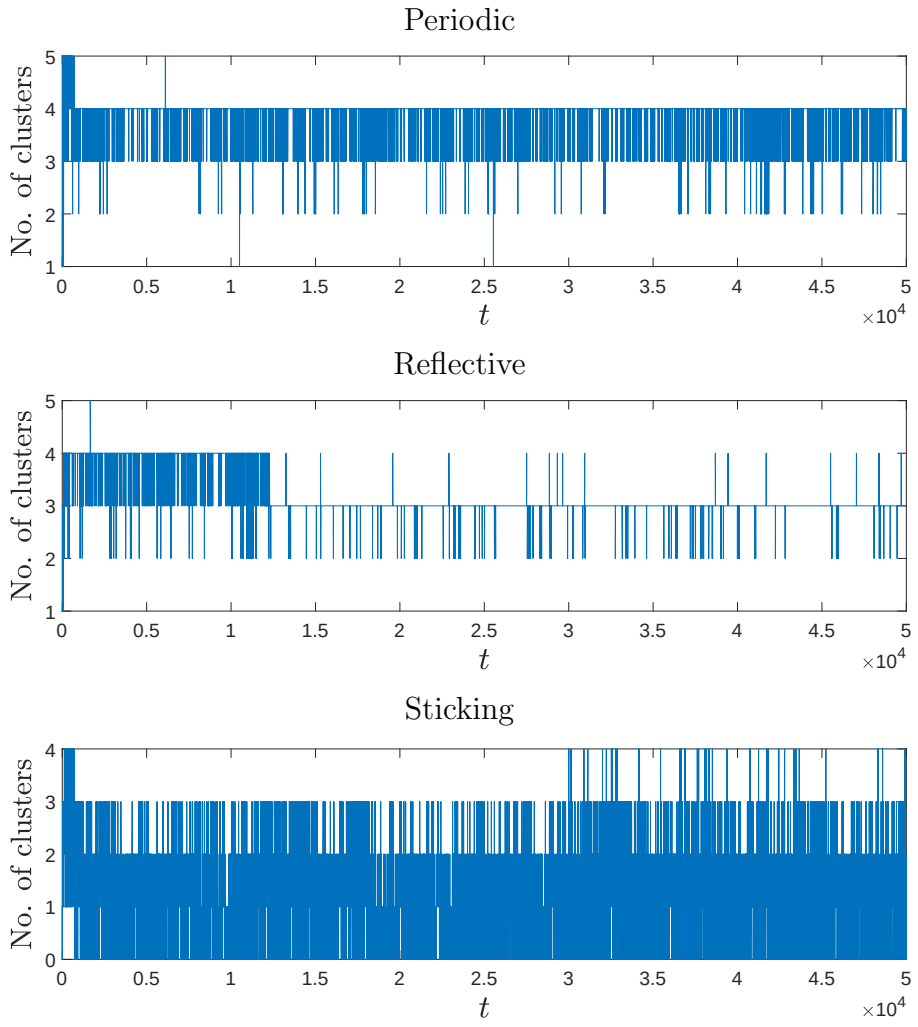

Figure 2.20: The number of clusters over time when using periodic, reflective and sticking boundaries. In all cases the number of clusters fluctuates, similar to Fig. 2.11.

so that an individual's decision takes into account the updates that have already happened in the sequence. This is known as asynchronous updating [40, 53, 100]. It has been shown that synchronous and asynchronous updating in an IBM can produce different results. In particular, synchronous updating can lead to greater temporal variation in the model as updating individuals' characteristics produces abrupt changes [40, 53]. In our model this may lead to animals stepping past each other and ending up further away as they move towards the previous position of their conspecific. However, it is not clear whether this will have a substantial effect on the formation of clusters. To test this, we compare the

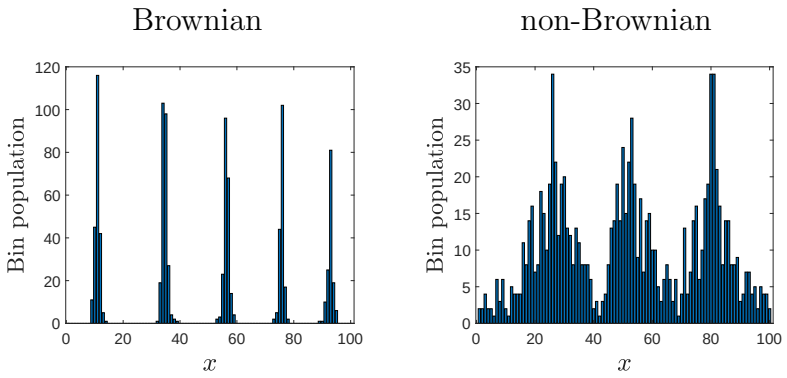

Figure 2.21: Example distributions of Brownian and non-Brownian walkers when using sequential movements. The parameters are the same as Fig. 2.10.

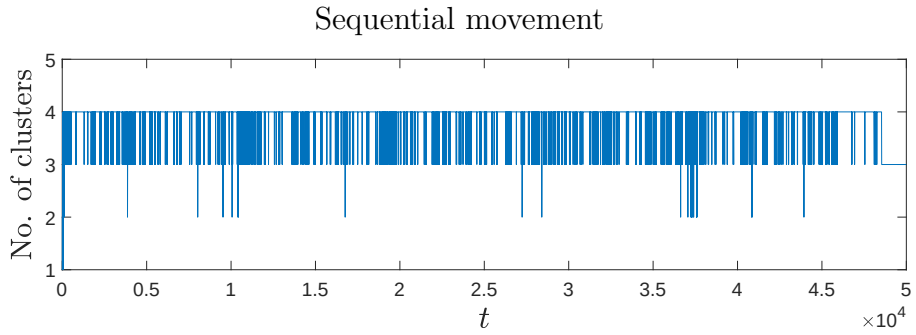

Figure 2.22: The number of clusters over time when using sequential movement in a population of non-Brownian walkers.

number of clusters and the cluster stability for populations of Brownian and non-Brownian walkers respectively.

Fig. 2.21 shows example distributions of Brownian and non-Brownian walkers using sequential movement. In both cases, the distributions are visually similar to those in Figs 2.5 and 2.10. In the case of Brownian walkers, the probability of different numbers of clusters obtained from 100 simulations is 0.03 for three clusters, 0.44 for four clusters, 0.51 for five clusters and 0.02 for six clusters. This is similar to the results in Table 2.4. For non-Brownian walkers, the temporal dynamics of the number of clusters shown in Fig. 2.22 has fluctuations similar to that shown in Fig. 2.11. We can therefore conclude that sequential movement does not affect the formation of clusters in our model.

2.3.4 Statistical properties of the spatial patterns

Morisita index

As we have shown above, density-dependent individual movement normally results in the formation of strongly heterogeneous spatial population distribution consisting of several clusters (when the dispersal kernel variance is not too large and the directional bias not too weak). Whilst this is clearly seen in the simulations results, the question is whether this self-organized heterogeneity could be described in a more quantitative way. There are several measures or indices that are used in statistical ecology for this purpose, e.g. see [101] for a short review. In particular, the Morisita index [157] has been widely used to quantify the heterogeneity of the spatial distribution [7, 95, 102]:

$$I_M \;=\; Q\,\frac{\sum_{k=1}^{Q} n_k(n_k-1)}{N(N-1)}. \tag{2.3.14}$$

The Morisita index provides a measure of how likely it is that two randomly selected individuals in a given distribution are found within the same bin compared to that of a random distribution [157]. It can be proved that, if the individuals are distributed randomly (with a constant probability density) then I_M is close to one, and it is greater than one if the individuals are aggregated [114].

Using the definition (2.3.14), we have calculated I_M for several different spatial population distribution as given by Figs. 2.3, 2.7, 2.10 and 2.14. The results are shown in Table 2.5. Obviously, the Morisita index is an adequate measure of the population aggregation: the conclusion as to which distribution is more aggregated based on the visual comparison appears to be in full agreement with I_M values. However, it is also readily seen that the Morisita index fails to distinguish between distribution with different number of clusters. For instance, the I_M value is close in the cases shown in rows 3 and 9 of the table; however, the number of clusters in the corresponding distributions is different. Similarly, the I_M

Table 2.5: The Morisita index calculated for various spatial population distributions. N.D. and P.L. stand for the normal distribution and the power law distribution, respectively; see Eqs. (2.2.2–2.2.3).

	Sources	Dispersal kernel	Number of clusters	Morisita index, I_M
1	Fig. 2.3 ($t = 100$)	N.D.	4	1.817
2	Fig. 2.3 ($t = 200$)	N.D.	4	3.438
3	Fig. 2.3 ($t = 500$)	N.D	4	8.065
4	Fig. 2.3 ($t = 1000$)	N.D.	4	8.872
5	Fig. 2.7	N.D.	2	1.204
6	Fig. 2.10 ($t = 100$)	P.L. ($\gamma = 2$)	4	1.230
7	Fig. 2.10 ($t = 10,000$)	P.L. ($\gamma = 2$)	4	1.352
8	Fig. 2.10 ($t = 30,000$)	P.L. ($\gamma = 2$)	3	1.346
9	Fig. 2.14	P.L. ($\gamma = 4$)	3	7.120

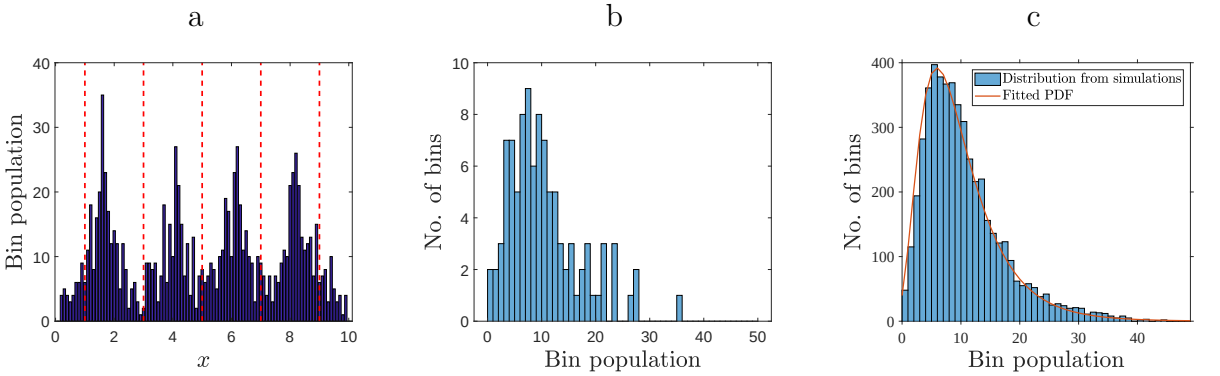

Figure 2.23: (a) The population distribution obtained in the case of the power law dispersal kernel (2.2.3) with $\gamma = 2$ and $k = 0.0036$ and other movement parameters as $R = 1$ and $P = 0.6$, vertical red lines indicates the hypothetical location where samples are taken. (b) Frequency distribution of sample values (all one hundred bins are used) obtained for the snapshot shown in (a). (c) Frequencies obtained from pooled multiple simulations, see details in the text; red curve shows the fitting of the data with a lognormal distribution, $R^2 = 0.996$.

value is approximately the same (up to the second digit) in rows 5 and 6, but the number of clusters is different. Also, the Morisita index is incapable of distinguishing between the different movement types: whilst rows 3 and 5 correspond to the Brownian walk, the distributions indexed in rows 6 and 9 are obtained for the non-Brownian walk.

Sample frequency distributions

In the above, we have shown that different patterns of individual animal movement result in an emerging spatial population distribution with apparently different properties. The

number of clusters, their size, shape, and their stability provide convenient theoretical measures to distinguish between the population distributions emerging in the populations of Brownian and non-Brownian walkers. However, although providing useful information about the pattern as a whole, they hardly provide any information about the local population density (such as is given, in our approach, by the population size in any given bin). Meanwhile, considering the problem in a more practical perspective, it is the local information that ecologists normally obtain in empirical studies, e.g. through sampling. The number of samples collected in any given animal population census can vary from, in rare cases, hundreds or even thousands of samples [5, 160, 232] to, rather typically, one or two dozen [21, 27] or, sometimes, a few or just one [15, 197]. Therefore, ecologists often have to operate with scarce spatial information that does not resolve details of the strongly heterogeneous population spatial distribution. As a result, the global properties of the distribution such as the location and the number of clusters (patches) remain obscure. An example is shown in Fig. 2.23(a) where red lines indicate the location where the samples were collected and hence the population density (or its proxy, e.g. trap count) is known. Note that in this example none of the distribution maxima has been sampled. We therefore investigate whether differences between population distributions can be picked up and quantified based on local or spatially unstructured information such as an array of values of the population density for a given species (or their proxy, e.g. trap counts) collected on a sampling grid with no reference to population aggregation.

One way to analyse the sampling data, especially in the absence of knowledge of the spatial pattern, is to consider the frequency distribution of sample values. This approach was used in several empirical studies [21, 45, 56, 207] and was shown to provide valuable insight into the properties of the corresponding population dynamics [176, 225]; see also [29, 260] for a more general framework. In order to demonstrate how to relate a given spatial pattern to the frequency distribution of sample values, let us consider the snapshot of the population distribution shown in Fig. 2.23(a). We assume that the population sizes

in different bins are statistically independent so that information obtained from all bins can be used, which gives an array of one hundred values of the population density. These numbers are arranged according to their frequencies resulting in the histogram shown in Fig. 2.23(b). The obtained frequency distribution has a jagged, irregular shape, which indicates that one hundred values is not enough to produce a stable, sensible distribution of sample values. To obtain a histogram with a better defined shape, we therefore pool together results of multiple simulation runs. For the given parameter set, the simulations

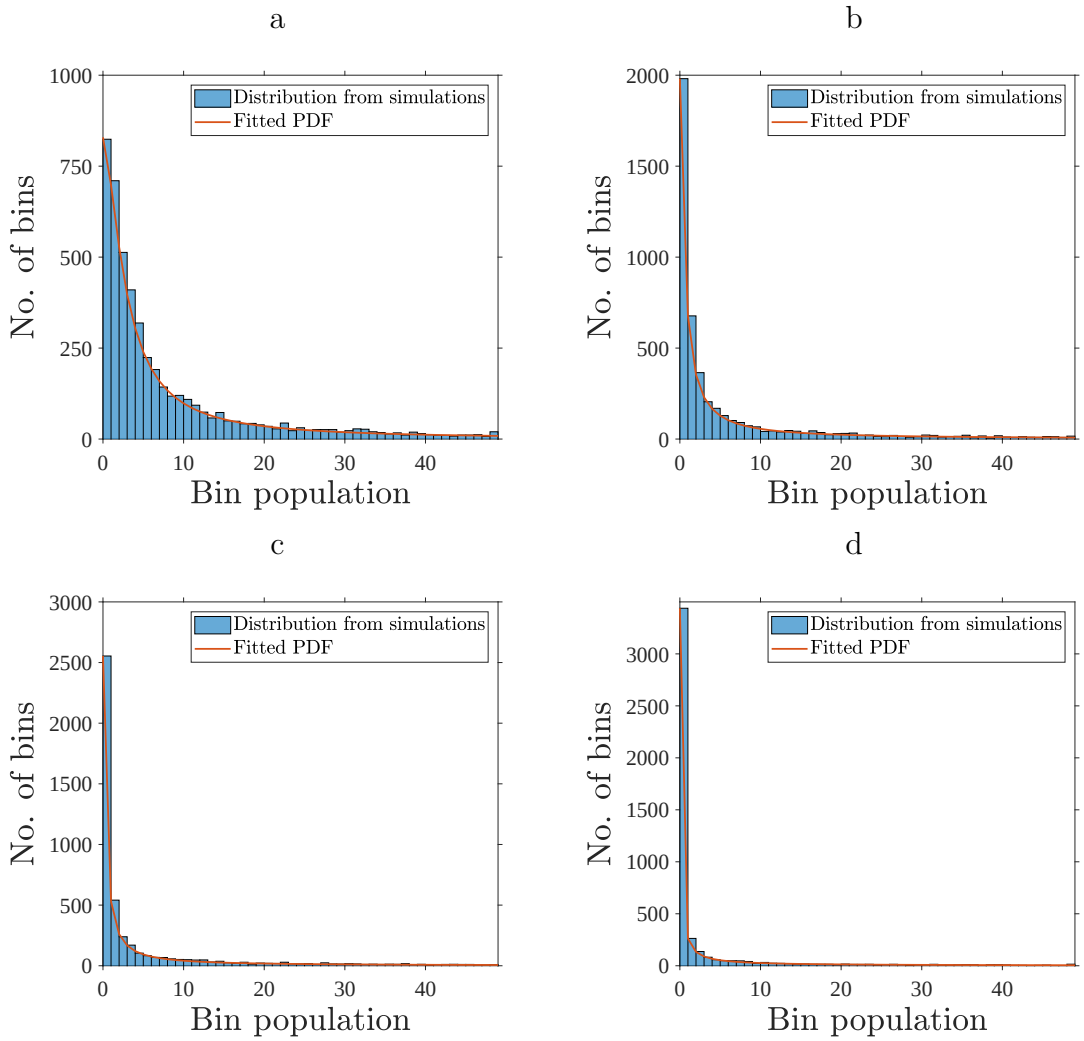

Figure 2.24: Frequency distribution of sample population density values obtained for the spatial population distributions simulated for different dispersal kernels: (a) power law (2.2.3) with $\gamma = 3$, (b) power law with $\gamma = 4$, (c) power law with $\gamma = 5$ and (d) normal distribution (2.2.2). Red curves show data fitting by a power law; see Table 2.6.

were repeated fifty times, thus producing altogether the pool of 5000 bin values that were then arranged into a histogram; see Fig. 2.23(c). It is readily seen that the histogram of sample value frequencies now has a much smoother shape; in particular, it can be fitted very well by a lognormal distribution, i.e. the red curve.

We now repeat the above procedure for different values of the power law exponent γ and for the normal distribution. Results are shown in Fig. 2.24. We readily observe that the properties of spatial population distributions (not shown here for the sake of brevity) emerging when the dispersal kernel is a power law (2.2.3) with $\gamma \geq 3$ is significantly different from the case when $\gamma = 2$ which corresponds to Lévy flights. Results obtained for larger values of γ are almost indistinguishable from the results obtained for the normal distribution, as can be seen in Figs. 2.24(c) and 2.24(d). All four frequency distributions shown in Fig. 2.24 can be fitted well by a power law, see Table 2.6 (note that the accuracy of the fitting increases with an increase in γ); however, it does not provide any sensible fitting for the sample value distribution obtained for $\gamma = 2$.

Table 2.6: Best-fit parameter values and R^2 values for the fitting of the sample frequency histograms shown in Fig. 2.24 by a power law $p(x) = c(h + x)^{-\mu}$.

	c	h	μ	R^2
$\gamma = 3$	$1.264 \cdot 10^6$	10.42	3.110	0.992
$\gamma = 4$	1578	0.8501	1.405	0.999
$\gamma = 5$	798.4	0.3977	1.261	1
Normal distribution	286.7	0.09068	1.035	1

2.4 Discussion and concluding remarks

In this chapter, we have formulated a 1D model to simulate animal movement within a closed domain, where individual movement is modulated by density-dependence, so that an animal is more likely to advance towards areas with a higher population density. The aim of this study has been to determine whether the inclusion of density-dependent movement leads to heterogeneous pattern formation and how the parameters impact the

spatial distribution. We have considered the spatial dynamics of a population where animals perform either Brownian or non-Brownian motion. In our simulation model, the individual movement is described by a dispersal kernel (probability distribution of travelled distances) which is parameterized, respectively, by the normal distribution or by a power law.

Having performed intense computer simulations for movement parameters varying over a broad range, we have determined that density-dependent individual movement does indeed result in the formation of animals clusters (patches of high population density), e.g. see Figs. 2.3, 2.5 and 2.10. The number of emerging clusters is a random variable, so that the population's aggregation properties are described by a probability distribution for a different number of clusters to appear (see Tables 2.1–2.3), not by a single number. The probability distribution (and hence the typical number of clusters) depends on the movement parameters such as the perception radius, the strength of density-dependence (directional bias) and the characteristic size of the movement step.

In the case where the directional bias is sufficiently strong and the movement domain is large, the properties of the animals clusters differ significantly between the populations of Brownian walkers and non-Brownian walkers. Whilst in the population of Brownian walkers the number of clusters does not change with time after an initial formation period, in the equivalent population of non-Brownian walkers with $\gamma = 2$, the clusters are dynamic so that in the course of time the system experience fast transitions between the states with different number of clusters (see Figs. 2.10, 2.11 and 2.13). In the case of non-Brownian walkers with $\gamma > 3$, the emerging clusters are stable.

The population dynamics of non-Brownian walkers exhibits two different transient time scales. The shorter time scale t_{rel} is associated with the 'usual' relaxation of the initial conditions (see Fig. 2.12). However, the initial distribution converges to a quasi-steady state, not an asymptotic state. The other, much longer time scale $t_{LT} \gg t_{rel}$ is associated with the lifetime of the quasi-steady state. At time $t \sim t_{LT}$, the system

experiences a fast transition from the quasi-steady state to its asymptotic state (e.g. from the 4/5-dynamics to the 3/4-dynamics, see Fig. 2.11). The system's dynamics therefore exhibits long term transient behaviour (see [93]);

The frequency distribution of local population density values ('samples') shows essentially different properties for the population of non-Brownian walkers (with $\gamma = 2$) and that of Brownian walkers. With an increase in γ, the frequency distribution for non-Brownian walkers experiences a gradual transformation, so that for larger values of γ it becomes virtually undistinguishable from the one obtained for the population of Brownian walkers (see Fig. 2.24).

In order to compare between the population dynamics of Brownian walkers and that of non-Brownian walkers, we had to establish a certain condition of equivalence between the two different movement processes. We used a condition based on equating the survival probabilities; see Eqs. (2.3.2–2.3.4). A question may arise about the robustness of this criterion with regard to the spatial and temporal scales involved [11]. Also, the sensitivity of the results to the chosen value of the survival probability P_s is a matter of discussion ($P_s = 0.9$ in our simulations), i.e. how different the results could be for a different value of P_s. With regard to the latter, we notice that, the larger P_s is, the larger the part of the kernel is that is included into the calculation. For the kernels of different type, it means that the effect of their different shape is going to be greater for larger values of P_s. Therefore, an increase in P_s is likely to make the difference between the two movement processes even more significant. In the opposite situation when P_s is small, only the central part of the kernel is included, so that the difference between the Gaussian and the power law is insignificant, see Eqs. (2.3.9).

In this chapter, we restricted our investigation to a hypothetical 1D case, i.e. the system with one spatial dimension. We want to emphasize that the 1D case is not at all abstract (in particular, it does not imply that animals live on a line): in terms of a more realistic 2D movement, the 1D system could correspond to either a narrow stripe

or a transect across the movement area. Yet the question remains as to how different the system's dynamics may be if the movement is considered in a fully isotropic 2D case, i.e. without any constraints on the values of y-coordinate.

We also notice that in the case of Brownian walkers, assuming that the environment is isotropic, the 'full' 2D movement splits to a product of two 1D movements for x and for y, i.e. $\rho(\Delta\mathbf{r}) = \rho(\Delta x)\,\rho(\Delta y)$ where $\Delta\mathbf{r}$ is the movement step along the 2D path, $(\Delta\mathbf{r})^2 = (\Delta x)^2 + (\Delta y)^2$, and each of $\rho(\Delta x)$ and $\rho(\Delta y)$ is given by (2.2.2). Therefore, in the case of Brownian walkers an intuitive extension of our results onto the 2D case is straightforward; in particular, one can expect the emergence of animal clusters with the properties similar to those observed in our 1D simulations.

In the case of non-Brownian walkers, especially for $\gamma < 3$, extension of our results onto the 2D case is less straightforward. Although it seems intuitive that the main features of the population dynamics, such as the formation of clusters, should remain valid also in that case, it becomes difficult to make any prediction about the shape and spacing of the clusters. This requires further work and will be explored in Chapter 3 where we will also examine how the cluster dynamics may be different in 2D.

Chapter 3

A Two-Dimensional Model of Density-Dependent Individual Movement

3.1 Introduction

The work in this chapter is based on our results in [69]. The aim for this study is to investigate the mechanisms behind the small-scale, within-generation spatial patterns formed as a result of density-dependent movement. As we have discussed in the previous chapter, the process of pattern formation in a population can be modelled by simple interactions between individuals, resulting in the emergence of collective behaviour [235]. In this chapter we expand on the model discussed in Chapter 2 with a stochastic model for two-dimensional (2D) individual-based movement which includes a density-dependent directional bias. Our aim is to analyse the spatio-temporal population dynamics in the more realistic 2D domain and understand how the degree of spatial aggregation in the population is determined by the type of individual movement.

In the previous chapter, we have confirmed that 1D density-dependent movement leads to the formation of spatial clusters. However, the results obtained in the 1D model

cannot be directly extended to a more realistic 2D case without more sophisticated rules of individual movement. Several new important questions arise, the definition of a 2D spatial cluster being one of them. The importance of accurate quantification of ecological spatial patterns has been acknowledged by scientists for decades [86, 131, 103] and it is clear that an irrelevant definition of a spatial cluster may result in irrelevant conclusions about the spatio-temporal population dynamics. Hence we define carefully the concept of a spatial cluster when our model is developed. Our definition incorporates two basic principles of cluster identification - measuring the distance to the nearest neighbour [44] and measuring the number of neighbours within a spatial unit [137] - to help us to analyse quantitative properties of the spatio-temporal dynamics such as number of clusters, the cluster spatial size, and the population within a cluster. Based on our definition of a spatial cluster we compare the results of the 2D model with the previous 1D model to demonstrate that, while density-dependent movement in 2D domains is responsible for cluster formation, it results in much more complex spatio-temporal dynamics.

Another question we are concerned with is how the quantitative properties of the spatial distribution respond to a change in the parameters of directed movement. The investigation of this question is important as it allows one to conclude on whether the process responsible for spatial pattern formation can be at least to some degree identified and understood by pattern analysis on its own [110, 149, 178]. As with the 1D model, the two cases we study in this chapter are where animals perform Brownian motion (i.e. described by a Gaussian dispersal kernel) [115, 218] and non-Brownian motion (described by a power law dispersal kernel) [245]. We therefore analyse how the spatio-temporal dynamics of the population distribution depend on key parameters in our model, i.e. the probability of directed movement and the perception radius, for both Brownian and non-Brownian walkers as we did in Chapter 2. The temporal stability of population clusters is explored in more depth in 2D and we argue that the analysis of spatial distributions alone may not be sufficient to determine the movement type. While the spatial distributions of

Brownian walkers and non-Brownian walkers can be indistinguishable when considering quantification of spatial clusters, their spatio-temporal dynamics are still different.

The work is organised as follows. In Section 3.2, we outline the rules of the model and introduce density-dependent movement. The definition of a cluster in 2D will be explained and validated to provide a reliable framework for further analysis. We justify our choice of parameters of directed movement in Section 3.3 and present the results of simulations of Brownian walkers with that parameter set. We then proceed to discuss the results of simulations of non-Brownian walkers with an 'equivalent' parameter set to allow for further comparison between Brownian and non-Brownian movement. Proceeding from this we directly compare results from simulations of Brownian walkers and non-Brownian walkers in Section 3.4. Finally, we offer discussion of the results and our conclusions in Section 3.5.

3.2 Model description

To simulate density-dependent animal movement in a 2D domain we use the individual-based modelling approach [36, 88, 113, 235] and closely follow the methods developed previously in our 1D model discussed in Chapter 2. For simulation of density-dependent random movement the position of each individual is given at a discrete moment in time $t_k,\ k = 0, 1, ...,\ t_{k+1} = t_k + \Delta t$ where Δt is the time increment. As in Chapter 2, we consider $\Delta t = 1$ for all time steps; for simplicity we drop the k and refer to t as the series of integers that are discrete time steps.

For a population of N animals, the location of the n_{th} animal at time t is given by $(x_n(t), y_n(t))$. If this is known, the position at time $(t + 1)$ is simulated as

$$(x_n(t+1), y_n(t+1)) = (x_n(t) + \Delta x, y_n(t) + \Delta y), \tag{3.2.1}$$

where $\Delta x,\ \Delta y$ are the spatial increments that the animal moves in the x and y direction

respectively during the time increment $\Delta t = 1$. The movement of animal n starts from an initial position $(x_n(0), y_n(0)) = (x_{n,0}, y_{n,0})$.

As the step size will be the radial distance an animal moves to from its previous position, it is convenient to consider the movement in terms of polar coordinates, (r, θ) with the centre at $(x_n(t), y_n(t))$. To define the increments $\Delta x,\ \Delta y$, we consider the radial distance $\Delta r = \sqrt{(\Delta x)^2 + (\Delta y)^2}$ that an animal will move during one time step and the direction θ in which the step is made. Therefore the change in x and y of the position of an individual at any given time step is given by

$$\Delta x = (\Delta r)cos(\theta), \quad \Delta y = (\Delta r)sin(\theta). \tag{3.2.2}$$

Following [49, 113, 235], we consider Δr to be a random variable distributed according to a certain probability density function $\rho(\Delta r)$ which we refer to as the dispersal kernel. For simplicity, we assume all animals in a population have identical movement behaviour so ρ is the same for all animals.

Since we are studying the spatial patterns of the population arising from different rules of individual movement, in particular Brownian and non-Brownian motion, we consider the same two cases as in Chapter 2. In the first case, the dispersal kernel is a normal distribution with a mean of 0 and a variance σ^2:

$$\rho(\Delta r) = \rho_G(\Delta r|0, \sigma^2) = \frac{1}{\sqrt{2\pi\sigma^2}} \exp\left(-\frac{(\Delta r)^2}{2\sigma^2}\right). \tag{3.2.3}$$

We note here that, as the radial distance an animal moves must be non-negative, we use a half-normal distribution in our computer simulations, as we did in Section 2.2.1 (see Eqs. 2.2.6 and 2.2.7). However, we also refer to σ from Eq. (3.2.3) as we did in Chapter 2 to make comparisons between 1D and 2D. We will refer to animals performing movement described by Eq. (3.2.3) as Brownian walkers.

In the second case, the dispersal kernel is given by the power law:

$$\rho(\Delta r) = \rho_P(\Delta r|k,\gamma) = \frac{C}{(k+\Delta r)^\gamma}, \tag{3.2.4}$$

where $k > 0$ and $\gamma > 0$ are parameters of the distribution and $C = (\gamma - 1)k^{\gamma-1}$ is the normalising coefficient, i.e. $\int_{-\infty}^{\infty} \rho(\xi)d\xi = 1$. Animals performing movement described by Eq. (3.2.4) will be referred to as non-Brownian walkers further in the text.

The formulation of Δr follows the same framework as the calculation of the step size Δx in our 1D model in the previous chapter, however the direction of movement given by the variable θ in a 2D domain will be different. For a non-density-dependent random walk, θ would be considered to be a random variable distributed according to a uniform distribution in the region $[0, 2\pi]$. To include density-dependent movement in the model, the definition of θ will have to be adjusted, the mechanism for which is introduced in the next section.

We consider movement in a closed domain of size $L_x \times L_y$ so that, for any n, $0 < x_n(t) < L_x,\ 0 < y_n(t) < L_y$ for all t. For simplicity we will only consider a square domain so that $L_x = L_y = L$. The closed boundaries are modelled by introducing an additional rule. Let the value of Δx or Δy generated for the $(n+1)$th step be such that either $x_n(t+1) < 0$, $x_n(t+1) > L$, $y_n(t+1) < 0$ or $y_n(t+1) > L$. Then this step is aborted, hence effectively changing the animal's decision to leave, and a new Δr and θ are generated to make sure that the animal remains inside the domain, i.e. $0 < x_n(t+1),\ y_n(t+1) < L$.

For the initial condition, we consider a population distribution that is uniform over the 2D domain. This involves generating the initial coordinates of each individual in the x and y direction using the probability density functions $\rho_{x0}(x)$ and $\rho_{y0}(y)$ which are both independent on space; $\rho_{x0} = \rho_{y0} = 1/L = const.$

3.2.1 Density-dependent movement

So far we have described a simulation procedure of independent animal movement where the movement of an individual is not dependent on the location of their conspecifics. This procedure is similar to those used in many other studies of spatio-temporal population dynamics [181, 218, 235]. Having constructed this model, we can now make adjustments so that the direction of movement θ of an individual is dependent on the position of other animals in their vicinity, thereby introducing density-dependence.

To account for this, we follow the method used in Chapter 2 and reintroduce the 'perception radius' $R \geqslant 0$ [190, 211]. This is the distance in any direction within which an individual can detect the presence of other animals. Only those animals within the perception radius at time t can affect the movement of the individual. This is illustrated in Fig. 3.1(a), where the perception radius is shown as the dotted circle around the individual in red.

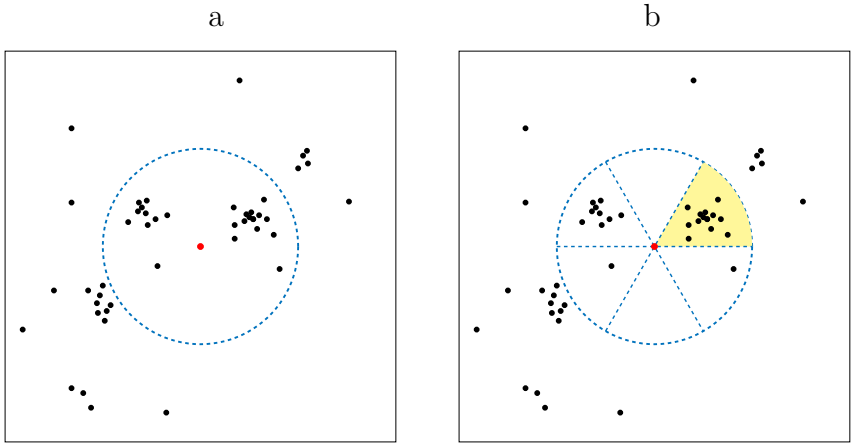

Figure 3.1: (a) An individual (shown in red) can detect the presence of other individuals within a circular domain defined by the perception radius, (b) the area within the perception radius split into segments with the most populated segment highlighted.

Once the perception radius R has been introduced, the next step is to identify regions with high population density within a circular domain defined by R. In our model, this is achieved by splitting a circle of radius R around an individual into S segments of equal

size. The number of neighbouring individuals in each segment is then counted to give the population within the segment and therefore to find the segment s^* with the largest population m_s. The mean angle θ_d of neighbours within only the segment s^* is then calculated as

$$\theta_d = \frac{\sum_{i=1}^{m_s} \theta_{n,i}}{m_s}, \tag{3.2.5}$$

where $\theta_{n,i}$ is the angle between animal n and animal i, (x_n, y_n) are the coordinates of the animal whose direction of movement we are calculating, and (x_i, y_i), $i = 1, ..., m_s$ are the coordinates of all neighbours within the segment s^*. Hence, θ_d is the angle of directed movement - the direction an animal will move if it 'decides' to move towards its conspecifics. An example is shown in Fig. 3.1(b) where the highlighted section is the one with the largest number of neighbours. The animal will move towards the centre of the neighbours in the highlighted segment. If more than one segment has the joint largest population then one of those segments is chosen with equal probability between them.

We now introduce a second parameter $P \in [0, 1]$ to quantify the strength of the directional bias. Let u be an auxiliary random variable which is uniformly distributed over the interval Ω,

$$\Omega = [P - 1, P]. \tag{3.2.6}$$

For undirected movement of a given individual, we introduce a variable θ_r, which has a uniform distribution over the region $[0, 2\pi]$. If the individual animal performs directed movement, we use the angle θ_d in (3.2.5). The direction of movement is then defined as follows:

$$\theta = \begin{cases} \theta_d, & \text{if } u \geqslant 0. \\ \theta_r, & \text{if } u < 0. \end{cases} \tag{3.2.7}$$

If $P = 1$ then the probability density function of u will be uniform in the region

$[0, 1]$ and therefore $\theta = \theta_d$, meaning an animal will always move towards an area of high density. Conversely, if $P = 0$ then the probability density function of u will be uniform in the region $[-1, 0]$ and therefore $\theta = \theta_r$, meaning an animal will move with a random walk independent of its conspecifics. In our study we consider $0 < P < 1$ so that there is always a degree of randomness in the direction of movement, i.e. an animal will sometimes 'ignore' its conspecifics and move in a completely random direction. Thus we refer to the parameter P as the probability of directed movement.

The number of segments

The number of segments S is a convenient parameter in our model as it allows us to avoid ambiguous cases when the direction of individual movement has to be determined. If the number of segments is exceedingly large, population clusters within the perception radius will be likely to be split up between several segments resulting in an incorrect conclusion about the mean angle as the variable m_s depends on S in (3.2.5). In addition, increasing the number of segments is more computationally expensive as the population has to be calculated for each segment within each animal's perception radius. On the other hand, if the number of segments is very small, we may have cases where two dense regions are positioned within the same segment (see Fig 3.2(a)) and the direction the individual will move will be between the dense regions rather than towards either of them.

The minimum number of segments S_{min} required to control the directed movement in our model can be defined under the requirement that, when clusters form, they will have a distance between each other greater than the perception radius R (otherwise those areas are likely to be drawn together and coalesce). For two areas of high density to be in the same perception radius of an individual while not within the perception radius of each other, the minimum angle α_{min} between them from the location of the individual must be $\alpha_{min} = \pi/3$ radians; see Fig 3.2(b). Hence, the minimum number of segments to guarantee that two clusters do not belong to the same segment is $S_{min} = 2\pi/\alpha_{min} = 6$

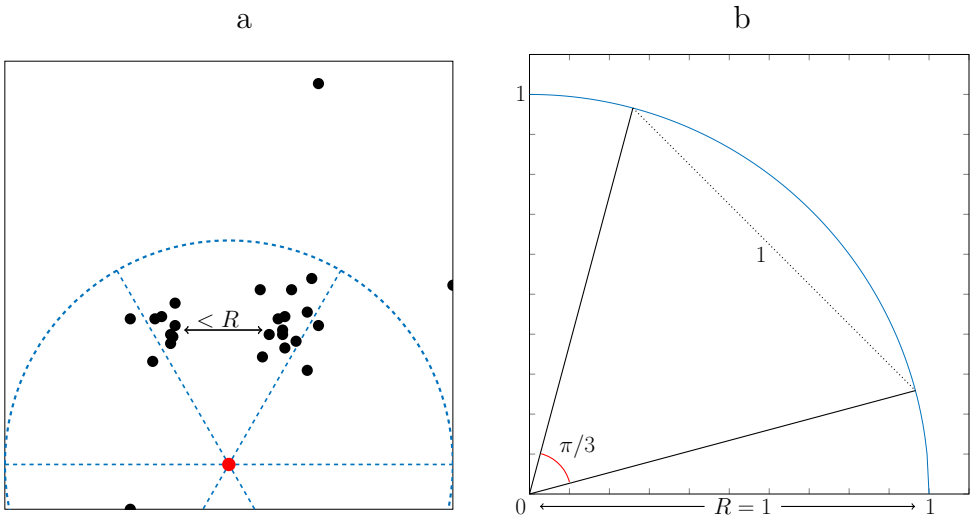

Figure 3.2: (a) The case where two clusters are contained within a single segment, (b) an illustration of a segment where that the largest distance between any two points within the segment is equal to R. The equilateral triangle shown for $R = 1$ has all angles equal to $\pi/3$.

and we use the value of $S = 6$ in our simulations (see [165] where the authors use the same number of six 'neighbouring cells' around each animal in their simulation framework).

Let us emphasize that the number of segments is an auxiliary parameter introduced to help us to avoid any ambiguity in the choice of the direction of movement as discussed above. While any choice of $S \neq 0$ makes cluster formation more pronounced, S is not critical for clusters to form. This is demonstrated in Section 3.4 and is visible in Figs. 3.24 and 3.25, showing distributions that emerge without the use of segments.

3.2.2 Cluster definition

The overall aim of our study is to analyse the dynamics of population clusters as a function of the movement parameters. Clusters can be loosely thought of as spatial sub-domains with higher population density than in surrounding sub-domains. Hence we have to approximate the population density from information we have about each individual in the domain before we develop a more formal definition of a cluster. For comparison with our results in the 1D model, it is appropriate to employ the method of 'bins' used previously (see the end of Section 2.2.1). However, it is worth considering other options

that could also be used in the 2D domain.

Data mining approaches such as hierarchical clustering [112, 152], k-nearest neighbour method [25] and algorithms such as DBSCAN [72] and OPTICS [10] have been used to group data points into clusters based on the distances between them. A similar method is to use a Voronoi diagram as in [229] where the density is inversely proportional to the size of the Voronoi cell (the area in which every point in that cell is closer to a single particle than any of its neighbours [14]). Kernel density estimation is another useful tool [39, 173, 205, 251] which has been used previously for finding clustering of different types of cells [155] and also in assessments of traffic accidents [9, 259] but a similar approach could be applied to the coordinates of a population. These methods and others that we do not consider may give slightly different results when defining a cluster. However, they do not remove the need for a density threshold to locate clusters, which must be chosen somewhat arbitrarily. The method of partitioning the domain into bins allows comparisons to be made between distributions and also benefits from being similar to the methods used for analysing a population distribution from trap count data, as will be seen in Chapter 6.

We therefore adapt the definition of a cluster from Section 2.2.1 for use in 2D. We partition the domain into a uniform square grid of BxB spatial sub-domains (bins) so that the length of a bin is L/B where L is the length of the domain. The number of animals inside a given bin divided by the area of the bin will then approximate the population density within the bin.

We say that a group of bins form a cluster if the following conditions hold:

- For a given parameter b_u, where $0 < b_u < 1$, there is a bin that contains a proportion of the total population that is larger than b_u.

- Any bin adjacent to a bin that forms part of a cluster also belongs to the cluster if it is greater than or equal to a second parameter b_l, where $0 < b_l < b_u$.

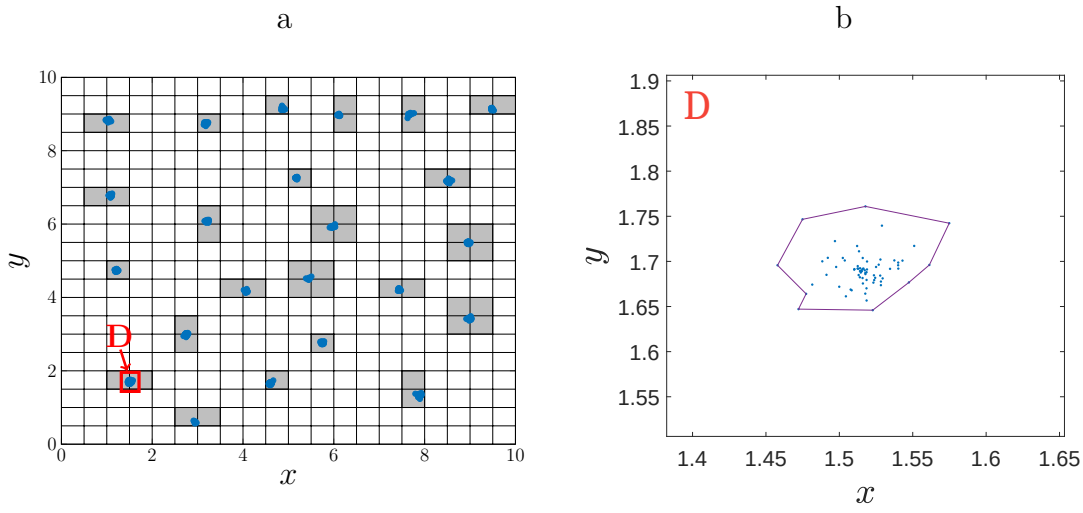

Figure 3.3: (a) The domain split into 20×20 bins with cluster-forming bins shaded and (b) An example of the boundary of a single cluster in region D.

One example of cluster identification above is shown in Fig. 3.3(a) where bins that form a cluster are shown as shaded areas in the domain. The number of clusters in the domain along with the cluster area (size) and population size within the cluster are useful properties for comparing cluster formation with different parameter sets in the model. These properties were calculated in the 1D model [68] so comparison between the two models can also be made. The population of each cluster is calculated based on the sum of bin populations for bins that contain a cluster but the spatial size of a cluster requires an extra step. As shown in Fig. 3.3(b), after a cluster is identified from bin populations, the 'boundary' function in MATLAB [145] is employed to ascertain the exact size of a 2D cluster by finding the convex hull of all individuals within those bins [65].

The number of bins

We note that the number of bins B is an arbitrary parameter in the definition of a cluster. The bin size has to be chosen so that it is sufficiently small to allow for low density bins to be found between clusters, i.e. clusters do not 'merge' together. It has also to be sufficiently large so that individuals that fluctuate to small distances away are still included as part of the clusters. We therefore study how the number of clusters in

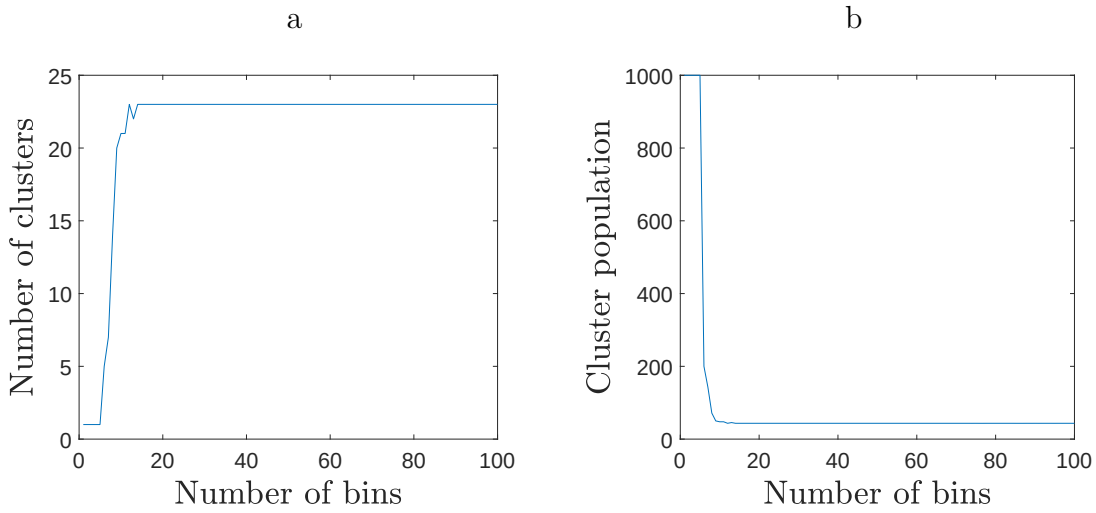

Figure 3.4: Sensitivity of the definition of cluster to the choice of the number of bins. The spatial distribution of the population of of Brownian walkers (3.2.3) is analysed at time $t = 1000$. The simulation parameters are $L = 10$, $N = 1000$, $P = 0.6$, $\sigma = 0.02$, and $R = 1$. The threshold number of bins is $B^* = 20$: the number of clusters and the mean cluster population do not change when a grid of $B^* \times B^*$ bins is further refined. (a) The number of clusters and (b) the mean cluster population when changing the number of bins (squared) when identifying clusters.

the domain is effected by our choice of the number of bins. Namely, we consider how the number of clusters will change if we use a different number of bins to identify clusters in the same spatial distribution. One example of the number of clusters along with the mean cluster population when changing the number of bins is shown in Fig. 3.4. It can be seen from the figure that the number of clusters and the cluster population become insensitive to the choice of the number of bins B when $B \geqslant B^*$, where $B^* = 20$ in this example. Furthermore, the results of our computational study reveal that, although a different choice of parameters in the problem will result in slightly different properties of the cluster, the threshold number of bins B^* remains the same and the number of clusters does not change if a $B^* \times B^*$ grid of bins is further refined. The cluster properties shown in Fig. 3.5, which analyses the clusters from a typical non-Brownian distribution, converge in a similar way but with some slight fluctuations to the number of clusters.

Table 3.1 shows the cluster properties calculated using varying bin sizes. When the number of bins is 20^2 or higher, we have a constant number of clusters but the mean

Table 3.1: The mean and standard deviation of properties of clusters that are formed by Brownian walkers with movement parameters $P = 0.6$, $R = 1$ and $\sigma = 0.02$, calculated using a different number of bins. The values in the table are taken over 10 simulations.

	10^2	20^2	30^2	50^2	100^2
N_c	21.8	24.9	24.9	24.9	24.9
	(1.87)	(2.13)	(2.13)	(2.13)	(2.13)
$A_c \times 10^{-2}$	5.82	1.42	1.33	1.20	0.922
	(4.31)	(0.0991)	(0.0726)	(0.0704)	(0.0689)
n_f	33.2	52.6	108	216	470
	(14.5)	(16.5)	(30.4)	(37.7)	(80.7)

cluster area decreases and the number of free individuals increases as the number of bins increases. When there is a large number of bins, it is more likely that individuals on the edge of a cluster will not be included into a cluster because they occupy a bin that is slightly below the threshold.

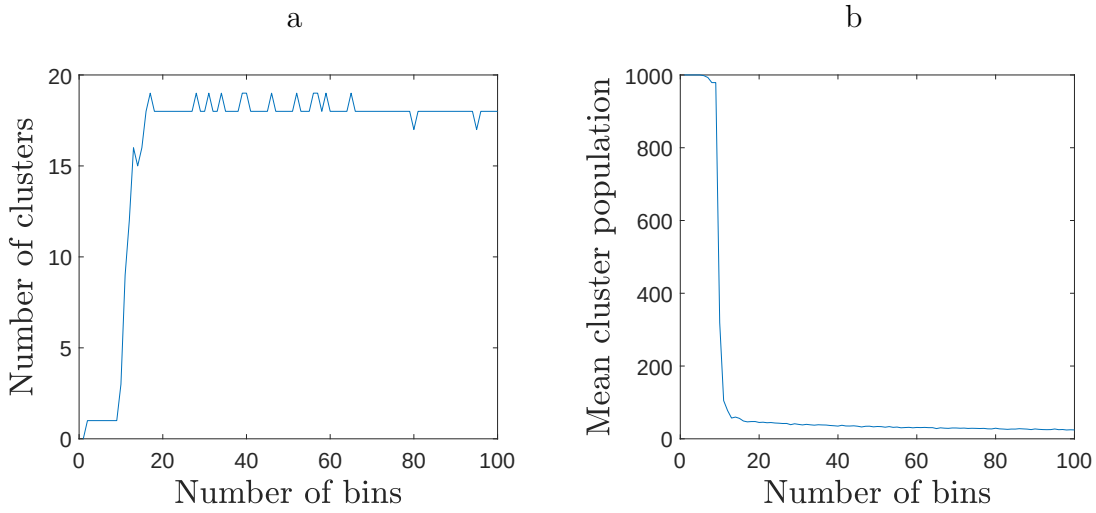

Figure 3.5: Sensitivity of the definition of cluster to the choice of the number of bins. The spatial distribution of the population of non-Brownian walkers (3.2.4) is analysed at time $t = 1000$. The simulation parameters are $L = 10$, $N = 1000$, $P = 0.6$, $\sigma = 0.02$, and $R = 1$. The threshold number of bins is $B^* = 20$: the number of clusters and the mean cluster population do not change when a grid of $B^* \times B^*$ bins is further refined. (a) The number of clusters and (b) the mean cluster population when changing the number of bins (squared) when identifying clusters.

In deciding an appropriate bin size, it may be useful to analyse the distances between individuals in the field. The nearest neighbour method is a commonly used method in

spatial analysis in ecology [81] and otherwise [25] where the mean and variance of the distances between a point and its nearest individual are calculated. We can do a similar analysis and find the distance between every possible pair of individuals to show the spatial scales between and within clusters. We calculate the distances for the distributions of a

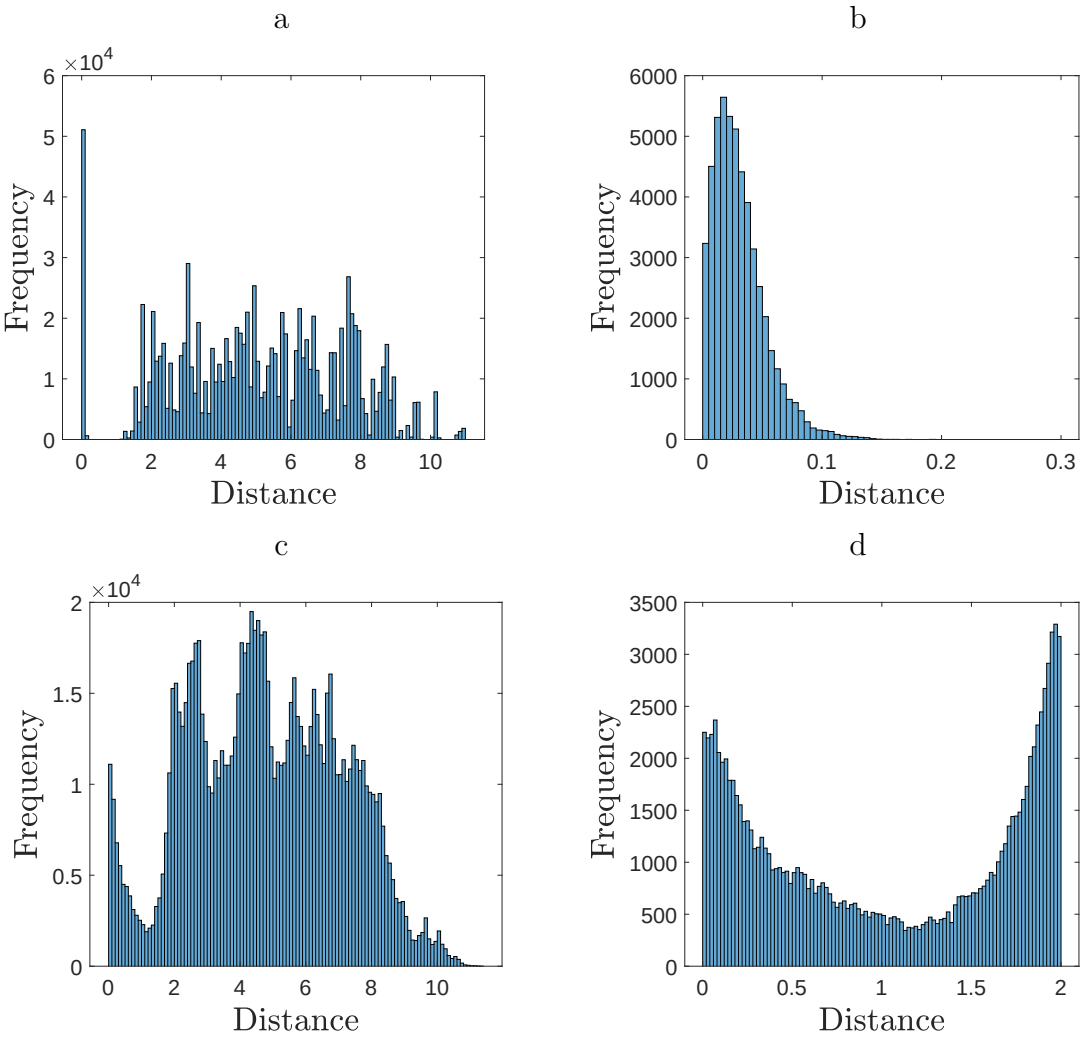

Figure 3.6: Frequency of distances measured between individual animals in two spatial distributions that have formed from Brownian and non-Brownian walkers respectively. The distance from every individual to all other animals is calculated at $t = 1000$, giving 1000^2 data points in each case. (a)-(b) Brownian walkers; see the distribution in Fig. 3.7(a) shows all distances, (b) shows the distances close to 0, i.e. for individuals within a cluster. (c)-(d) non-Brownian walkers; see the distribution in Fig. 3.8 (c) shows all distances, (d) shows the distances between 0 and 2, i.e. the area where pairs can be within a cluster, in neighbouring clusters or with individuals outside clusters.

typical simulation of Brownian and non-Brownian walkers. Fig. 3.6 shows the frequency with which different distances occur. Fig. 3.6(a) shows a large amount of pairs have a distance close to 0 in the population of Brownian walkers, suggesting that those pairs are in the same cluster. Very few have a distance of length close to 1 and the distance between pairs that are not in a cluster ranges from roughly 1.5 to 11.

Fig. 3.6(b) shows the spike close to 0 in more detail. The distribution peaks at around 0.02 before decreasing to a level where there are only 10 distances measured between 0.15 and 0.2 and none at all between 0.2 and 1.1. This tells us that the diameter of the clusters are all less than 0.2 and also shows that clusters cannot be within a distance of 1 from each other, due to the perception radius R. The scales of distances within and between clusters can also explain the regions of stability in Fig. 3.4. We can see that the number of clusters and mean cluster population and area have a large shift between 5 and 15 bins, when the bin size is between 2 and 0.6, which is the region where the minimum distance between clusters occurs.

The results are not so clear for the distribution of non-Brownian walkers as shown in Fig. 3.6(c)-(d). Because of the amount of individuals in between clusters, we do not have a range where no distances between individuals occur. Fig. 3.6(d) shows the minimum point in the distribution of distances is roughly 1.2 but, depending on our bin size, most of the distances in the region of 0.5 and 1.5 will be made up of distances where at least one of the individuals is free.

A grid of bins that would be sensible for both distributions would have to have bin sizes that are in the region $[0.1, 0.5]$ for the Brownian distribution. This is the region $[0.2, 1]$ halved as two neighbouring bins can make up part of the same cluster and so the distance over two bins should be restricted to this region. The non-Brownian case may require a slightly more restrictive region $[0.2, 0.5]$ but the results do not tell us as much as the Brownian distribution case.

Overall, from studying two example distributions of Brownian and non-Brownian walk-

ers, we have enough information to justify a choice of the number of bins in the grid. In the Brownian case the properties of clusters are less sensitive to the change of bins than in the non-Brownian case but in both there is a region starting at slightly fewer than a grid of 20x20 bins, where there are not significant changes. Taking all the above information into account, we believe a 20x20 grid of bins is sufficient for analysing the properties of clusters.

Once the number of bins B has been defined, we choose the cluster thresholds based on the requirement that, for a cluster to be counted, there must be a bin with at least double the average bin population density and the cluster ends when a bin is reached which is below the average density. This allows most areas of high population density to be identified without noise significantly affecting the results. Since the average bin population density can be estimated as N/B^2 on a grid of $B \times B$ bins, we define $b_u = 2N/B^2$ and $b_l = N/B^2$.

3.3 Simulation results

In this section we study the properties of the spatial distribution of a population where the individuals perform the density-dependent random movement described in Section 3.2. We particularly want to examine how the properties of the spatial distribution change subject to the type of random movement as defined by the dispersal kernel (3.2.3) or (3.2.4), and the choice of the controlling parameters for density-dependent movement, i.e. the perception radius R, and the probability of directed movement P.

For the rest of this chapter, we consider a square domain with length $L = 10$ and the total population size $N = 10,000$. We use a 20×20 grid of bins in all simulations with cluster thresholds $b_u = 0.005$ (i.e 0.5% of the total population N) and $b_l = 0.0025$ (i.e 0.25% of N). We also note that the variance σ^2 in the dispersal kernel (3.2.3) we use in our simulations has to be small compared to L so that the boundary conditions do not dominate the dynamics. Similarly the perception radius R must be smaller than

L but bigger than the typical step size to allow for several clusters to form. If R is too large in comparison to L then each animal will be influenced by the majority of the rest of the population and all animals will congregate in a single cluster in the centre of the domain, as shown in 1D in Fig 2.1. Alternatively, if R is too small in comparison to the typical step size, each animal will only be influenced by few others and in the subsequent time step is likely to have moved to an area where entirely different conspecifics are now influencing their movement, never allowing clusters to form.

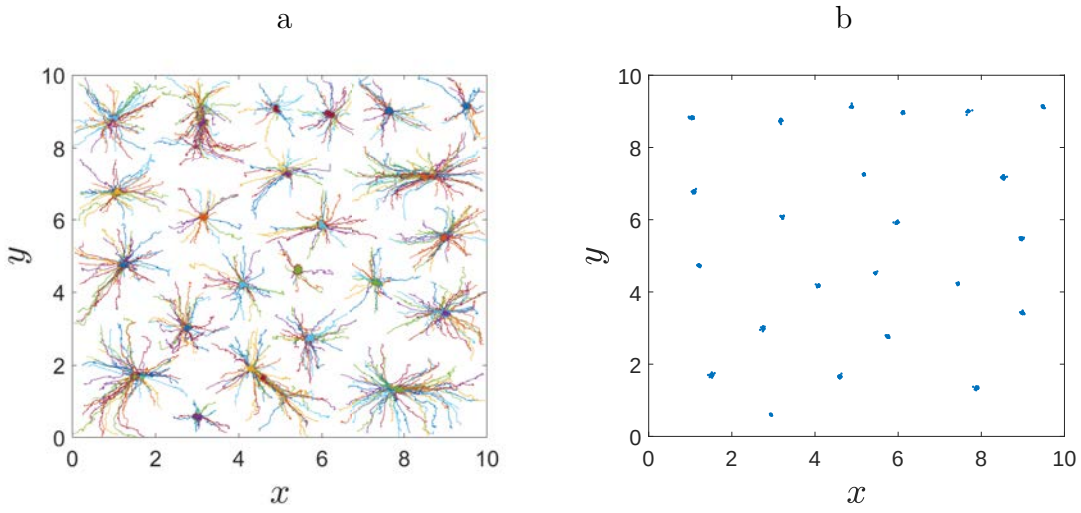

Figure 3.7: Examples of the (a) individual animal paths over 1000 time steps and (b) final distribution of animals after 1000 time steps of a simulation of a population of Brownian walkers.

Typical simulation results are shown in Fig. 3.7 for Brownian walkers and Fig. 3.8 for non-Brownian walkers. The density-dependent movement parameters used are $P = 0.6$, $R = 1$. For Brownian walkers we use the normal distribution kernel (Eq. (3.2.3)) with $\sigma = 0.02$, and for the non-Brownian walkers we use the power law distribution kernel (Eq. (3.2.4)) with $\gamma = 2,\ k = 0.0036$. In both cases density-dependent individual movement has resulted in the formation of a number of clusters. In the case of Brownian walkers, all individuals converge to points in the domain as can be seen in Fig. 3.7(a) where individual animal paths are shown. The formation of distinct clusters as time progresses is shown in Fig. 3.7(b). In the case of non-Brownian walkers, it is possible to see some

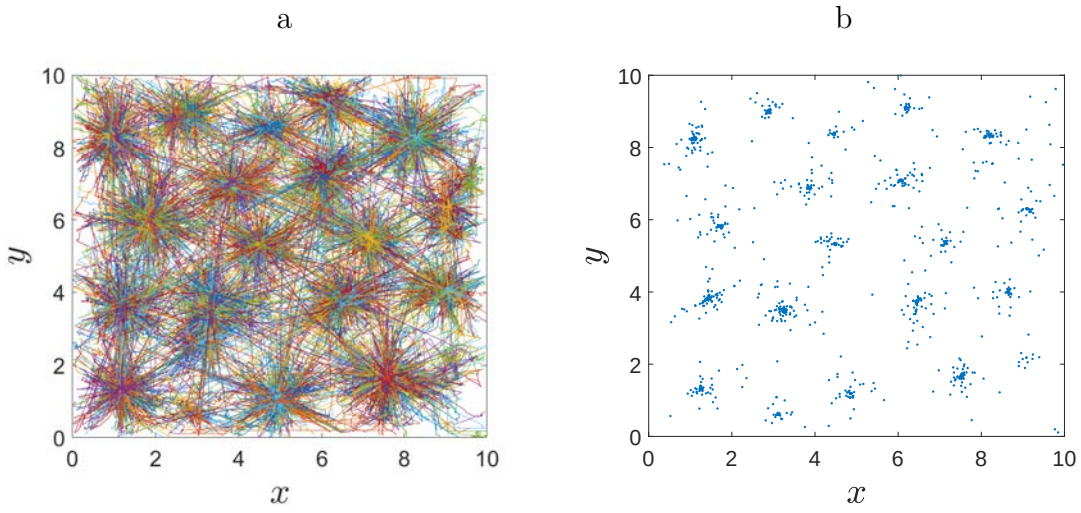

Figure 3.8: Examples of the (a) individual animal paths over 1000 time steps and (b) final distribution of animals after 1000 time steps in a simulation of a population of non-Brownian walkers.

of the large step sizes in Fig. 3.8(a) which are characteristic of the power law dispersal kernel. Therefore clusters are not so visually distinct as in the Brownian walkers case but there are still several clusters that emerge as shown in Fig. 3.8(b). Therefore we can now examine how the type of motion and the parameter values change the number of clusters formed in the domain and their properties.

3.3.1 Brownian walkers

We want to investigate the properties of the spatial distributions and compare our results with the 1D model and we begin with the case of Brownian motion. It has been discussed in Section 2.4 that in the case of Brownian walkers one can expect the emergence of 2D animal clusters with properties similar to those observed in 1D simulations. We therefore choose the 'baseline' movement parameters as $\sigma = 0.02$, $P = 0.6$ and $R = 1$ to make our 2D simulation consistent with the 1D model.

One example of the development of the spatial distribution over time is shown in Fig. 3.9. The formation of clusters is already seen at time $t = 100$, with no apparent difference between the distributions at times $t = 1000$ and $t = 10,000$. This suggests that

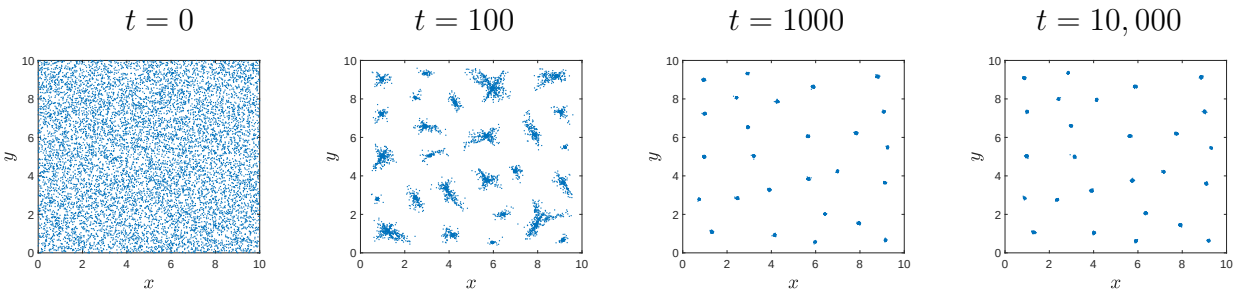

Figure 3.9: The spatio-temporal dynamics emerging from a random-uniform initial distribution of a population of Brownian walkers at time $t = 0$. Movement parameters are $P = 0.6$, $R = 1$ and $\sigma = 0.02$. (a) $t = 0$, the initial distribution of the population; (b) $t = 100$, the formation of clusters already begin at small times; (c) $t = 1000$ and (d) $t = 10,000$, clusters are 'temporally stable', as there is no visible change in the number of clusters and their shape over time.

the system evolves to a steady spatial distribution as in the 1D model. To investigate this further, we calculate the number of clusters and their population and spatial size using the definition of a cluster in Section 3.2.2. To determine the population and spatial size of the clusters we calculate the mean number of individuals in each cluster and also the mean area that each cluster covers for all clusters identified in the system at a particular time step. The evolution of those properties over time is shown in Fig. 3.10 up to $t = 1000$. Although the system never reaches a steady state in a strict sense due to fluctuations in the population and area of clusters, it is readily seen that the properties converge and do so in a timescale $t \approx 200$. Extending the simulation time up to $t = 20,000$ shows that the quasi-steady state holds as no further changes are seen.

Stable formation of clusters is further confirmed by results in Fig. 3.11 where spatio-temporal dynamics are examined for a lower probability, $P = 0.2$, of directed movement. In this case, we expect the initial timescale of cluster formation to be longer when P is small, and this can be seen in Fig. 3.11, showing cluster properties over a time period of $t = 20,000$. The convergence of cluster properties now happens at approximately $t = 600$ and there are larger fluctuations in the mean cluster population. This is because individuals will be more likely to move in and out of clusters than for higher values of P.

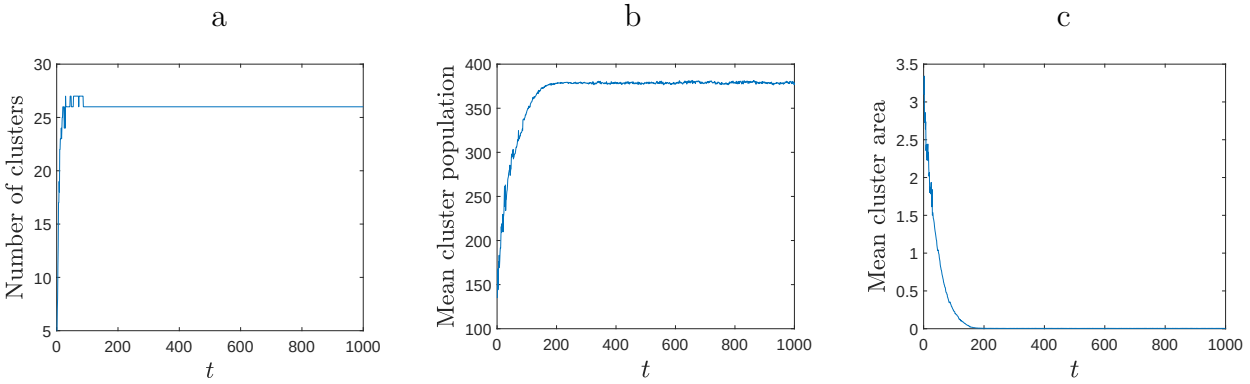

Figure 3.10: An example of the development of clusters over time when the probability of directed movement is $P = 0.6$. The other parameters are $R = 1$ and $\sigma = 0.02$. The quantitative properties of the spatio-temporal dynamics are (a) the number of clusters, (b) the mean cluster population, and (c) the mean cluster area. The mean values of the cluster properties have been calculated from all the clusters that emerge in one simulation. The quantitative properties converge in a timescale $t \approx 200$.

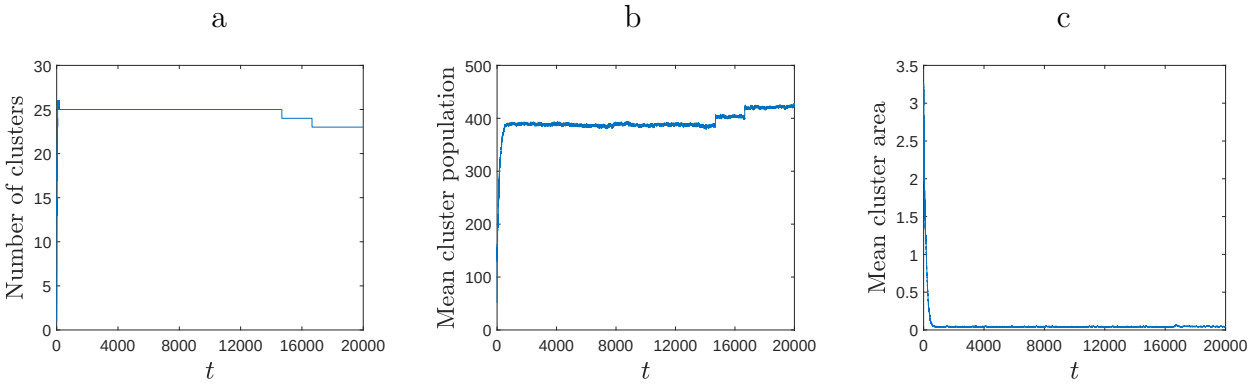

Figure 3.11: An example of the development of clusters over time when the probability of directed movement is $P = 0.2$. The other parameters and the figure legend are the same as in Fig. 3.10. The quantitative properties converge in a timescale $t \approx 600$.

Table 3.2: The mean and standard deviation of properties of clusters that form with different values of probability of directed movement P at $t = 10,000$, $R = 1.0$, $\sigma = 0.02$; N_c is the mean number of clusters, A_c is the mean cluster area, n_f is the mean number of free individuals. The standard deviation for every mean value is shown in brackets below the mean. The values in the table are taken over 10 simulations.

	$P = 0.1$	$P = 0.2$	$P = 0.3$	$P = 0.4$	$P = 0.5$	$P = 0.6$	$P = 0.7$	$P = 0.8$	$P = 0.9$
N_c	23.4	24.2	25.0	24.9	25.1	24.9	24.8	24.9	24.9
	(2.011)	(2.486)	(2.108)	(2.378)	(2.283)	(2.132)	(2.251)	(2.601)	(2.514)
$A_c \times 10^{-2}$	28.31	10.41	4.97	3.07	2.15	1.42	1.09	0.79	0.55
	(1.556)	(0.4148)	(0.2604)	(0.1695)	(0.07051)	(0.09906)	(0.04305)	(0.03562)	(0.03313)
n_f	499.4	222.2	138.1	111.2	80.3	52.6	52.4	58.3	40.1
	(68.96)	(42.50)	(51.99)	(45.41)	(26.29)	(26.55)	(26.82)	(23.17)	(26.51)

Table 3.3: The mean and standard deviation of properties of clusters that form with different values of the perception radius R at $t = 10,000$, $P = 0.6$, $\sigma = 0.02$. The legend is the same as in Table 3.2. The values in the table are taken over 10 simulations.

	$R = 1$	$R = 2$	$R = 2.523$	$R = 3$	$R = 4$	$R = 5$	$R = 100$
N_c	24.9	6.4	4.2	3.2	1	1	1
	(2.132)	(0.8433)	(0.6325)	(0.4216)	(0)	(0)	(0)
$A_c \times 10^{-2}$	1.42	2.30	2.80	2.82	3.26	4.10	3.24
	(0.09906)	(0.08758)	(0.1704)	(0.1499)	(0.4446)	(0.4149)	(0.5782)
n_f	52.6	24.9	12.9	15.2	1.8	1.9	6.9
	(26.55)	(20.99)	(9.927)	(13.92)	(5.007)	(4.434)	(8.293)

Tables 3.2 and 3.3 show how the number of clusters, the mean cluster area and the number of free individuals, i.e. animals that are not within a cluster, depend on the parameters of directed movement. For each parameter set, 10 simulations are made up to $t = 10,000$. We then record the number of clusters, the number of free individuals and the mean cluster area of all clusters in each simulation and take the mean of these numbers from all 10 simulations, giving the data in the tables.

As we vary the probability of directed movement, P, there are fewer individuals that will move further away from the centre of a cluster as P increases because at each time step they have a high probability of moving directly towards the centre. Therefore we expect that the animals will be clustered very densely and all animals will be contained within a cluster when P is large. This conclusion is confirmed by the results in Table 3.2. It is readily seen from the table that there is no significant trend in the number of clusters as P increases, but the cluster area and the number of free individuals decreases.

Table 3.3 shows the change in cluster properties when we vary the perception radius R. The significant trend when R is increased is that the number of clusters decreases with only individual clusters appearing when $R \geqslant 4$. This is because for large R each cluster will attract animals over a larger area. Since no two clusters can be within the perception radius of each other without coalescing, there will be space in the domain only for fewer clusters. We note that the value $R = 2.523$ in the table presents the case when the area within the perception radius covers 20% of the domain, i.e. the same proportion of the domain as when $R = 1$ in the 1D domain with $L = 10$. The mean number of clusters is $N_c = 4.2$ for $R = 2.523$ and is similar to the mean number of clusters in the 1D model with $R = 1$ which is $N_c = 4.56$ (calculated from the results shown in Table 2.1). We also note that clusters (as we have defined them) are difficult to accurately identify until R is one order of magnitude greater than σ (see Fig. 3.12) and we therefore apply the requirement $R \gg \sigma$ when we proceed in our study so we can be confident that the cluster properties are correct.

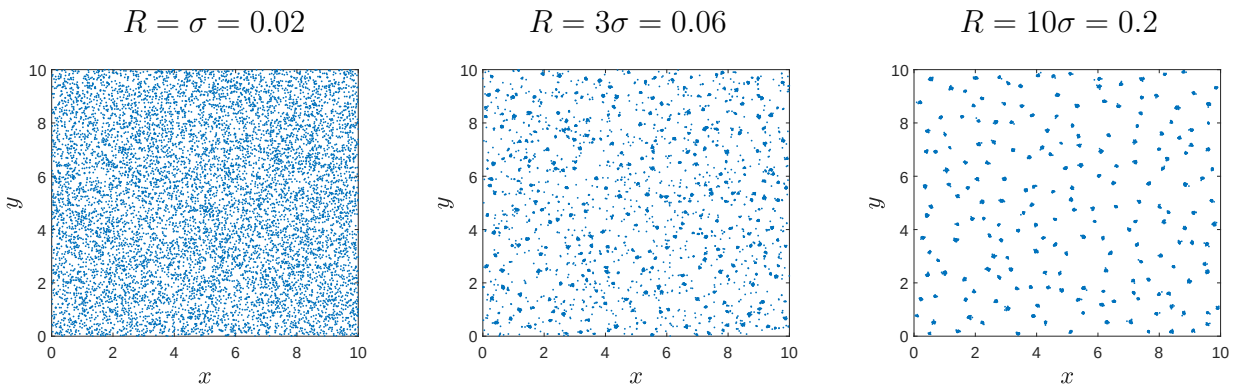

Figure 3.12: Example distributions of a population of 10,000 Brownian walkers at $t = 10,000$ with small R. Other movement parameters are $P = 0.6$ and $\sigma = 0.02$.

Table 3.4: The mean and standard deviation of properties of clusters that are formed by Brownian walkers with different values of σ. The legend is the same as in Table 3.2. The cluster properties are analysed at time $t = 10,000$, other movement parameters are $P = 0.6$ and $R = 1$.

	$\sigma = 0.01$	$\sigma = 0.02$	$\sigma = 0.04$	$\sigma = 0.08$	$\sigma = 0.2$
N_c	25.8	24.9	24	19.1	11.5
	(1.81)	(2.13)	(1.16)	(1.46)	(0.850)
$A_c \times 10^{-2}$	0.355	1.42	5.18	19.2	78.2
	(0.0158)	(0.0991)	(0.227)	(0.914)	(5.66)
n_f	31.4	52.6	129	257	623
	(20.0)	(26.6)	(36.6)	(53.6)	(80.9)

Now that we understand how the density-dependent movement parameters P and R influence cluster formation we also want to check how the cluster properties are related to the basic characteristics of random movement, i.e. how they depend on the mean step size of Brownian walkers. Since we cannot directly control the mean step size in our computer simulations, we use the relationship from Eq. (2.2.7) and vary the parameter σ in simulations instead. The results are shown in Table 3.4 where it is readily seen from the table that the choice of σ effects the number of clusters, the mean cluster area and the number of free individuals. As σ increases (and the mean step size μ_f increases too), animals are more likely to take larger steps away from a cluster, leading to clusters with a larger area and in turn this means fewer clusters can exist in the domain as clusters must be a certain distance away from each other. Taking a larger mean step size also means

that animals are more likely to move entirely away from a cluster, leading to a higher number of free individuals. The change in properties is also visible in the example spatial distributions shown in Fig. 3.13.

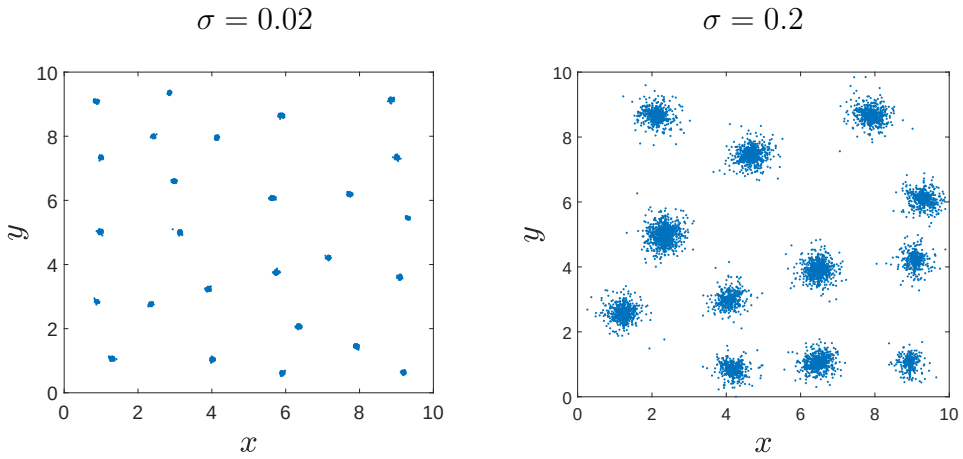

Figure 3.13: Example distributions of a population of 10,000 Brownian walkers at $t = 10,000$ when $\sigma = 0.02$ and $\sigma = 0.2$. Other movement parameters are $P = 0.6$ and $R = 1$.

Finally, we briefly investigate how cluster properties are affected if we change our definition of the perception radius R. Let us introduce a 'decaying' perception range in the model when animals located closer to the individual are seen with a greater probability. The decaying perception radius can be modelled for each individual as follows. The distance d to all other animals is calculated and, for each other animal, the distance d is then compared to a random number r generated from a uniform distribution in the region $[R_0, R_1]$, where the radius $R_0 > 0$ and $R_1 > R_0$. If $r - d \geqslant 0$ then the animal is seen with probability 1 and influences the direction of movement. If $r - d < 0$, then the animal is not seen and has no influence on the direction of movement. Since $R_0 < r < R_1$, any distance $d \leqslant R_0$ will guarantee $r - d \geqslant 0$ and therefore the animal will definitely be seen and a distance $d > R_1$ will guarantee $r - d < 0$ and the animal will not be seen. Thus all animals within the radius of R_0 are seen, while only a fraction of the population located within the ring $R_0 < d < R_1$ is seen and no animals at the distance $d > R_1$ are seen.

The results obtained when we vary parameters R_0 and R_1 are presented in Table 3.5

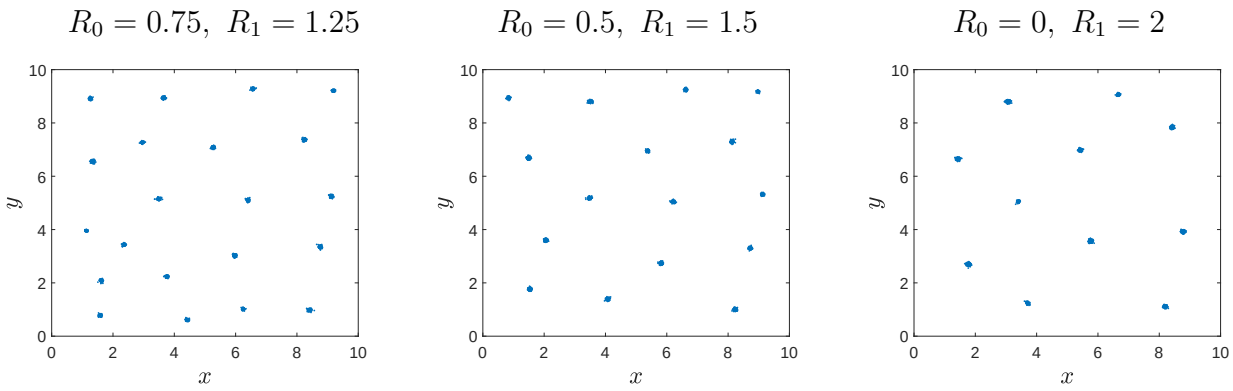

Figure 3.14: Example distributions of a population of 10,000 Brownian walkers at $t = 10,000$ with a decaying perception radius. Other movement parameters are $P = 0.6$ and $\sigma = 0.02$.

(see also Fig. 3.14). From the results shown in the table, we conclude that introduction of the decaying perception range preserves cluster formation as clusters still form even when $R_0 = 0$. Meanwhile, the number of clusters decreases, as the size of the ring $R_0 < d < R_1$ is increased. This is similar to what happens when we use our previous definition of the perception radius and increase R (see Table 3.3). This is probably because, even though the probability of being 'seen' is small close to R_1, for a large population over a large number of time steps it will happen frequently enough for two clusters within the distance R_1 of each other to coalesce. Thus, our previous conclusion about the influence of the perception radius is confirmed as the average perception radius $(R_0 + R_1)/2$ can still be considered as a parameter of the density-dependent movement responsible for the

Table 3.5: The mean and standard deviation of properties of clusters that are formed by Brownian walkers with a decaying perception radius with different values of R_0 and R_1 at $t = 10,000$, other movement parameters are $P = 0.6$ and $R = 1$. The legend is the same as in Table 3.2. The values in the table are taken over 10 simulations.

	$R = 1$	$R_0 = 0.75,\ R_1 = 1.25$	$R_0 = 0.5,\ R_1 = 1.5$	$R_0 = 0,\ R_1 = 2$
N_c	24.9	21.7	17.6	10.1
	(2.13)	(1.06)	(1.51)	(0.876)
$A_c \times 10^{-2}$	1.42	1.42	1.58	1.95
	(0.0991)	(0.0909)	(0.0927)	(0.133)
n_f	52.6	81.8	49	40.6
	(26.6)	(58.4)	(19.9)	(25.0)

number of clusters.

We conclude from the results in this section that the choice of the density-dependent movement parameters P and R influence the size and number of clusters respectively. The simulation results show a strong relationship between the number of clusters and the perception radius R. On the other hand, there is no significant relationship between the number of clusters and the probability of directed movement, P. Varying P in the model results in a change of the cluster density while clusters with few or no free individuals are formed when P is sufficiently high. A similar effect can be observed when we decrease the mean step size through varying σ. Meanwhile, we want to emphasize the importance of the parameter P in our model. When $P = 0$, animals move independently of their conspecifics and introduction of the perception radius alone will not result in cluster formation (see also the discussion in Section 3.4).

Also, given the dependence of cluster properties from the parameters of 2D density-dependent movement, we can confirm the assumption made in Section 2.4 that the formation of clusters in a 2D domain shares similar properties to the 1D model when Brownian walkers are considered. In particular, we see the same stable formation of clusters as shown in Figs. 3.10 and 3.11 and a similar number of clusters are formed when we use a 2D counterpart of the perception radius in the 1D model. Thus, a 1D model of density-dependent movement can be considered as a proxy for a study of 2D Brownian walkers to allow for significant computational savings and we can use conclusions made in Chapter 2 about the balance between parameters of random movement (i.e. the mean step size) and directed movement (i.e. the probability P and the perception radius R).

3.3.2 Non-Brownian walkers

In this section we consider non-Brownian motion simulated by a power law distribution (3.2.4). In order to make a sensible comparison between the results obtained for the dispersal kernel given by the normal distribution and those obtained for the power law we

use the same condition of equivalence established at the start of Section 2.3.2. This gives us k from the power law distribution (3.2.4) in terms of σ from the normal distribution (3.2.3):

$$k = 1.16\sqrt{2\sigma^2}\left(10^{\frac{1}{\gamma-1}} - 1\right)^{-1}. \tag{3.3.1}$$

When the exponent of the power law is $\gamma \leqslant 2$, then the distribution is heavy tailed and is used to simulate Lévy flight [138, 244, 245]. As we increase γ, the tail of the distribution becomes more like that of the normal distribution, and so we should expect the results to become similar to the results obtained for Brownian walkers as happened in the 1D model (see Section 2.3.2). Hence, for most simulations we set $\gamma = 2$ but we will discuss the effect of changing γ further below. When analysing the clusters that form, we continue to use the definition in Section 3.2.2 with a grid of 20×20 bins and thresholds $b_u = 0.5\%$ of the total population N and $b_l = 0.25\%$ of the total population N. We also use the movement parameters $P = 0.6$, $R = 1$ and, following Eq. (3.3.1) with $\gamma = 2$ and $\sigma = 0.02$, we get $k = 0.0036$ to make our simulations comparable to Brownian walkers.

The development of the spatial distribution of non-Brownian walkers with the above choice of parameters is shown in Fig. 3.15. We see that areas of high population density form but they are not as clear and dense as the clusters formed by Brownian walkers. The clusters appear to form in the first 100 time steps and there is no obvious further congregation of the population between the distributions at $t = 500$ and $t = 20,000$ from visual inspection although the number of clusters does appear to have changed.

The properties of the clusters formed by non-Brownian walkers are plotted in Fig. 3.16 for $P = 0.6$ and Fig. 3.17 for $P = 0.2$. When the probability of directed movement is sufficiently high, i.e. $P = 0.6$, the number of clusters drops several times in the first 4000 time steps and once more at $t \approx 8000$. The number of clusters then stays steady at $N_c = 18$ for the remaining time steps in the simulation. The mean cluster population

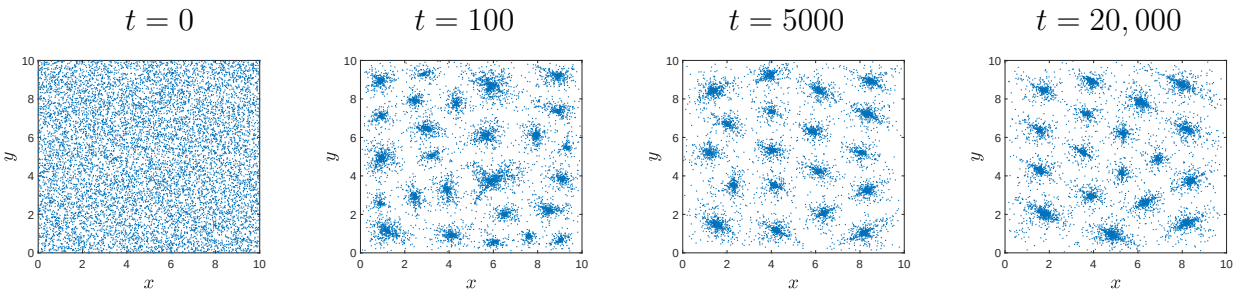

Figure 3.15: The spatial distribution of a population emerging from a random-uniform initial distribution at time $t = 0$. The population moves according to a power law dispersal kernel (3.2.4) and the movement parameters are $P = 0.6$, $R = 1$, $\gamma = 2$, and $k = 0.0036$.

shifts when the number of clusters changes (when two clusters merge, there will obviously be an increase in the mean cluster size) but is otherwise stable with small fluctuations as individuals move in and out of clusters. The mean cluster area stays relatively stable despite shifts in the number of clusters, suggesting that the number of clusters and the cluster population have no impact on the spatial size of the cluster. When the probability of directed movement is $P = 0.2$, as shown in Fig. 3.17, the number of clusters over time is no longer fixed and instead fluctuates between 16 and 17 clusters, occasionally dropping to 15 and once to 14 clusters. The mean cluster population and area also fluctuate, much more wildly than for when $P = 0.6$ but there are no large shifts in either of those properties after the initial formation. The dynamics of a fluctuating number of clusters is similar to the dynamics seen in non-Brownian walkers in the 1D model.

The results in Fig. 3.16 and 3.17 suggest that the stability or dynamism of the clusters is dependent on the probability P of directed movement. When $P = 0.6$ the system produces quasi-stable clusters, i.e. the number of clusters does not fluctuate although there may be occasional changes in the number of clusters. When $P = 0.2$ however, we have a system where the number of clusters constantly fluctuates. We further investigate the dynamics of these clusters by calculating the rate of change of the number of clusters. Namely, we introduce a time interval consisting of ΔT time steps and a binary function $b(t)$, where $b(t) = 0$ if there is no change in the number of clusters over one time step, and

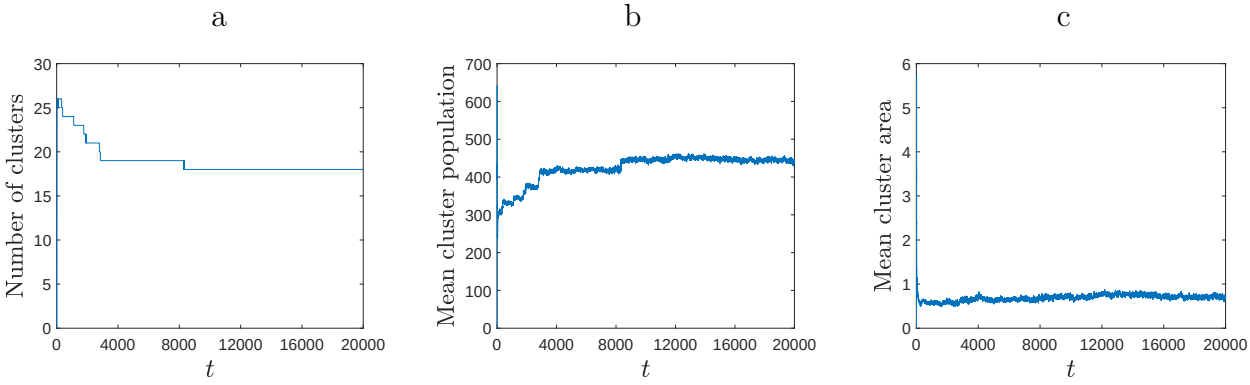

Figure 3.16: The development of clusters over time. The population moves according to a power law dispersal kernel (Eq. (3.2.4)) and the movement parameters are $P = 0.6$, $R = 1$, $\gamma = 2$ and $k = 0.0036$. The quantitative properties of the spatio-temporal dynamics are (a) the number of clusters, (b) the mean cluster population , and (c) the mean cluster area. The system produces quasi-stable clusters with no strong fluctuations in the quantitative properties.

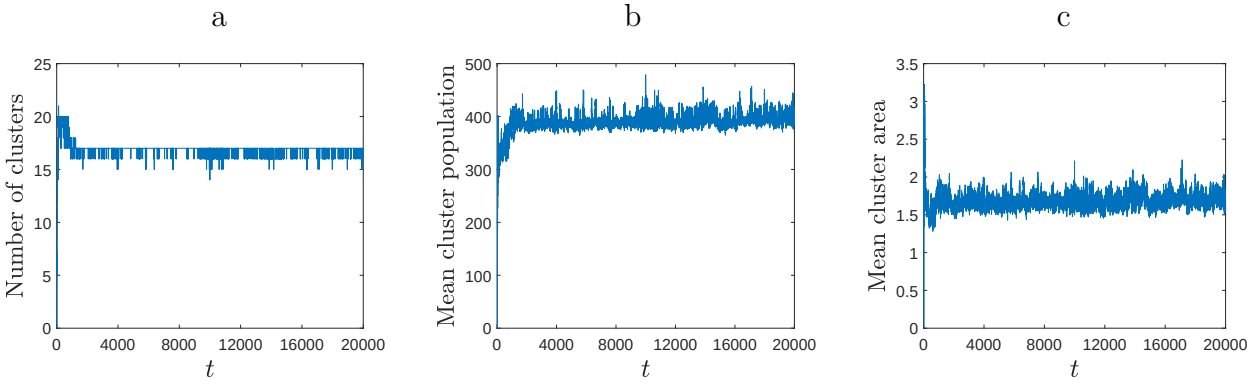

Figure 3.17: The development of clusters over time. The population moves according to a power law dispersal kernel (Eq. (3.2.4)) and the movement parameters are $P = 0.2$, $R = 1$, $\gamma = 2$ and $k = 0.0036$. The quantitative properties of the spatio-temporal dynamics are (a) the number of clusters, (b) the mean cluster population , and (c) the mean cluster area. The number of clusters fluctuates with time resulting in fluctuations in the other quantitative properties.

$b(t) = 1$ if the number of clusters changed between $t-1$ and t. The number of fluctuations $F(t)$ is then defined as

$$F(t) = \sum_{i=t-\Delta T}^{i=t} b(t_i). \tag{3.3.2}$$

The number of fluctuations $F(t)$ computed for $\Delta T = 100$ when $P = 0.2$ is shown in Fig. 3.18, where the value $F(t)$ at each time step is averaged over 10 simulations. It is seen from the figure that, after an initial time period, the number of fluctuations stays around

10 over time ΔT. In contrast, $F(t)$ calculated when $P = 0.6$ drops to close to 0 within 100 time steps and remains there for the rest of the simulation.

In Table 3.6 we calculate the cluster properties when R is increased. This shows that, as with Brownian walkers (see Table 3.3), the perception radius affects the number of clusters with only individual clusters appearing for $R \geqslant 4$.

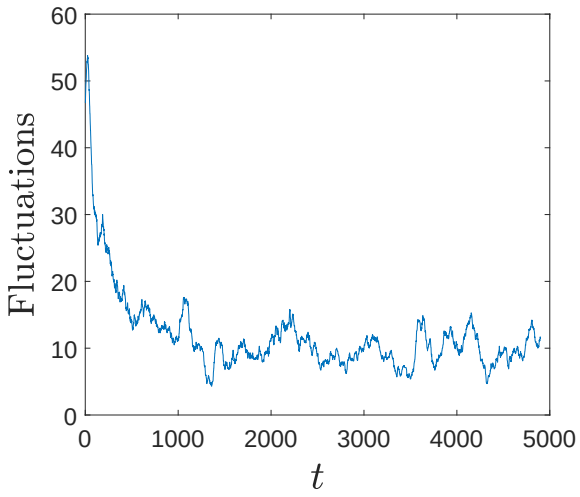

Figure 3.18: The number of fluctuations in the number of clusters per $\Delta T = 100$ time steps averaged over 10 simulations. The populations in each simulation move according to a power law dispersal kernel (3.2.4) and the movement parameters are $P = 0.2$, $R = 1$, $\gamma = 2$ and $k = 0.0036$.

As discussed above, if the exponent of the power law, γ, is increased from $\gamma = 2$, the tail of the distribution decays quicker, becoming more like that of the normal distribution.

Table 3.6: The mean and standard deviation of properties of clusters that are formed by non-Brownian walkers with different values of R at $t = 10,000$, the other movement parameters are $P = 0.6$, $k = 0.00365$ and $\gamma = 2$. The values in the table are taken over 10 simulations.

	$R = 1$	$R = 2$	$R = 2.523$	$R = 3$	$R = 4$	$R = 5$	$R = 100$
N_c	20.7	4.5	3.8	1.9	1	1	1
	(1.45)	(0.527)	(0.422)	(0.738)	(0)	(0)	(0)
A_c	0.643	2.50	2.76	6.02	9.13	9.46	9.10
	(0.0457)	(0.359)	(0.318)	(2.75)	(0.541)	(0.595)	(0.611)
n_f	1998	1657	1639	1454	1286	1295	1321
	(62.3)	(109)	(63.2)	(136)	(50.4)	(45.6)	(51.9)

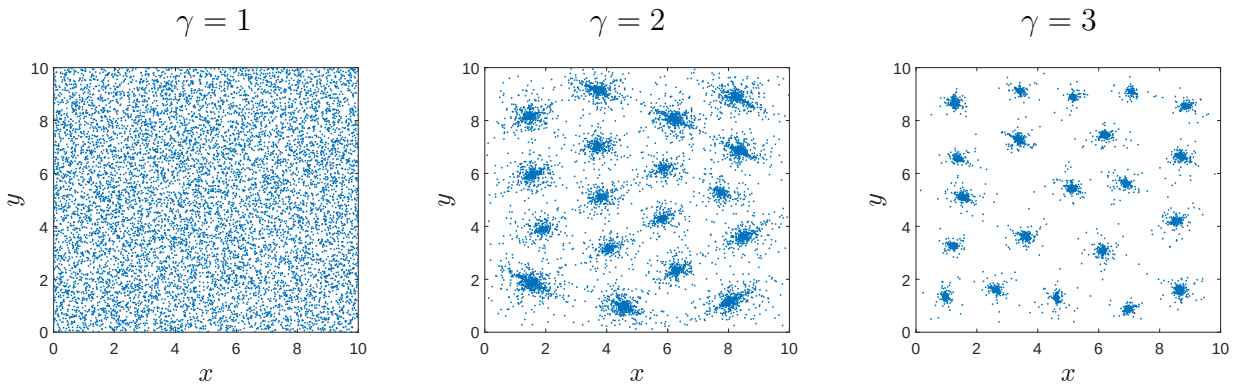

Figure 3.19: The population distribution at $t = 10,000$ of non-Brownian walkers using the power law distribution (3.2.4) to generate the step size with $\gamma = 1,\ 2,\ 3$.

Table 3.7: The mean and standard deviation of properties of clusters at $t = 10,000$ that form in 10 simulations with different movement regimes, N_c is the mean number of clusters, A_c is the mean cluster area, n_c is the mean cluster population. The standard deviation for every mean value is shown in brackets. The parameters are $R = 1$, $P = 0.6$, $k = 0.0036$, and $\sigma = 0.02$ in the Gaussian case.

Properties	$\gamma = 2$	$\gamma = 3$	$\gamma = 4$	$\gamma = 5$	Gaussian
N_c	20.7 (1.15)	20.1 (0.876)	22.7 (1.77)	23.3 (1.94)	24.9 (2.13)
A_c	0.643	0.248	0.118	0.0792	0.0153
	(4.57×10^{-2})	(2.11×10^{-2})	(1.2×10^{-2})	(8.75×10^{-3})	(1.05×10^{-3})
n_c	388 (22.3)	466 (22.8)	430 (36.1)	424 (39.1)	402 (36.9)

We found in the 1D model that as γ is increased, the distributions that are produced become more similar to those produced by Brownian walkers. We expect that the same will hold true in the 2D model and we now examine the distributions that are produced with $2 \leqslant \gamma \leqslant 5$ and compare them with the population distribution of Brownian walkers. Table 3.7 shows that indeed, the properties of the clusters are more similar to the Gaussian dispersal kernel case when γ is higher. One notable difference is that when γ increases, so does the number of clusters (and standard deviation of the number of clusters). When γ is lower, there is a greater chance of individuals making larger steps. Intuitively, this means that clusters may have to be further apart otherwise they would merge together. The mean cluster area decreases as γ increases because the probability of an individual taking a large step away from the centre of the cluster is lower. We also see that, apart from $\gamma = 2$

when there are a large number of free individuals, the mean cluster population decreases as γ increases. This can be explained by the increase in the number of clusters since the whole population, which remains constant, is split between more clusters, resulting in smaller cluster populations. We note that when $\gamma = 1$, no clusters emerge in the population; see Fig. 3.19(a). This is due to the high probability of an individual moving very long distances within the domain. Therefore each individual will be consistently moving around the entire domain, never forming into clusters.

We now briefly discuss how basic characteristics of non-Brownian movement determined by (3.2.4) influence cluster formation. The investigation of this question is less straightforward than in the case of Brownian walkers (see Section 3.3.1) as the power law distribution does not have a finite mean when $\gamma \leqslant 2$. Thus we pool together the movement step sizes made by all animals (i.e. $N = 10,000$) in the population of non-Brownian walkers over 100 time steps and compute the 'mean step size' μ_n based on that information. Since the 'mean step size' μ_n obtained from direct computation depends on the parameter k in (3.2.4), we can vary it by varying k in in our computer simulations. Furthermore, as k is related to the parameter σ of the Brownian motion by (3.3.1), a relationship between σ and μ_n can also be established. The results are shown in Table 3.8, where we take a similar range of σ as in Table 3.4. Given the value σ, we find k from (3.3.1) and then determine μ_n from direct computation.

Table 3.8: A comparison between σ, k and the 'mean step size' μ_n for non-Brownian walkers. Given the value k, the mean step size μ_n is calculated from the first 100 steps of $N = 10,000$ animals in the simulated data.

	$\sigma = 0.002$	$\sigma = 0.01$	$\sigma = 0.02$	$\sigma = 0.2$
k	3.65×10^{-4}	1.82×10^{-3}	3.65×10^{-3}	3.65×10^{-2}
μ_n	3.08×10^{-3}	0.0120	0.0218	0.139

In Table 3.9 we calculate cluster properties when k is increased and therefore the 'mean step size' is increased according to the results in Table 3.8. It can be seen from the table that the same conclusion can be made as we had for Brownian walkers in Section 3.3.1,

i.e. the number of clusters N_c decreases as μ_n increases. It is worth noting, however, that cluster properties are different when the non-Brownian walkers are compared to Brownian walkers through the relationship between parameters in Table 3.8. For all values of σ we use in our simulations, the cluster size and number of free individuals is always larger for non-Brownian walkers (cf. Table 3.4). These results are also illustrated in Fig. 3.20 (cf. Fig. 3.13).

Table 3.9: The mean and standard deviation of properties of clusters that are formed by non-Brownian walkers with different values of k at $t = 10,000$, the other movement parameters are $P = 0.6$, $R = 1$ and $\gamma = 2$. The values in the table are taken over 10 simulations.

	$k = 3.65 \times 10^{-4}$	$k = 1.82 \times 10^{-3}$	$k = 3.65 \times 10^{-3}$	$k = 3.65 \times 10^{-2}$
N_c	22.5	21.1	20.7	17.1
	(1.72)	(1.45)	(1.15)	(1.20)
$A_c \times 10^{-2}$	39.9	52.8	64.3	99.4
	(2.90)	(4.93)	(4.57)	(7.50)
n_f	1675	1839	1998	2592
	(46.8)	(71.3)	(62.3)	(111)

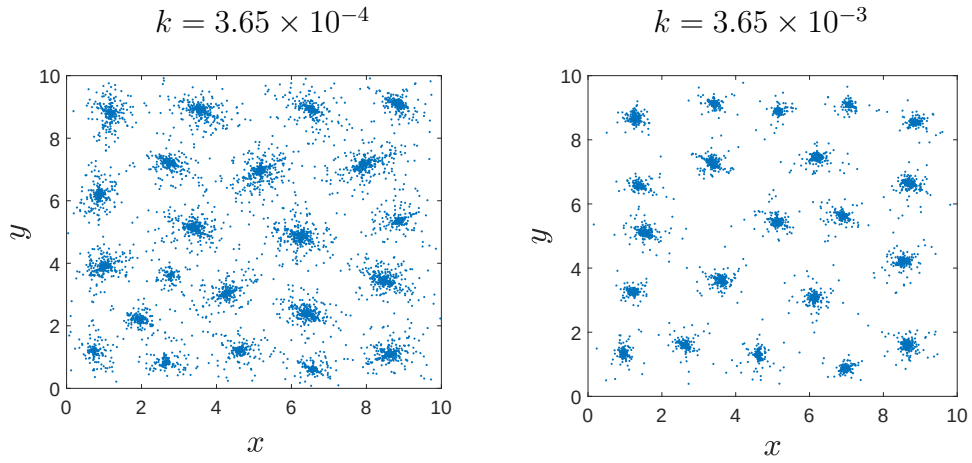

Figure 3.20: Example distributions of a population of 10,000 non-Brownian walkers at $t = 10,000$ when $k = 3.65 \times 10^{-4}$ and $k = 3.65 \times 10^{-3}$. Other movement parameters are $P = 0.6$, $R = 1$ and $\gamma = 2$.

The simulations in this section show, as in the case of Brownian walkers, density-dependent movement by non-Brownian walkers results in the formation of clusters. However, like in the 1D case, the clusters formed by non-Brownian walkers are less dense

than Brownian walkers and take a longer time to form. Also, the emergence of dynamic clusters, when the probability P of directed movement is low, has been revealed in the 2D case; see Fig. 3.17. Although the dynamics of fluctuating clusters in non-Brownian walkers was discussed in the previous chapter, the dependence on the probability of directed movement is a new result.

3.4 Comparison of Brownian and non-Brownian walkers

In this section we investigate the question of whether similar spatio-temporal dynamics of a population can emerge from Brownian and non-Brownian motion when different values of P are used. We have shown in the previous sections that the probability of directed movement largely controls the size of the clusters that are produced; see Fig. 3.21 where the mean area of a cluster is shown to decrease as P increases. We have already established above and in our discussion of the 1D model that the distributions produced by Brownian walkers are more dense than non-Brownian walkers. However, a numerical study reveals that there is an overlap where, for Brownian walkers with $P < 0.1$, there is a corresponding value of P for non-Brownian walkers that produces clusters with the same area.

Let us label the probabilities P of directed movement we use for Brownian and non-Brownian walkers as P_B and P_n respectively. To investigate further the similarities between clusters produced for Brownian walkers when $P_B < 0.1$ and non-Brownian walkers when $P_n > 0.1$, we compare the quantitative properties of clusters, i.e. the mean number of clusters, mean cluster population and mean area of clusters as well as the number of free individuals. We also measure the degree of aggregation in the population defined by the Morisita index [157]:

$$I_M = B \frac{\sum_{k=1}^{B} n_k(n_k - 1)}{N(N-1)} \tag{3.4.1}$$

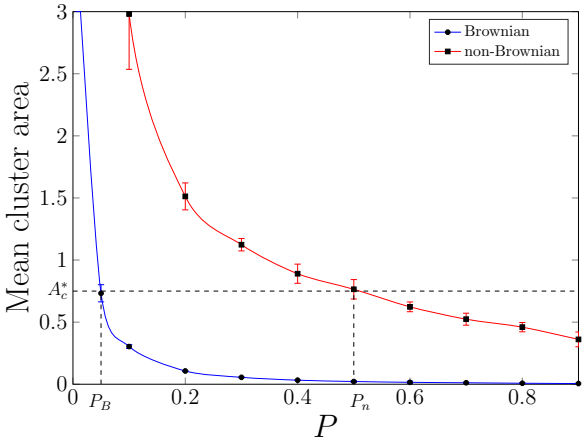

Figure 3.21: The mean area of clusters produced by Brownian and non-Brownian walkers for the probability of directed movement $P \in [0.01, 0.9]$. The mean values of the cluster area in the graph are taken over 10 simulations for each value of P and the error bars show the standard deviation. For non-Brownian walkers, no clusters are formed when $P < 0.05$. The other movement parameters are $R = 1$, $\sigma = 0.02$, $k = 0.0036$ and $\gamma = 2$. Vertical dotted lines show two values of the probability P (i.e. $P_B = 0.05$ for Brownian walkers and $P_n = 0.5$ for non-Brownian walkers) that correspond to the same mean area of clusters $A_c^* \approx 0.75$.

where B is the number of bins, n_k is the number of animals in bin k and N is the total population. The Morisita index provides a measure of how likely it is that two randomly selected individuals in a given distribution are found within the same bin compared to that of a random distribution. It has already been used in our study of 1D spatial distributions to quantify their heterogeneity. However, it is worth noting again that the Morisita index alone cannot be employed to compare various spatial distributions. Though it provides a measure of aggregation, the index (3.4.1) does not provide any information about the number of clusters or how they are distributed. Therefore it can only be used as an additional tool for comparing spatial distributions alongside the other quantitative properties of the clusters.

In Table 3.10, we present the mean and standard deviation of features of the spatial distribution for Brownian walkers with certain values of P_B between 0.01 and 0.09 and non-Brownian walkers with P_n between 0.1 and 0.9. From close inspection of the data in the tables, we see that the properties of clusters are similar for Brownian and non-

Table 3.10: The mean and standard deviation of properties of clusters formed by Brownian and non-Brownian walkers at $t = 10,000$ that form in 10 simulations with different movement regimes, N_c is the mean number of clusters, n_c is the mean cluster population, A_c is the mean cluster area, n_f is the mean number of free individuals, I_M is the Morisita index. Other parameters are $R = 1$, $\gamma = 2$, $\sigma = 0.02$, and $k = 0.0036$.

Brownian walkers	$P_B = 0.01$	$P_B = 0.02$	$P_B = 0.05$	$P_B = 0.08$	$P_B = 0.09$
N_c	11.9	17.5	20.9	21.9	23.2
	(0.989)	(1.27)	(1.73)	(2.18)	(2.66)
n_c	512.1	413.1	425.9	431.1	412.3
	(42.9)	(29.4)	(39.3)	(50.1)	(53.9)
A_c	3.263	1.648	0.7324	0.4127	0.3538
	(0.220)	(0.106)	(0.0600)	(0.0318)	(0.0198)
n_f	3937	2803	1159	657.5	563.6
	(318)	(162)	(138)	(115)	(84.5)
I_M	1.346	2.273	6.766	10.81	10.47
	(0.0298)	(0.102)	(0.539)	(1.09)	(1.42)
Non-Brownian walkers	$P_n = 0.1$	$P_n = 0.2$	$P_n = 0.5$	$P_n = 0.8$	$P_n = 0.9$
N_c	13.6	19.1	20.3	20.6	19.9
	(1.78)	(1.37)	(1.57)	(1.90)	(1.66)
n_c	449.0	345.2	385.5	415.5	442.2
	(66.0)	(24.9)	(34.1)	(39.3)	(45.7)
A_c	2.981	1.513	0.7643	0.4664	0.3716
	(0.490)	(0.124)	(0.0705)	(0.0481)	(0.0499)
n_f	3997	3437	2221	1508	1268
	(190)	(209)	(116)	(75.8)	(118)
I_M	1.299	2.131	6.157	12.03	17.76
	(0.0171)	(0.0449)	(0.450)	(1.56)	(5.86)

Brownian walkers when the probability of directed movement is approximately 10 times higher for non-Brownian walkers than for Brownian walkers, $P_n \sim 10P_B$. The exception to this relationship is when we compare clusters obtained for $P_B = 0.09$ and $P_n = 0.9$ as only the cluster population and area are similar, while the other properties start to diverge from each other as the probability increases.

Fig. 3.22 shows example distributions for simulations of Brownian and non-Brownian walkers at $t = 10,000$ with various values of P_B and P_n. Visual inspection of these figures confirms that properties of clusters are similar when $P_n \sim 10P_B$ but only for $P_B \leqslant 0.05$, $P_n \leqslant 0.5$. As P increases the similarities of the cluster decrease and the

spatial distributions are not as similar, as illustrated when $P_B = 0.08$ and $P_n = 0.8$.

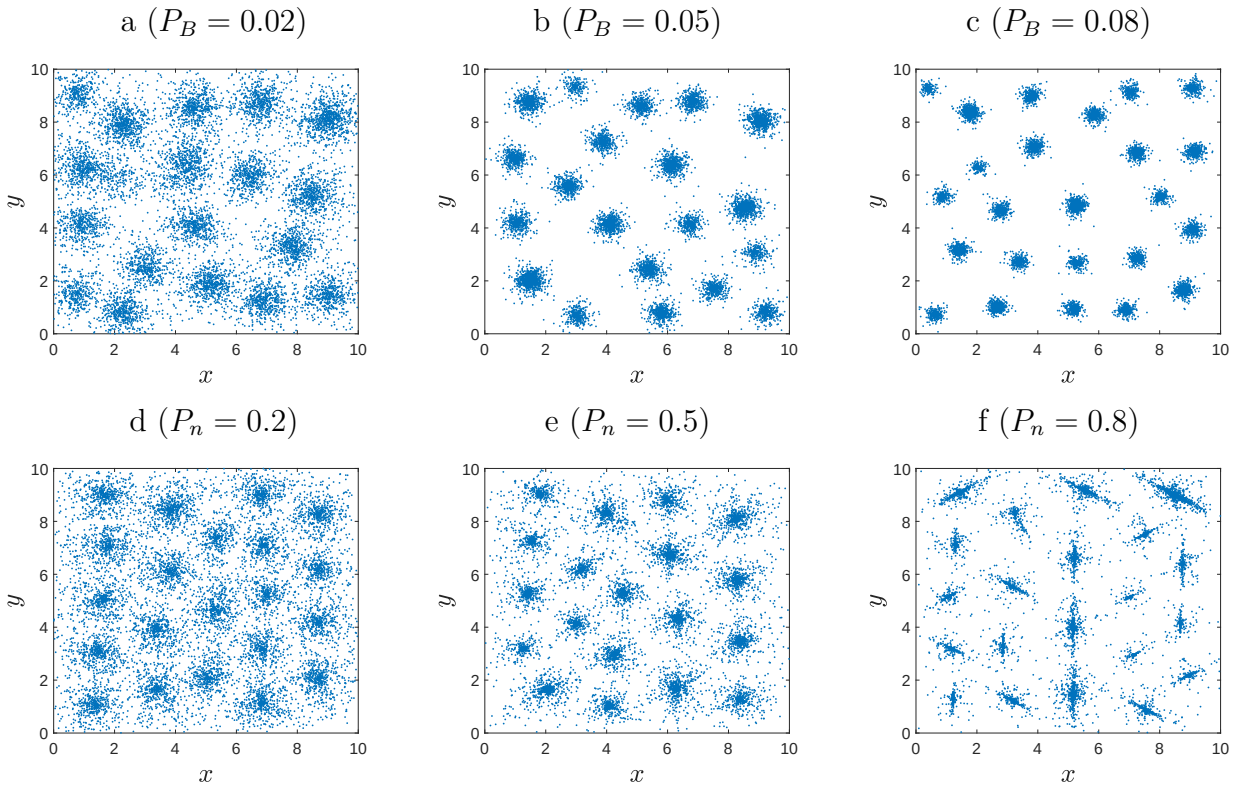

Figure 3.22: Example distributions of Brownian walkers (top) and non-Brownian walkers (bottom) at $t = 10,000$ with varying probabilities of directed movement. Probabilities P_B and P_n are shown in brackets for Brownian and non-Brownian walkers respectively. The other movement parameters are $R = 1$, $\sigma = 0.02$, $k = 0.0036$ and $\gamma = 2$.

One result of directed movement in the 2D model is that for large P the shape of clusters becomes 'stretched'. One example of stretched clusters can be seen in Fig. 3.22(f) when $P_n = 0.8$ showing the distribution formed by non-Brownian walkers. To measure the difference between the shapes of a 'stretched' cluster of Fig. 3.22(f) and a 'uniform disk' cluster of Fig. 3.22(c), we analyse the distribution of angles from the centre of the cluster in each spatial distribution of animals in a cluster. Namely, the median position $\mathbf{r}_m$ of all animals within the cluster is calculated for spatial distributions in Fig. 3.22(c) and Fig. 3.22(f). We then find the angle of each animal to the point $\mathbf{r}_m$ and then re-orientate each cluster in the spatial distribution so that the peak angles are at $\pm\pi/2$. This allows us to use data from all the clusters in the distribution to generate a histogram of angle

frequencies as shown in Fig. 3.23 (a,c). The slope from the peak at $\pi/2$ can then be fitted with a power law distribution as shown in Fig. 3.23(b,c). From examining the figures and fitting the slope from $\pi/2$ to π we conclude that the clusters produced by Brownian and non-Brownian walkers have a very different shape indeed, despite having similar cluster properties.

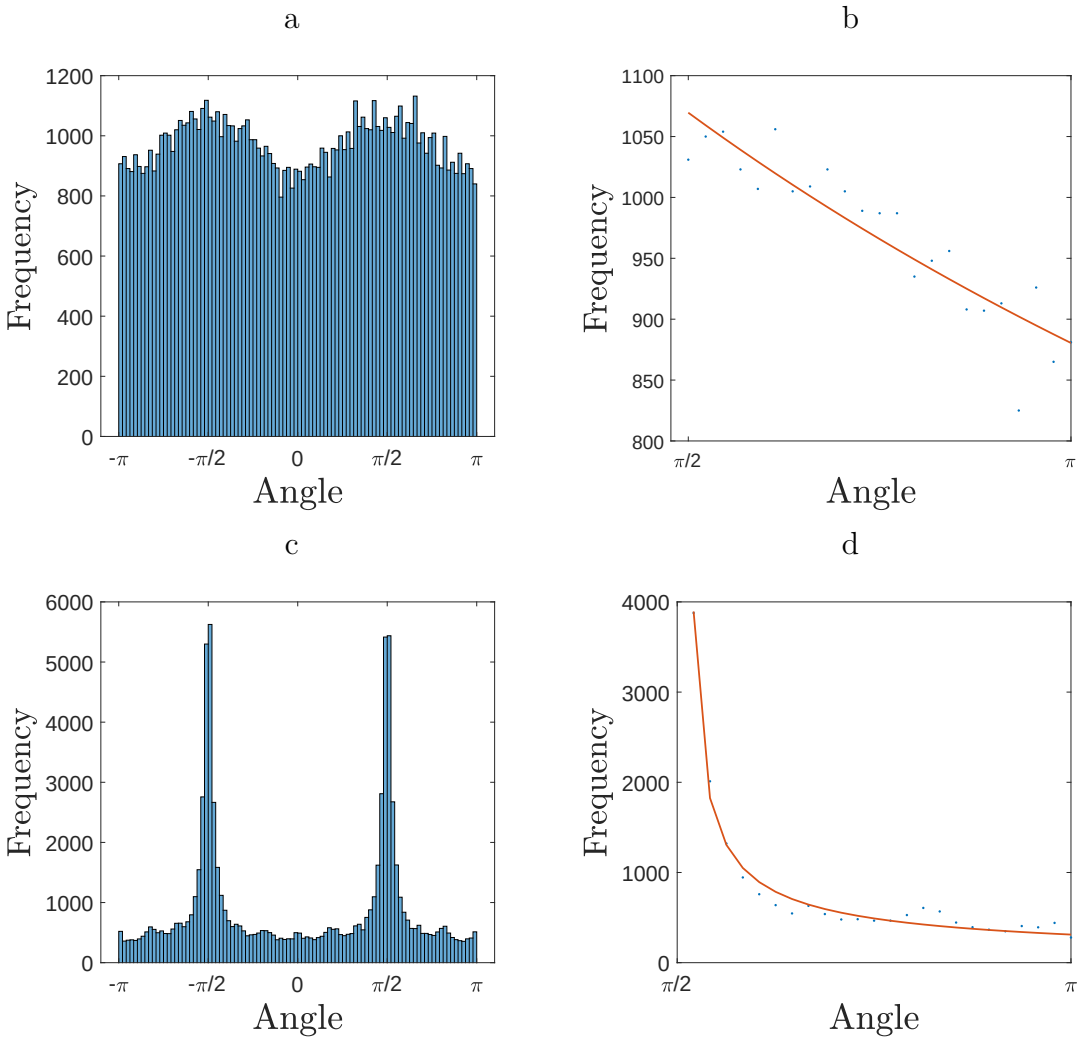

Figure 3.23: (a) The distribution of angles between animals in a cluster and the centre of the cluster for all clusters shown in Fig. 3.22 produced by Brownian walkers when $P_B = 0.08$ (a,b) and non-Brownian walkers when $P_n = 0.8$ (c,d). The distribution between $\pi/2$ and π fitted with a power law distribution is (b) $6941/(6.558+\theta)^{0.989}$ with $R^2 = 0.83$, and (d) $404/(-0.037+\theta)^{0.632}$ with $R^2 = 0.98$.

Formation of 'stretched' clusters may be in part due to the formulation of our model

where the area inside an animals perception radius is split into segments. We can investigate this by changing the number of segments from $S = 6$, which has been used in all previous simulations, and by removing the use of segments altogether. If we remove segments, as demonstrated in Fig. 3.24(a,b) for non-Brownian walkers when $P = 0.2$ and $P = 0.8$, we see that the stretching of clusters no longer occurs. The pattern of clusters otherwise appears to be similar to previous simulations, with regular spacing between clusters. When we change the number of segments from $S = 6$ to $S = 5$, as seen in Fig. 3.24(c,d), the stretching patterns still appear when P is large. From visual inspection, the pattern of clusters that emerges is similar to that when $S = 6$, shown in Fig. 3.22(d,f), although the shape of the stretching appears different, likely due to the arrangement of the segments.

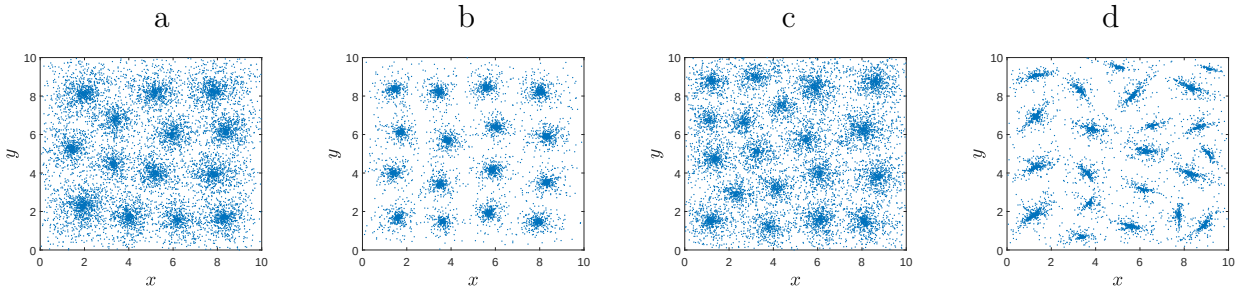

Figure 3.24: Example distributions at $t = 10000$ of non-Brownian walkers. (a,b) Without segments, (c,d) with 5 segments, (a,c) $P = 0.2$, (b,d) $P = 0.8$. Other movement parameters are $R = 1$ and $\sigma = 0.02$.

To investigate the impact of not using segments further, we simulate Brownian walkers with and without segments. This is shown in Fig. 3.25, showing that there is very little difference in the pattern of clusters produced or the time taken for the clusters to become stable. However, from visual inspection of the distributions shown in Figs. 3.24 and 3.25(a,b), it appears that when segments are not used the number of clusters is smaller than when they are. This is confirmed in Fig. 3.25(c), showing that when segments are not used, fewer clusters form on average. Without segments, the average number of clusters is 22.5 compared to 24.9 when segments are used (see Table 3.2). We also note

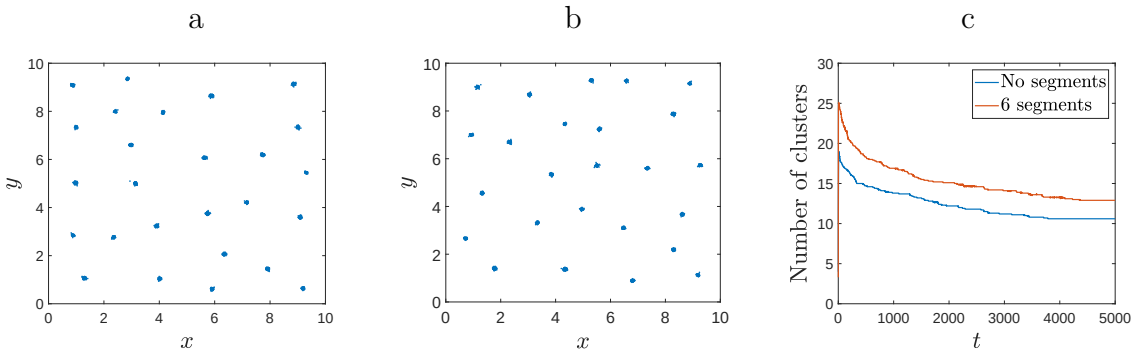

Figure 3.25: (a,b) Example distributions at $t = 10000$ of Brownian walkers with movement parameters $P = 0.6$, $R = 1$ and $\sigma = 0.02$. (a) With 6 segments. (b) Without segments. (c) The mean number of clusters formed in 10 simulations over 5000 time steps.

that when varying the number of segments between $S = 4$ and $S = 8$, there was no change in the number of clusters that form.

A possible reason for this could be that when segments are not used, it is more likely that an animal will move between two areas of high density rather than picking one to move towards. This in turn means that in the initial stages of cluster development, there will be a higher number of individuals between areas of high density. When there is a significant population outside a cluster but still within the perception radius, this can 'pull' the cluster towards that direction by a small amount. If this happens to two clusters so that each cluster is within the perception radius of the animals within the other cluster then they will coalesce to form one cluster. Therefore, we have slightly fewer clusters forming. As we can see from Fig. 3.25(c), the difference in the mean number of clusters is immediate, suggesting that this effect only happens in the first few time steps before clusters are fully formed. Once the clusters have formed, they behave similarly to when there are segments.

We also note that the regular pattern formed by the position of clusters does not appear related to the number of segments as it appears both with and without the use of segments. The arrangement of clusters, which is close to a hexagonal pattern is probably a result of circle packing theory. The theory states that regular hexagonal packing is the

densest arrangement of identical circles [42]. In the case of cluster formation, the clusters themselves can act as circles with a radius equal to the perception radius and therefore their densest possible arrangement will be in a hexagonal pattern. However, due to the stochastic nature of the simulations, the densest arrangement of clusters will not necessarily emerge. Moreover, the position of clusters is not fixed and they can merge together if they become too close leading to the pattern of clusters being asymmetrical. This will form a cluster that has a larger distance to its neighbouring clusters than necessary as its new position will be somewhere between the position of the two original clusters. This gives us the pattern such as that seen in Fig. 3.1(a) of clusters that are all over a certain distance apart but have a degree of randomness to their position. When the clusters are stable, this pattern is preserved. However when the clusters are dynamic, the space between clusters has many free individuals. This can lead to a cluster being formed in the space or other nearby clusters being pulled into the space by the free individuals. Therefore the uniform pattern of clusters is retained.

We believe that the use of segments makes sense biologically as an animal is unlikely to move in a direction which it perceives to be the mean position of its conspecifics rather than a direction which it perceives to have the highest density. The use of segments narrows down the direction an animal will decide to move to a region that contains the highest density. We acknowledge however, that there may be other methods of modelling density-dependent movement that do not result in stretched clusters and further study is required to understand the phenomenon.

We have seen above that the appearance of dynamic clusters, i.e. spatio-temporal dynamics where the number of clusters fluctuates over time, is dependent on the probability P_n of directed movement in non-Brownian walkers. For example, dynamic clusters appear when $P_n = 0.2$ in Fig. 3.17(a), yet there are no dynamic clusters when $P_n = 0.6$ in Fig. 3.16(a). Meanwhile, it immediately follows from comparison of Figs. 3.16(a) and 3.17(a) that dynamic clusters are not a feature of the system of non-Brownian walk-

ers for all values of P_n. Furthermore, if we suppose that Brownian walkers with the $P_B = 0.02$ produce similar clusters to non-Brownian walkers with the 'counterpart' probability $P_n = 0.2$, then we might expect those clusters to be dynamic when the spatio-temporal dynamics of Brownian walkers is considered. However, as Fig. 3.26(a) shows, the clusters appear to be stable with only a shift in the number of clusters happening at $t \approx 3500$. This is obviously different to the dynamics of non-Brownian walkers when $P_n = 0.2$ on the same timescale.

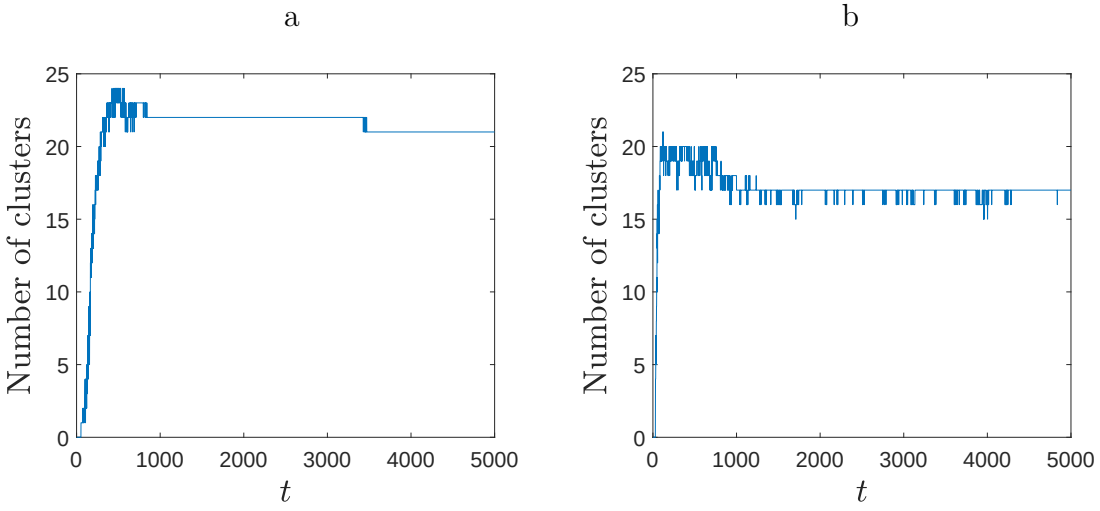

Figure 3.26: The number of clusters over time for (a) Brownian walkers with $P_B = 0.02$ and (b) non-Brownian walkers with $P_n = 0.2$. The other movement parameters are $R = 1$, $\sigma = 0.02$, $k = 0.0036$ and $\gamma = 2$.

We can therefore conclude that for certain probabilities of directed movement, the distributions produced by Brownian and non-Brownian walkers can appear similar. This only holds for $P_B < 0.05$ for Brownian walkers for some corresponding P_n for non-Brownian walkers. While some cluster properties remain similar, the shape of clusters and the cluster stability are not. Moreover, as P_B increases, other properties such as the number of free individuals produced by each movement type diverge and when $P_B > 0.1$ there is no corresponding P_n that will produce a similar distribution. Due to the difference in cluster stability, we have the important result that while the spatial distributions of

Brownian walkers and non-Brownian walkers can be indistinguishable when considering certain cluster properties, the spatio-temporal dynamics are still different.

3.5 Discussion and conclusions

In this chapter, the model of density-dependent movement described in Chapter 2 has been extended to 2D spatial domains. Our aim for both chapters has been to relate the problem of understanding of population spatial patterning to another major focus in ecology, namely, to the effect of different individual movement patterns [196, 235, 245]. We therefore considered the spatial dynamics of a population where animals perform either Brownian or non-Brownian density-dependent motion.

We have designed the formulation of the process of directed movement in a 2D domain: while the size of a random jump is consistent between the 1D and 2D cases, the introduction of an angle of movement in the 2D model influences how directed movement works. Namely, when the probability of directed movement is $P = 0.5$ in the 1D model, there is unbiased random movement as there is an equal chance of an animal moving towards the area of higher density. In the 2D model, having the probability $P = 0.5$ does not result in unbiased random movement as the animal will move directly towards the area of highest density in 50% of time steps and at any other angle the other 50%. Therefore, it is only the value $P = 0$ that produces unbiased random movement in the 2D model. This makes it difficult to compare the results of the 1D and 2D models when changing P directly. Instead, in this chapter we have shown how the spatial distributions are dependent on P throughout the range of $P \in (0, 1)$. We have also investigated how the spatial distributions depend on the perception radius R - another parameter required to formulate rules of density-dependent movement in the model.

3.5.1 Brownian walkers

We concluded in Chapter 2 that the formation of clusters in a population of Brownian walkers would be similar in 1D and 2D models. Indeed, in the case of Brownian walkers and assuming that the environment is isotropic, the 'full' 2D movement splits to a product of two 1D movements for x and for y, i.e. $\rho(\Delta\mathbf{r}) = \rho(\Delta x)\,\rho(\Delta y)$ where $\Delta\mathbf{r}$ is the movement step along the 2D path, $(\Delta\mathbf{r})^2 = (\Delta x)^2 + (\Delta y)^2$, and each of $\rho(\Delta x)$ and $\rho(\Delta y)$ is given by (3.2.3). In this study we have confirmed that density-dependent movement in 2D spatial domains results in the formation of animal clusters and, exploring the changes in cluster properties as the parameters change, we have found that the relationship between parameters and the distribution is the same in 1D and 2D problems. The number of clusters formed in a 2D domain is random although within a range that is dependent on the movement parameters, particularly the perception radius R. When we set the area within the perception radius to be the same proportion of the domain in the 2D model as the 1D model, the mean number of clusters in 2D is 4.2, while in 1D the mean number of clusters is 4.44 (calculated from when $R = 1$ in Table 2.1). In both studies, increasing the perception radius led to fewer clusters. In both 1D and 2D cases, given that P is sufficiently high then dense clusters were formed with few or no free individuals. Only when P was very close to the value where the movement becomes unbiased (i.e. $P \approx 0.52$ in 1D, $P \approx 0.01$ in 2D) did the random movement not result in stable clusters. When P was such that clusters did form in 2D, they were always stable and although there were occasional changes in the number of clusters, Brownian walkers never produced dynamic, rapidly fluctuating clusters.

3.5.2 Non-Brownian walkers

The formation of clusters by a population of non-Brownian walkers in the 2D model was less predictable having studied the results in 1D spatial domains. We found that indeed,

clusters were formed in the population of non-Brownian walkers. Similarly to the 1D model, for the same parameter choice the properties of 2D clusters differ significantly between populations of Brownian and non-Brownian walkers. The non-Brownian walkers produce fewer clusters that are less dense and there are many more free individuals in the domain in comparison to Brownian walkers with equivalent movement parameters.

It has been revealed in our 2D study that there are similarities between properties of clusters formed by Brownian walkers with $P < 0.1$ and non-Brownian walkers with a value of P approximately 10 times larger. This conclusion, however, does not hold for the stability of clusters as Brownian walkers do not produce dynamic clusters for any P. Thus, the analysis of spatial distributions alone may not be sufficient to conclude about the movement type: the spatial distributions of Brownian walkers and non-Brownian walkers can be indistinguishable when considering certain cluster properties but the spatio-temporal dynamics are still different.

Another new feature of the 2D problem is that the clusters of non-Brownian walkers are dynamic but only when P is sufficiently low. In our study of the 1D model, we concluded that non-Brownian walkers produced dynamic clusters while Brownian walkers usually produced stable clusters. However, by analysing the dynamics with varying values of P in the 2D model, we have now found that 2D clusters produced by non-Brownian walkers are not always dynamic.

3.5.3 Summary of cluster dynamics in the 2D model

We have shown that the probability of directed movement, P, has a significant effect on the properties of clusters that arise from density-dependent movement of both Brownian and non-Brownian walkers. When $P = 0$, animals move independently of their conspecifics and therefore the system will preserve an initial statistically uniform distribution for Brownian and non-Brownian walkers. As P increases, at some point the system will shift so that the distribution contains clusters. This will occur at a different value of P

depending on the movement type. For non-Brownian walkers, clusters will begin to form at $P \approx 0.05$ but for Brownian walkers this probability value will be much lower, $P \approx 0.01$.

When clusters are formed in a population of Brownian walkers, they are largely stable over time (apart from occasional shifts when clusters merge), as shown in Fig. 3.26(a) with $P = 0.02$. However, for clusters that are formed in a population of non-Brownian walkers with a low value of P, the number of clusters is dynamic, as shown in Fig. 3.26(b) with $P = 0.2$. At some point between $P = 0.2$ and $P = 0.6$ another shift occurs for non-Brownian walkers and the clusters that are produced become stable, as seen in Fig. 3.16(a).

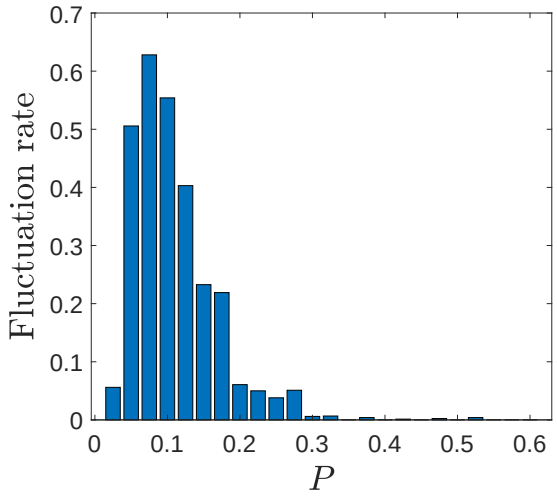

Figure 3.27: The rate of fluctuations in the number of clusters between $t = 4000$ and $t = 5000$ in a population of non-Brownian walkers when P increases from $P = 0.025$ to $P = 0.6$ with the increment $\Delta P = 0.025$. The populations in each simulation move according to a power law dispersal kernel (3.2.4) and the movement parameters are $R = 1$, $\gamma = 2$ and $k = 0.0036$. The frequencies are averaged over three simulations for each value of P.

It is difficult to study the exact points of transition when increasing P as it would involve numerous simulations. We therefore cannot say for certain whether the shifts from the 'no clusters' region in P to 'dynamic clusters' to 'stable clusters' happen suddenly, neither can we determine the length of the transition state between the two. However, we can approximately find the regions of different dynamics by running multiple simulations

with varying P. Fig. 3.27 shows the number of fluctuations in the non-Brownian walkers case when P increases with the increment 0.025. Between $P = 0.05$ and $P = 0.175$ we have a very high rate of fluctuations that starts decreasing as P increases. For $P = 0.2$ to $P = 0.275$ there are still a small number of fluctuations which then suddenly drops to almost no fluctuations happening at $P = 0.3$ and above. The results shown in the figure do suggest a sharp shift in the dynamics, first from no clusters to highly dynamic clusters at $P = 0.05$ which then has a slow shift to moderately dynamic clusters at $P = 0.2$ and another sharp shift to stable clusters at $P = 0.3$.

As discussed above, the number of clusters is dependent on our definition and choice of threshold parameters and bin size. We chose parameters so that the properties of clusters would not be sensitive to small changes in those parameters. However at transitions between dynamics of the distributions the choice of parameters may have a greater effect. Further to this, we have not formally defined what we mean by stable and dynamic clusters. It is clear that Fig. 3.26(b) shows dynamic clusters but if the number of transitions was decreased there must be a threshold at which point we would consider the system to no longer be showing dynamic clusters and this issue requires further investigation. The importance of cluster 'stability' will be discussed further in Chapter 6 where we propose a framework for targeted pesticide application on high density patches. A certain level of temporal stability is required to be able to target patches but further study will be required to produce a specific stability threshold.

This model, along with the 1D model discussed in Chapter 2 is partially motivated by recent experimental work on the distribution and movement of the grey field slug in agricultural fields [78, 180]. In Chapter 4, we analyse movement data of slugs to determine whether they display density-dependent movement. Although it is difficult to establish the existence of directed movement as described by the model in this chapter, it is possible to detect changes in behaviour due to population density.

Chapter 4

Patterns of Individual Movement of the Grey Field Slug in an Arable Field

4.1 Introduction

This chapter consists of our work presented in [67]. As proven in Chapters 2 and 3, density-dependent animal movement can result in the formation of high density patches. This can be a factor on a short within-generation time as our model has shown, but also on a longer multi-generation time scale [74, 97, 261]. In this chapter, we focus our attention to the movement of slugs in an agricultural environment. Previous studies have shown that the spatial distribution of slugs are often patchy and preliminary investigations have not found a significant correlation between slug distribution and environmental factors such as the properties of the soil [78]. Field studies have suggested that slug movement could be regulated by density-dependent mechanisms, so that the movement pattern of an individual slug is different when con-specifics are present nearby [252]. However, the evidence is scarce and often anecdotal rather than documented, partly because of technical problems relating to slug tracking. It is likely that density-dependent movement and

environmental factors both play a role and work is ongoing to determine the combination of factors involved in patch formation [78, 79, 80].

While data on individual animal movement of mammals, birds and fish are abundant [66, 82, 217], movement data for invertebrates such as snails, worms and slugs in their natural environment remain relatively scarce. One reason for that is the small body size, which, given the current development of radio-tag technology, often makes their tagging difficult or even impossible (but see [17]). Other methods of marking are available but methods such as harmonic radar and RFID (radio frequency identification) tagging make it easier to find organisms without having to interfere with their behaviour.

In this chapter, we report the results of the first field study on individual movement of the grey field slug to use a unique combination of field tracking technology that determines the location of slugs when both above and below the soil, in conjunction with a relevant theoretical framework to support analysis and interpretation of the data collected. The experiment was designed specifically to investigate the existence of density-dependence which has allowed us to obtain important evidence, which would be difficult to achieve with a different approach. Slugs were collected in an arable field, radio-tagged and released back into the field. Two different types of treatment were used: "sparse release" and "dense release". In the sparse release, slugs were placed at equally spaced locations in an arable field sufficiently far away from each other to minimize encounters (approximately two meters apart). The existence of density dependence was investigated using the second treatment (dense release) in which slugs were released as a group, i.e. initially placed close to each other (within 20 cm from nearest neighbour). In both treatments, the position of each slug was tracked for about ten hours using known time steps. The experimental work described in this chapter was undertaken by colleagues at Harper Adams University, for a more detailed explanation of the tracking procedure, see [80].

The data produced by the experiments were of the form of coordinates of each slug in the field at discrete moments of time. We therefore approximate their movement path

as a series of straight lines between their known locations. This is a well established method [64, 113, 116, 235] and also fits well with our random walk model (see Chapters 2 and 3) whereby we simulated individual movement with straight line steps. The tracking data were analysed using the Correlated Random Walk (CRW) framework [64, 235, 257]. A correlated random walk is one which shows a degree of directional persistence, i.e. an animal is likely to continue moving in the same direction in two subsequent time intervals, and often fits well when analysing animal movement paths. The framework includes analysis of movement features such as the mean speed, mean scaled squared displacement, the straightness of the movement path and the frequency a slug moves. It also considers the theoretical rate of spread which can be compared to the data by calculating the distribution of turning angles and the net squared displacement.

We have found that all components of the slug movement pattern exhibit significantly different properties in the cases of sparse and dense release, clearly suggesting that density-dependence is a factor regulating slug movement in the agricultural environment. Results from this data can be used to inform our model and in Chapter 5 we show how the variations in movement with population density can lead to the formation of patches.

4.2 Data collection

A technique for implanting RFID tags beneath the body wall of fully grown slugs has been recently developed, allowing individuals to be accurately tracked in the field [80]. Comparison of tagged and untagged slugs in laboratory tests have shown that after a 14-day post-insertion recovery period, no significant differences occurred between survival rates, egg batch production, food consumption or locomotor behaviour (velocity; distance travelled). The method has subsequently been used to follow movement of individuals for extended periods of time, showing that most slugs ($\sim 80\%$) forage within a limited area. For example, 5 weeks after release in the field, the mean overall distance from their release point in work conducted in spring was 78.7 ± 33.7 cm, and 101.9 ± 24.1 cm in autumn

experiments [80]. The slugs that stay locally during the experiments are thought to do so because they are already within a patch and those that travel further are moving between patches. The observations suggested that locomotor behaviour promotes the stability of the patchy distribution of slugs in arable fields, but further work to determine mechanisms leading to the small foraging area was required.

The potential for density-dependent individual movement to influence slug foraging patterns was investigated by recording the movement of individual slugs above and below the soil surface in an experiment conducted during the period of higher slug activity in autumn (5-25 November 2016), in a commercial winter wheat field (Shropshire, UK; 52_46001.260 N, 002_34050.140 W). A rectangular 6×5 grid with 2m between adjacent traps was established in the study field, with a single unbaited refuge trap consisting of an upturned terracotta plant pot saucer (18 cm diameter; LBS Horticulture Supplies, Lancashire, UK) set at each node. The spacing of trapping nodes reduced the potential for mutual interference between slugs when later released and tracked. Assessments prior to the experiment indicated that there was a low population of slugs (mean of < 1 per trap) evenly distributed across the selected study area, reducing the potential for naturally occurring individuals to influence the behaviour of experimental animals. No rainfall was recorded throughout the experiment and low spatial variation in moisture content of the soil was noted across the study area, thus minimizing any differential effects on individual slug movement.

Two slugs were taken from the trap at each grid node (5 November) and placed individually in labelled tubes before being returned to the laboratory and maintained singly in a 250 ml circular plastic rearing container under light/temperature regimes reflecting UK autumn conditions (10:14 light:dark cycle; photophase = 15°C, scotophase = 10°C) and at a constant 60% humidity [80]. Lettuce leaves were offered ad libitum to each slug as food and replaced with fresh leaves daily, and all slugs were allowed a 48 h acclimation period before being used in experiments [80].

Following the acclimation period, a RFID tag with a unique code was implanted into each slug using the previously developed procedure [80]. Slugs were gently anaesthetized by exposing them to a CO_2 rich environment for 20 seconds or until they were fully extended. The needle of an MK165 implanter (Biomark USA) was positioned on the left side about three-quarters of the way along the full length of the body from the anterior end, level with the top of the keel, and with the its tip pointing forward. It was inserted by applying gentle pressure until the tip was no longer visible, and an 8 x 1 mm tag (chip and antenna coil encased in glass; HPT8 tag, Biomark USA) was released. Following tagging, each slug was returned to its rearing cage and maintained under the above conditions for the 14 day recovery period; any slug displaying abnormal behaviour or other symptoms of injury was discarded.

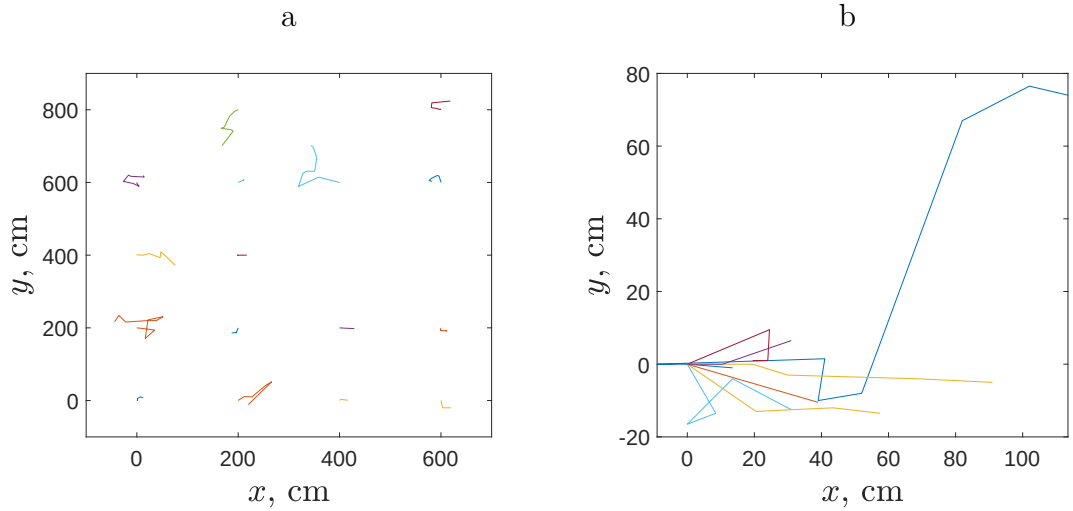

Figure 4.1: The trajectories of slugs from the (a) sparse release and (b) dense release.

After a 14-day recovery period, the slugs were allotted at random to one of two treatments before being released back onto the field trapping grid at dusk. Seventeen tagged slugs were each released singly (sparse release), using the nodes on which they had originally been caught to ensure appropriate spacing between slugs and thus minimising mutual contact. In the dense release treatment, eleven tagged slugs were released in close proximity to each other (approximately 20 cm between nearest neighbours). Numbering grid

nodes sequentially from the top left corner of the grid matrix of 5 rows and 6 columns, the first row contains traps 1-6; in second row the node immediately below node 1 is node 7; et seq. Using this notation, the slugs in the dense release treatment were released on node 18, i.e. approximately in the middle of the area covered by the trapping grid. Movement of each slug in both the sparse and dense release treatments during the following 10 hour period, was tracked by mapping its position on a 2-dimensional horizontal plane on 10 occasions, using a HPR Plus reader and racket antenna (Biomark, USA); see Fig. 4.1. Both treatments were run simultaneously, and there were no less than 20 minutes between each assessment although the exact time interval was dependent on the degree of difficulty of locating individuals. The system allowed the position of each slug to be detected whether above or below the soil surface, and the location of each detection was marked using a marker peg and the time of the assessment recorded. To reduce the impact of the accumulation of any minor errors in measurement that may have accrued between sequential markers, the peg location in relation to the original release point were determined and the distance between sequential markers calculated by triangulation. All slugs were located at each trapping assessment, and combining all assessments slugs were found to be on the soil surface on 79.3% of occasions. Temperature readings taken using a soil temperature probe (Vegetronix, USA) were verified by comparison with the Harper Adams University weather station (situated 650 m from the experimental site on similar open ground and at the same altitude), and fluctuations across the area and during the total time of the experiment never exceeded 3°C.

4.3 Data analysis

The nature of the slug movement data collected in the field experiment (i.e. position on or beneath the soil surface observed at discrete moments of time) makes it possible to analyse the slug locomotory track in terms of the discrete-time random movement framework [64, 113, 116, 235]. Within this framework, a curvilinear movement path is

approximated by a broken line (see Fig. 4.2) and the movement of an individual slug is parameterized by the following frequency distributions:

1. The distribution of the step sizes along the movement path (i.e. the distance between sequential pairs of recorded positions; Fig. 4.2) or the corresponding average speed.

2. The distribution of turning angle (the angle between the straight lines drawn between sequential pairs of recorded positions; Fig. 4.2).

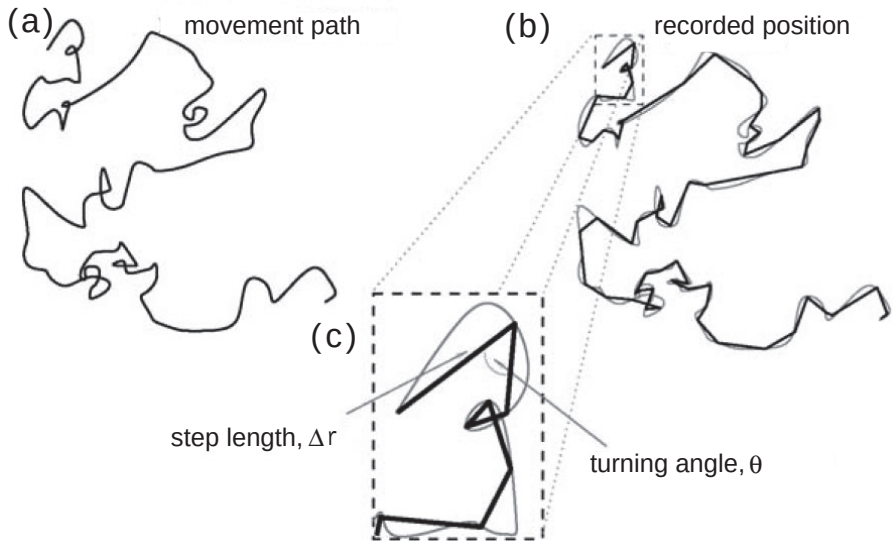

Figure 4.2: A sketch of animal movement path and its discretization (adapted from [113]). (a) The original movement path is normally curvilinear. (b) Due to the limitations of the radio-tracking technique, position of the animal is only known at certain discrete moments of time; correspondingly, the curve is approximated by a broken line. (c) The movement path as a broken line is fully described by the sequence of the step sizes along the path, i.e. the distances travelled between any two sequential recorded positions, and the sequence of the corresponding turning angles.

Once all the information is available, it is possible to calculate the mean squared displacement as a function of time [116, 156]. Additionally, in the case where the movement consists of alternating periods of active movement and immobility (periods with no recorded displacement resulting from feeding or inactivity, hereafter referred to as "resting time"), one should also consider the distribution of the corresponding periods.

4.3.1 Speed, squared displacements and the straightness index

It is apparent from the data that slug movement is intermittent, with periods of locomotion interspersed between periods in which they remain motionless. Tables 4.1 and 4.2 show, for the sparse and dense releases respectively, the number of 'active' time intervals when the slugs were moving. Periods during which slugs were motionless are marked by the zeros in Tables 4.1 and 4.2, but all these individuals resumed their movement during the following day, confirming that they were alive throughout the assessment period. We therefore retain the zeros in the data for the subsequent analysis.

The baseline discrete-time framework considers animal position at equidistant moments of time. However, in the field experiment (as described in Section 4.2), time taken to locate slugs at each assessment resulted in the time interval varying between measure-

Table 4.1: Slug mean speed (averaged over the whole movement path), the mean SSD (see Eqs. (4.3.3) and (4.3.5), respectively) and the straightness index in the case of sparse release for each of 17 slugs used in the experiment. Here the straightness index is calculated using Eq. (4.3.4) where the values of the step size are immediately available from our field data.

Slug number in protocol	Active steps (out of total 10)	Mean speed, $< v >$	Mean SSD, $< \sigma^2 >$	Straightness index, s
1	4	0.0313	0.1681	0.7459
2	10	0.4731	14.6612	0.1758
3	8	0.1844	3.3475	0.7140
4	8	0.1781	3.0618	0.2231
5	7	0.3121	10.2142	0.7709
6	3	0.0389	0.2944	0.8337
7	2	0.0310	0.5091	0.8947
8	4	0.0670	0.7159	0.7055
9	6	0.4062	23.9861	0.1374
10	2	0.0400	0.4931	0.9088
11	2	0.0651	0.9406	1.0000
12	0	0	0	–
13	8	0.3719	12.9547	0.5115
14	6	0.1863	5.4126	0.4252
15	7	0.0847	0.9628	0.3668
16	3	0.0402	0.4149	0.4495
17	2	0.0774	1.4697	0.7685

Table 4.2: Slug mean speed (averaged over the whole movement path), the mean SSD (see Eqs. (4.3.3) and (4.3.5), respectively) and the straightness index in the case of dense release for each of 11 slugs used in the experiment. Here the straightness index is calculated using Eq. (4.3.4) where the values of the step size are immediately available from our field data.

Slug number in protocol	Active steps (out of total 10)	Mean speed, $< v >$	Mean SSD, $< \sigma^2 >$	Straightness index, s
1	7	0.2946	12.4178	0.6825
2	0	0	0	–
3	4	0.0826	1.3006	0.9623
4	0	0	0	–
5	0	0	0	–
6	4	0.0887	1.4682	0.5321
7	3	0.0456	0.8170	0.4969
8	1	0.0222	0.3004	1
9	1	0.0734	2.9659	1
10	4	0.2137	5.6046	0.9965
11	2	0.0660	1.1160	0.9896

ments (sparse release treatment: 27-87 mins; dense release treatment: 20-103 mins). The step size, i.e. the displacement during one time interval, depends in part on the duration of that interval, hence risking bias in the results. We address this issue by scaling the step size by the duration of the corresponding time interval, i.e. by considering the average speed during the step:

$$v_k(i) \quad = \quad \frac{|\Delta \mathbf{r}|_k(i)}{\Delta t_k(i)}, \quad i = 1, 2, \ldots, T, \tag{4.3.1}$$

where

$$|\Delta \mathbf{r}|_k(i) \quad = \quad |\mathbf{r}_k(t_i) - \mathbf{r}_k(t_{i-1})|, \tag{4.3.2}$$

is the displacement of the kth slug during the ith time interval, i.e. the distance between the two sequential positions in the field. Here T is the total number of steps made by the given slug during the full period of the experiment (in our field data, for all slugs $T = 10$).

For each individual slug, we then calculate the mean average velocity over all steps

along the movement path:

$$< v >_k \;=\; \frac{1}{T}\sum_{i=1}^{T} v_k(i). \tag{4.3.3}$$

The results for the sparse and dense releases are shown in Tables 4.1 and 4.2, respectively; see also Fig. 4.3(a).

The mean speed of slug movement, although being an important factor for slug dispersal, does not provide enough information about the rate at which the slug increases its linear distance from the point of release, because it does not provide information on the frequency of turning or the turning angle. In order to take that into account, we calculate the straightness index [64], i.e. the ratio of the total displacement (distance between the point of release and the final position at the end of the experiment) to the total distance travelled along the path:

$$s_k \;=\; \frac{|\mathbf{r}_k(t_T) - \mathbf{r}_k(t_0)|}{\sum_{i=1}^{T} |\Delta\mathbf{r}|_k(i)}, \tag{4.3.4}$$

where t_0 is the time of slug release and t_T is the time of the final observation. The actual distance travelled is approximated by the length of the corresponding broken line (see the dark solid line in Fig. 4.2).

The straightness index quantifies the amount of turning (a combination of the frequency and angles of turns) along the whole movement path, i.e. over the whole observation time, but it says nothing about the rate of turning on the shorter time scale of a single 'step' along the movement path. To account for this, along with the mean speed we calculate the mean scaled squared displacement (SSD):

$$< \sigma^2 >_k \;=\; \frac{1}{T}\sum_{i=1}^{T} \sigma_k^2(i) \qquad \text{where} \qquad \sigma_k^2(i) \;=\; \frac{|\Delta\mathbf{r}|_k^2(i)}{\Delta t_k(i)}, \tag{4.3.5}$$

see Tables 4.1-4.2 and Fig. 4.3(b). For the same value of mean speed, a larger value of

the SSD corresponds to a straighter movement on the timescale of a single step, with a smaller turning rate.

An immediate observation from visual analysis of the data shown in Fig. 4.3 is that both slug velocities and the SSD are smaller in the case of dense release than in the sparse release. Therefore, a preliminary conclusion can be drawn that average slug movement is slower in the dense release compared to the sparse release treatment.

4.3.2 Turning angles

We now proceed to analyse the distribution of turning angles. The histogram of different values of the angle is shown in Fig. 4.4. Let us consider first the case of sparse release (see Fig. 4.4(a)). We readily observe that the distribution is roughly symmetrical and has a clear maximum at $\theta_T = 0$. The latter indicates that, on this timescale, slug movement is better described as a CRW than standard diffusion [49, 235]. Indeed, standard diffusion (also known as the simple random walk) assumes that there is no bias in the movement direction, in particular there is no correlation in the movement direction in the intervals before and after the recorded position, which means that the turning angle is uniformly

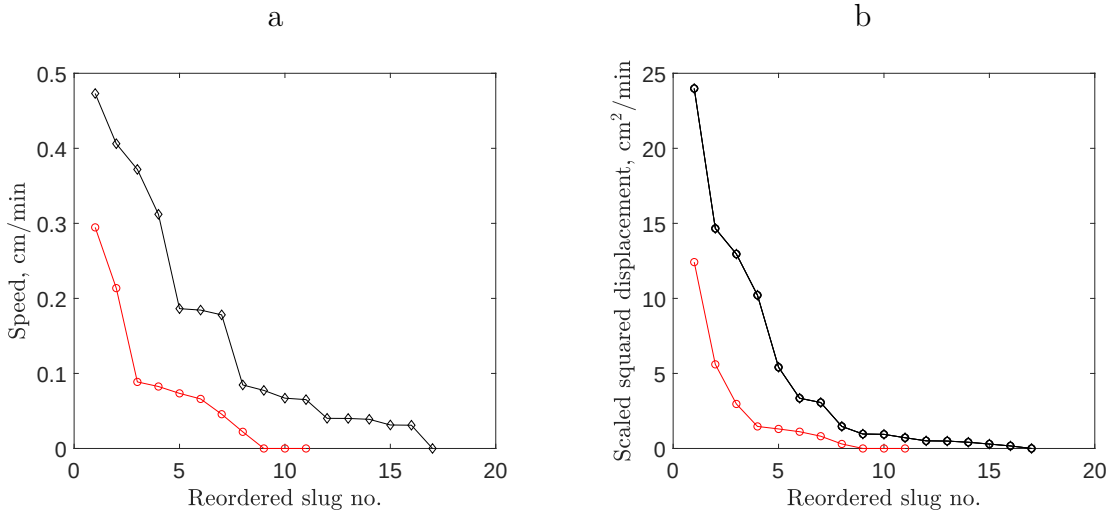

Figure 4.3: (a) Slug average velocities and (b) slug average SSD, black diamonds for the sparse release and red circles for the dense release.

distributed over the whole circle. On the contrary, in the case where a correlation between the movement directions exists (hence resulting in the CRW), the distribution of the turning angle has a peak at zero. This is in agreement with the results of previous studies on animal movement (in particular, invertebrates [116, 144]) as well as a general theoretical argument [196].

In order to provide a more quantitative insight, we look for a functional description of the turning angle distribution using several distributions that are commonly used in movement ecology. The results are shown in Table 4.3. We establish that the turning angle data are best described by the exponential distribution. Somewhat unexpectedly, it outperforms the Von Mises distribution, although the latter is often regarded as a benchmark and its use has some theoretical justification [49]. However, the exponential distribution of the turning angle has previously been observed in movement data on some other species, e.g. on swimming invertebrates [83].

The distribution of turning angles obtained in the case of dense release exhibit different features; see Fig. 4.4(b). In this case, the distribution is not symmetric and has a clear

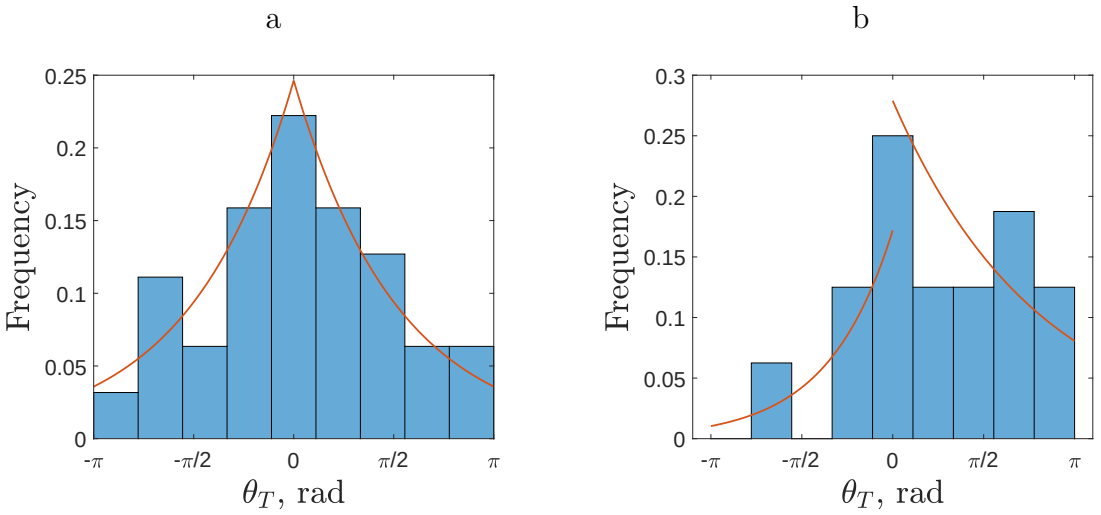

Figure 4.4: Frequency distribution of the turning angle in the case of (a) sparse and (b) dense releases of slugs. In calculating the turning angle, the periods of no movement were disregarded. The red curve shows the best-fitting of the data with the exponential function; see details in the text.

Table 4.3: The R^2 values for the turning angle movement data (in case of sparsely released slugs) described by different standard frequency distributions. The corresponding data are shown in Fig. 4.4(a).

Distribution	Best fit	R^2
Uniform	0.1	< 0.001
Piecewise Linear	$0.205 - 0.0603\|\theta\|$	0.789
Von Mises	$\frac{0.672\exp(0.807\cos(\theta))}{2\pi I_0(0.807)}$	0.766
Power Law	$36.1(4.28 + \|\theta\|)^{-3.39}$	0.785
Exponential	$1.63\exp(-\|\theta\|/0.246)$	0.793

bias towards positive values: the mean turning angle corresponding to the data shown in Fig. 4.4(b) is $< \theta_T >= 0.772 \approx \pi/4$ radians. Since the slugs used in the dense release are from the same cohort as those used in the sparse release, we consider this bias as an effect of the slug density: the movement pattern of an individual slug is affected by the presence of con-specifics. We discuss possible mechanisms of the density dependence in Section 4.5.

An attempt to describe the turning angle data from the dense release by a symmetric distribution returns low values of R^2 (see Table 4.4). However, the accuracy of data fitting comparable with the sparse release can be achieved by using an asymmetric distribution, i.e. where the corresponding function has different parameters for the positive and negative values of the angle. The results are shown in Table 4.5.

Table 4.4: Examples of distributions fitted to the turning angle of all densely released slugs, excluding no movements.

Distribution	Best fit	R^2
Uniform	0.1	2.22×10^{-16}
Piecewise Linear	$0.193 - 0.0537\|\theta\|$	0.391
Von Mises	$\frac{0.670\exp(0.658\cos(\theta))}{2\pi I_0(0.658)}$	0.351
Power Law	$36.0(4.85 + \|\theta\|)^{-3.20}$	0.370
Exponential	$1.92\exp(-\|\theta\|/0.220)$	0.376

The turning angle data shown in Fig. 4.4 were obtained using all active steps along the movement paths. However, since periods of slug movement alternate with periods of

Table 4.5: Examples of asymmetric frequency distributions fitted to the turning angle of all densely released slugs, excluding no movements. The corresponding data are shown in Fig. 4.4(b).

Distribution	Best fit $\theta < 0$	Best fit $\theta > 0$	R^2
Uniform	0.05	0.15	0.348
Piecewise Linear	$0.128 + 0.0448\theta$	$0.259 - 0.0627\theta$	0.750
Von Mises	$\frac{0.351 \exp(1.19 \cos(\theta))}{2\pi I_0(1.19)}$	$\frac{0.990 \exp(0.491 \cos(\theta))}{2\pi I_0(0.491)}$	0.707
Power Law	$185(4.24 + \lvert\theta\rvert)^{-4.78}$	$32.7(5.61 + \lvert\theta\rvert)^{-2.74}$	0.727
Exponential	$0.172 \exp(-\lvert\theta\rvert/1.12)$	$0.279 \exp(-\lvert\theta\rvert/2.53)$	0.734

resting, it may raise the question of the relevance of the turning angle at the locations where slugs remained motionless for some time. In order to check the robustness of our results, we now repeat the analysis to calculate the turning angle differently by omitting the segments adjoined with the rest position. The results are shown in Fig. 4.5. In this case, a reliable fit may not be possible due to there being insufficient data. However, a visual inspection of the corresponding histograms suggests that the main properties of the turning angle distribution agree with those observed above for the bigger data set. Namely, in both cases the distribution has a clear maximum at $\theta_T = 0$ (this is seen particularly well in the case of sparse release). In the case of sparse release the distribution is approximately symmetric, while in the case of dense release there is a clear bias towards positive values. We therefore conclude that the properties of the turning angle distribution are robust with regard to the details of its definition. We note here that the turning angle along with the step sizes provides enough information to analyse individual movement in the random walk framework [64, 113, 116, 235]. The absolute angle may also be used to analyse movement directions [26, 61], but we do not do this here and would expect to reach the same conclusions.

4.3.3 Movement and resting times

Our field data shows that, while foraging, slugs do not move continuously but alternate periods of movement and rest; see the second column in Tables 4.1 and 4.2. Such behaviour

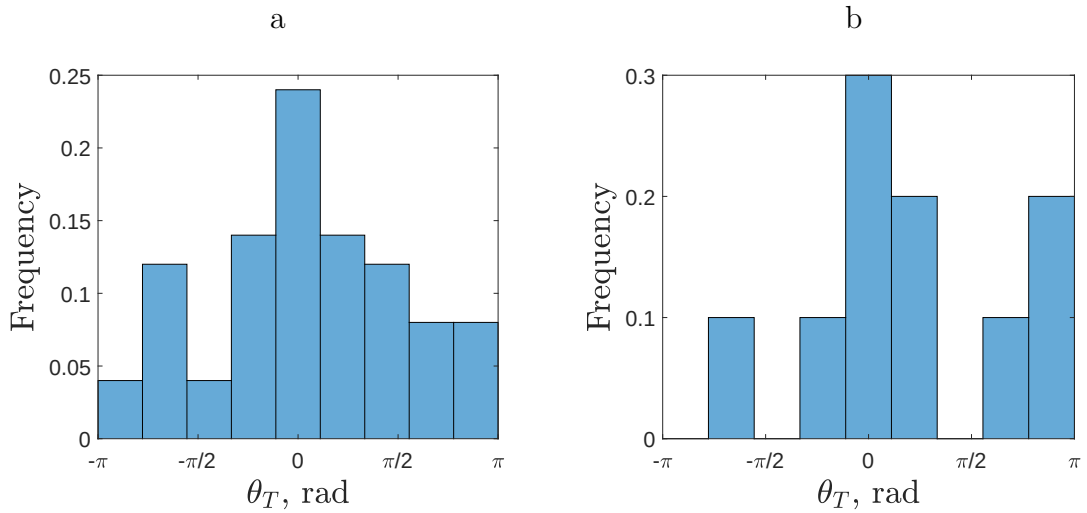

Figure 4.5: Frequency distribution of the turning angle in case of (a) sparse release, (b) dense release. The turning angle is only calculated for consecutive movements, i.e. if a slug does not move during a time step then its previous angle of movement is not used.

is typical of many animal species [144, 240]. In this section, we analyse the proportion of time that slugs spend moving, in particular to reveal the differences, if any, between the sparse and dense release.

Fig. 4.6 shows the corresponding data where for the convenience of analysis the slugs are renumbered in a hierarchical order, so that slug 1 spends the highest proportion of time moving, slug 2 has the second highest, etc. We readily observe that the sparse release slugs tend to move more frequently than those from the dense release treatment: slugs that move for more than half of the total observation time constitute about 50% of the group in the case of sparse release but less than 30% in the case of dense release.

In order to make a more quantitative insight, we endeavour to describe the data using several standard distributions; see Tables 4.6 and 4.7. Figs. 4.7 and 4.8 show, for the sparse and dense release respectively, the description of the data on the frequency of movement with several standard distributions. Interestingly, although the visual inspection of the quality of the data fit may favour either the logistic or the log-Cauchy distribution, we find that the normal distribution performs better than others both in sparse and dense release treatments. Importantly, however, the parameters of the distribution are different

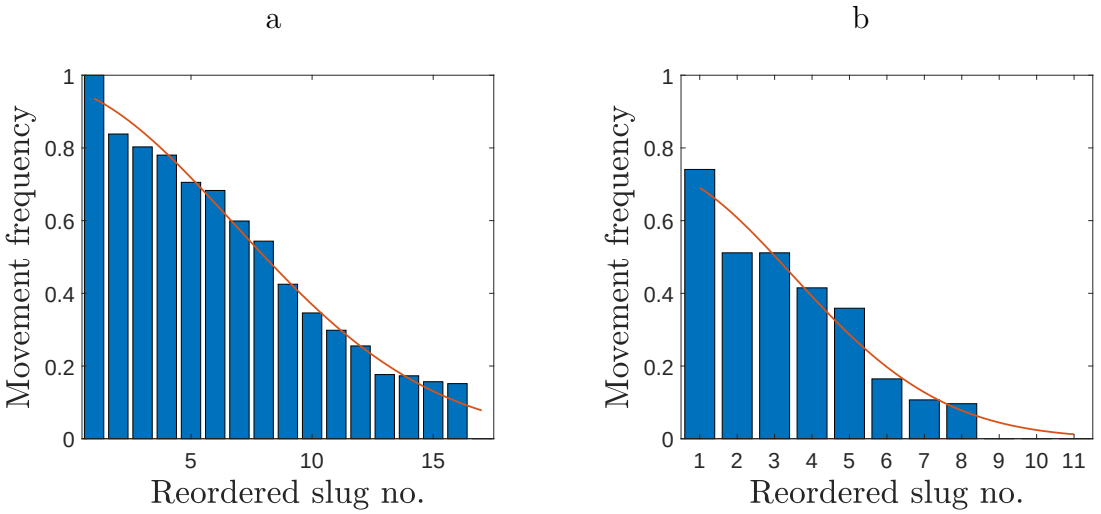

Figure 4.6: Distribution of the proportion of the total time spent in movement in case of (a) sparse release and (b) dense release. The red curve shows the best-fit of the data with the normal distribution; see details in the text.

Table 4.6: The R^2 values for the proportion of movement time described by different standard frequency distributions in the case of sparse release.

Distribution	Best fit	R^2
Linear	$0.994 - 0.0586x$	0.978
Normal	$3.21\frac{\exp(-0.5(x+1.47)^2/(8.21^2))}{8.21\sqrt{2\pi}}$	0.983
Power Law	$13900(20.3+x)^{-3.10}$	0.916
Exponential	$1.18\exp(\frac{-x}{8.37})$	0.945
Cauchy	$\frac{19.0}{6.65\pi}\frac{6.65^2}{(x-1.56)^2+6.65^2}$	0.962
Log-Cauchy	$\frac{13.4}{x\pi}\frac{1.07}{(\ln x-1.92)^2+1.07^2}$	0.977
Weibull	$8.89\frac{1.18}{7.25}\frac{x}{7.25}^{1.18-1}e^{(-(x/7.25)^{1.18}}$	0.971
Logistic	$17.4\frac{\exp(-(x-0.189)/4.66)}{4.66(1+\exp(-(x-0.189)/4.66))^2}$	0.980

between the two cases; in particular, the standard deviation appears to be approximately twice as large in the case of sparse release. Arguably, it confirms the above conclusion that slugs move more frequently or for longer in the case of sparse release. Slugs released as a group tend to spend considerably more time at rest compared to the slugs released individually.

To avoid a possible bias due to the different group size (17 slugs in the sparse release and 11 in the dense release), we now rearrange the data in terms of the proportion

Table 4.7: The R^2 values for the proportion of movement time described by different standard frequency distributions in the case of dense release.

Distribution	Best fit	R^2
Linear	$0.710 - 0.0743x$	0.930
Normal	$1.12\frac{\exp(-0.5(x+0.573)^2/(4.03^2))}{4.03\sqrt{2\pi}}$	0.966
Power Law	$42500(12.1+x)^{-4.24}$	0.910
Exponential	$0.998\exp(\frac{-x}{3.68})$	0.933
Cauchy	$\frac{6.79}{3.12\pi}\frac{3.12^2}{(x-0.932)^2+3.12^2}$	0.925
Log-Cauchy	$\frac{5.22}{x\pi}\frac{1.13}{(\ln x-1.21)^2+1.13^2}$	0.928
Weibull	$3.30\frac{1.25}{3.53}\frac{x}{3.53}^{1.25-1}e^{(-(x/3.53)^{1.25}}$	0.953
Logistic	$6.46\frac{\exp(-(x-0.232)/2.27)}{2.27(1+\exp(-(x-0.232)/2.27))^2}$	0.958

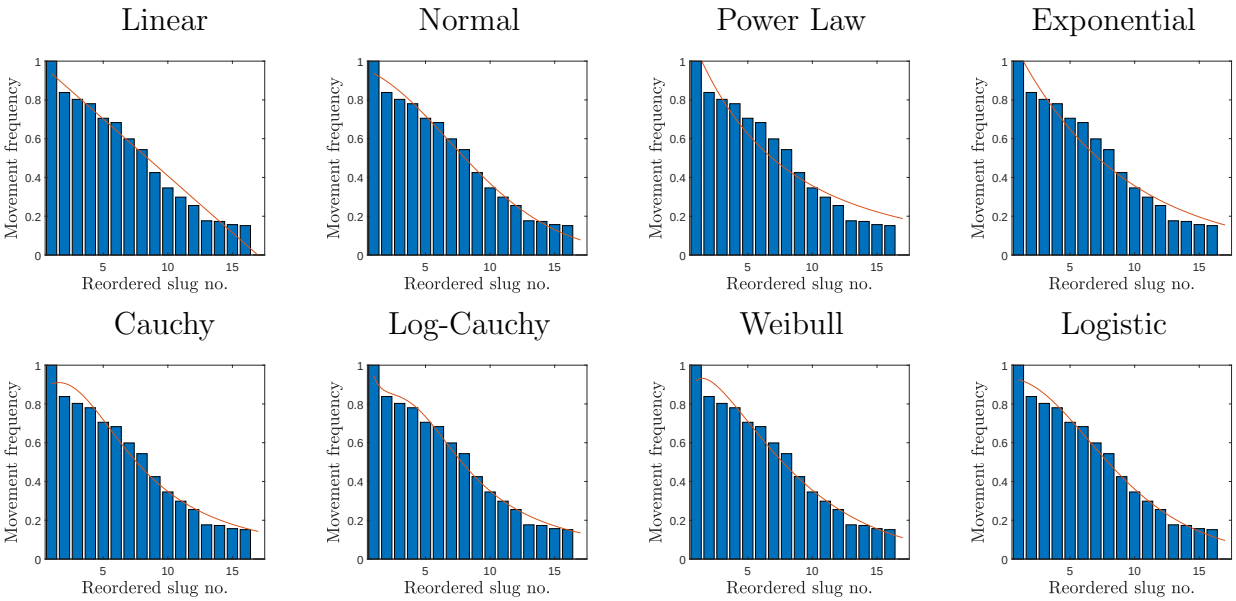

Figure 4.7: Distribution of the proportion of the total time spent in movement in the case of sparse release. The red curve shows the best-fitting of the data with various standard distributions (as in the figure legend). The corresponding values of R^2 (quantifying the quality of fit) are shown in Table 4.6 in the main text.

of the group that moves with a given frequency. The results are shown in Fig. 4.9. Although the amount of data in this case does not allow us to describe them using a particular function, the two cases clearly exhibit distributions with different properties. In particular, the average movement frequency is 0.467 for the sparse release and 0.264 for the dense release, and the corresponding variances are 0.090 and 0.065, respectively.

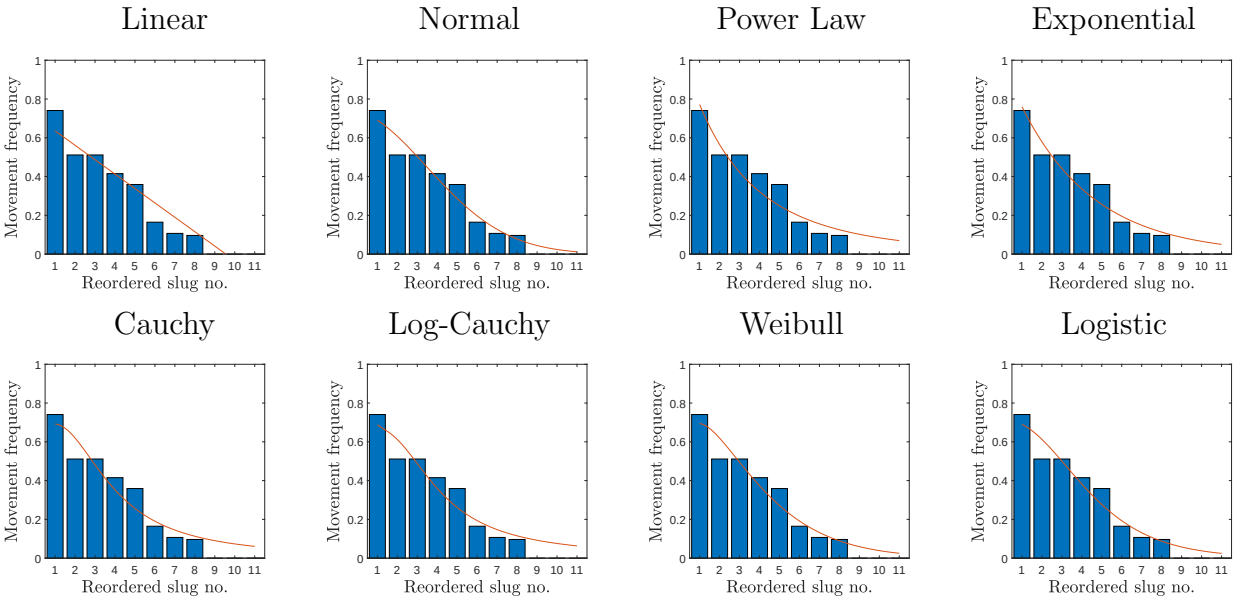

Figure 4.8: Distribution of the proportion of the total time spent in movement in the case of dense release. The red curve shows the best-fitting of the data with various standard distributions (as in the figure legend). The corresponding values of R^2 (quantifying the quality of fit) are shown in Table 4.7 in the main text.

To further quantify the differences, Fig. 4.10 shows the number of slugs moving in each observation interval. Once again, we observe that the graph exhibits essentially different properties between the two releases. In particular, over the first interval, the majority

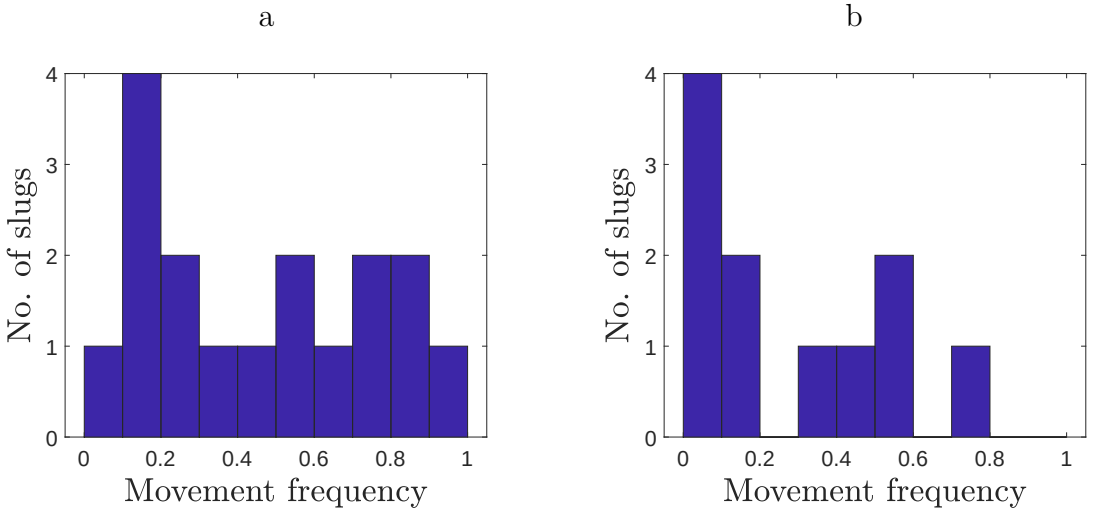

Figure 4.9: Distribution of the movement frequencies in case of (a) sparse release and (b) dense release.

of slugs (14 out of 17) move in the case of sparse release but none of the slugs move in the case of dense release. In the second half of the observation time (intervals 6-10) on average about 50% of slugs (8 out of 17) move in the case of sparse release but only about 25% of slugs (2-3 out of 11) move in the case of dense release.

Based on the differences between the two releases, we conclude that the presence of con-specifics is the factor that affects the distribution of slug movement time. Thus, along with the results of the previous sections, it suggests that slug movement is density-dependent.

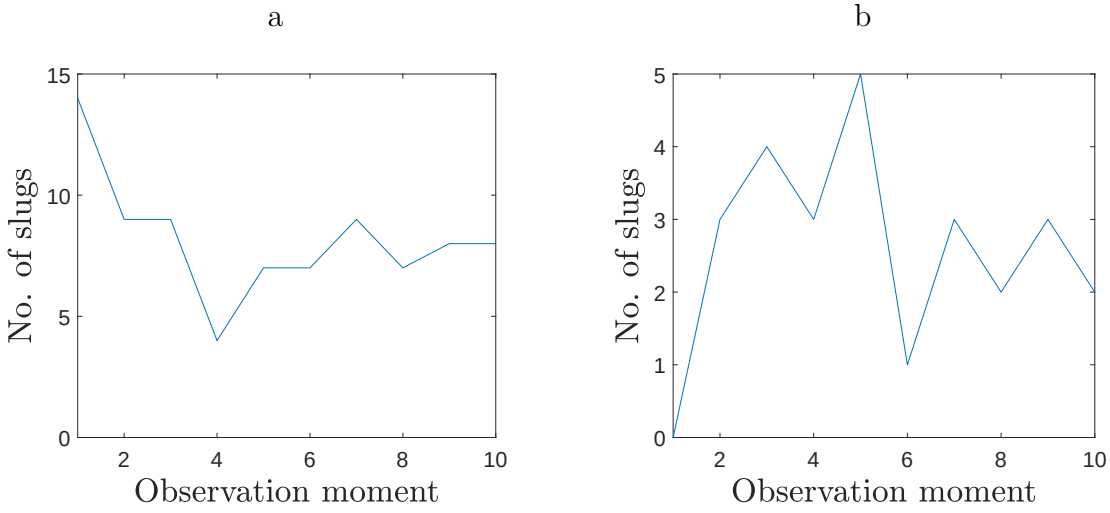

Figure 4.10: The number of moving slugs at each observation moment in case of (a) sparse release and (b) dense release.

4.4 Rate of spread

It is a generic property of animal movement, especially during foraging, that individuals tend to move away from their original position - in our experiment, their release point. For many theoretical and practical reasons, assessment of the 'rate of spread' is often required (the rate at which the animals move away), e.g. by estimating the dependence of their mean squared displacement (MSD) on time. In this section, we analyse the rate of spread using different approaches to further investigate the differences in movement

between the sparse release and the dense release.

4.4.1 Mean squared displacement

When analysing patterns of individual animal movement, a key question is how far the animals can spread over a given duration of time. In case of a random movement (see [235] for the discussion of the "bugbear of randomness"), the rate of spread is conventionally quantified by the dependence of the mean squared displacement (MSD) on time.

Once sufficient data is available for the distribution of the turning angle and the displacement per unit time for an individual animal, its MSD can be predicted using the Correlated Random Walk (CRW) framework [116, 235]. However, that would require a much larger amount of individual movement data than is available from our field experiment. We therefore have to pool the data from several individual slugs. We readily observe (Fig. 4.11) that the CRW predicts a faster rate of displacement in the case of sparse release. We also observe that the theoretical prediction (shown by the red line) is in good agreement with the data on the average slug displacement over the first 200 minutes of slug movement. However, the variance of the actual slug position grows rapidly with time: starting from approximately 150-200 minutes after release, it becomes so large that the prediction has little practical value.

One reason for the large variance of the calculated MSD is that there is considerable variability between the movement behaviour of different individual slugs, e.g. in terms of their mean velocity (see Tables 4.1 and 4.2). In order to minimize the effect of individual differences while maintaining a sufficient volume of data for the analysis, we now quantify the rate of spread by analysing the data on the Scaled Squared Displacement (SSD) from slugs that show similar movement properties.

A well established theory [49, 235, 245] suggests that the MSD should follow the power law, which we scale by the duration of the corresponding time interval, hence to obtain

the Scaled Squared Displacement (SSD):

$$\frac{|\Delta \mathbf{r}|^2}{\Delta t} \sim (\Delta t)^{\gamma-1}, \tag{4.4.1}$$

where the exponent γ depends on the movement type, i.e. $\gamma = 1$ in case of the diffusive movement [115, 235] and $\gamma > 1$ in case of a faster movement which is often referred to as "superdiffusive" if $1 < \gamma < 2$, ballistic if $\gamma = 2$ and "superballistic" if $\gamma > 2$. The case of slower spread with $0 < \gamma < 1$ is called the "subdiffusive" movement.

It is useful to comment on the geometry of the corresponding graph. It is readily seen that the graph of relation (4.4.1) is given by a straight line for the ballistic case $\gamma = 2$, a convex curve for the superdiffusive case $1 < \gamma < 2$ and a concave curve for the superballistic if $\gamma > 2$.

We begin with the case of sparse release. Fig. 4.12(a) shows the cumulative data for the SSD for slugs 3 and 4, which have very similar values of mean velocity (see Table 4.1). (We mention here that, where possible, one should avoid pooling together movement data of individuals with different movement characteristics as such pooling may lead to unrealistic, superficial results, e.g. see [183].) We readily observe that the 'cloud' of data points has a clear maximum at intermediate values of Δt. This does not fit into the standard theoretical framework that predicts the SSD to be a monotonously increasing function of time as discussed above. It indicates that the SSD over the entire range cannot be linked to a single movement behaviour. We therefore assume that the slug movement occurs as a result of the interplay between two different movement behaviours, one prevailing at smaller time intervals (e.g. the CRW) and the other one prevailing at larger time intervals. Correspondingly, we endeavour to describe the SSD data by a piecewise function that is an increasing function at smaller time (on the left of the dashed vertical line) and a decreasing function at larger time (on the right of the dashed vertical line). Following the established theory discussed above [49, 245], we describe the SSD by

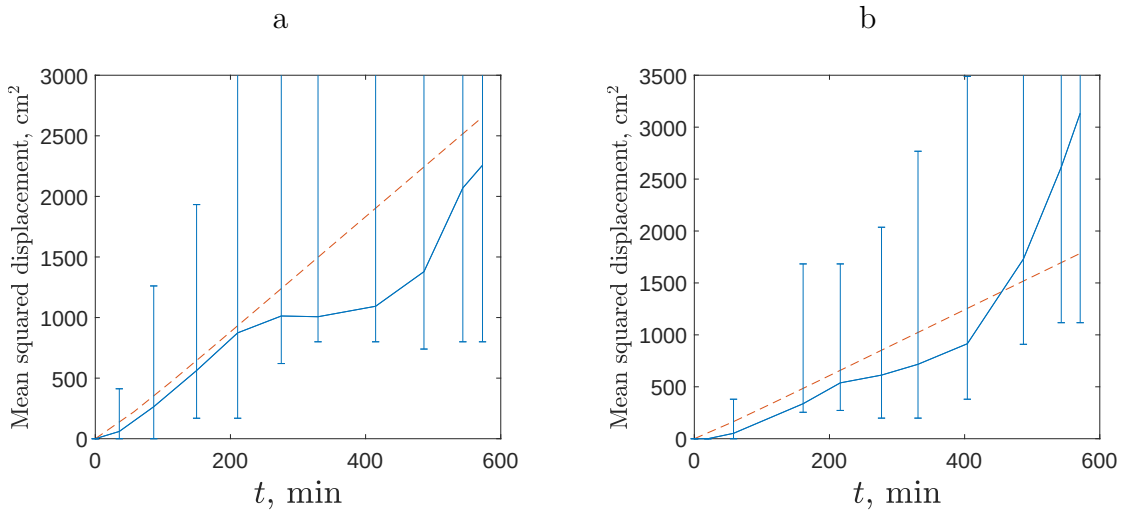

Figure 4.11: Mean squared displacement vs time averaged over all slugs in case of (a) sparse release and (b) dense release. Blue solid line shows the data, the red dashed line shows the theoretical prediction. The vertical lines show the actual range for the position of individual slugs from the field data

the power law.

We readily observe from Fig. 4.12(a) that the SSD is a rapidly increasing function of time (much faster than linear), suggesting that slug movement on this short timescale

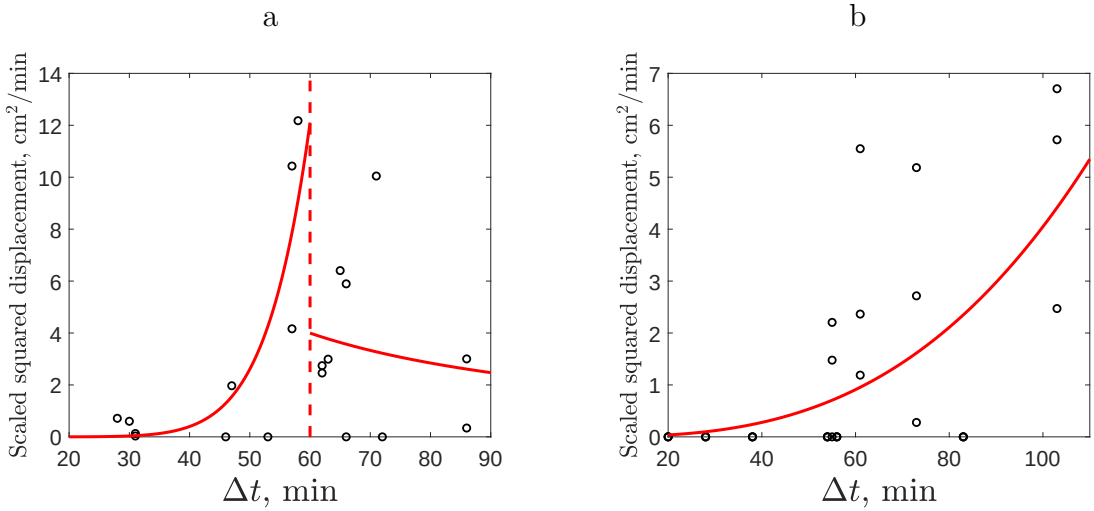

Figure 4.12: Values of the Scaled Squared Displacement vs time. (a) Data for slugs 3 and 4 in the sparse release (see Table 4.1) and its best fitting by the piecewise power law (red curve) with $1.01 \cdot 10^{-16} \cdot (\Delta t)^{9.62}$ for $27 < \Delta t \leq 60$ and $508 \cdot (\Delta t)^{-1.18}$ for $60 < \Delta t \leq 87$, $R^2 = 0.513$. (b) Data for slugs 3, 6 and 7 in the dense release (see Table 4.2) and its best fitting by the power law (red curve) with $5.81 \cdot 10^{-6} \cdot (\Delta t)^{2.92}$, $R^2 = 0.394$.

can be classified as "superdiffusive" or even "super-ballistic" [121, 245]. The CRW with the properties of superdiffusive movement has previously been observed for some other invertebrate species [200]. For larger time intervals, slugs movement slows down. Our results show that the dependence of the SSD on time is then well described by a power law with a negative exponent. Arguably, it suggests the "subdiffusive" movement pattern [245]. We hypothesize that this might be a manifestation of homing behaviour. Although evidence for homing behaviour in slugs is scarce [84, 203], it is well established in some other ground-dwelling invertebrates species, e.g. see [63] and references therein. We will further discuss this issue in Section 4.5.

Interestingly, the data distribution of SSD in the case of dense release exhibits considerably different properties. Figure 4.12(b) shows the pooled data from slugs 3, 6 and 7. We readily observe that in this case the data are not peaked at the intermediate time but show a clear trend to increase. There is no indication of slowing down at the longer timescale and the best fitting is achieved by a simple power law (red curve) with the exponent larger than 2, thus suggesting superdiffusive movement over the entire observation time.

The reason for using a piecewise curve is that visual inspection of the data points in 4.12(a) indicates that a single power law curve would not be a suitable fit. We suggest that the data could be fit by two power law functions, indicating different types of movement on different time scales and trial different junction points, which we label α, that appear close to the peak. However, this increases the number of parameters fitted to the data, which introduces the danger of overfitting [94]. To justify this option, we calculate the Akaike Information Criterion (AIC). AIC is a statistical measure, used for comparing models which takes into account the number of parameters of the model [3]. The best model for approximating the data is the one with the lowest AIC value. AIC is defined as

$$\mathrm{AIC} = 2k - 2\log L, \tag{4.4.2}$$

Table 4.8: A piecewise power law function fitted to $(\Delta x)^2/\Delta t$ plotted against Δt for sparsely released slugs 3 and 4. The two values of R^2 are for each section of the fit.

α	$x < \alpha$	$x > \alpha$	R^2	AIC_C
55	$0.0633x^{0.566}$	$4.32 \times 10^{8}x^{-4.41}$	0.012, 0.248	112
57	$1.10 \times 10^{-14}x^{8.40}$	$1.67 \times 10^{10}x^{-5.28}$	0.623, 0.215	113
60	$1.01 \times 10^{-16}x^{9.62}$	$508x^{-1.18}$	0.754, 0.026	110
63	$8.20 \times 10^{-5}x^{2.68}$	$1.43 \times 10^{6}x^{-3.01}$	0.263, 0.103	119
65	$6.09 \times 10^{-5}x^{2.76}$	$4.51 \times 10^{4}x^{-2.22}$	0.303, 0.049	119
70	$8.30 \times 10^{-4}x^{2.08}$	$8.43 \times 10^{12}x^{-6.58}$	0.214, 0.243	119

where k is the number of parameters and L is the maximum of the likelihood function for the model [163]. As the sample size is small in our data set, an adjusted measure, AIC_C, is required to prevent overfitting [34],

$$\text{AIC}_C = \text{AIC} + \frac{2k^2 + 2k}{n - k - 1}, \tag{4.4.3}$$

where n is the number of data points. The best fitting continuous power law curve is $(\Delta x)^2/\Delta t = 0.098(\Delta t)^{0.869}$ with $R^2 = 0.077$ and $\text{AIC}_C = 113$. This is higher (and therefore a worse model) than the best fitting piecewise function as $\text{AIC}_C = 110$ when $\alpha = 60$. This shows that when accounting for the extra parameters, the piecewise curve is still a better fit than a single power law curve for the scaled squared displacement over time. To be thorough, Fig. 4.13 shows the results of fitting the values of SSD obtained in the case of sparse release by a piecewise power law subject to different values of α. The corresponding values of R^2 and AIC are shown in Table 4.8. It can be seen that a different choice of α with an adequate fit would not change our conclusions.

Note that strictly speaking relation (4.4.1) is only valid in an idealized case where the turning angle is distributed uniformly over the circle, i.e. there is no correlation between any two consequent movements along the path. A more realistic case is given by the Correlated Random Walk (CRW) where the distribution of the turning angle is lumped around the movement direction during the preceding interval [116]. In the case of

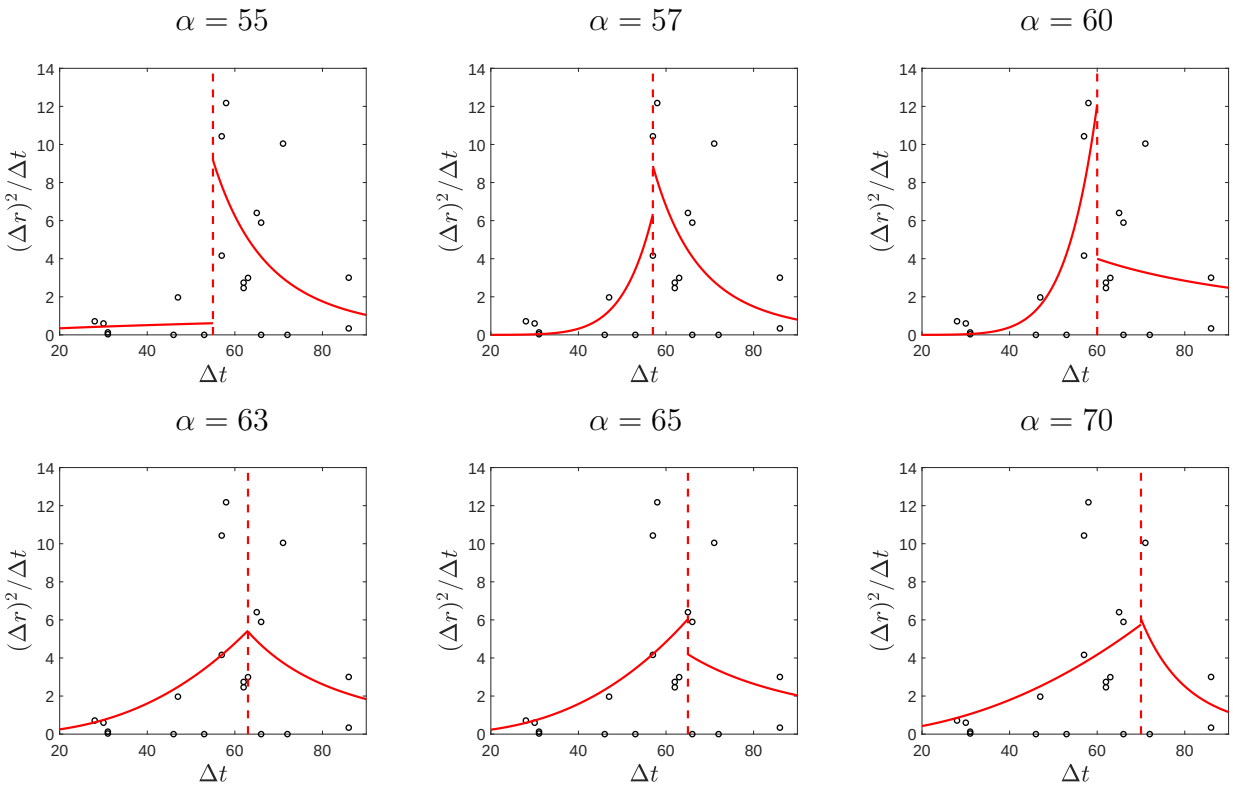

Figure 4.13: $(\Delta x)^2/\Delta t$ plotted against Δt for sparsely released slugs 3 and 4, fitted with a piecewise linear function which is split at α.

equidistant observation moments (i.e. a constant time step), the dependence of the MSD on the number of steps n along the movement path is given by the following equation [116]:

$$|\Delta\mathbf{r}|^2(t) \quad = \quad \langle l^2\rangle n + \frac{2c\langle l\rangle^2}{1-c}\left(n - \frac{1-c^n}{1-c}\right) \qquad \text{where} \qquad n = \frac{t}{(\Delta t)_0}. \qquad (4.4.4)$$

Here $(\Delta t)_0$ is the duration of (fixed) time step and $\langle l\rangle$ and $\langle l^2\rangle$ are, respectively, the mean and the variance of the step size distribution (assuming that they exist, which implies a thin-tailed distribution of the step size [49]) and c is the mean value of the cosine of the turning angle. If the turning angles were distributed uniformly over the circle, i.e. $c = 0$,

expression (4.4.4) turns into

$$|\Delta\mathbf{r}|^2(t) \;=\; \langle l^2\rangle n \;\sim\; t, \tag{4.4.5}$$

which corresponds to $\gamma = 1$ in (4.4.1) and hence to the case of diffusive spread.

In the general case $c \neq 0$, expression (4.4.4) describes the movement that in the course of time slows down from the almost ballistic movement $|\Delta\mathbf{r}|^2 \sim t^2$ to the diffusion motion $|\Delta\mathbf{r}|^2 \sim t$ [49]. Indeed, it is readily seen that

$$|\Delta\mathbf{r}|^2 = \langle l^2\rangle n + \frac{2c\langle l\rangle^2}{1-c} \sim n \sim t, \tag{4.4.6}$$

for a large number of steps n, and therefore the walk becomes diffusive in the long term. In order to obtain the expression for small number of steps, for the sake of simplicity let us consider the case with a high directional persistence, so that $c = 1 - \delta$ where $\delta \ll 1$. Then

$$1 - c^n = 1 - (1-\delta)^n \approx n\delta - \frac{1}{2}n(n-1)\delta^2 \tag{4.4.7}$$

(omitting terms containing higher orders of δ) so that Eq. (4.4.4) becomes

$$|\Delta\mathbf{r}|^2 = n\langle l^2\rangle + \langle l\rangle^2(1-\delta)n(n-1) \sim n^2 \sim t^2. \tag{4.4.8}$$

Therefore, the graph of the SSD in the case where the animal performs the CRW is also given by a concave curve but with slopes different from the one predicted by Eq. (4.4.1). Thus, should one of them provide a better description of the data than the other one, that should allow us to identify the corresponding movement pattern, e.g. CRW vs super-ballistic. However, the concavity of the graph may be difficult to observe if c is not close to one.

4.4.2 Size and area of the patch

It is well established that in their natural environment, the spatial distribution of the grey field slug is heterogeneous, forming patches of high population density separated by areas with low population density [78, 180]. In applications, e.g. for efficient pest management which is our motivation for this study, it is important to understand how one can determine the patch location, how its boundary can be determined [178, 185] and how fast patches evolve with time. There is considerable field evidence that patches of high slug density are stable in time, at least within a given season [78, 180]. In addition, there are many theoretical results showing that density-dependent individual movement is a factor that can increase patch stability and even lead to patch (cluster) formation [68, 97, 136, 238]. Correspondingly, in this section we analyse the field data on slug movement in the context of patch dynamics.

The 'patch' can be defined in several different ways. We notice here that, while a

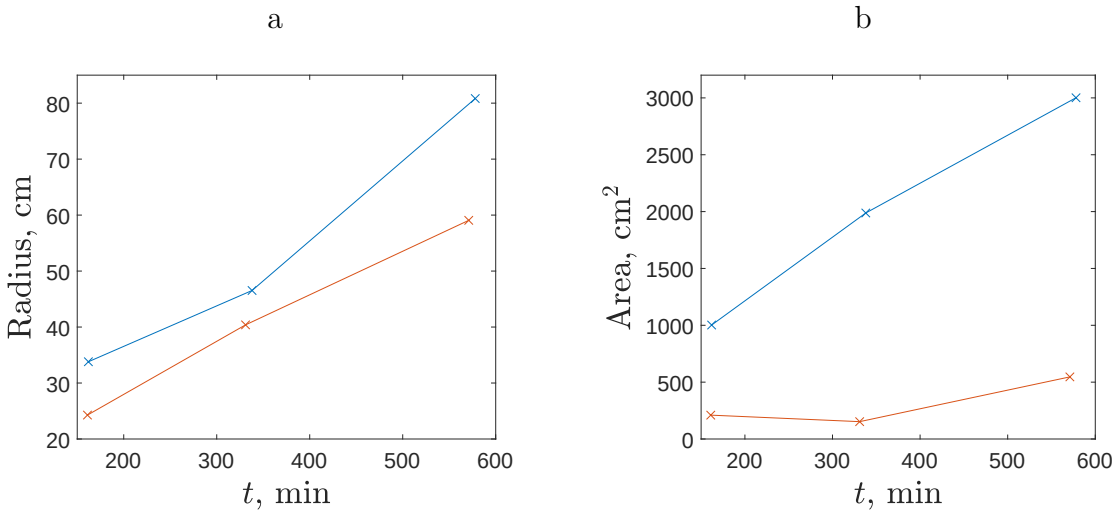

Figure 4.14: The radius (a) and the area (b) of the slug "patch" (cluster) shown after 4, 7 and 11 time steps as the time that the data was recorded are approximately the same for both sparse and dense releases. In (a), the patch is defined as a circle that envelopes the closest 90% of slugs to the origin, its radius thus being the distance of its farthest slug. In (b), in order to calculate the area the convex hull of the closest 90% of slugs was used. Blue and red colours are for the sparse and dense releases, respectively.

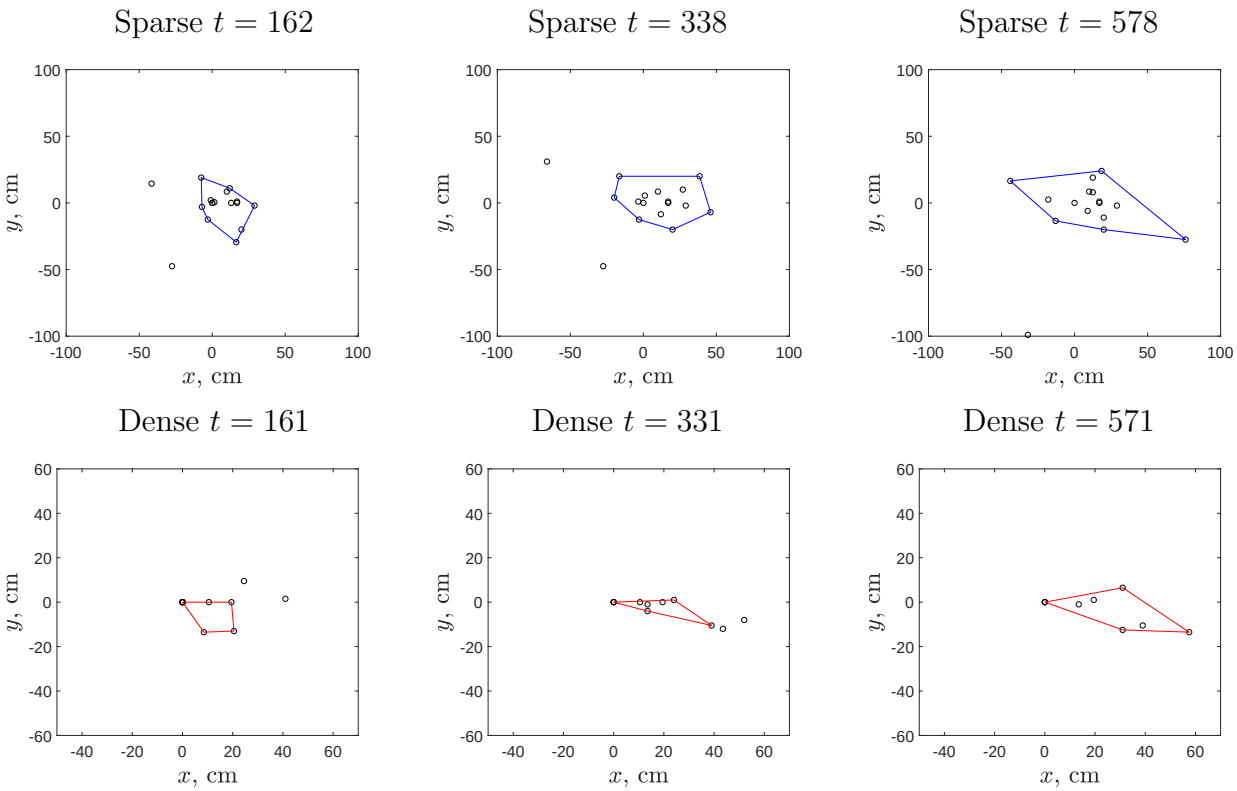

Figure 4.15: The slug patch (as defined by the convex hull that envelopes 90% of slugs closest to the origin) at different sequential time points after (top) sparse and (bottom) dense release. The time (in minutes) corresponds to time steps 4,7 and 11 used in Fig. 4.14.

considerable proportion of the slug population is found in high-density patches, a (small) number of slugs can usually be found in the areas between the patches, although it remains unclear whether it is a result of a different movement behaviour (e.g. with a lesser strength of density dependence) or a random fluctuation. We therefore define the patch as the area that contains approximately 90% of the total number of slugs released in the given experiment.

In the case of dense release, the above definition can be applied straightforwardly; see the red line in Fig. 4.14(a). In sparse releases, the patch is virtual rather than real: in order to make the results comparable between the two releases, the start point for each individual movement path is translated to a common origin. The radius of the corresponding virtual patch vs time is shown in Fig. 4.14(a) by the blue line. We readily

observe that the patch grows faster in the case of sparse release.

Apart from the size of the high density patch, as is quantified above by its radius, another important aspect is its shape. Indeed, the radius is not sufficient if the patch shape significantly deviates from the circle, e.g. is elongated: in this case, the same population can be spread over much larger distances. To take the effect of shape into account, arguably the area occupied by the patch should be considered along with the patch size.

In the light of the above, we analyse what is the patch shape and how it develops in time following sparse and dense releases. The results are shown in Figs. 4.14(b) and 4.15. We observe that the shape is similar in the two treatments. However, the difference between the two releases in terms of the area of the patch is clear, with the area growing considerably faster in the case of sparse release.

4.5 Discussion

A good understanding of the individual movement factors that determine the spatial distribution of invertebrates in their natural environment is needed for various purposes. Other than for pest management, which is our motivation for this work, it is also necessary in the conservation of endangered species for example. Density-dependent individual movement is one such factor as it is known to contribute to the formation of pronounced spatial heterogeneity and to the temporal stability (i.e. persistence over long periods of time) of patches of high population density. The existence of density dependence, although obvious in some species (e.g. through the formation of swarms) may be difficult to detect in other species, especially where the 'sociality' resulting in animal grouping is missing. In Chapters 2 and 3 we discuss an alternative mechanism that results in patch formation, auto-taxis, where density-dependent individual movement is more likely to be in the direction of higher population density. However, in spite of the well developed theory, auto-taxis is difficult to identify in field data and there are only a few cases where

its existence has been unambiguously proven.

In this chapter, the aim was to investigate the existence of density-dependence in the movement of the grey field slug. Slugs were radio-tagged and their movement tracked in a field experiment with two different treatments, i.e. following release as either a group (dense release) or with individuals placed far away from each other (sparse release) so that they were unlikely to encounter each other for the duration of the experiment. Slug movement data was analysed using the discrete-time random walk framework [49, 64, 235, 257] that parameterises the movement with frequency distributions for its three essential components: the step size, the turning angle, and the proportion of movement/resting time.

Our analysis reveals that the properties of all three movement components are significantly different between the sparse and dense releases, with the general tendency that slugs move faster and longer distances in the case of sparse release, i.e. in the absence of the con-specifics in their vicinity. We have further confirmed it by estimating the rate at which the 'patch' (the area containing 90% of the group) grows with time. Consistently with the above, we obtained that the patch grows faster in the case of sparse releases. Arguably, this result has an immediate interpretation that density-dependence has a positive effect on the stability of slug patches.

A question may arise here as to why slugs move faster and longer distances in the case of sparse release. As a probable answer, the reduced encounter rate with conspecifics or signs of conspecifics (e.g. chemical signals, slime trails, etc.) may result in movement being interrupted less often and contribute to a lower turning frequency (the latter linearising the track), in combination resulting in a greater rate of displacement. This may result in more rapid displacement between than within patches.

One of the interesting findings of our study is the strongly biased distribution of the turning angles observed in the case of dense release. Although our data do not allow for the identification of the corresponding movement behaviour, candidate contributory

mechanisms are known from the literature. It has previously been shown that the grey field slug is able to re-locate refuges from distances of 1m or even larger [203], and that some slug species (e.g. the pulmonate slug *Limax pseudoflavus*) follow the slime trails of their con-specifics [52]. The use of chemical information has also been shown to influence homing in two pulmonate slugs [51, 84]. In the case of the grey field slug, trail following has been recorded but occurs less frequently (8% of trail encounters) and is only exhibited when reproductively active, a small part of their lifetime [252]. Our results, however, indicate that, in spite of its relatively low frequency, the slime trail following, and possibly chemical signals, may be factors contributing to the turning angle bias. Indeed, in the case of dense release, fresh trails are abundant within a small area and even a relatively small proportion of the tailgating slugs can result in a noticeable bias in the turning angle distribution. Note that the persistent bias in the turning angle suggests that the corresponding movement paths are spiral-like, This, in turn, may result in increased cohesion of high density patches: indeed, a slug moving along a spiral would remain in the vicinity of the patch for a much longer time (see Fig. 4.16).

We have also shown that the presence of con-specifics has a more subtle effect on the individual movement by changing the way in which the SSD depends on the duration of the movement interval: the SSD is a monotonously increasing function of time in the case of dense release but a non-monotonous hump-shaped function in the case of sparse release. This may indicate that, in the absence of con-specifics, the individual slug movement behaviour is timescale dependent.

On the small timescale, slug movement occurs faster than is predicted by the standard Brownian (diffusive) motion. The question however remains whether this faster movement occurs because of the correlation between subsequent steps as described by the CRW or the movement is of a different type, i.e. superdiffusive or even superballistic (see Eqs. (4.4.1 and (4.4.4)). To answer this question, we compare the quality of data fitting provided by the power law with different exponents. Recall that, while the range of exponent values

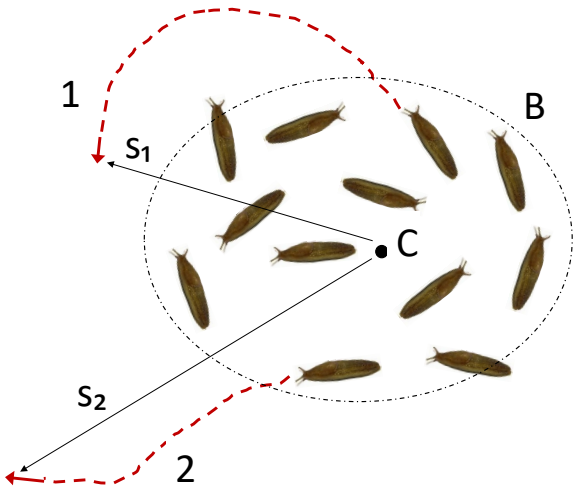

Figure 4.16: Sketch of the effect of animal movement path's geometry on the patch temporal stability. Here point C is the centre of the patch, B is the hypothetical patch boundary, lines 1 and 2 are two movement paths with different properties, and s_1 and s_2 are the distance from the patch centre after a given time. For approximately the same distance travelled along the path, a slug that moves along a spiral-like path (line 1) will on average remain significantly closer to the patch centre (note $s_1 < s_2$) and/or to the patch boundary than a slug that moves along an approximately straight line (line 2).

for the SSD dependence on time is the same for the CRW and for the superdiffusive movement, i.e. between 0 and 1 (cf. Eq. (4.4.1) with $1 < \gamma < 2$ and Eqs. (4.4.6–4.4.8)), for the superballistic movement the exponent is larger than 1. Our results (see Fig. 4.12) show that the exponent is consistently larger than 2, which leads us to the conclusion that, on the shorter time scale, slugs display superballistic movement.

This conclusion about superballistic movement (often referred to in the literature as the Lévy walk) is in good agreement with some other studies on invertebrates. In particular, the Lévy walk type movement was observed in mud snails [126] and Drosophila larvae [216]. Interestingly, a study on the movement behaviour of walking Tenebrio beetles [200], while observing a superballistic movement, concluded that the correlated random walk can produce a movement pattern indistinguishable from the Lévy walk. An unambiguous identification of the movement pattern requires the movement data from multiple temporal scales as the pattern can be scale dependent, e.g. being superballistic at small

scales but slowing down to diffusion at large temporal scales [58, 231]. Such slowing down can happen due to different mechanisms, e.g. as a behavioural response to meeting con-specifics [58] or due to the inherent effect of the environmental friction [231]. Here we hypothesize that slowing down of slug displacement (as observed in the case of the sparse release, see Fig. 4.12(a)) can also result from the homing behaviour. Alternatively, a well developed theory [198] in agreement with some empirical studies [109, 156] predicts that the Lévy walk type movement can arise as the asymptotical regime of the composite random walk when the scales involved are sufficiently broad to allow for the excitation of a large number of elementary movement modes. Therefore, although our study indicates the superballistic movement of slugs at a small timescale (one day), further investigation is needed to reveal the movement properties on a larger timescale (e.g. weeks or months).

In summary, using a novel combination of mathematical and biological techniques to investigate the effect of slug population density on their locomotory behaviour, in our study we have found that all components of the slug movement (mean speed, turning angles and movement/resting times) exhibit significantly different properties in the cases of sparse and dense releases. As a result, the slugs released as a group dispersed more slowly than those released individually. In particular, the turning angle of those released as a group (dense release) displayed a clear anticlockwise bias. This clearly suggests that the density is a factor regulating slug movement in the agricultural environment. While the dense release included eleven tagged individuals, however, there was only one group. Further work is therefore required to confirm these preliminary findings, which may provide an insight into the behavioural mechanisms underpinning the stability of the high density patches that are a feature of their recognized heterogeneous distribution in arable fields.

In Chapter 5, we use the results from this study to model a population with density-dependent movement parameters to determine whether this behaviour can lead to stable patch formation. Knowledge of patch stability would facilitate the targeting of pesticide

applications to discrete areas of the field, thus providing an approach to more sustainable slug control. Although the scales of movement analysed in this chapter are much smaller than that of an arable field which can cover hundreds of metres, the influence of density-dependence on small scale individual movement can be important for patch stability over large time and spatial scales. Over larger time intervals than covered in this chapter, slugs that are within a patch will not move far, as has been shown in previous experiments [80]. We would expect slugs in areas of low population density to either find a patch or be more likely to move much larger distances across the field, as 20% of slugs were found to do in previous studies [80]. Possible methods for pesticide targeting assuming the existence of patches with temporal stability are discussed in Chapter 6.

Chapter 5

A Model of Density-Dependent Individual Movement Informed by Experimental Data

5.1 Introduction

The analysis of tracking data from grey field slugs in Chapter 4 has shown clear evidence that individual slug movement is density-dependent. It is possible to use these results to develop further the individual based model, discussed in Chapters 2 and 3, towards a realistic approximation of slug movement in a field. Although the data did not allow us to determine whether the direction of slug movement changes in the way we have modelled it in previous chapters, our data analysis does provide substantial information that can be used to determine other characteristics of individual movement in the model.

We have shown in Chapters 2 and 3 that density-dependence influencing the direction of movement can produce clusters of high population density. Pattern formation has also been previously shown to occur when the direction of movement is random but the average speed of animals is density-dependent [135, 136]. This suggests that variations in movement features discussed in Chapter 4, such as the movement frequency and turning

angle, may also have the potential for producing patterns in population density. This can be tested through the construction of an IBM, incorporating the results from the previous chapter, where individual movement characteristics will change depending on the local population density.

In this chapter we examine the population distributions that emerge when we model two types of movement: 'sparse' movement based on the data from sparsely released slugs that we use to approximate how slugs move when they are not in a cluster, and 'dense' movement that we use to approximate how slugs move within a cluster. The purpose of study in this chapter is to determine whether patterns will form in the population, what conditions are required for this to occur and whether they remain stable over long time periods. While we do not attempt to analyse the characteristics of patterns, we do determine whether patches form and if so, whether they persist over long time intervals. Detailed discussion of slug patches found in experimental data can be found in Chapter 6.

5.2 Model description

The velocity distribution, turning angle distributions and movement ratio from the two datasets are used to fit our parameter values (see Sections 4.3.1, 4.3.2 and 4.3.3 respectively). Unlike the models discussed in Chapters 2 and 3, we do not include a probability of directed movement, as that information is already expressed in the distribution of turning angles. We aim to determine whether the two types of movement alone can lead to the formation of clusters.

As in Chapter 3, the location of the n_{th} animal at time t is given by $(x_n(t), y_n(t))$. The position at time $(t+1)$ is then simulated as

$$(x_n(t+1), y_n(t+1)) = (x_n(t) + \Delta x, y_n(t) + \Delta y), \tag{5.2.1}$$

where $\Delta x,\ \Delta y$ are the spatial increments that the animal moves in the x and y direction respectively during the time increment $\Delta t = 1$. The movement of animal n starts from an initial position $(x_n(0), y_n(0)) = (x_{n,0}, y_{n,0})$.

We consider the radial distance $\Delta r = \sqrt{(\Delta x)^2 + (\Delta y)^2}$ that an animal will move during one time step and the direction θ in which the step is made. As we are concerned with variation in turning angle as discussed in Section 4.3.2, the angle of movement at the time step $[t,\ t+1]$ is calculated as $\theta(t+1) = \theta(t) + \theta_T$ where $\theta_T \in [-\pi, +\pi]$ is the turning angle. Then the change in x and y of the position of an individual at any given time step is given by

$$\Delta x = (\Delta r)\cos(\theta), \quad \Delta y = (\Delta r)\sin(\theta). \tag{5.2.2}$$

5.2.1 Movement parameters

Most of the movement parameters will be taken from the results obtained in Chapter 4. In the data, time was measured in minutes and the space in centimetres. We set the model parameters so that Δt equates to 30 minutes, i.e. $t = 30t^*$ where t^* is the time in minutes. This is a typical time interval used in the experiment. We use $L = L^*$ for our length scale so it directly relates to the distance in centimetres. For all simulations in this chapter we set $L = 1000$ which is approximately equal to the experimental area in the sparse release (see Fig. 4.1(a)).

The movement ratio for slugs in the simulation can be simply based on the mean movement ratios of all slugs in each data set. As discussed in Section 4.3.3 this gives a probability of moving at any given time step as 0.467 for the sparse release and 0.264 for the dense release. For the purposes of our model, it is suitable to round these movement probabilities to $P_m^s = 0.5$ for sparse movement and $P_m^d = 0.25$ for dense movement.

The process is slightly more complicated in choosing the movement type and fitting step size parameters. As we are simulating resting times separately from the generation

of step size, we want to approximate the distribution of step sizes from the movement velocities only when a slug moves. Therefore we remove all zero values and multiply each velocity by Δt to be representative of the movement in the chosen time scale. The step sizes Δr, of all sparse and dense release slugs are shown in Fig. 5.1(a,c) and (b,d) respectively. There is insufficient data to conclusively determine the type of movement that slugs undergo and so the data is fitted to the distributions used as the dispersal kernel in Chapters 2 and 3 as an approximation. Therefore, as in those chapters, the model will be of a population of either Brownian or non-Brownian walkers.

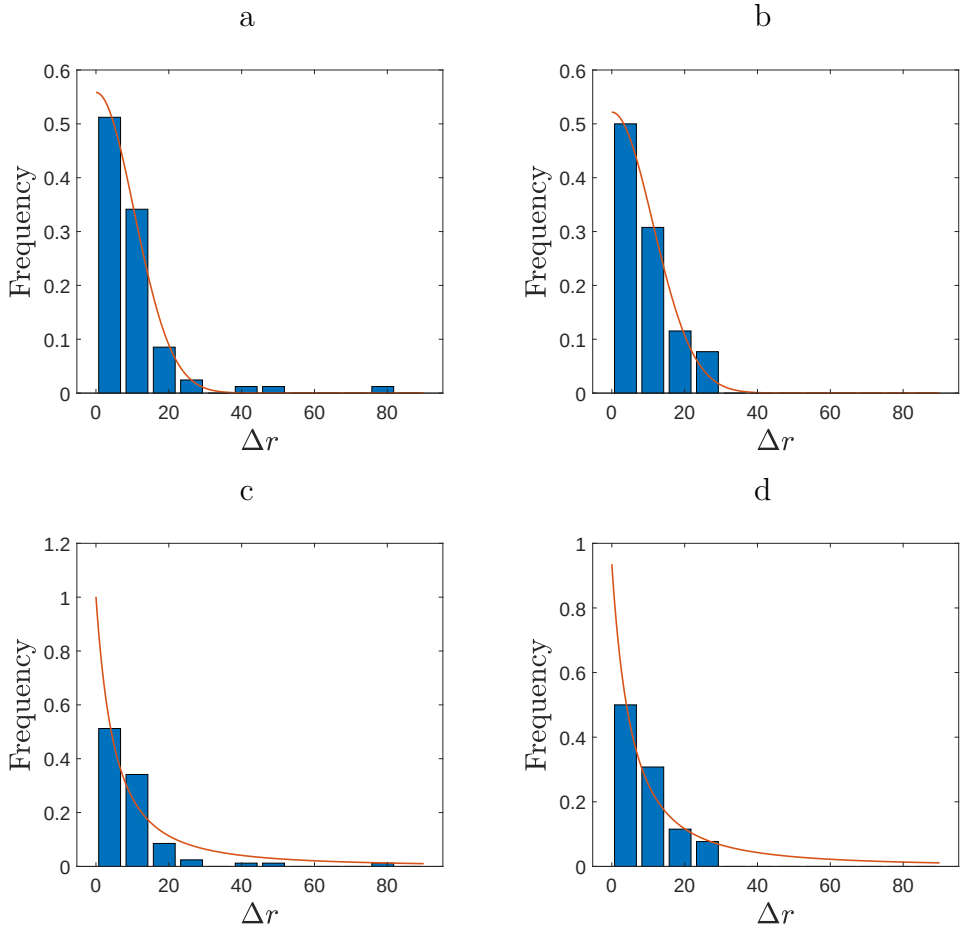

Figure 5.1: Frequency distribution of the step sizes calculated by multiplying non-zero velocities by Δt in the case of (a,c) sparse release, (b,d) dense release. The distributions are fitted to a (a,b) half-normal distribution and a (c,d) power law distribution with $\gamma = 2$. The relevant fitted parameters and R^2 values are (a) $\sigma = 10.46$, $R^2 = 0.993$, (b) $\sigma = 11.25$, $R^2 = 0.992$, (c) $k = 10.15$, $R^2 = 0.923$ and (d) $k = 10.91$, $R^2 = 0.949$.

The distribution of Δr shown in Fig. 5.1 and described in the figure caption can be used to generate the step sizes in our model. For Brownian walkers we will use the normal distribution (Eq. 3.2.3) with $\sigma = 10.46$ for sparse movement and $\sigma = 11.25$ for dense movement. For non-Brownian walkers we will use the power law distribution (Eq. 3.2.4) with $\gamma = 2$ and $k = 10.15$ for sparse movement and $k = 10.91$ for dense movement.

As shown in Tables 4.3-4.5, we can also fit the turning angle. Fig 4.4 shows that the sparse release slugs have a clear preference for a turning angle close to zero. For the dense release, there appears to be a bias towards a positive turning angle, however as the correlation is less pronounced than in the sparse release, we initially assume that there is a uniform distribution of turning angles, i.e. there is an equal probability of a slug moving in any direction regardless of its previous direction of movement.

We model a correlated random walk for sparse release slugs with a Von Mises distribution. This is not the best fit according to Table 4.3 but it is not significantly worse and, as discussed in Section 4.3.2, a more regularly used distribution for modelling correlated random walks than the others in the table. Therefore we have probability density function for turning angles given as

$$\rho_{VM}(\theta_T|\mu,\kappa) = \frac{\exp(\kappa\cos(\theta_T - \mu))}{2\pi I_0(\kappa)}, \tag{5.2.3}$$

with $\mu = 0$ and $\kappa = 0.8$ (rounded from the result shown in Table 4.3).

5.2.2 Density-dependent movement parameters

Having established how we will model the two different types of movement behaviour we can now include them in the same simulation. To do this we need to reintroduce the perception radius R and a new parameter, the density threshold d. Now, if the average density within an individuals perception radius is above the density threshold, that individual will move with dense movement. If the average density is below the

threshold it will move with sparse movement.

For each slug, the local density is given by

$$D_l = \frac{m}{\pi R^2} \tag{5.2.4}$$

where m is the number of other slugs within the perception radius, i.e. for slug i, the total number of slugs from $j = 1, ...N,\ j \neq i$, that satisfy $\sqrt{(x_i - x_j)^2 + (y_i - y_j)^2} < R$.

We also introduce an auxiliary variable u to determine whether a slug moves or rests. For each slug at each time step, u is drawn from a uniform distribution in the region $[0,\ 1]$ and movement occurs when $u < P_m$, where P_m is the movement probability (notated as P_m^d and P_m^s for dense and sparse movement respectively).

Therefore, the dispersal kernel for Brownian walkers will be given by

$$\rho(\Delta r) = \begin{cases} \rho_G(\Delta r|0, \sigma_s^2) & \text{if } D_l < d, \text{ and } u < P_m^s \\ \rho_G(\Delta r|0, \sigma_d^2) & \text{if } D_l \geqslant d, \text{ and } u < P_m^d \\ \{0\} & \text{otherwise,} \end{cases} \tag{5.2.5}$$

and the distribution of turning angles is given by

$$\rho(\theta_T) = \begin{cases} \rho_{VM}(\theta_T|0, \kappa), & \text{if } D_l < d, \\ \rho_U(\theta_T), & \text{if } D_l \geqslant d \end{cases} \tag{5.2.6}$$

where ρ_G is the normal distribution (see Section 3.2, Eq. 3.2.3), ρ_{VM} is the Von Mises distribution and ρ_U is a uniform distribution in the region $[-\theta,\ \theta]$. For non-Brownian walkers the normal distribution is replaced by a power law distribution (see Eq. 3.2.4).

To begin, we choose the density threshold to be the average density of the whole domain, $d = 0.01$ for $N = 10,000$ and $L = 1000$. We note that the average population density, dictated by our choices of N and L, is useful as it allows us to clearly see patterns

in the population, whether it is realistic for a slug population is undetermined. Although methods such as taking trap counts can provide information on relative abundance, the absolute numbers of slugs in arable fields is unknown [78, 79]. Variations to the population size are examined in Section 5.3.2. For a baseline estimate of the perception radius we look within a potential range $R_0 < R < R_1$, where R_0 and R_1 are the minimum and maximum possible values of R respectively. R_0 is determined by the scales of movement seen in the experimental data. We note that the maximum step sizes recorded in the experimental work were no larger than $\Delta r = 80$ (see Fig. 5.1). It would be unrealistic for the typical step size to be larger than the perception radius as it should be able to perceive the area that is moving into. Our choice for R_1 is based on the initial distribution of sparse release slugs from the experimental data in Chapter 4 and estimation from biologists [249]. We assume that slugs cannot see each other in the sparse release and as can be seen in Fig. 4.1(a), they are roughly 200 cm apart, so we may choose any $R < 200$. For this reason we choose $R = 100$ for the following simulations. Other values of the perception radius and the density threshold are explored in Section 5.3.1.

5.3 Simulation results

We can now simulate the slug movement of sparse and dense release slugs to determine whether or not patches of high density will form. For the initial distribution of sparse slugs, we use the same protocol as in Chapters 2 and 3 and generate each position from a uniform distribution across the whole field. To simulate a dense release, we confine the initial positions to a single cluster in the centre of the domain. We therefore generate each position in the region of a circle of radius R_i. The initial radial distance from the centre of the domain is generated from a uniform distribution in the region $[0,R_i]$ and the angle to the centre of the domain is generated from a uniform distribution in the region $[0,2\pi]$. These value are then used to calculate the initial x and y coordinates. Our choice of R_i and therefore the initial average density of the dense release is arbitrary and initially we

choose the density to be 10 times higher than the sparse release so that $R_i = \sqrt{10/\pi}$.

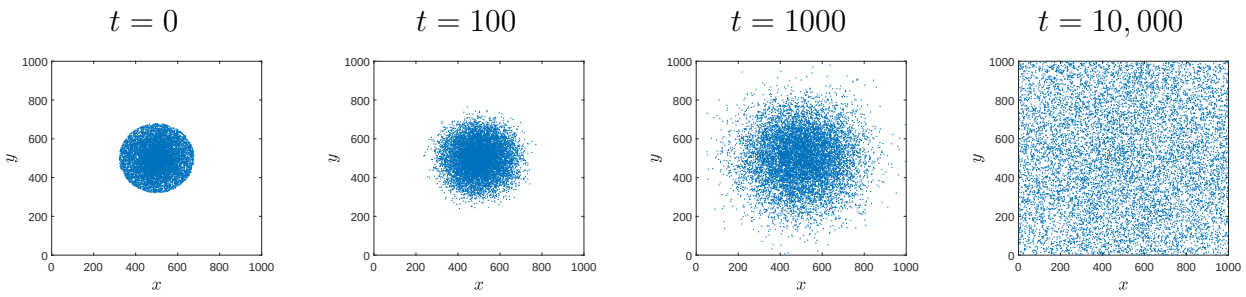

Figure 5.2: The distribution of 10,000 slugs simulated with Brownian walkers that only undergo movement which simulates movement from the dense release.

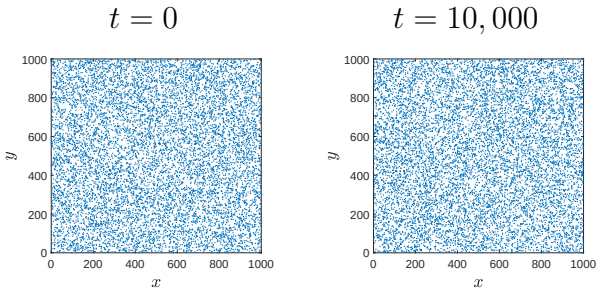

Figure 5.3: The distribution of 10,000 slugs simulated with Brownian walkers that only undergo movement which simulates movement from the sparse release.

First we examine the distributions that evolve from a population that only moves with either sparse or dense movement. As we might expect, slugs released in a uniform distribution whose movement approximates the sparse release stay in a uniform distribution and do not cluster (see Fig. 5.3). For slugs that move only with an approximation of the dense release, we can see from Fig. 5.2 that although many slugs stay close to the centre of the cluster for some time, by $t = 10,000$ they have entirely dispersed and their distribution also becomes uniform.

Now we combine both movement types into one simulation, where the behaviour of an individual will change if the population density within its perception radius R moves beyond the threshold d. Figs. 5.4-5.7 show the distributions that form from this regime. It can be readily seen that patterns do emerge and are still visible after large time intervals. We show the distribution in contour plots (Figs. 5.5 and 5.7) so that the patterns may be

easily seen. This is done by splitting the domain into a grid of bins, as we did in Chapters 2 and 3 for our definition of clusters. The contour plots display an interpolation of the discrete local densities.

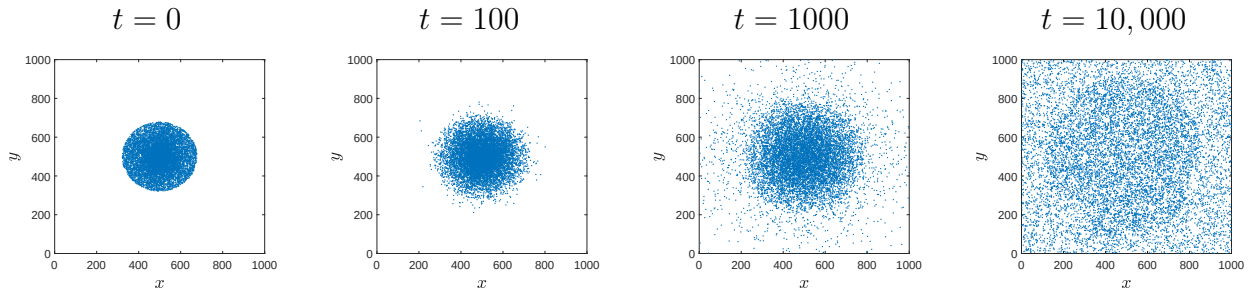

Figure 5.4: The distribution of 10,000 slugs simulated with Brownian walkers that have changeable movement parameters depending on their local density. Density-dependence parameters are $d = 0.01$, $R = 100$. The initial distribution is a dense release.

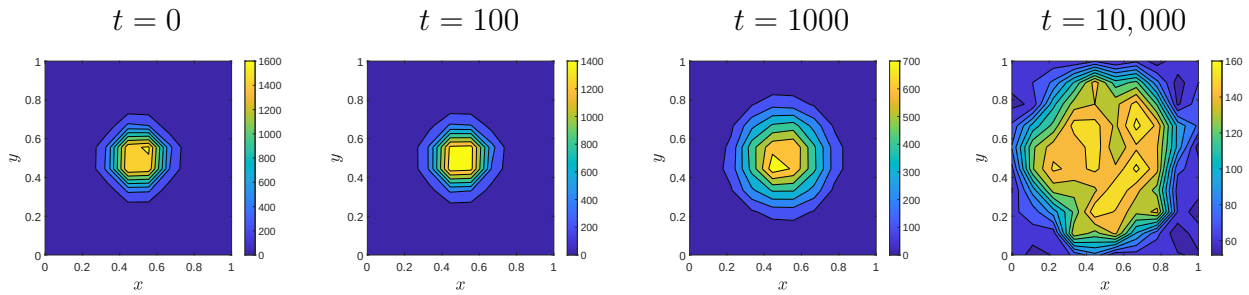

Figure 5.5: The contour plots showing the density corresponding to Fig. 5.4.

We may also examine whether patterns will form from a population of non-Brownian walkers as we did in previous models discussed in Chapters 2 and 3. The results from these models indicated that clusters can occur from non-Brownian walkers but they were not as dense or stable as Brownian walkers when using an equivalent set of parameters. In this model, we choose the parameters discussed in Section 5.2.1, from the distribution shown in Fig. 5.1(c,d).

Figs. 5.8 and 5.9 show the resulting distribution from an example simulation of non-Brownian walkers where all other parameters are the same as Figs. 5.6 and 5.7. From visual inspection it appears that there is no pattern formation for non-Brownian walkers. This is likely due to a higher amount of larger step sizes when moving so that individuals

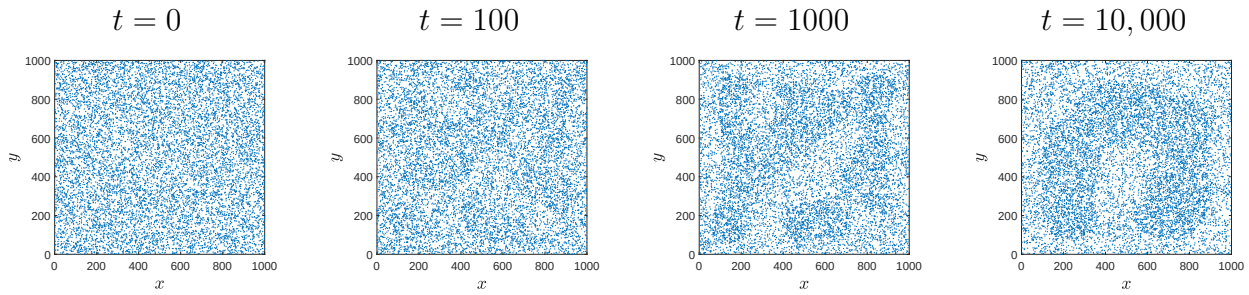

Figure 5.6: The distribution of 10,000 slugs simulated with Brownian walkers that have changeable movement parameters depending on their local density. Density-dependence parameters are $d = 0.01$, $R = 100$. The initial distribution is a sparse release.

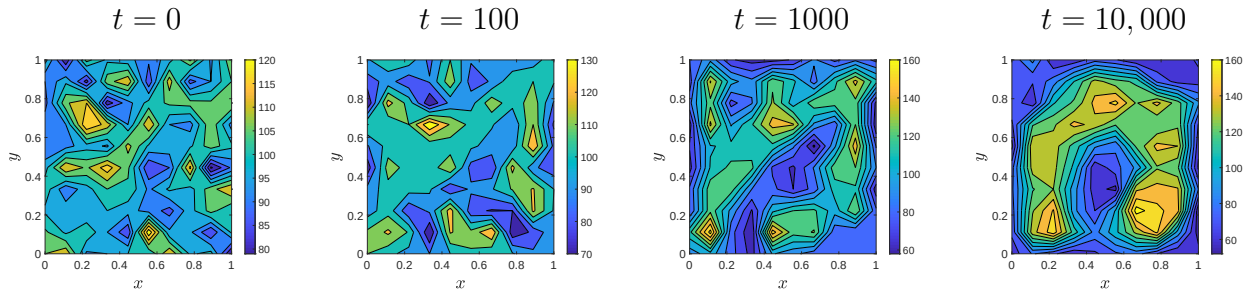

Figure 5.7: The contour plots corresponding to Fig. 5.6.

are less likely to remain in a dense area for a long period of time. Non-Brownian movement simulated with a power law dispersal kernel with $\gamma = 2$ describes superballistic movement, which we discuss in Sections 4.4.1 and 4.5. Our conclusion from the previous chapter is that slugs may move by superballistic movement on short time scales. However, in fitting the distributions in Fig. 5.1 we can see that a fat tailed distribution does not fit well to the dense release data set where there is no step size higher than $\Delta r = 30$ in a single time interval. It would be more appropriate in the sparse release data set where this occurred three times, suggesting that the differences in movement could also be modelled by using different probability functions as the dispersal kernel. However, as we do not appear to have pattern formation for non-Brownian walkers and the R^2 values are higher for a normal distribution fitted to the data, we only consider Brownian walkers for the remainder of this chapter.

As mentioned above, for dense movement we choose a uniformly distributed turning

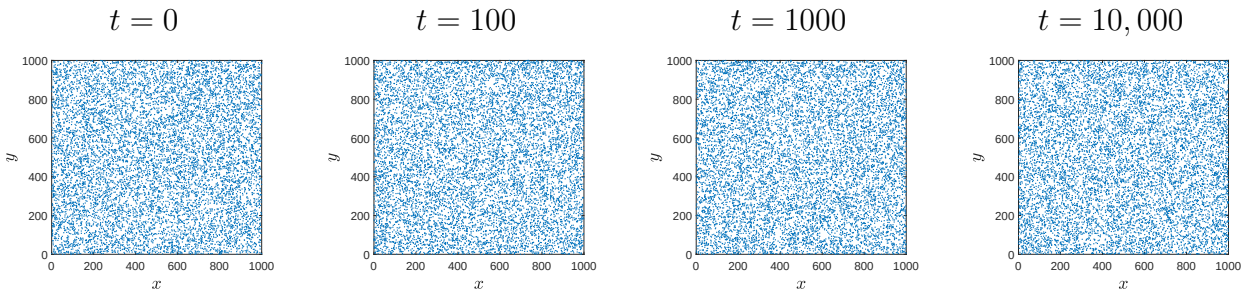

Figure 5.8: The distribution of 10,000 slugs simulated with non-Brownian walkers that have changeable movement parameters depending on their local density. Density-dependence parameters are $d = 0.01$, $R = 100$. The initial distribution is a sparse release.

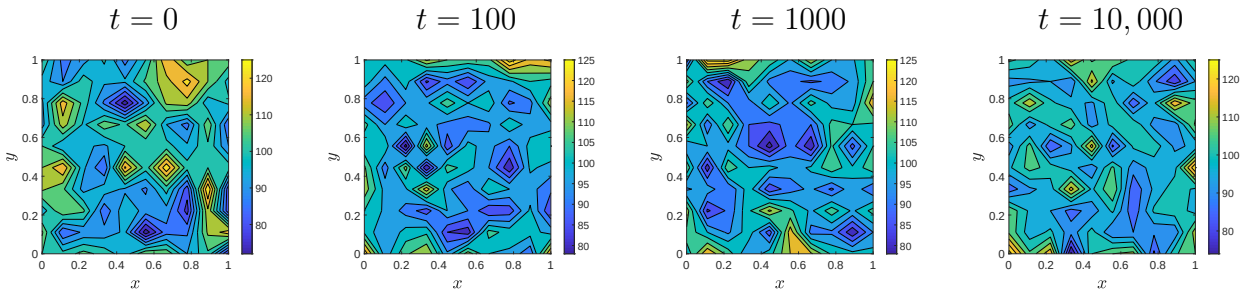

Figure 5.9: The contour plots corresponding to Fig. 5.8.

angle as we assume that when in a high population density, slugs will have no desire to move long distances from their current position. However, as suggested in Section 4.3.2 and shown in Table 4.5, the turning angle data is not uniformly distributed. We therefore introduce a CRW into dense movement instead of a uniformly distributed turning angle. As is done with the sparse movement, we use the Von Mises distribution, however the ratio of negative to positive turning angles in the data is not equal (25% of the turns are negative, 75% are positive) and the value of κ (see Eq. 5.2.3) is different for each direction. From the data shown in Table 4.5, we have parameters for the negative and positive turning angles as $\kappa_n = 1.2$ and $\kappa_p = 0.49$ respectively.

If all other parameters are kept the same as Fig. 5.6, the simulation produces distributions such as those shown in Figs. 5.10 and 5.11. It can be seen from the figures that pattern formation is similar to when using the uniform distribution, as we might expect. Further exploration into the turning angle distribution of slugs and its effect on pattern

formation requires further study and more experimental data, however this is beyond the scope of this study. We therefore continue in this chapter assuming a uniform distribution of turning angles when in high density.

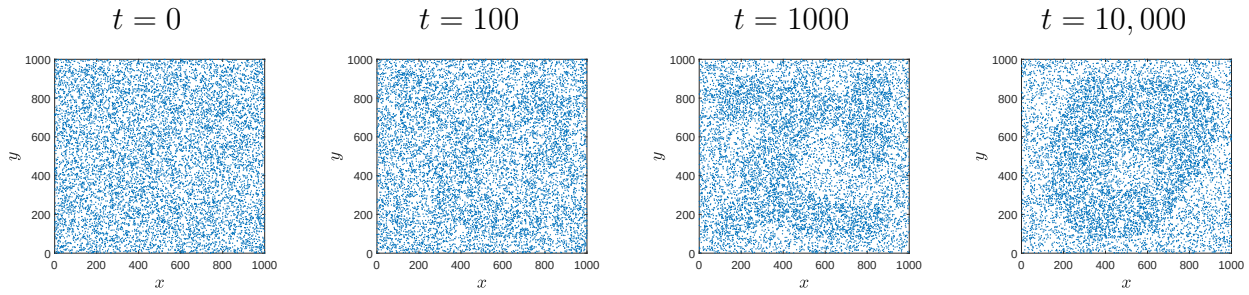

Figure 5.10: The distribution of 10,000 slugs simulated with Brownian walkers that have changeable movement parameters depending on their local density and both movements use a correlated random walk. Density-dependence parameters are $d = 0.01$, $R = 100$. The initial distribution is a sparse release.

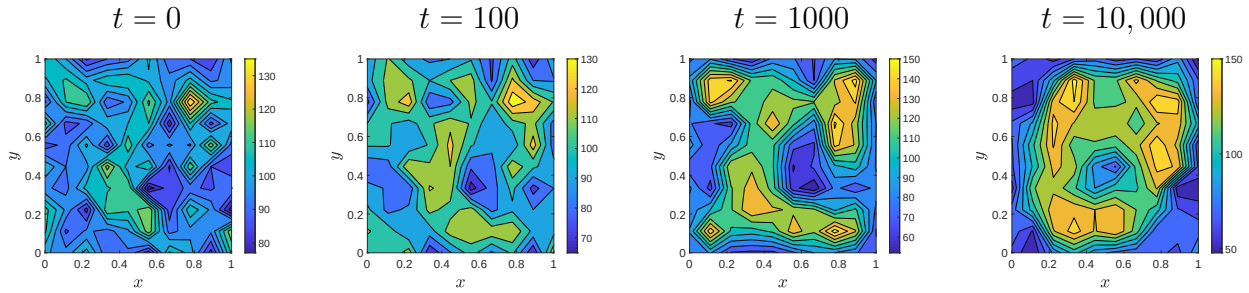

Figure 5.11: The contour plots corresponding to Fig. 5.10.

5.3.1 Varying the density-dependent parameters

To determine the effect of the perception radius and the density threshold that determines the movement type, we simulate varying d (Figs. 5.12 and 5.13) and R (Figs. 5.14 and 5.15). It can be clearly seen from visual inspection of the distribution that $d = 10^{-2}$ is the choice most likely to produce patches. When varying the perception radius, patches appear for $R \geqslant 50$. Multiple patches can be seen from the distributions when $R = 50$ and $R = 100$ but when $R = 300$ only one patch emerges in the domain.

This is confirmed by calculating the Morisita Index [157],

$$I_M = B \frac{\sum_{k=1}^{B} n_k(n_k-1)}{N(N-1)}, \tag{5.3.1}$$

where B is the number of bins, n_k is the number of animals in bin k and N is the total population (see discussion in Sections 2.3.4 and 3.4). The Morista Index for a quasi-uniform distribution is $I_M = 1$ and will increase for a more aggregated distribution. At $t = 10,000$, the mean Morisita Index for 10 simulations with $d = 0.6,\ 0.8,\ 1$ and 1.2×10^{-2} is $I_M = 1.01, 1.03, 1.06$ and 1.01 respectively. For $R = 10,\ 50,\ 100$ and 300, $I_M = 1.01,\ 1.05,\ 1.06$ and 1.07 respectively. In all cases the increase is small because most bins still have similar population densities, however it is apparent that the patches with the higher density in the case of $d = 10^{-2}$ makes the distribution slightly more heterogeneous when measured by the Morisita Index.

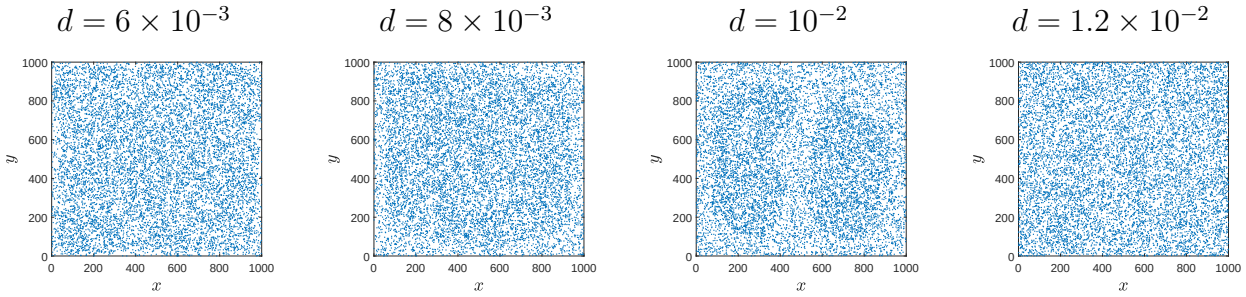

Figure 5.12: The distribution of $N = 10,000$ slugs at $t = 10,000$ simulated with Brownian walkers that have changeable movement parameters depending on their local density. For all simulations $R = 100$ and d has been chosen from trial and error to find cases where patches form. The initial distribution is a sparse release.

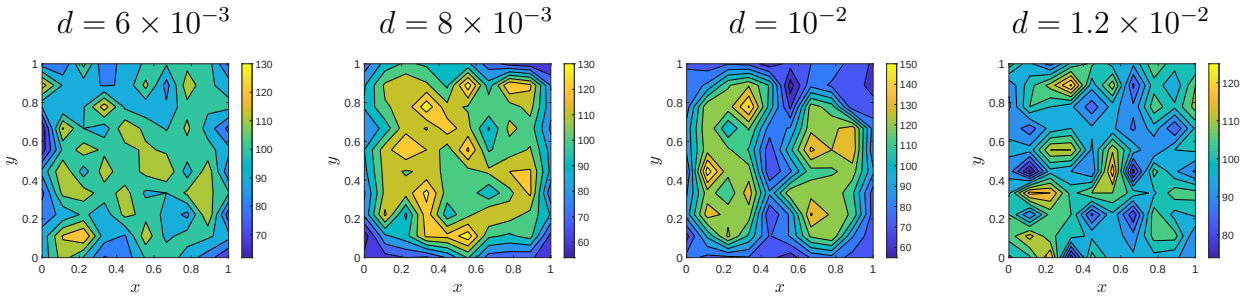

Figure 5.13: The contour plots corresponding to Fig. 5.12.

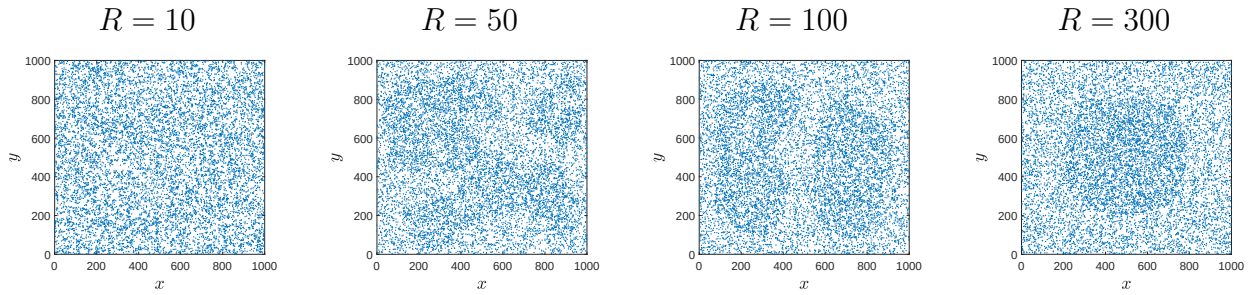

Figure 5.14: The distribution of $N = 10,000$ slugs at $t = 10,000$ simulated with Brownian walkers that have changeable movement parameters depending on their local density. For all simulations $d = 10^{-2}$. (a) $R = 10$ (b) $R = 50$, (c) $R = 100$, (d) $R = 300$, The initial distribution is a sparse release.

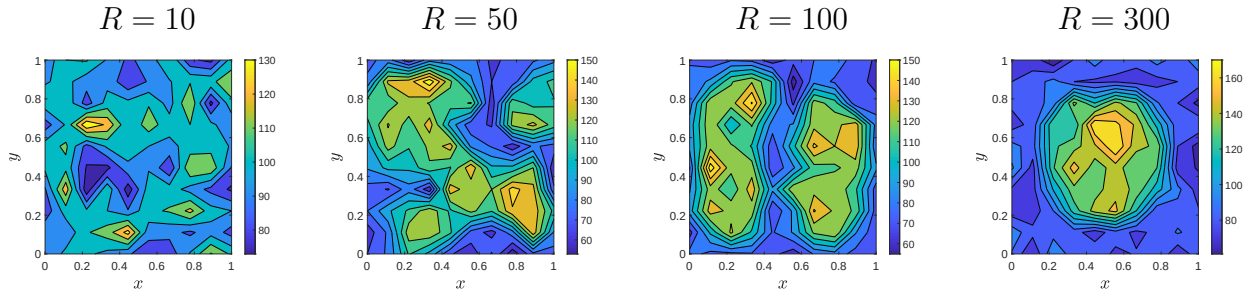

Figure 5.15: The contour plots corresponding to Fig. 5.14.

5.3.2 Effect of the average population density on pattern formation

To determine the population density needed for patches to form, we simulate using different values of N. Figs. 5.16 and 5.17 show the distribution of slugs in a domain of length $L = 1000$ with different population densities and different choices of the density threshold d. As shown in Fig. 5.12, when $N = 10,000$, a value of d that is equal to the total population density, $d = 10^{-2}$, is a good choice for pattern formation. In this case, there are always a proportion of slugs in the population that are in a dense region and the remaining slugs will be in a sparse region. If the average population density is not similar to the threshold d then slugs are likely to be moving with just one type of movement and, as it is the combination of different movement types that produces patterns, they will

stay in a quasi-uniform distribution. It logically follows that pattern formation will be dependent on both d and N. This is confirmed in the bottom row of Fig. 5.16 where it can be seen that a high density patch forms for $N = 5000$, $d = 5 \times 10^{-3}$ but there aren't any visible patches for lower values of d.

For lower densities, there do not visually appear to be any patches that form at all. The mean Morisita Index from 10 simulations does suggest a slight aggregation though for the three cases where d is roughly equal to the average density: $N = 5000$, $d = 5 \times 10^{-3}$, $N = 2500$, $d = 2 \times 10^{-3}$ and $N = 1000$, $d = 10^{-3}$. In these cases the Morisita Index has a small rise to 1.05 but in all other cases remains within 10^{-3} of 1, corresponding to a uniform distribution. This suggests that although it may not be possible to identify through visual inspection, pattern formation can still occur when the average population density is low, provided d is also small.

5.4 Discussion

In Chapter 4 we showed that slugs show different movement behaviours when they are released together to when they are released far apart. Via the model discussed in this chapter, we have now demonstrated that this change of behaviour has the potential to produce patches of high population density. These patches only visibly appear when the density threshold is approximately equal to the average density in the domain, when a reasonable proportion of slugs are in a dense or sparse area at any given time.

Although the conditions for patches in this model are restrictive, we have shown that patches can emerge from a quasi-uniform distribution in a homogeneous environment. In reality, environmental factors such as soil moisture and temperature are likely to effect slug movement and create heterogeneity in population distribution. Density-dependent movement of the sort described in this chapter combined with heterogeneity that already exists are more likely to produce lasting patches even if the environmental effects are removed as long as there are a sufficient number of slugs moving with each type of movement.

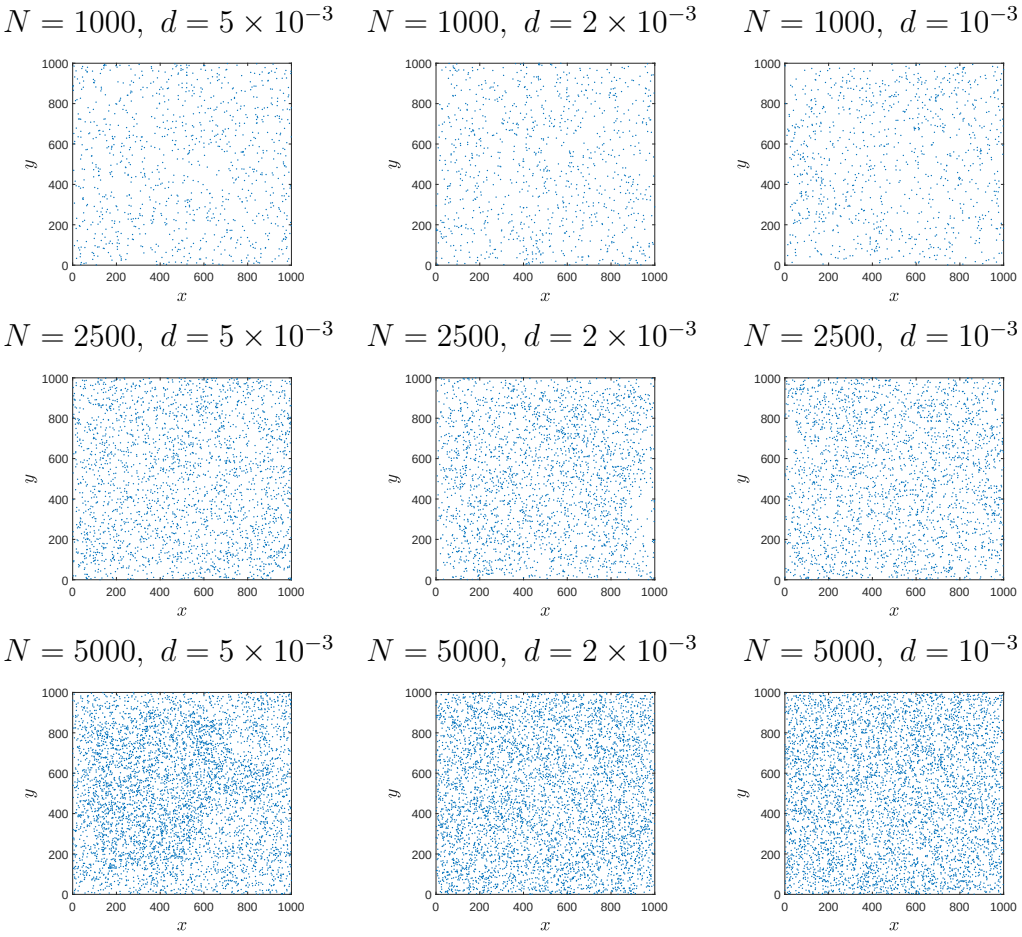

Figure 5.16: The distribution of N slugs at $t = 10,000$ simulated with Brownian walkers that have changeable movement parameters depending on their local density. The initial distribution is a sparse release.

In this chapter we showed that the density dependent movement analysed in Chapter 4 produces clusters that are temporally stable. This has been tested up to $t = 10,000$ which equates to 5000 hours, or nearly 7 months. Modelling has allowed us to examine the dynamics seen in field experiments on extended temporal scales. In future, we can also extend the spatial scales to investigate how patches form over an entire arable field. Although the spatial scales of movement in a single time step are small, the patch dynamics on larger spatial scales and over large temporal scales can therefore be studied. In Chapter 6, we examine slug trap counts taken from real arable fields which show that patches of high slug density do indeed form and investigate how they may be identified and targeted

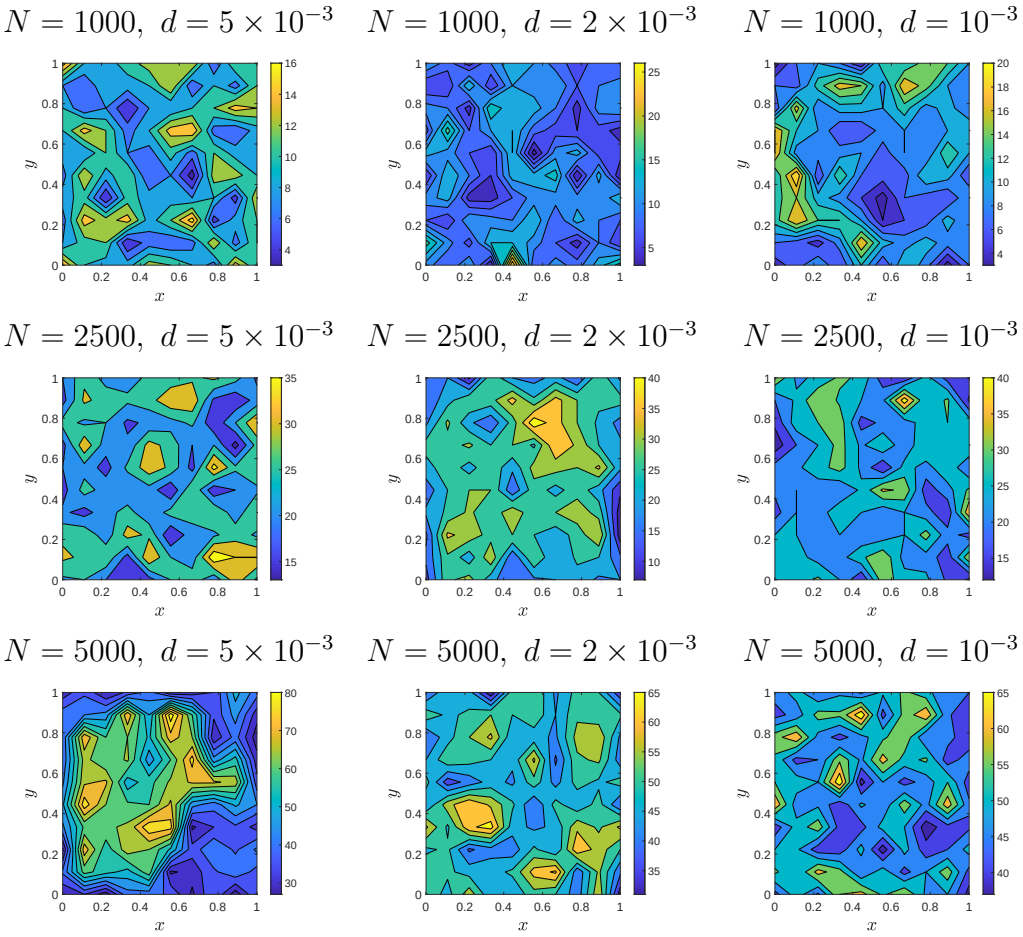

Figure 5.17: The contour plots corresponding to Fig. 5.16.

so that pesticide application will be more efficient. The results from this chapter suggest that the movement dynamics of slugs produce patches that are temporally stable if their movement is different inside a patch from outside a patch. This is crucial if the targeted application of pesticide is to be a viable option for farmers, where patch stability over the entire growing season is required.

Chapter 6

Towards a Targeted Pesticide Application Protocol for the Grey Field Slug

6.1 Introduction

In this chapter, we develop a prototype protocol for the targeted use of pesticides so that the application of pesticide is more efficient and overall usage is reduced. The work presented here is based on our results in [179]. It is designed to be of a practical nature and attempts to take into consideration realistic concerns that a farmer may have in a pesticide application protocol. In previous chapters we concluded that density-dependent individual movement can produce patches of high density that are stable over time. However in this chapter we are not concerned with the reasons for patchy population distributions and we make the assumption that they are a feature of slug distributions and are temporally stable.

As in Chapter 4, the grey field slug is the species we examine to discuss the optimal application of pesticide to strongly heterogeneous pest distributions and the issues that need to be resolved for successful targeting of pesticides in selected spatial domains. For

many years slug control in arable crops has relied on molluscicide pellets applied to the entire field when the slug population exceeds defined thresholds. Meanwhile, it has been reported in numerous studies [12, 28, 78] that the spatio-temporal dynamics of the slug population results in heterogeneous spatial patterns of the slug density in arable fields whereby readily detected patches of higher slug numbers are interspersed within areas of lower slug densities irrespective of the population size. Moreover, as we have shown in Chapter 4, there is evidence that slugs behave differently in areas of high population density in such a way that could cause stable patches to form. A patchy distribution of slugs may offer significant potential for reducing use of pesticides in agricultural fields. If a commercially viable method of identifying their location and size can be established then application of pesticides may be targeted at high slug density patches alone, leaving areas with lower slug numbers untreated.

In this chapter, we explain how to incorporate targeted application of pesticides into a hypothetical protocol based on the threshold slug population abundance. The benefits of the targeted use of pesticides will be clearly demonstrated when we investigate data on slug abundance collected in several commercial fields. The prototype protocol is sufficiently flexible to be readily extended to other pest species that display a heterogeneous distribution. Meanwhile there remain several open questions that may constrain further development of the protocol, one of them being a definition of spatial patches. We argue that a generic definition of a patch as any spatial sub-domain with a closed boundary that has non-zero population density is not efficient when targeted use of pesticide is considered. Hence the generic definition of a spatial patch will be revisited to allow for the inclusion of various additional constraints on patch size and population density within the patch. We then investigate the impact of those constraints on the pesticide application procedure.

This chapter is organised as follows. In Section 6.2 we introduce a generic targeted pesticide application procedure in a case where a population of grey field slugs has to be

controlled. The section is focused on identification of areas with non-zero slug density with consequent application of pesticide in those areas, no matter how low the slug density is in each patch. In Section 6.3 we compare the results of Section 6.2 with a standard pesticide application protocol based on a threshold population abundance and demonstrate how the targeted application procedure should be modified to take the threshold number into account and to avoid pesticide application in areas with low population density. We then show in Section 6.4 that a targeted use of the pesticide protocol depends heavily on the definition of a spatial patch and a single control parameter such as the population threshold in the current standard monitoring/control protocol cannot accommodate important information about patch size. An alternative to the 'single threshold' based approach is then to introduce two control parameters in order to quantify both the pest abundance in each patch and the patch size. Thus, we explain in Section 6.4 how to take into account the pest density and the patch size in the pesticide application protocol. Finally, conclusions are discussed in Section 6.5.

6.2 The baseline method

The aim in this section is to explain a hypothetical pesticide application protocol that can be considered as a prototype for targeted use of pesticide. In this and the next section we demonstrate our approach by using the baseline case of the grey field slug population.

Data on slug abundance were collected by researchers at Harper Adams University in several commercial winter wheat fields between autumn 2015 and autumn 2017 [78]. A standard experimental design was established for the research in all fields in both cropping years. Refuge traps consisting of upturned 18 cm diameter, plastic plant pot saucers were placed in a regular 10×10 grid with distance $h = 10$ meters between nearest traps. Sampling grids were installed at a minimum of 20 meters from the nearest field edge. The number of slugs under each refuge trap were recorded after traps had been left undisturbed for 14 days, and thereafter at regular intervals.

An important assumption in this study was that the sampling grid used for collection of slug data was sufficiently fine to provide accurate information about both the heterogeneous spatial slug distribution and the total slug abundance in the field. Although the above assumption is essential for our discussion, we recognise that using such a fine sampling grid (i.e. 100 traps per hectare) is not realistic in routine data collection for commercial pest management. Determining a minimum number of sampling locations required for accurate reconstruction of spatial density patches is a challenging question that requires further careful study. While the above question is beyond a scope of this study, it is briefly discussed in Chapter 7.

The dataset we use to introduce our approach is a spatial distribution of the slug population obtained from trap counts collected on 18 November 2016 from a commercial arable field sown with winter wheat, located at South Kyme, Lincolnshire, UK. The trap count data collected in the field are shown in Table 6.1, and the spatial slug distribution reconstructed from this data is shown in Fig. 6.1 where the total length L of the sampling grid (100 m) in both directions is converted to the non-dimensional unit length $L = 1$; see below in Section 6.2.1 for further explanation of the conversion of the GPS coordinates in the physical domain to the grid coordinates in the unit square. Given that a regular grid of traps is used in the monitoring routine, the distance h between traps and the coordinates of each trap are readily calculated in the converted domain. The continuous distribution shown in the figure has been obtained from the discrete data in Table 6.1. We interpolate the data, using piecewise linear interpolation, to give a continuous population density function defined at every point of the domain of interest in order to visualise slug density (see Fig.6.1(a)). A slug patch is defined as any spatial sub-domain with the closed boundary where the population density is greater than zero.

For the sake of discussion in this section we assume that pesticide will be applied in our hypothetical protocol to any slug patch in the field, no matter how low the slug density is within the patch. Thus the first step in our procedure is to identify the boundaries

Table 6.1: Trap count values taken from a regular sampling grid of 10×10 traps in the South Kyme field on 18 November 2016.

1	0	0	1	0	2	0	0	3	0
4	1	0	0	0	0	0	1	0	0
0	0	0	0	0	1	0	0	0	0
0	0	0	0	1	1	0	1	0	1
1	2	0	1	0	1	0	0	0	0
2	2	1	0	0	0	0	0	0	0
0	1	1	0	0	0	1	1	0	0
0	0	0	0	0	0	0	0	0	1
0	0	0	0	0	0	1	2	0	1
0	1	0	0	1	0	0	0	0	0

of spatial patches that are clearly seen in Fig. 6.1(a). This is done by converting the data in Table 6.1 into binary data (i.e. producing the presence/absence map from the original data). Consider trap count C_i in the ith refuge trap $i = 1, 2, \cdots, N$, where N is the number of traps in the field, and let h be the distance between neighbouring grid points on a regular sampling grid. For each data point, if the trap count is $C_i > 0$ then we set $C_i = 1$ and if $C_i = 0$ it remains set as 0. This produces a binary table showing only the location of slugs (as linked to the position of each trap in the field) and not the quantity. Neighbouring values of 1 in the horizontal or vertical direction are then said to be in the same patch and we can therefore count distinct patches in the field and define their boundaries.

The patch boundaries are visualised in Fig. 6.1(b). We assume that every trap is installed at the centre of its square catchment area and the catchment area has the linear size of $h/2$, where h is the distance between neighbouring traps. Hence a slug patch which appears as an isolated non-zero trap count in Table 6.1 will have the same area as trap catchment area $A = h \times h$. That assumption is illustrated in Fig. 6.1(b) where the regions shown in green within slug patches are regions enclosed by neighbouring traps that contain slugs and the outer region shown in blue has the width of $h/2$. Hence, in patches shown purely in blue, there are only one or two traps where slugs were found and

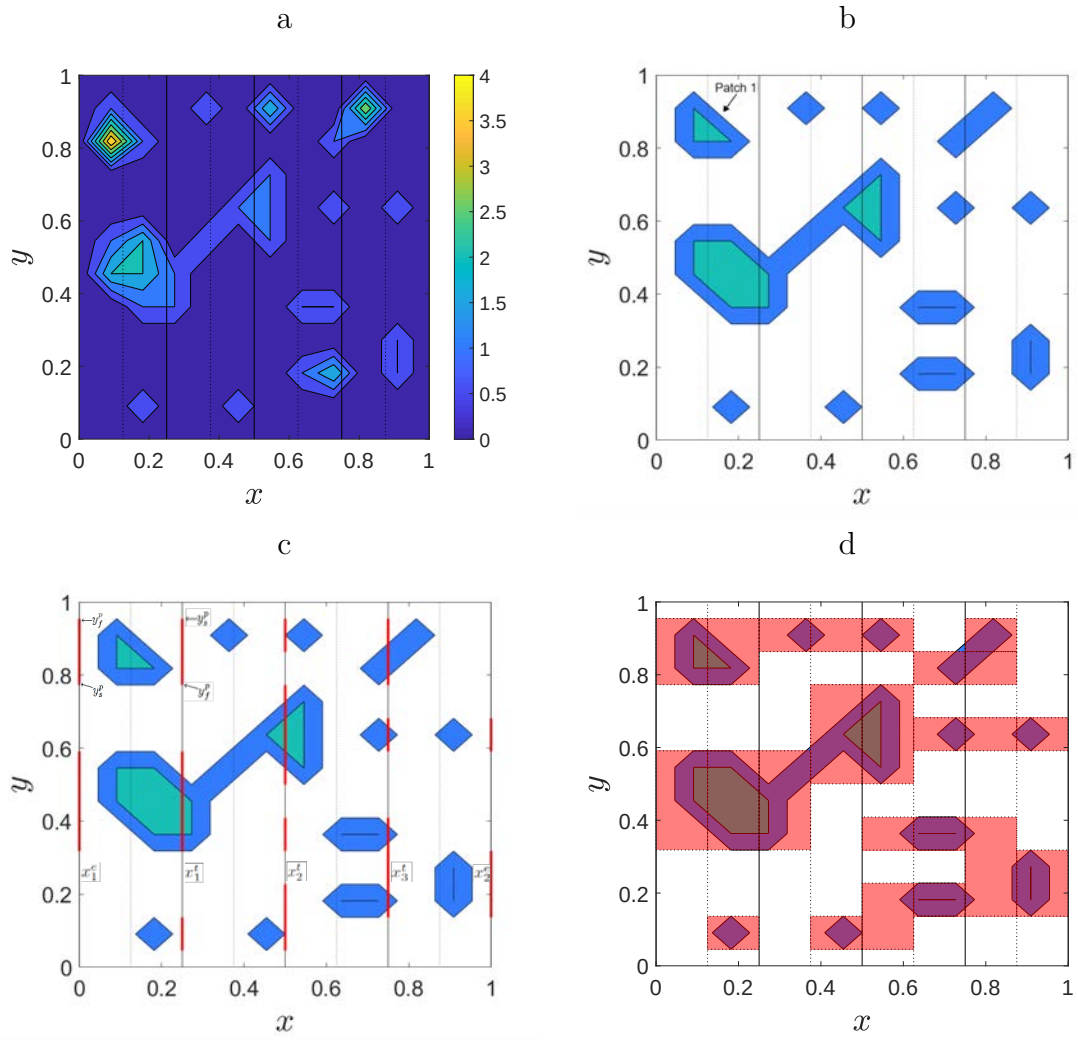

Figure 6.1: Trap counts were taken on a sampling grid of 10 by 10 locations in the South Kyme field on 18 November 2016 (see details in the text), the corresponding numerical values are given in Table 6.1. The total length L of the sampling grid (100 m) in the x and y directions is rescaled as $L = 1$. The continuous distributions and patch boundaries shown in the figure are obtained from linear interpolation. (a) The slug spatial distribution reconstructed from trap counts based on linear interpolation between trap locations. (b) Contour plot showing slug patches (areas of light green colour in the figure) with the boundary region (blue colour). (c) Contour plot showing slug patches mapped onto the tracks. The mappings are shown as red lines along the track indicating the points from where pesticide should be applied. (d) Contour plot showing slug patches with pesticide applied in red shaded areas. Pesticide used $M = 45.5\%$.

their neighbouring traps did not contain slugs.

We now model the application of pesticide so that the entire area of a patch is covered.

The pesticide is applied when the spreader is moved along a track in the field and in our model we assume that the field has three interior tracks that are shown as solid vertical lines in Fig. 6.1(c). Each vertical track in the figure is completely defined by its x-coordinate, x^t, and we then label the tracks as x_1^t, x_2^t and x_3^t respectively. We also assume that two external tracks (i.e. vertical boundaries $x = 0$ and $x = 1$ labelled as x_1^e and x_2^e in Fig. 6.1(c)) can be used for pesticide spreading, the pesticide can be spread in either direction from a track (i.e. to the left and to the right), and the pesticide is uniformly distributed between the track and the midpoint between two tracks. Therefore if a patch on one side of the track is detected, pesticide will be spread in a rectangular block.

The track lines and the midpoints between tracks are represented in Fig. 6.1(b-d) as solid and dotted lines respectively. In our algorithm we define projection of each slug patch onto track lines and those coordinates are used to generate rectangular domains where pesticide will be applied. For each slug patch p to be handled, the algorithm outputs the track label (as explained above) and the coordinates y_s^p and y_f^p along the track where pesticide should start being applied and stop being applied.

Consider, for example, the first slug patch labelled as 'patch 1' at the upper left corner of Fig. 6.1(b). In order to cover that patch with pesticide, it should be applied when the spreader moves from point y_s^p to y_f^p along track x_1^e and when it then moves in the opposite direction from point y_s^p to y_f^p along track x_1^t; see Fig. 6.1(c). The above information is recorded, is stored along with the patch label, and the same analysis is made for any slug patch detected in the field. As a result, the algorithm returns all data required for targeted use of pesticides in the field. The output data are illustrated in Fig. 6.1(c): spreading of pesticide will happen when the spreader moves along each interval shown in red.

Once the output information has been obtained, the rectangular domains are restored to contain each patch where the pesticide should be spread. The areas of the field where pesticide is applied can be seen by the shaded areas in Fig. 6.1(d). The total area A of

pesticide applied to the field is calculated by summing the area of each shaded rectangular block. Since the total field area is $A^* = L \times L = 1$ and assuming that total coverage of the field would use $M^* = 100$ mass units of pesticide (i.e. 100% of pesticide), we can find the percentage of pesticide M used by targeting only the patches as $M = A \times M^*$. In the case of South Kyme, when the patches are targeted from three internal tracks and two external tracks, only $M = 45.5\%$ of pesticide is used.

6.2.1 GPS coordinate transformation

In this section we explain briefly a process that will transform coordinates from the unit square, as we have used in Section 6.2, to actual GPS coordinates in the field. The coordinates of the four corner traps in the sampling grid are required as an input and we geometrically transform those coordinates into the unit square. The transformation can then be used to convert any GPS coordinates from the field into unit square coordinates to be further used in our pesticide targeting procedure. The unit square can be transformed back to the GPS coordinates and any coordinate from the unit square can be converted to GPS coordinates. This will be necessary when determining the start and finish points for

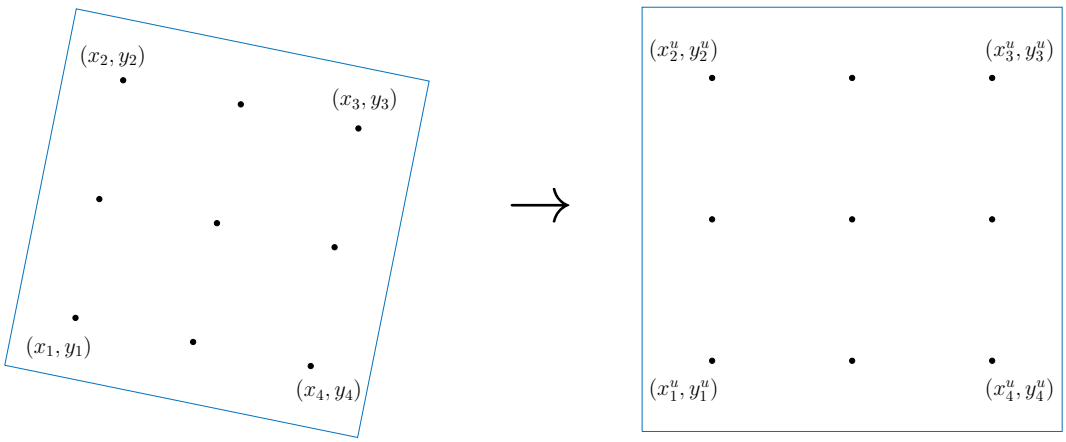

Figure 6.2: An example of a field with nine traps and the coordinates of the four corner traps transformed into the unit square.

applying pesticide in the field. The experimental data used in this chapter is of the form of a uniform square grid of trap counts, making it easy to transform to a unit square to apply a targeting algorithm and convert back to GPS coordinates. It is entirely possible to apply additional transformations a different layout of traps but we do not consider that here.

We consider the GPS coordinates (x, y) and the four corner traps to be (x_i, y_i) for $i = 1, ..., 4$ going clockwise starting from the bottom left point as shown in Fig. 6.2. The coordinates (x, y) are then changed according to the transformation that turns the corner coordinates into a unit square. However, we need the traps to be in the interior of the unit square and not on the boundary, therefore we position the corner points at distances of $\frac{h}{2}$ from the boundary: $(\frac{h}{2}, \frac{h}{2})$, $(\frac{h}{2}, 1-\frac{h}{2})$, $(1-\frac{h}{2}, 1-\frac{h}{2})$ and $(1-\frac{h}{2}, \frac{h}{2})$ where h is the distance between traps. The first step is to translate the coordinates so that $(x_1, y_1) = (0, 0)$ so that we can make our rotation and scaling transformation. Therefore

$$(x_t, y_t) = (x - x_1, y - y_1). \tag{6.2.1}$$

As we know the traps are already set out in a square of 100 m, the only remaining transformations required are rotation and rescaling. The rotation matrix is given as

$$M_r = \begin{bmatrix} \cos(\theta) & -\sin(\theta) \\ \sin(\theta) & \cos(\theta) \end{bmatrix} \tag{6.2.2}$$

and the scaling matrix is

$$M_s = \begin{bmatrix} \frac{1-h}{x_l} & 0 \\ 0 & \frac{1-h}{y_l} \end{bmatrix}, \tag{6.2.3}$$

where

$$\theta = \tan^{-1}\left(\frac{y_4 - y_1}{x_4 - x_1}\right) \tag{6.2.4}$$

is the angle from the horizontal between the bottom left and right corners and

$$x_l = \sqrt{(x_1 - x_4)^2 + (y_1 - y_4)^2}, \tag{6.2.5}$$

$$y_l = \sqrt{(x_1 - x_2)^2 + (y_1 - y_2)^2} \tag{6.2.6}$$

are the distances between (x_1, y_1) and (x_4, y_4), and (x_1, y_1) and (x_2, y_2) which reduces the size from the distance between the corners to a distance of $1 - h$. Although in this report we only take the case of a square grid of traps when measured in metres, this is not necessarily square when taking GPS coordinates, therefore the scaling in the x and y directions are not the same.

By multiplying these matrices together we are left with one transformation matrix to apply to the translated (x_t, y_t) to get our new coordinates for the unit square (x_u, y_u).

$$\boldsymbol{T} = \begin{bmatrix} \cos(\theta) & -\sin(\theta) \\ \sin(\theta) & \cos(\theta) \end{bmatrix} \begin{bmatrix} \frac{1-h}{x_l} & 0 \\ 0 & \frac{1-h}{y_l} \end{bmatrix} = \begin{bmatrix} \frac{(1-h)\cos(\theta)}{x_l} & \frac{-(1-h)\sin(\theta)}{y_l} \\ \frac{(1-h)\sin(\theta)}{x_l} & \frac{(1-h)\cos(\theta)}{y_l} \end{bmatrix}. \tag{6.2.7}$$

$$\begin{bmatrix} x_t^u \\ y_t^u \end{bmatrix} = \boldsymbol{T} \begin{bmatrix} x_t \\ y_t \end{bmatrix} \tag{6.2.8}$$

Then we reposition away from the boundary so that

$$(x^u, y^u) = (x_t^u + \frac{h}{2}, y_t^u + \frac{h}{2}). \tag{6.2.9}$$

To find (x, y) from coordinates in the unit square (x^u, y^u), we translate the coordinates back to the unit square and use the inverse matrix to translate back to GPS coordinates.

$$(x_t^u, y_t^u) = (x^u - \frac{h}{2}, y^u - \frac{h}{2}). \tag{6.2.10}$$

$$\begin{bmatrix} x_t \\ y_t \end{bmatrix} = \boldsymbol{T^{-1}} \begin{bmatrix} x_t^u \\ y_t^u \end{bmatrix}, \tag{6.2.11}$$

where

$$\boldsymbol{T^{-1}} = \begin{bmatrix} \frac{(1-h)\cos(\theta)}{x_l} & \frac{-(1-h)\sin(\theta)}{y_l} \\ \frac{(1-h)\sin(\theta)}{x_l} & \frac{(1-h)\cos(\theta)}{y_l} \end{bmatrix}^{-1} = \frac{1}{(1-h)^2} \begin{bmatrix} x_l\cos(\theta) & x_l\sin(\theta) \\ -y_l\sin(\theta) & y_l\cos(\theta) \end{bmatrix}. \tag{6.2.12}$$

Finally we have

$$(x, y) = (x_t + x_1, y_t + y_1). \tag{6.2.13}$$

6.3 Threshold-based pesticide application

The example of the South Kyme field in the previous section is convenient for the purpose of illustration of our approach as it presents a patchy spatial distribution with very distinct slug patches. However, if the data in Table 6.1 were considered under more realistic conditions, then no pesticide would be used at all. Monitoring and control protocols usually require that a management action is only applied if an estimate of the average trap count (or the average density) exceeds a given management threshold [224]. Although individuals from different slug life stages are unlikely to have the same negative impact on crops, average trap count in this study reflected normal commercial practice in referring to total trap count (adult + sub-adult + juvenile slugs). Let us define the average trap count S as

$$S = \frac{1}{N}\sum_{i=1}^{N} C_i, \tag{6.3.1}$$

e.g. see [57, 219] where C_i is the trap count in the ith refuge trap and N is the number of traps in the field. In most pesticide application protocols average trap number S has to be checked against the imposed action threshold value S_{th} and pesticide will only be applied if $S \geqslant S_{th}$. Let us define a threshold value in our hypothetical protocol as $S_{th} = 5$

Table 6.2: Analysis of trap count data collected on several commercial fields. P is the number of patches where a slug patch is considered as an isolated sub-domain with the non-zero slug density (see details in the text). The average trap count S is calculated as in Eq. (6.3.1). The amount of pesticide M needed to cover all patches in the field is calculated as the percentage of the amount needed to cover the entire field.

Field	Date	P	$M\%$	S
Uppington	04.01.16	2	100	1.78
Uppington	19.01.16	4	100	1.29
Uppington	01.02.16	5	92.5	1.65
Uppington	16.02.16	12	32.5	0.2
Adney Corner	30.11.15	13	35.0	0.25
Adney Corner	14.12.15	14	77.5	0.69
Adney Corner	29.01.16	3	100	0.98
Adney Corner	16.02.16	18	55	0.42
Stoney Lawn	07.12.15	1	100	3.02
Stoney Lawn	06.01.16	1	100	5.98
Stoney Lawn	11.01.16	1	100	6.21
Stoney Lawn	14.01.16	2	100	6.03
Stoney Lawn	18.02.16	1	100	9.13
Badjics	18.12.15	5	91.3	1.61
Badjics	06.01.16	2	100	2.24
Badjics	20.01.16	2	100	1.60
Badjics	18.02.16	1	100	4.00
Adney Middle	08.12.15	4	100	1.20
Adney Middle	22.12.15	1	100	1.68
Adney Middle	14.01.16	1	100	2.28
Adney Middle	18.01.16	1	100	4.00
Adney Middle	12.02.16	1	100	2.35

(note this is higher than the usual thresholds used in commercial practice which can be up to a mean of 4 slugs per trap depending on the crop or crop condition being treated). In our model case of the South Kyme field the average trap count is $S = 0.49$ and is much less than S_{th}. Given a very low number of slugs, there is no need to apply pesticide.

The above conclusion about the use of pesticide is further confirmed by data in Table 6.2 where we show the result of our algorithm applied to spatial distribution of slugs in several commercial fields. Again we assume that total coverage of the field would use $M = 100$ mass units of pesticide. The analysis of the amount of pesticide M (column 4

in the table) reveals that in most cases the entire field will be covered by pesticide if we aim to control all slug patches without taking the threshold value into account. On the other hand, it is seen from the table that the average trap count S in column 5 is well below the threshold value for many commercial arable fields presented in the table and pesticide application is not required in those fields at all. We conclude from comparison of columns 3, 4 and 5 that in most cases presented in the table we have a small number of slug patches (column 3) and the slug density is low within each patch. Hence our next step is to incorporate the threshold criterion in our algorithm in order to avoid application of pesticide to slug patches with low slug density.

To explain our approach, let us consider another example where slug data were collected in a field in Stoney Lawn, Shropshire, UK, on 14 January 2016. The main difference between this dataset and the South Kyme dataset considered previously is that there is a much larger slug population in Stoney Lawn. Table 6.3 shows the trap count values where the values range from 0 to 48 with average $S = 6.03$ and we also note that the majority of trap counts are at least 1.

The spatial slug distribution reconstructed from the data in Table 6.3 is shown in Fig. 6.3(a). The patch identification procedure explained in Section 6.2 is then applied and patch boundaries are shown in Fig. 6.3(b) where we can see one very large patch covering the majority of the field. Therefore, if we were to apply the algorithm as in the previous example of the South Kyme field, almost the entire field would need to be targeted. Meanwhile, visual inspection of spatial slug distribution in Fig. 6.3(a) reveals that there are several areas of low slug density where pesticide is not required along with one area of very high density where the pesticide must be applied. Let us recall that in the targeted use of pesticide procedure in Section 6.2 we have defined slug patch as any sub-domain of the non-zero slug density in the field. However that simplistic definition is not efficient when the density of slugs varies in different patches. A more careful definition of patches is therefore required to allow for selection of patches with high density which

Table 6.3: Trap count values from the 10×10 sampling grid in the Stoney Lawn field. Trap counts were taken on 14 January 2016.

11	0	2	0	5	7	9	1	1	7
21	1	0	3	1	3	15	3	7	0
10	0	6	2	2	0	8	0	3	4
16	0	2	2	1	2	23	2	5	3
1	6	0	2	4	7	18	4	4	0
18	0	1	2	14	12	10	2	5	0
32	5	3	2	5	1	34	6	6	0
15	3	1	0	12	2	48	4	8	2
2	3	0	4	10	4	20	3	2	1
1	17	7	9	3	4	17	3	4	2

should be incorporated into the targeted use of pesticide protocol.

6.3.1 The threshold-based protocol

When a pesticide is applied uniformly across the whole field, the threshold S_{th} is a key parameter in the monitoring and control protocol as it determines whether pesticide application is required or not. Therefore, one method of choosing the patches to target would be to list the traps in descending order of the size of the trap count. The average trap count S is then calculated according to (6.3.1). If the average trap count is above the threshold S_{th}, the trap with the maximum trap count is marked to be targeted and the area of potential pesticide application is defined. The average trap count S is then recalculated under the assumption that the trap already marked to be targeted now has a zero trap count. If the new average trap count in (6.3.1) is still above the threshold then the trap with maximum remaining trap count is also marked to be targeted. The average trap count S is again recalculated with any traps that have been targeted set to zero along with any other traps in the area of pesticide application. The above procedure is repeated until the recalculated average value S is below the threshold or below the targeted pest suppression.

We analyse the average trap count by rewriting expression (6.3.1) in Section 6.3 as

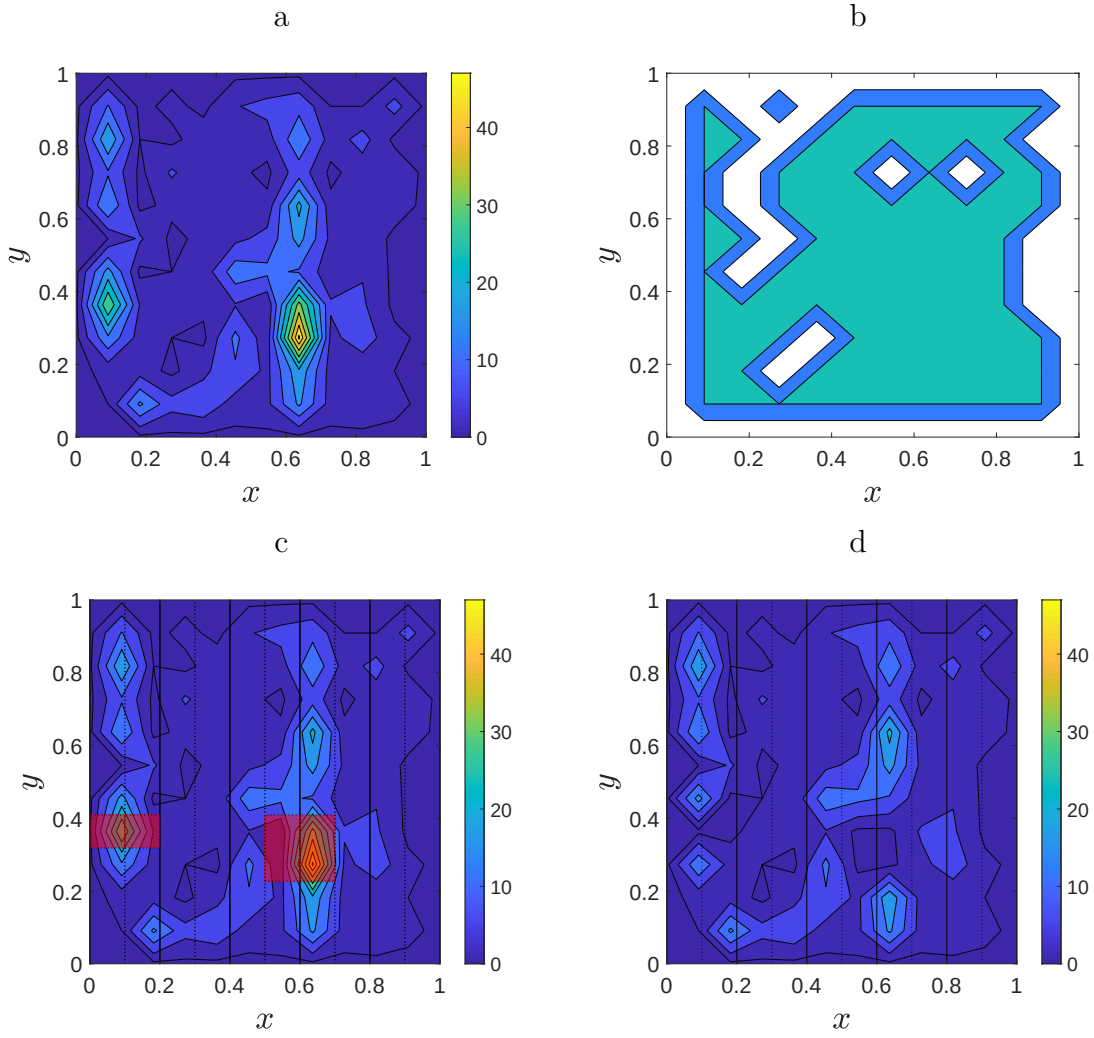

Figure 6.3: Trap counts were taken on a regular sampling grid of 10 by 10 locations in the Stoney Lawn field on 14 January 2016 (see also Table 6.3). The total length L of the sampling grid in the x and y directions is rescaled as $L = 1$. The continuous distributions of the slug density in the field shown in the figures were obtained from linear interpolation of the discrete data. (a) The slug spatial distribution reconstructed from trap counts in Table 6.3. (b) Contour plot showing areas with the non-zero slug density at Stoney Lawn. (c)-(d) Application of the thresholding procedure with a threshold of $S_{th} = 5$. (c) Two patches with the highest slug density are identified and pesticide will be applied in red shaded areas only. (d) The distribution of slugs after the pesticide has been applied. The field has an original average trap count of $S = 6.03$. After the application of pesticide, the new average trap count is $S = 4.71$. The amount of pesticide used was 7.5% of that which would be used to cover the entire field.

follows:

$$S = \frac{1}{N}\sum_{i=1}^{N} C_i = \frac{1}{N}\sum_{i=1}^{N}(S_{th} + C_i - S_{th}) = S_{th} + \frac{1}{N}\sum_{i=1}^{N}(C_i - S_{th}), \tag{6.3.2}$$

where we notice that the difference $C_i - S_{th}$ for any trap count C_i can be negative, positive or zero value. Let N_1 traps have the trap count $C_j < S_{th}$, $j = 1, 2, \cdots, N_1$, and N_2 traps have the trap count $C_i \geqslant S_{th}$, $i = 1, 2, \cdots, N_2$, where $N_1 + N_2 = N$. We then rearrange the sum in (6.3.2) as

$$S_{th} - S = \frac{1}{N}\left(\sum_{j=1}^{N_1}(S_{th} - C_j) - \sum_{i=1}^{N_2}(C_i - S_{th})\right), \tag{6.3.3}$$

where both sums in (6.3.3) are positive because of the definition of trap counts C_j and C_i.

Clearly the condition $S_{th} - S > 0$ holds if we have

$$\sum_{j=1}^{N_1}(S_{th} - C_j) > \sum_{i=1}^{N_2}(C_i - S_{th}). \tag{6.3.4}$$

Let us find the highest trap count in the sum $\sum_{i=1}^{N_2}(C_i - S_{th})$ and denote it as C_{i^*}. Suppose that the pesticide has been applied to the area around the trap i^* only and all slugs have been killed in that area as a result of pesticide application. We can therefore consider the trap count in that trap as $C_{i^*} = 0$ after pesticide application and the expression (6.3.3) becomes

$$S_{th} - S = \frac{1}{N}\left(\sum_{j=1}^{N_1+1}(S_{th} - C_j) - \sum_{i=1}^{N_2-1}(C_i - S_{th})\right), \tag{6.3.5}$$

where the trap count $C_{i*} = 0$ now contributes to the first sum on the right-hand side of (6.3.5). We then check the condition (6.3.4) again and, if it does not hold, we find the highest trap count in the remaining sum $\sum_{i=1}^{N_2}(C_i - S_{th})$ and repeat our analysis of (6.3.5) as

Table 6.4: (a) Example trap counts in a 3×3 sampling grid. (b) New number i is assigned to each trap as the trap counts C_i are ordered in the descending order. Traps 1 and 2 with trap count $C_1 = 31$ and $C_2 = 20$ respectively (shown in bold in the table) must have zero trap count to ensure that the average trap count is $S < S_{th} = 5$. Hence those traps are marked for pesticide application (see details in the text).

a

11	20	2
31	1	0
8	4	6

b

i	1	2	3	4	5	6	7	8	9
C_i	**31**	**20**	11	8	6	4	2	1	0

above till the condition (6.3.4) becomes true. It is obvious from (6.3.4) that the number T of traps marked for pesticide application can only be $T \leqslant N_2$ and we minimise the number T by selecting a trap with the highest trap count at every step of our algorithm.

We illustrate selection of patches with high slug density by considering the model example of trap counts in a hypothetical sampling grid of 3×3 locations. Let trap counts collected on that grid be as shown in Table 6.4. The total number of slugs in the table is 83 with an average trap count $S = 9.22$. Let us set the threshold $S_{th} = 5$. As the average trap count S is above the threshold the first step is to target the highest trap count. The trap counts are reordered in the descending order and traps are renumbered accordingly. The highest trap count of 31 now is in the first trap. Assuming none of the other traps are in the area where pesticide is applied, the trap count of 31 is set to 0. Hence the new average trap count is $S = 5.78$. This is still over the threshold and so the next highest trap count, 20, is targeted giving a new average of 3.56. Since the average trap count is now less than the threshold, we can ignore all remaining traps when applying pesticide.

One important observation which should be incorporated into the procedure is that the pellet applicator is restricted to moving along defined tracks applying pellets to a swathe extending outwards on either side. Because of those restrictions when pesticide is applied to a targeted area around a trap, other traps within that area may have pesticide applied to them irrespective of the trap count(i.e. despite not being specifically marked out to be targeted). We therefore have to set counts from such traps to zero before the

next iteration of the procedure.

Returning to the example of the field in Stoney Lawn, using the above procedure requires the areas around only three traps to be targeted before an average value $S < S_{th} = 5$ is obtained. The average of all trap counts in Stoney Lawn is $S = 6.03$ but after targeting the traps with values 48, 34, and 32 (the three highest counts as seen in Table 6.3) the average is reduced to $S = 4.71$. The patches of high slug density to be targeted are shown in Fig. 6.3(c).

As explained above, after the pesticide has been applied, we assume that any trap within the area targeted by pesticide has a zero trap count. In the Stoney Lawn field three traps were marked for pesticide treatment, but an additional four were also within the swathe in which pellets were applied when the spreader moved along each track. Hence we have seven traps in total where the trap count is set to zero after pesticide application. Those 'new' zero trap counts are taken into account in formula (6.3.1) when the average is calculated after pesticide application. The trap counts in the traps that have pesticide applied account for 22.9% of the total number of slugs in the field (132 out of 603) but the pesticide used is now only $M = 7.5\%$ of the amount required to cover the entire field. The resulting hypothetical distribution of slugs after the pesticide has been applied is shown in Fig. 6.3(d).

If we use the same example of the Stoney Lawn field but change the threshold to $S_{th} = 3$, a higher number of traps will be required to be targeted to reduce the average S below the threshold. In this case, 10 traps are chosen for targeting with 23 traps having pesticide applied in total. Fig. 6.4 shows the outline of the patches to be targeted in relation to the distribution of slugs. The average slug count from the remaining traps is reduced to $S = 2.91$. The trap counts set to zero after pesticide application account for 51.7% of the total population (i.e. 312 out of 603 slugs) and the amount of pesticide used is 26.2%. Conversely, if the threshold S_{th} is increased then fewer traps will be targeted. If $S_{th} = 6$ then only one trap with the trap count of 48 will be targeted and if $S_{th} = 7$

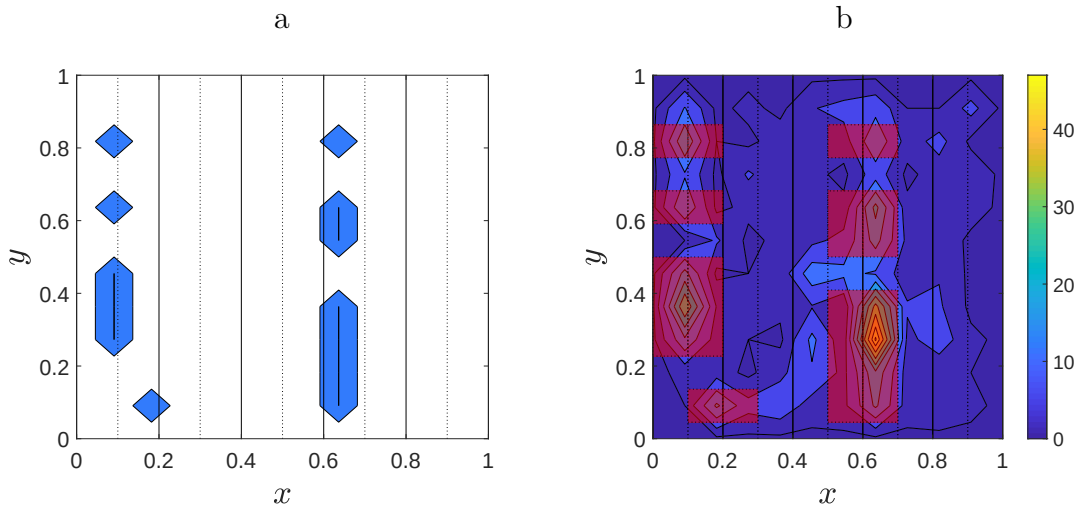

Figure 6.4: Targeted application of pesticide in the Stoney Lawn field with a threshold of $S_{th} = 3$. (a) Contour plot showing slug patches to be targeted. (b) The spatial distribution reconstructed from data in Table 6.3) with pesticide to be applied in red shaded areas after slug patches to be targeted have been identified. The field has an average trap count $S = 6.03$ and after the application of pesticide the new average trap count is $S = 2.91$. The amount of pesticide used is now 26.2% of what would be used to cover the entire field.

Table 6.5: The results of targeted pesticide application based on the threshold value $S_{th} = 4$. The average trap count is calculated before (S) and after (S_{new}) pesticide application; see details in the text. The amount of pesticide M needed to cover marked areas in the field is calculated as the percentage of the amount of pesticide needed to cover the entire field. C_{max} is the highest remaining trap count after pesticide application.

Field	Date	S	S_{new}	$M\%$	C_{max}
Stoney Lawn	06.01.16	5.98	3.97	22.50	11
Stoney Lawn	11.01.16	6.21	3.76	23.75	13
Stoney Lawn	14.01.16	6.03	3.95	15.00	18
Stoney Lawn	18.02.16	9.13	3.51	41.25	12
Badjics	18.02.16	4.00	3.78	2.50	11
Adney Middle	18.01.16	4.00	3.81	1.25	11

then there will be no pesticide applied in the field as the average trap count $S = 6.03$ is already below the threshold.

6.3.2 Targeting patches with high slug density: examples

We now investigate the threshold-based protocol in more detail by employing it for decision making on pesticide application in several fields in Shropshire which have relatively high average trap count $S \geqslant 4$ (Table 6.2). Spatial distributions of slugs in those fields are shown in Fig. 6.5 and patches with high slug density are clearly visible in each field. We assume that those fields are subject to pesticide application as they exceed a threshold value $S_{th} = 4$. The results of pesticide application are shown in Table 6.5. The average trap count S calculated for original spatial distribution in each field is compared with the new average trap count S_{new} recalculated after pesticide application. It is seen from the table that S_{new} is below the threshold value in all fields. Notice, however, that the heterogeneous spatial distribution remains and slug patches are visible in all fields after pesticide application (Fig. 6.5). Only a fraction of the total population is treated as a result of the threshold-based protocol and in several cases just one or two patches should be removed in order to meet the condition $S \leqslant S_{th}$.

One example of very small pesticide usage is given by the Badjics field where it is sufficient to treat only one of the patches with higher population density to reduce the overall population level in the area studied to below threshold level (cf. Fig. 6.5(e)(i) and (e)(ii) where the spatial distribution is shown before and after pesticide application respectively). It requires $M = 1.25\%$ to treat the patch and move the average trap count at the Badjics field below the threshold. However, despite the condition $S \leqslant S_{th}$ being formally fulfilled, the new average trap count $S = 3.81$ remain very close to the threshold. It can be seen from the spatial distribution in Fig. 6.5(e)(ii) that the slug patches still have relatively high population density. Hence a more careful definition of the pesticide application protocol may be required, and we discuss an alternative approach in the next section.

Let us now investigate what happens when we change the number of tracks used by

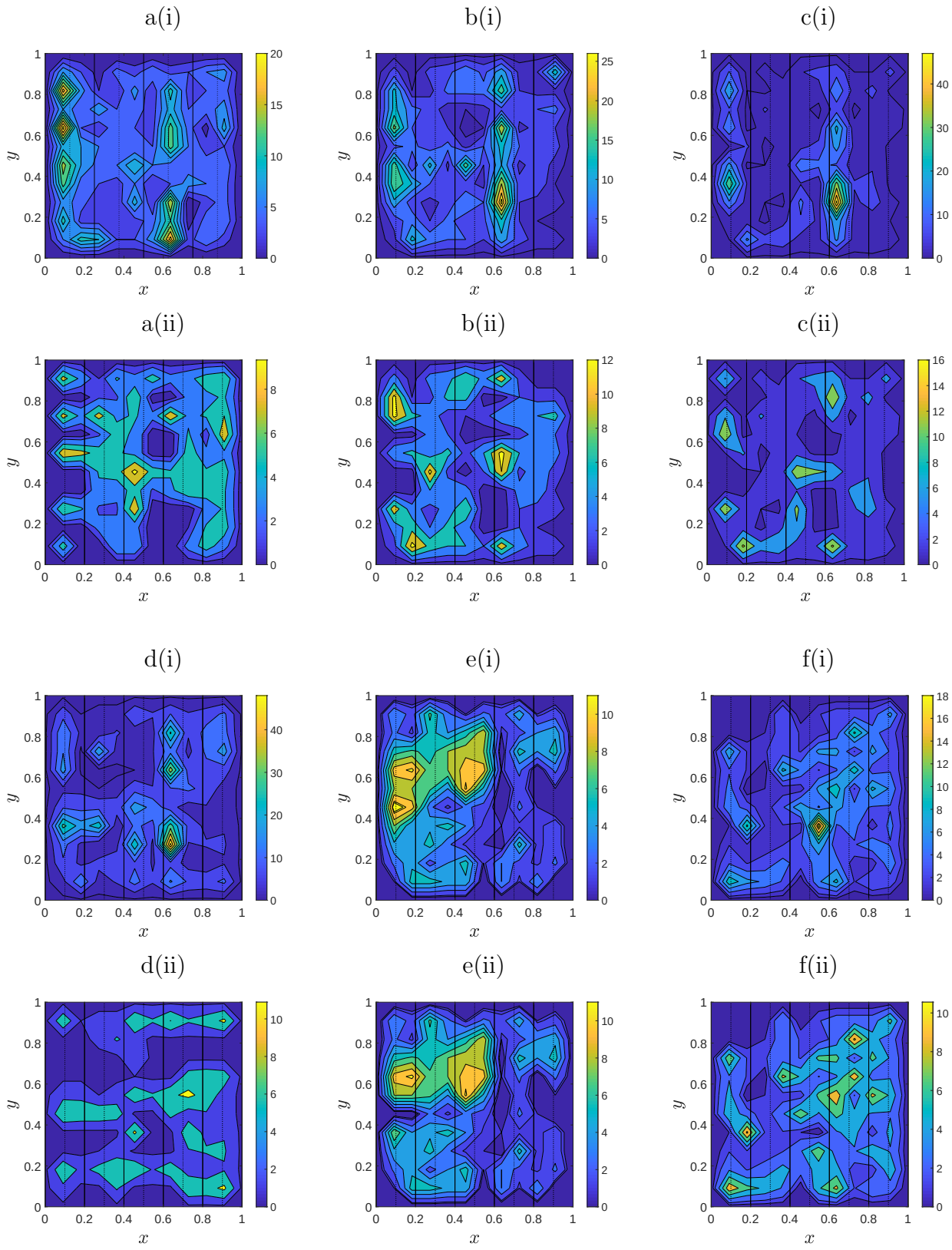

Figure 6.5: The spatial distribution of slugs from trap counts (i) before and (ii) after pesticide has been applied to targeted traps. The action threshold is $S_{th} = 4$. (a)-(d) represent spatial distributions at the Stoney Lawn field on 06.01.2016 (a), 11.01.2016 (b), 14.01.2016 (c), and 8.02.2016 (d), (e) the Badjics field on 18.02.2016 and (f) the Adney Middle field on 18.01.2016.

Table 6.6: The results of targeted use of pesticide when the number of interior tracks is increased from 3 (see previous examples) to 4. The threshold value is $S_{th} = 4$. The legend is as in Table 6.5.

Field	Date	S	S_{new}	$M\%$	C_{max}
Stoney Lawn	06.01.16	5.98	3.64	24.00	10
Stoney Lawn	11.01.16	6.21	3.91	19.00	13
Stoney Lawn	14.01.16	6.03	3.67	16.00	17
Stoney Lawn	18.02.16	9.13	3.80	38.00	12
Badjics	18.02.16	4.00	3.78	2.00	11
Adney Middle	18.01.16	4.00	3.81	1.00	11

the pellet applicator when moving across the field. The results are shown in Table 6.6 where the number of interior tracks is increased from 3 (as in previous examples) to 4. We anticipate that if we were to increase the number of tracks in the field, we would be able to target the patches with a smaller total area more accurately and fewer traps that are not targeted will have pesticide applied to them. However, the results presented in Table 6.6 do not justify using extra tracks for more efficient pesticide application. It is seen from the table that the amount of pesticide used in each field remains approximately the same (or even increases in some cases) when another track is added to the route. Thus the optimal number of tracks in the field remains an open question and development of a reliable protocol with regard to this issue will require further study.

Finally, we investigate how the pesticide consumption depends on the threshold value employed in the protocol. We anticipate from our discussion in Section 6.3.1 that changing

Table 6.7: The results of targeted use of pesticide when the threshold number S_{th} varies (see the threshold value S_{th} in brackets). The legend is as in Table 6.5.

Field	Date	$M\%(S_{th} = 3)$	$M\%(S_{th} = 4)$	$M\%(S_{th} = 5)$
Stoney Lawn	06.01.16	40.00	22.50	12.50
Stoney Lawn	11.01.16	33.75	23.75	12.50
Stoney Lawn	14.01.16	26.25	15.00	7.50
Stoney Lawn	18.02.16	50.00	41.25	26.25
Badjics	18.02.16	13.75	2.50	0
Adney Middle	18.01.16	12.50	1.25	0

the threshold value will change the amount of pesticide used on the field. The total amount of pesticide applied when the threshold is decreased to $S_{th} = 3$ and increased to $S_{th} = 5$, compared with the original threshold $S_{th} = 4$ is shown in Table 6.7. One obvious conclusion arising from the results in the table is that the amount of pesticide applied is reduced when a larger value of the threshold is used in the pesticide application protocol. It is interesting to note, that pesticide consumption decreases quite significantly when the threshold is increased. In the extreme case of the Stoney Lawn field on 18.02.2016 (line 4 of Table 6.7) we originally have the average trap count $S = 9.13$ (see Table 6.5). Applying the threshold $S_{th} = 3$ requires 50% of the field area to be treated with pesticide and reduces the average trap count to $S_{new} = 2.67$ while applying the threshold $S_{th} = 5$ requires almost half that area to be treated ($M = 26.25\%$) and leaves the average trap count after pesticide application as $S_{new} = 4.97$.

We can conclude from the above examples that targeted use of pesticide allows one to significantly decrease the amount of pesticide required to reduce the average trap count below a defined threshold. However, one problem with the protocol is that it is not clear from our use of the average trap count above whether it results in the optimal choice of traps for pesticide targeting. Consider, for example, a relatively low average trap count, such that just one trap has to be targeted to meet the condition $S \leqslant S_{th}$. In cases such as in Fig. 6.5(f)(i) there is one trap count that is considerably higher than the others and thus identifying a clear target for pesticide application. However, in Fig. 6.5(e)(i) there are several trap counts that are much higher than the rest, and targeting one trap in this case will reduce the average trap count to below the threshold while having little effect on the overall spatial distribution of slugs in the field (which is partly determined by environmental factors). Moreover, while the protocol reduces the average trap count below the threshold by making the average number of slugs in each selected patch lower, it does not result in smaller slug patches. In the case of the Stoney Lawn field, 14.01.2016, with threshold $S_{th} = 5$, targeted application of pesticide met the condition $S < S_{th}$ yet

it resulted in 93 traps having been left untargeted out of 100 and patchy distribution of slugs has been preserved. Hence, the targeted use of pesticide resulting from the protocol based on the average trap count alone, neglects the patch size which is another important property of heterogeneous spatial slug distribution. In the next section we discuss possible modifications to the protocol that address explicitly the spatial distribution of slugs.

6.4 Multi-parametric identification of patches in the targeted use of the pesticide protocol

It has been argued in the previous section that the threshold-based protocol does not take into account spatial characteristics of discontinuous (patchy) distributions and it therefore remains uncertain whether the protocol offers an optimal selection of spatial sub-domains where pesticide should be applied. Uncertainty associated with the choice of traps for targeting when the spatial structure of slug distribution is neglected can be illustrated by the following simple example. Consider a linear transect across a hypothetical field where trap counts in traps spaced at equal distances are $[2, 6, 27, 15, 8, 6, 7, 19, 11, 4]$. The average trap count is $S = 10.4$. For the sake of simplicity in this example we assume that if a trap is targeted then pesticide will be applied over that trap only and neighbouring traps will not be caught in the area of pesticide application as can happen in the two-dimensional domains. Fig. 6.6(a) shows the contribution of each trap count towards the average trap count (see stacked block A). In the pesticide application protocol based on the single threshold value S_{th} as explained in Section 6.3.1 the traps are targeted one by one, starting with the largest trap count and descending towards the smallest, until the average trap count S after pesticide has been applied is less than the threshold S_{th}. However, the above method of selecting traps for targeting is not unique. It can be seen from the figure there are several alternative combinations of trap counts which collectively meet the condition $S < S_{th}$ (see stacks B, C and D in Fig. 6.6(a)) and it remains unclear

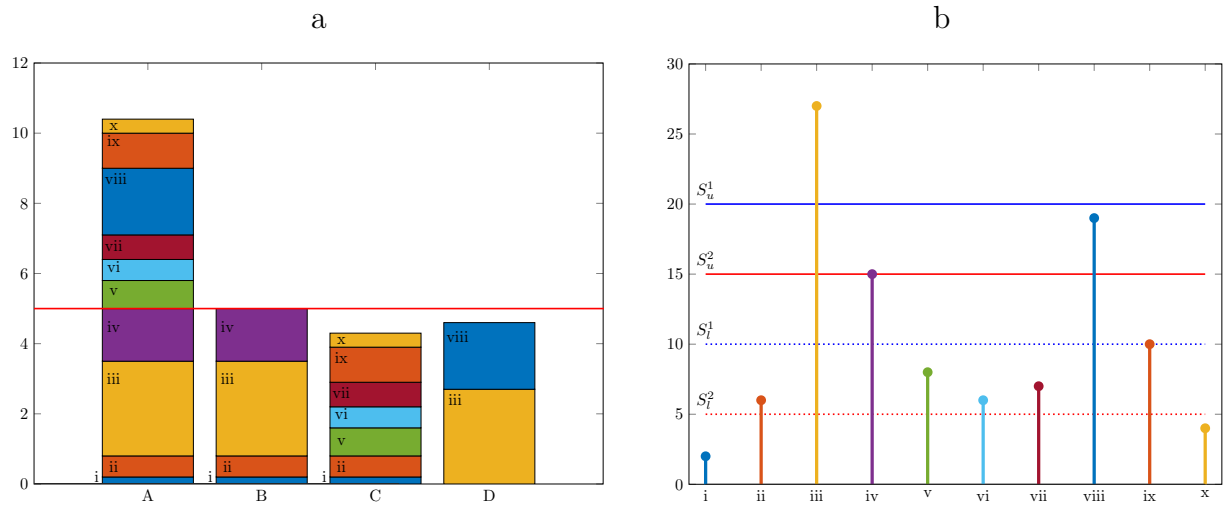

Figure 6.6: A transect test case of trap counts. Roman numerals i–x are used for traps numbering. (a) The threshold based approach (see Section 6.3). Each coloured block in stacked bar A represents the contribution of each trap towards the average $S = 10.4$ (going from trap i at the bottom to trap x at the top). The threshold is set at $S_{th} = 5$; see red solid horizontal line in the figure. To satisfy our aim of reducing the average as $S \leqslant S_{th}$, we need to remove blocks until the trap counts stack is smaller than the threshold. That can be achieved in various ways; see stacks B, C and D in the figure. (b) The 'double threshold' approach. The trap count in each trap along the transect is shown as a coloured stem in the figure. The solid lines are the upper threshold S_u set to 20 (blue) and 15 (red). The dashed lines are the lower threshold S_l set to 10 (blue) and 5 (red).

from the protocol which combination is optimal.

Our algorithm for trap selection in Section 6.3.1 is based on the implicit definition of slug patch as a sub-domain with the high slug density. This definition does not take into account the spatial size of any single patch as the slug abundance is considered as the dominant feature of patch. An alternative definition, however, could be based on the geometric size of patch where the area occupied by the patch is considered as its main characteristic and the following protocol takes this factor into account.

6.4.1 Definition of patch characteristics: slug abundance in a patch vs. patch size

As we could see in Section 6.2 the most straightforward way to define a spatial patch would be to label any isolated spatial sub-domain with non-zero population density as a patch. The above definition accounts for patch size automatically, yet it may result in redundant pesticide application when the population density across the entire field is low. We therefore proceed with a more prescribed definition of patch size where only patches with relatively high population abundance will be considered.

The concept underpinning the modified definition of patch size is to identify key trap counts to be targeted, and then by examining the neighbouring trap catches, determine whether the patch has ended or whether it also covers the area assessed by these traps. The above suggestion requires two thresholds S_u and S_l (*i.e.* the upper and lower thresholds). The procedure to find patches is then to firstly identify all trap counts with a value greater than or equal to upper threshold S_u and mark those traps in the sampling grid. For each of these points in the grid, we then consider the neighbouring trap counts. If a neighbouring trap count has a value greater than or equal to the lower threshold S_l, then it is included as part of the patch. The process is then repeated iteratively for all new traps included in the patch until no neighbouring trap catch is found to exceed S_l. Note that this is essentially the same definition described in Sections 2.2.1 and 3.2.2 to locate clusters from bin populations in our individual based models.

Consider again the transect example introduced in Fig. 6.6 and let us now show the trap count in each trap along the transect as a coloured stem in Fig. 6.6(b) where trap numeration and colour scheme is the same as in Fig. 6.6(a). Let us establish upper threshold $S_u^1 = 20$ (blue solid horizontal line) and lower threshold $S_l^1 = 10$ (blue dotted horizontal line). Then there is only the trap count in trap iii which is greater than the upper threshold and there will be only one small patch around trap iii and trap iv, as

all neighbouring trap counts are below the lower threshold. However if we decrease the lower threshold and use $S_u^1 = 20$ and $S_l^2 = 5$, shown with the solid blue and red dotted line, then there will be one large patch covering the area around trap ii to trap ix, as all of these traps have trap counts exceeding the lower threshold and at least one of the trap counts is above the upper threshold. If we also decrease the upper threshold and use $S_u^2 = 15$ and $S_l^2 = 5$ (the two red horizontal lines in Fig. 6.6(b)), then we also get one large patch covering trap ii to trap ix as lowering the upper threshold does not result in marking any new traps outside of this area. Finally, if we consider $S_u^2 = 15$ and $S_l^1 = 10$, there are two trap counts in Fig. 6.6(b) that are higher than the upper threshold, two trap counts higher than the lower threshold and there are several traps between them with the trap counts below the lower threshold. Therefore we will have two distinct patches, one covering traps iii and iv and one covering traps viii and ix.

6.4.2 Example of the two-parametric patch identification

Let us label the pesticide procedure where the lower and upper thresholds are introduced as a 'double threshold' protocol. We conclude from the above consideration that the upper threshold S_u largely determines the number of patches to be targeted and the lower threshold S_l determines both the size of those patches and the number of situations where two patches can be considered as having merged into one. Let us further illustrate the 'double threshold' protocol by applying it to the Stoney Lawn field on 14.01.2016 (see data in Table 6.3 and the spatial distribution in Fig. 6.3). This protocol yields different results to the 'single threshold' based approach discussed in Section 6.3.

Table 6.8 shows the results of the 'double threshold' protocol when we fix the lower threshold as $S_l = 5$ and vary the upper threshold from $S_u = 5$ to $S_u = 40$. When the upper threshold is increased, we can see that the number of patches and targeted traps decreases as expected. The results of this can be seen in Fig. 6.7 where S_u is set to 10, 20, 30 and 40. In the figure, the size of the individual patches is always the same but the

Table 6.8: A comparison of the results of applying the double threshold protocol using data from the Stoney Lawn field on 14.01.2016, but with different upper threshold values S_u. The lower threshold is $S_l = 5$. P is the number of patches, T is the percentage of traps targeted for pesticide application, S_{new} and $M\%$ are as in Table 6.5.

S_u	P	$T\%$	S_{new}	$M\%$
5	9	38	0.43	73.75
10	4	33	0.64	70.00
20	3	30	0.97	67.50
30	2	26	1.56	57.50
40	1	22	2.29	50

number of patches decreases as S_u increases. When $S_u = 10$ there will be at least one trap in each of the four patches that has a trap count higher than S_u; see Fig. 6.7(a). However only one of those patches has a trap with a count exceeding $S_u = 40$; see Fig. 6.7(d).

Consider now Table 6.9 where we fix the upper threshold to $S_u = 20$ and vary the lower threshold S_l from $S_l = 2$ to $S_l = 20$. This allows us to confirm how the two thresholds define the patches and how varying them changes the outcome.

As explained above, the upper threshold controls the number of patches and the lower threshold determines the size of the individual patch. When we decrease the lower threshold, we can see that the number of targeted traps always increases but the number of patches will either decrease or stay the same. This is because the maximum number of

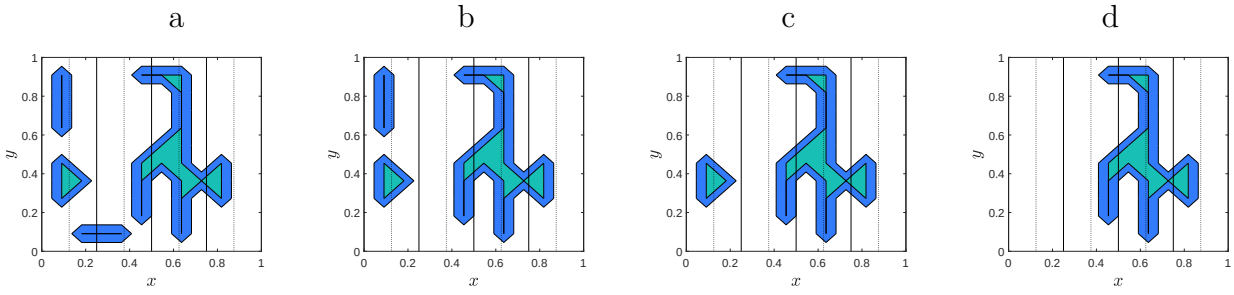

Figure 6.7: A comparison between the results of the patch definition at the Stoney Lawn field on 14.01.2016 with the lower threshold set to $S_l = 5$ and varying upper thresholds. Contour plots showing slug patches (areas of light green colour in the figure) with boundary region (blue colour). (a) Upper threshold is $S_u = 10$ (b) $S_u = 20$ (c) $S_u = 30$ (d) $S_u = 40$.

Table 6.9: A comparison of the results of applying the double threshold protocol using different lower thresholds to data from the Stoney Lawn field on 14.01.16. The upper threshold is $S_u = 20$. The legend is the same as in Table 6.8.

S_l	P	$T\%$	S_{new}	$M\%$
20	4	6	3.95	15.0
15	4	10	3.06	25.00
10	3	16	1.96	43.75
6	3	24	0.97	67.50
4	3	41	0.23	83.75
3	2	54	0.0	100
2	2	71	0.0	100

patches with a fixed S_u will be found when $S_l = S_u$ and the traps that have counts that exceed this threshold often belong to separate patches. This can be seen in Fig. 6.8(a) and in the top row of table 6.9. There are six traps targeted when $S_u = S_l = 20$ but three of them are in the same patch. As S_l decreases, more traps that were neighbouring those in the patch will be incorporated into that patch as soon as their trap count exceeds the new value of S_l; see Fig. 6.8(b)-(c). Eventually, with decreasing S_l, the patches will become large enough to merge together and hence we have a decreasing number of patches; see Fig. 6.8(d).

The 'double threshold' approach offers a stricter control on the patch size in comparison with the 'single threshold'-based protocol. Meanwhile applying the double threshold protocol on its own does not guarantee that the average trap count will be $S < S_{th}$ after

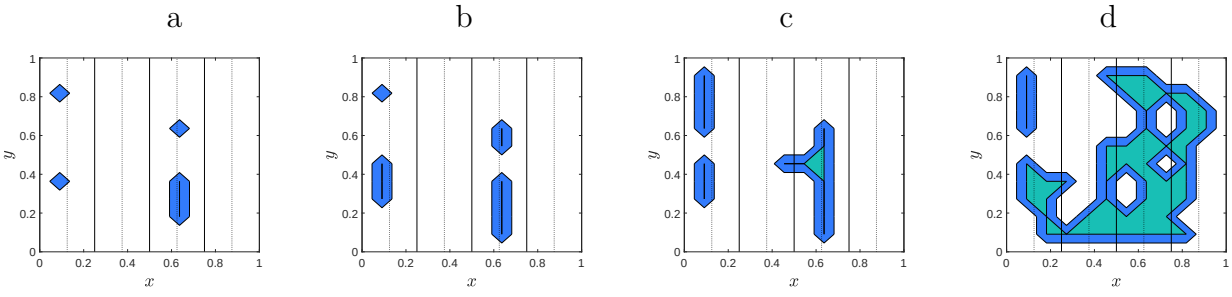

Figure 6.8: A comparison between the results of the patch definition at the Stoney Lawn field on 14.01.2016 with the upper threshold $S_u = 20$ set to 20 and varying lower thresholds. Contour plot legend as in Fig. 6.7.(a) $S_l = 20$ (b) $S_l = 15$ (c) $S_l = 10$ (d) $S_l = 3$.

pesticide application. Hence our next goal is to combine both 'single threshold' and 'double threshold' approaches into one protocol, therefore ensuring that a new average trap count is lower than the threshold S_{th} while also acknowledging the spatial properties of the patches. The details of a unified protocol are explained below.

6.4.3 A unified approach to definition of slug patch

A unified approach summarises our discussion about an optimal definition of slug patch in a targeted use of pesticide procedure where we now design a pesticide application protocol to take into account both the slug density in the patch and the patch size. The protocol utilizes the algorithms discussed in Sections 6.3.1 and 6.4.1 and consists of two respective steps. The first step is, as in the single threshold based approach developed in 6.3.1, to determine the traps that must be targeted to reduce the average trap count below the given threshold. That should reveal slug patches with the high slug density irrespective of their spatial size. We then follow the procedure from the 'double threshold' approach developed in Section 6.4.1 and apply lower threshold S_l to the traps identified for targeting in step 1. Therefore, any neighbouring traps with a trap count above S_l will also be targeted thus defining the size of the patches requiring treatment. For simplicity, it may be appropriate to set $S_l = S_{th}$, i.e. all neighbouring traps with counts higher or equal to the threshold should also be targeted.

Consider our baseline example of the Stoney Lawn field on 14.01.16. In this case $T = 3$ traps are targeted in two patches when we set the threshold $S_{th} = 5$. If a pesticide was applied this would reduce the average trap count from $S = 6.03$ to $S = 4.71$ and it would require $M = 7.5\%$ of the pesticide amount used to treat the whole field (see Table 6.7). However, if instead of applying pesticide we go to step 2 of our unified protocol, then additional traps are targeted under the condition that trap count C_i in the ith trap is $C_i > S_l$ provided the ith trap is a neighbour of any of the three traps initially marked for targeting by step 1. If we then apply the lower threshold $S_l = S_{th} = 5$, this increases the

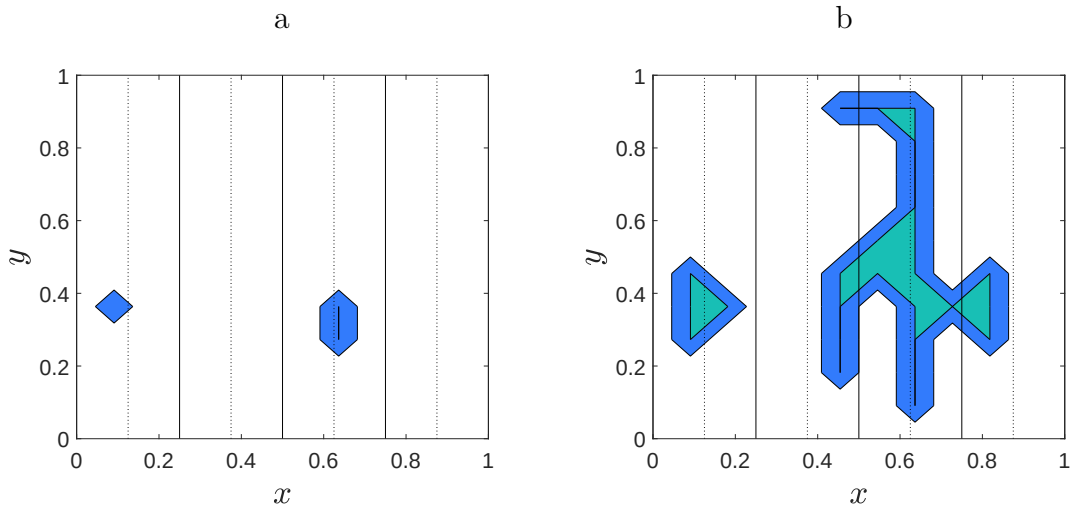

Figure 6.9: The targeted trap counts in the Stoney Lawn field on 14.01.16. Contour plot legend as in Fig. 6.7. (a) the single threshold approach applied only ($S_{th} = 5$) and (b) an additional lower threshold applied ($S_l = 5$).

number of traps targeted to $T = 26$, still making up two individual patches as shown in Fig. 6.9, and the new average trap count is $S_{new} = 1.56$ after pesticide application. The area treated with pesticide relates to the amount used and it increases from $M = 7.5\%$ to $M = 57.5\%$ mass units.

Table 6.10 shows the results of the combined protocol after the first and second step of patch identification when the threshold S_{th} is varied. In the table, S^1 and $M^1\%$ are the average trap count and the area treated with pesticide if the decision to treat is made at

Table 6.10: Results from the combined protocol on Stoney Lawn 14.01.16 with the varying threshold S_{th}. The field had an average trap count of $S = 6.03$ prior to pesticide application. The lower threshold at the second step of the combined protocol is $S_l = S_{th}$. S^1 and $M^1\%$ are the average trap count and the area treated with pesticide that would result from treatment decisions being made at the first step of the combined protocol (see details in the text), S^2 and $M^2\%$ are the average trap count after pesticide application and the area treated with pesticide following decisions made at the second step of the protocol.

S_{th}	S^1	$M^1\%$	S^2	$M^2\%$
3	2.91	26.2	0	100
4	3.95	15.0	0.23	83.75
5	4.71	7.50	1.56	57.50
6	5.49	2.50	2.29	50.00

the first step of the combined protocol. Those values are compared to S^2 and $M^2\%$ which are the average trap count after pesticide application and the area treated when decision making occurs at step 2. It is seen from the table that the addition of a lower threshold that takes into account patch size significantly reduces the average trap count S_{new} after pesticide application yet it increases the amount of pesticide used. When $S_{th} = S_l = 6$, after applying the combined approach the average trap count is reduced to $S = 2.29$, far less than the threshold S_{th} but it requires $M = 50\%$ of the field to be treated. In contrast, the single threshold based protocol (i.e. the first step of the combined approach) would use only $M = 26.2\%$ of the total pesticide to reduce the average trap count to $S = 2.91$.

It can be concluded from the study case considered in this section that the combined protocol uses pesticide in a less efficient way in comparison to the standard threshold based approach. Nevertheless, the combined protocol may be more effective in real world applications as it may be important to target large areas to slow down or stop slug patches reforming as may happen if smaller areas are targeted when the surrounding areas have reasonably large trap counts.

6.5 Conclusions

In this chapter we have established a theoretical basis for a prototype targeted pesticide application protocol that allows the selective control of a pest population in agricultural fields. The protocol is based on the analysis of a strongly heterogeneous spatial distribution of the pest population using field data collected from commercial fields. Although the conclusions are applicable to many pest species, the grey field slug was selected as the baseline case for our study as there is extensive evidence that the spatial distribution this species in arable crops is strongly heterogeneous [222, 28, 12, 159]. Our approach identifies the areas of high slug density (slug patches) and pesticide is applied selectively to those areas alone, differing from most existing commercial practices in which the entire field is uniformly treated. Our model demonstrates that the approach results in con-

siderable savings in the total crop area treated, and thus the amount of pesticide used, potentially contributing to current environmental sustainability priorities and yielding a small positive effect on profit margins.

While the suggested protocol provides a platform from which multiple opportunities relating to selective application of pesticides can be pursued, it requires further validation and development to facilitate cost-efficacy and commercial viability before it can be considered for use by practitioners. The most challenging issue that has still to be resolved is the definition of a spatial patch. We have argued in Section 6.3 that a generic definition of a patch as any spatial sub-domain with a closed boundary that has a non-zero population density is not efficient when targeted use of pesticide is considered. Indeed, the above definition implies that pesticide is applied to every patch in the field, irrespective of its size or the pest density within it. Under more realistic conditions, the definition of patch will require some additional constraints. Depending on economic and environmental goals, practitioners will require the identification of sufficiently large patches with a population density that exceeds a defined level. It has been shown in Section 6.4 that different approaches to defining a patch will lead to different conclusions about the spatial pattern of pest distribution and consequential variability in the area of a crop identified for treatment with pesticides (cf. Fig. 6.7 and Fig. 6.8). We therefore conclude that the definition of a spatial patch has to be carefully considered before it can be employed in a targeted-treatment protocol. Heterogeneous spatial distributions of various animals have been a focus of intense study in past decades and reliable statistical measures have been developed to classify the degree of animal aggregation in a spatial domain (e.g. see [230, 253]). However, the extent to which it is possible to exploit previous research results in spatial analysis undertaken as a part of an investigation of the problem of targeted use of pesticides is unclear. The definition of a spatial patch requires careful investigation in future work as it becomes dependent on the conditions of the control protocol. Furthermore, the targeted use of pesticide procedure discussed in this chapter requires 'temporal

stability' of patches. Since the decision about patch boundaries is essentially based on the analysis of trap counts, the time scale of the trapping protocol implies that the procedure cannot be applied to species who form volatile patches where the patch boundaries change rapidly with time. The definition of temporal stability of a patch depends on the definition of a patch and those two issues should be investigated further together.

Another important question that our study raises is the economic reliability of threshold values. Established monitoring and control protocols are based on the assumption that treating pest populations to prevent them reaching or exceeding defined threshold levels should avoid (or at least alleviate) economic damage being caused by the pest. The targeted use of pesticide procedure relies heavily on the above assumption, but we have demonstrated that it can result in significant numbers of pests remaining in locations surrounding those that have been targeted. Thus, despite having reduced the population to sub-threshold level, it is possible that the remaining individuals may form a nucleus for pest resurgence after the efficacy of the pesticide has declined, resulting in rapid reformation of patches, particularly if there is an environmental driver for clustering in those areas. It might be argued that the current practical use of thresholds have been based partly on the assumption that a large proportion of the population is removed after treatment, and thus the economic calculations underpinning them incorporate these considerations (firstly by reducing post-treatment crop losses sufficiently to make treatment cost-effective and secondly by reducing the rate at which resurgence occurs). On the other hand, approaches in which treatments are applied to entire fields may result in the post-application average trap count being unnecessarily much smaller than the threshold value.

In this chapter we made the assumption that the trap counts accurately approximate slug population density in the field. However, the accuracy of our approximations is dependent on the number of traps, if the grid of traps is too coarse, important information may be missed [176, 180]. It may not be viable for farmers to monitor 100 traps as has

been done in this study to obtain a high level of accuracy. Therefore, analysis of individual slug movement and computational models, such as those discussed Chapters 4 and 5, can provide important information about the spatial scales of patches. Although the data analysed in Chapter 4 was collected over several hours, the modelling work in Chapter 5 showed the formation and stability of patches over much larger time periods. In future work this can also be scaled up to the entire field to establish the number of patches and their sizes. With the addition of simulated traps to the model, we can also assess the minimum number of traps required to accurately identify patches.

The current study offers a basis from which recalculation of thresholds can contribute to more sustainable use by application of reduced volumes of pesticide through more careful targeting. We have demonstrated that a definition of more accurate thresholds will require more information about the heterogeneous spatial distributions of pest populations and we require two control parameters quantifying both the pest abundance in each patch and the patch size in monitoring and control protocols. Therefore, while farmers may not be able to make immediate use of our results, the potential reduction in pesticide that we have demonstrated indicates the value of continuing to investigate slug patch dynamics and pest targeting regimes.

Chapter 7

Concluding remarks

7.1 Discussion and conclusions

In this thesis we have been concerned with the spatial distributions of pest species within an arable field. Pests cause significant damage to arable crops and require methods to control their populations. Application of pesticides is the most common means of pest control, however they are costly and can have damaging effects on the environment. Typically, pesticides are administered across an entire field, however a more efficient targeted approach is possible if the distribution of the pest population is known. In this thesis, we have investigated the formation of heterogeneous spatial distributions in a population and examined possible ways that high density patches can be identified for targeting. In particular, we have examined the spatial population distributions that emerge from when individual movement patterns are dependent on the local population density. This was done in the context of a particular pest species, the grey field slug, which are shown to display density-dependent movement through our analysis of tracking data.

In Chapters 2 and 3, an IBM was built to simulate the individual movement of an unspecified species that performs density-dependent movement such that animals are more likely to move towards their con-specifics. Two types of animal movement have been

considered: Brownian and non-Brownian motion. In the simulation model, the individual movement is described by a dispersal kernel (probability distribution of travelled distances) which is parametrised, respectively, by the normal distribution or by a power law. Many realisations of the IBM simulations in 1D and 2D have shown that density-dependent individual movement do indeed result in the formation of multiple clusters (patches of high population density) when using an appropriate set of parameters.

Having established the emergence of clusters, which can be clearly seen from visual inspection of figures such as Figs. 2.3, 2.10, 3.7 and 3.8, we could continue to investigate the relationship between the parameter values that determine density-dependent movement and the spatial distribution. To do this, a definition of a cluster had to be devised. The definition we chose, which involved partitioning the domain into bins and applying thresholds to find clusters (see Sections 2.2.1 and 3.2.2), required a careful study to ensure that the properties we measured were accurate and useful. Other methods for defining a cluster could have also produced valid results and these are discussed in Chapter 3. However, we believe our definition is the most suitable as it allows for comparison between simulated distributions and also to empirical data, as it is similar to the methods used for analysing a population distribution from trap count data, as seen in Chapter 6. Assuming that trap counts are accurate representations of slug density within their catchment area, the relative number of slugs in traps as a proportion of the total population can be directly compared to simulated bin populations. In future work, this can allow for comparisons to be made between sample frequency distributions in simulated and empirical data, as done in Section 2.3.4. Bin populations and trap counts as a proportion of the total population can also be used as a metric to fit the model to experimental data.

With clusters defined, this allowed an examination of the different cluster properties and how they change with the choice of parameters and type of movement. A key result is that the number of emerging clusters is a random variable, and the typical number of clusters that appear depends on the movement parameters, particularly the perception

radius. The typical cluster size and the number of free individuals (those that are not within a cluster) is heavily dependent on the density dependence and the characteristic size of the movement step. The relationships between parameters and cluster properties are similar for the 1D and 2D models. For example, in both models an increase in the perception radius leads to a decrease in the number of clusters and the cluster size increases when either the probability of density-dependent movement is decreased or the characteristic step size is increased. When we set the area within the perception radius to be the same proportion of the domain in the 2D model as the 1D model, the mean number of clusters in 2D is 4.2, while in 1D the mean number of clusters is 4.56. This supports the claim, made in Section 2.4, that we would expect to see similar results for a 2D model as in the 1D model, especially for Brownian walkers. We also saw that the results were similar in the case for non-Brownian walkers as well, although for certain choices of the probability of directed movement, non-Brownian walkers could produce stable clusters in 2D where they did not in 1D.

As mentioned above, knowledge of the stability of a cluster or patch is essential for the targeted application of pesticide. In cases where the directional bias is sufficiently strong and the movement domain is large, the properties of the clusters differ significantly between populations with the different movement types: Brownian walkers and non-Brownian walkers. In the 2D model of Brownian walkers, when P was such that clusters did form, they were always stable although there were occasional changes in the number of clusters. Brownian walkers never produced dynamic, rapidly fluctuating clusters. This was not the case in 1D where Brownian walkers could produce dynamic clusters (see Fig. 2.9) but this could only occur when P is close to 0.5. In most cases, they were also stable. In the equivalent population of non-Brownian walkers in 1D the clusters were dynamic for all values of P that were tested and there were fast transitions between states with different number of clusters. This also holds in the 2D model but only when P is sufficiently low. This suggests the possibility that knowledge of the stability of clusters or

patches that a population forms can be determined by a measure of an individual animals density-dependence and their movement type. We have also shown that it requires more than measuring the properties of clusters of a 'snapshot' of the spatial distribution at a given time to determine what type of movement animals are moving by and therefore whether the clusters are stable or not. Although the spatial distributions may be similar, the spatio-temporal dynamics can still differ (see Section 3.4).

Our investigation in Chapters 2 and 3 is of a generic, unspecified animal species. We have proven that the process that has been modelled can result in the formation of clusters and the results could apply to any scenario with density-directed dependent individual movement. However, this study was motivated by the recent studies of the distribution and movement of the grey field slug in agricultural fields [78, 180], the results of which we analyse in Chapters 4, 5 and 6. In the previous studies, the spatial distribution of slugs was shown to be remarkably patchy and preliminary correlation analysis performed did not reveal any significant correlation between the distribution of slugs and the physical properties of soil [78]. Research is ongoing to determine the effect of environmental heterogeneity on slug patch formation but it is thought that both social and environmental factors contribute [78, 79, 80]. The analysis of slug tracking data in Chapter 4 clearly shows a difference in movement behaviour when an animal has con-specifics nearby and the potential that this has to form patches is demonstrated in Chapter 5. The knowledge that patch formation is an inherent trait of slug movement suggests that a targeted application of pesticide is feasible and the potential ways that this problem can be addressed are demonstrated in Chapter 6.

We have found, through analysis of tracking data in Chapter 4, a clear difference between movement patterns when slugs are released separately or together. This is displayed in the difference in the mean speeds (see Fig. 4.3), the time spent moving (see Fig. 4.6) and also the growth of the size of the slug patch (see Fig. 4.14). While these results suggest that slug movement is dependent on the population density, it is not clear

whether there is any directed movement as modelled in Chapters 2 and 3. However, the distribution of turning angles does show a clear bias in the case of the dense release (see Fig. 4.4) whereas the distribution of turning angles for sparse release slugs is symmetric around $\theta = 0$. This could be as a result of slime trail following or other mechanisms of density-dependent movement.

The results from this study are promising but further analysis and data collection would be required to make firm conclusions about all aspects of slug movement. To be able to determine the movement type and more accurately determine the strength of density-dependence, more data should be collected from a larger amount of slugs over a longer time period. However, using the data available to create a realistic model of slug movement, as discussed in Chapter 5, has produced some encouraging results which indicate that variability in only the movement frequency and turning angle in the random walk with population density can be sufficient to form a patchy distribution in a homogeneous environment. A larger amount of slug tracking data showing how individual movement changes with population density would allow us to make more specific conclusions about patch formation and the conditions required for it to occur.

It should be noted that the assumption of the randomness of the animal movement is context-specific; in particular, it depends on the type of movement. For instance, animal movement during their migration can hardly be regarded as random. However, animal movement during foraging can often be treated as random (e.g. see [115, 235]) and described accordingly, i.e. by considering the constituting elements of the movement path as random variables described by certain probability distributions. We have made the assumption that this approach is appropriate in our analysis of tracking data and when modelling random movement.

Confirmation of the density-dependence of slug movement and the formation of a patchy population distribution is a positive result for prospective applications of our research in pest management. As we discuss in Chapter 6, slug patches are required to be

temporally stable for a targeted application of pesticide to work. As shown in Chapters 2 and 3, strong density-dependence leads to stable clusters, particularly if individuals move by Brownian motion but also for non-Brownian walkers if the probability of density-dependence is high (see Fig. 3.27).

In Chapter 6, a theoretical basis for a prototype targeted pesticide application protocol has been established that allows the selective control of a pest population in agricultural fields, under the assumption that patches are stable. The protocol is based on the analysis of strongly heterogeneous spatial distributions of a slug population using field data collected from commercial fields. Our approach identifies the areas of high slug density and pesticide is applied selectively to those areas alone, differing from many existing commercial protocols in which the entire field is uniformly treated. The model demonstrates that the approach results in considerable savings in the amount of pesticide used, potentially contributing to current environmental sustainability priorities and yielding a small positive effect on profit margins.

Throughout all of the chapters, a recurring issue that had to be addressed was how to define a patch of high population density in a way that is useful to our study. As discussed above, there are many methods to achieve this when information is known about the position of every individual in the population. However, when analysing trap counts, there is a great deal of uncertainty and we have to make the assumption that the trap count is truly representative of the surrounding area. While average trap counts have long been used to provide information on population abundance in ecological applications or when making pest management decisions [8, 98, 250], it has been recently demonstrated [174, 175] that the spatial heterogeneity of a population distribution can make the task of evaluating population abundance challenging. The problem is exacerbated by the fact that a coarse sampling grid is usually employed in a monitoring/control protocol and it has been shown that in the this case the estimate of population abundance becomes essentially a random variable [180]. A very fine sampling grid has been used in the

field experiment discussed in Chapter 6, therefore the average trap count is likely to be a reliable estimate of the pest population in the field. However, this is not usually the case in regular pest monitoring procedures and further study is needed, along with collaboration with biologists and farmers, to determine the most efficient way to accurately locate slug patches and decide where to apply pesticide.

7.2 Future work

For the work discussed in Chapters 2, 3 and 5, we have built a flexible framework for an individual-based model of a population that has density-dependent movement. There are many directions in which this work can be taken to build on these results. A sensible next step would be to expand upon the work done in Chapter 5, with the addition of more data and sophisticated data fitting to be able to produce a realistic model of slug movement. Of particular interest would be a method of accurately measuring the strength of density-dependence and determine how that varies with population density. This is likely to be a continuous relationship, rather than the binary approximation we made in the model.

There are many other properties of the model that could be adjusted to incorporate aspects of real pest movement. One of the current assumptions in our model is that there is no limit to the population density, as can be seen in the very dense clusters such as Figs. 2.3 and 3.7. This could be changed by giving animals a physical size rather than being modelled as particles. Individuals would then not be allowed to overlap with one another. This could be modelled by terminating the step if an individual collides with another and could have a big impact on the spatial dynamics, particularly in the case of non-Brownian walkers where large steps may currently pass through many other individuals. Terminating the movements step changes the asymptotics of the dispersal kernel by truncating its tail and hence diminishes the difference between Brownian and non-Brownian walkers. This would significantly change the results if we applied it to our 1D model, discussed in Chapter 2, where collisions would be very common. Since

encounters would happens much less often in the 2D case than in the 1D case, one can expect that the population dynamics would be significantly different in different spatial dimensions. In particular, one can expect that the difference between the Brownian and non-Brownian walkers will be more significant in a higher dimensional space.

Other possible developments of the model to prevent improbably high population densities would be to have a repelling force, as has been modelled previously in the case of flocks and herds [89, 90]. Similarly, the strength of density-dependent directed movement when an animal is already in an area of high population density could be reduced or 'switched off' in a similar way to the model in Chapter 5 where we have two types of movement: dense and sparse. In Chapter 4 we have established that slugs move less in higher density areas but it may be the case that at a certain density, the reverse happens and slugs are likely to move more often to escape the high density region. This is something that may be revealed with more tracking experiments.

To further combine the theoretical model with the data analysis, inclusion of traps into the domain would allow comparisons between the simulated data and the trap counts discussed in Chapter 6. The analysis could follow similar work previously done [1, 2, 181, 185] and could allow further fitting of parameters that cannot be determined by tracking data. Further along, application of pesticide to 'kill' individuals in the simulation could be added, allowing the comparison of different targeting strategies in a theoretical model. Environmental data showing factors such as temperature and soil moisture could also be analysed to determine whether this effects slug movement and could also be included in a future IBM.

Another area of future work would be to investigate equation-based models of heterogeneous spatial distributions in order to provide a more rigorous insight into the problem of pattern formation. Studies on nonlinear partial differential equations (PDEs) have often been motivated by a real-world problem, in particular one of biological origin. Starting

from the pioneering work in the early 20th century [75, 124, 236], PDE-based models became a powerful research approach in biology and ecology [37, 129, 142, 161].

To examine the ways that slug patches may form, diffusion-type models could be developed to study environmental and population density-dependent factors separately. Environmental factors are density-independent and hence they could be modelled by a linear Fokker-Planck equation with a diffusion coefficient that is dependent on space [22]. Fokker-Planck diffusion would be necessary for this study because of the assumptions made when deriving the equation from the random walk: the Fokker–Planck law assumes that movement speed depends on the conditions at the starting point of each step whereas Fick's law (resulting in the standard diffusion equation) assumes that the speed of each step of movement depends on the conditions at the end point of that step. Fick's and Fokker-Planck's laws of diffusion give identical results when the diffusion is homogeneous but with spatial heterogeneity the results will differ greatly [22, 204]. Fokker-Planck models have been shown to generate pattern formation in a heterogeneous environment [22, 204] and are therefore a good description for population dynamics where individuals move differently based on local information [38]. In the context of simulating pattern formation, the spatial variation in the diffusion coefficient will correspond to heterogeneity in an environment: A favourable environment will lead to a slower animal movement and thus low diffusivity and an unfavourable environment will lead to faster animal movement and high diffusivity.

The 2D Fokker-Planck diffusion model would be of the form:

$$\frac{\partial}{\partial t}u(\mathbf{r},t) = \nabla^2 \left(D_1(\mathbf{r})u\right), \tag{7.2.1}$$

supplemented by initial and boundary conditions, where $u(\mathbf{r},t)$ is the population density, $\mathbf{r} = (x,y) \in \Omega \subset \mathbf{R}^2$, $\nabla = (\frac{\partial}{\partial x}, \frac{\partial}{\partial y})$, and $t > 0$ is time. The idea of using Fokker-Planck diffusion as a model of pattern formation in heterogeneous environment is relatively new,

especially in the 2D space [23, 204], and recent investigations have been done only by simulations. However it may be possible to solve Eq. (7.2.1) analytically. Although a general solution may be difficult to find, preliminary considerations showed that the analytical solution could be found by means of an appropriate change of variables [186] for a special (but biologically sensible) choice of the diffusion function $D_1(\mathbf{r})$ possessing certain symmetry (e.g. cylindrical).

The model of density-dependent diffusion would take the form, as in [92, 186], of a non-linear PDE:

$$\frac{\partial}{\partial t}u(\mathbf{r},t) = \nabla\left(D_2(u)\nabla u\right). \tag{7.2.2}$$

The diffusion coefficient dependence on the population density u would simulate animal movement in a similar way to the IBM in Chapter 5, i.e. corresponding to slow animal movement when in an area of high population density and fast movement in an area of low population density. The solution properties depend on the form of $D(u)$ and in previous studies such as [186, 208], $D(u)$ has been an increasing function which has resulted in a travelling wave solution. Several other forms of $D(u)$ could be considered to investigate biological pattern formation. Solutions for a few different forms of $D(u)$ have been found analytically in the 1D case using the Aronson–Newman approach [186] and have also been studied using approximate analytical solutions such as variational iterative method [96, 208]. It may be possible to find an analytical solution of Eq. (7.2.2) in the 2D space in the case where the problem possess certain symmetry. In particular, for the initial condition possessing cylindrical symmetry Eq. (7.2.2) becomes quasi-1D and a modification of the Aranson-Newman methods would still apply.

The results of these two models could also be brought together by considering the synergetic model combining the effect of both environmental and density-dependent interactions. The corresponding general model taking into account both interaction types

includes both terms and hence is given by a nonlinear Fokker-Planck-diffusion model:

$$\frac{\partial}{\partial t}u(\mathbf{r},t) = \nabla^2\left(D_1(\mathbf{r})u\right) + \nabla\left(D_2(u)\nabla u\right). \tag{7.2.3}$$

To solve this problem, one could use a combination of analytical tools suggested for Eqs. (7.2.1) and (7.2.2); in particular, using a change of variables, especially for the cases with symmetry. Numerical solutions of Eq. (7.2.3) could also be found for a special choice of functions $D_1(\mathbf{r})$ and $D_2(u)$ and appropriate initial conditions. This PDE-based approach would compliment the results from the IBM simulations presented in this thesis.

The research discussed in this thesis has made good progress towards establishing the plausibility and effectiveness of targeted pesticide application. We believe that further study on patch identification and the temporal stability of patches should continue as it is an essential step to confirming the efficiency of targeted pesticide application. The pressure to reduce overall pesticide use is likely to continue into the future but we have made some important steps into demonstrating how this can be done.

List of References

[1] D. Ahmed, S. Benhamou, M. Bonsall, and S. Petrovskii. Three-dimensional random walk models of individual animal movement and their application to trap counts modelling. *Preprint*, 2020.

[2] D. Ahmed and S. Petrovskii. Analysing the impact of trap shape and movement behaviour of ground-dwelling arthropods on trap efficiency. *Methods Ecol Evol*, 10(8):1246–1264, 2019.

[3] H. Akaike. A new look at the statistical model identification. *IEEE T Automat Contr*, 19(6):716–723, 1974.

[4] M. C. Alavanja, M. K. Ross, and M. R. Bonner. Increased cancer burden among pesticide applicators and others due to pesticide exposure. *CA-Cancer J Clin*, 63(2):120–142, 2013.

[5] C. J. Alexander, J. M. Holland, L. Winder, C. Woolley, and J. N. Perry. Performance of sampling strategies in the presence of known spatial patterns. *Ann Appl Biol*, 146(3):361–370, 2005.

[6] A. Alyokhin, M. Baker, D. Mota-Sanchez, G. Dively, and E. Grafius. Colorado potato beetle resistance to insecticides. *Am J Potato Res*, 85(6):395–413, 2008.

[7] M. Amaral, S. Pellico Netto, C. Lingnau, and A. Figueiredo Filho. Evaluation of the morisita index for determination of the spatial distribution of species in a fragment of araucaria forest. *Appl Ecol Env Res*, 13(2):361–372, 2015.

[8] J. T. Anderson, F. L. Zilli, L. Montalto, M. R. Marchese, M. McKinney, and Y.-L. Park. Sampling and processing aquatic and terrestrial invertebrates in wetlands. In *Wetland techniques*, pages 143–195. Springer, 2013.

[9] T. K. Anderson. Kernel density estimation and k-means clustering to profile road accident hotspots. *Accident Anal Prev*, 41(3):359–364, 2009.

[10] M. Ankerst, M. M. Breunig, H.-P. Kriegel, and J. Sander. Optics: ordering points to identify the clustering structure. In *ACM Sigmod record*, volume 28, pages 49–60. ACM, 1999.

[11] H. A. Araújo and E. P. Raposo. Lévy flights between absorbing boundaries: Revisiting the survival probability and the shift from the exponential to the sparre-andersen limit behavior. *Phys Rev*, 94(3):032113, 2016.

[12] G. A. Archard, D. A. Bohan, L. Hughes, and C. W. Wiltshire. Spatial sampling to detect slug abundance in an arable field. *Ann Appl Biol*, 145(2):165–173, 2004.

[13] B. C. Arnold. *Pareto Distributions Second Edition*. Chapman and Hall/CRC, 2015.

[14] F. Aurenhammer. Voronoi diagrams—a survey of a fundamental geometric data structure. *ACM Comput Surv*, 23(3):345–405, 1991.

[15] M. Baars and T. S. Van Dijk. Population dynamics of two carabid beetles at a dutch heathland: I. subpopulation fluctuations in relation to weather and dispersal. *J Anim Ecol*, 53(2):375–388, 1984.

[16] N. Bacaër. *A short history of mathematical population dynamics*. Springer Science & Business Media, 2011.

[17] S. E. Bailey. Foraging behaviour of terrestrial gastropods: integrating field and laboratory studies. *J Mollus Stud*, 55(2):263–272, 1989.

[18] F. Bartumeus, M. G. E. da Luz, G. M. Viswanathan, and J. Catalan. Animal search strategies: a quantitative random-walk analysis. *Ecology*, 86(11):3078–3087, 2005.

[19] S. L. Bates, J.-Z. Zhao, R. T. Roush, and A. M. Shelton. Insect resistance management in GM crops: past, present and future. *Nat biotechnol*, 23(1):57, 2005.

[20] D. Bearup, C. M. Benefer, S. V. Petrovskii, and R. P. Blackshaw. Revisiting Brownian motion as a description of animal movement: a comparison to experimental movement data. *Methods Ecol Evol*, 7(12):1525–1537, 2016.

[21] D. Bearup, S. Petrovskii, R. Blackshaw, and A. Hastings. The impact of terrain and weather conditions on the metapopulation of *Tipula paludosa* in South-Western Scotland: linking pattern to process. *Am Nat*, 182(3):393–409, 2013.

[22] M. Bengfort, H. Malchow, and F. M. Hilker. The Fokker–Planck law of diffusion and pattern formation in heterogeneous environments. *J. Math. Biol.*, 73(3):683–704, 2016.

[23] M. Bengfort, I. Siekmann, and H. Malchow. Invasive competition with Fokker-Planck diffusion and noise. *Ecol. Compl.*, 34:134–138, 2018.

[24] S. Benhamou. How many animals really do the Lévy walk? *Ecology*, 88(8):1962–1969, 2007.

[25] K. Beyer, J. Goldstein, R. Ramakrishnan, and U. Shaft. When is "nearest neighbor" meaningful? In *International conference on database theory*, pages 217–235. Springer, 1999.

[26] S. Blanche, J. Casas, F. Bigler, and K. E. Janssen-Van Bergeijk. An individual-based model of *Trichogramma* foraging behaviour: parameter estimation for single females. *J Appl Ecol*, pages 425–434, 1996.

[27] B. Boag, K. Mackenzie, J. McNicol, R. Neilson, et al. Sampling for the New Zealand flatworm. In *Proc. Crop Protection in Northern Britain 2010*, pages 45–50, 2010.

[28] D. A. Bohan, D. M. Glen, C. W. Wiltshire, and L. Hughes. Parametric intensity and the spatial arrangement of the terrestrial mollusc herbivores *Deroceras reticulatum* and *Arion intermedius*. *J Anim Ecol*, 69(6):1031–1046, 2000.

[29] B. M. Bolker. *Ecological models and data in R.* Princeton University Press, 2008.

[30] R. J. Brenner, D. A. Focks, R. T. Arbogast, D. K. Weaver, and D. Shuman. Practical use of spatial analysis in precision targeting for integrated pest management. *Am Entomol*, 44(2):79–102, 1998.

[31] P. Broly, R. Mullier, J.-L. Deneubourg, and C. Devigne. Aggregation in woodlice: social interaction and density effects. *ZooKeys*, (176):133, 2012.

[32] D. Brown, D. Giles, M. Oliver, and P. Klassen. Targeted spray technology to reduce pesticide in runoff from dormant orchards. *Crop Prot*, 27(3):545 – 552, 2008.

[33] J. M. Bullock, R. E. Kenward, and R. S. Hails. *Dispersal Ecology: 42nd symposium of the British ecological society*. Cambridge University Press, 2002.

[34] K. P. Burnham, D. R. Anderson, and K. P. Huyvaert. AIC model selection and multimodel inference in behavioral ecology: some background, observations, and comparisons. *Behav Ecol Sociobiol*, 65(1):23–35, 2011.

[35] M. J. Butler IV, A. B. MacDiarmid, and J. D. Booth. The cause and consequence of ontogenetic changes in social aggregation in new zealand spiny lobsters. *Mar Ecol Prog Ser*, 188:179–191, 1999.

[36] J. A. Byers. Wind-aided dispersal of simulated bark beetles flying through forests. *Ecol Model*, 125(2-3):231–243, 2000.

[37] H. M. Byrne and M. A. J. Chaplain. Growth of necrotic tumors in the presence and absence of inhibitors. *Math Biosci*, 135:187–216, 1996.

[38] R. S. Cantrell, C. Cosner, and Y. Lou. Movement toward better environments and the evolution of rapid diffusion. *Math Biosci*, 204(2):199–214, 2006.

[39] R. Cao, A. Cuevas, and W. G. Manteiga. A comparative study of several smoothing methods in density estimation. *Comput Stat Data An*, 17(2):153–176, 1994.

[40] G. Caron-Lormier, R. W. Humphry, D. A. Bohan, C. Hawes, and P. Thorbek. Asynchronous and synchronous updating in individual-based models. *Ecol Model*, 212(3-4):522–527, 2008.

[41] L. M. Carrascau, J. C. Alonso, and J. A. Alonso. Aggregation size and foraging behaviour of white storks *(Ciconia cinconia)* during the breeding season. *Ardea*, 78:399–404, 1990.

[42] H.-C. Chang and L.-C. Wang. A simple proof of Thue's theorem on circle packing. *arXiv preprint*, page 1009.4322, 2010.

[43] P.-C. Chavy-Waddy and T. Kolokolnikov. A local PDE model of aggregation formation in bacterial colonies. *Nonlinearity*, 29(10):3174, 2016.

[44] P. J. Clark and F. C. Evans. Distance to nearest neighbor as a measure of spatial relationships in populations. *Ecology*, 35(4):445–453, 1954.

[45] D. Clarke-Harris and S. J. Fleischer. Sequential sampling and biorational chemistries for management of lepidopteran pests of vegetable amaranth in the Caribbean. *J Econ Entomol*, 96(3):798–804, 2003.

[46] J. Clobert, M. Baguette, T. G. Benton, and J. M. Bullock. *Dispersal ecology and evolution*. Oxford University Press, 2012.

[47] E. Codling, N. Hill, J. Pitchford, and S. Simpson. Random walk models for the movement and recruitment of reef fish larvae. *Mar Ecol Prog Ser*, 279:215–224, 2004.

[48] E. Codling, J. Pitchford, and S. Simpson. Group navigation and the "many-wrongs principle" in models of animal movement. *Ecology*, 88(7):1864–1870, 2007.

[49] E. A. Codling, M. J. Plank, and S. Benhamou. Random walk models in biology. *J R Soc Interface*, 5(25):813–834, 2008.

[50] B. Collignon, A. Séguret, and J. Halloy. A stochastic vision-based model inspired by zebrafish collective behaviour in heterogeneous environments. *Roy Soc Open Sci*, 3(1):150473, 2016.

[51] A. Cook. Homing by the slug *Limax pseudoflavus*. *Anim Behav*, 27:545–552, 1979.

[52] A. Cook. Field studies of homing in the pulmonate slug *Limax pseudoflavus* (Evans). *J Mollus Stud*, 46(1):100–105, 1980.

[53] D. Cornforth, D. G. Green, and D. Newth. Ordered asynchronous processes in multi-agent systems. *Physica D: Nonlinear Phenomena*, 204(1-2):70–82, 2005.

[54] I. D. Couzin, J. Krause, R. James, G. D. Ruxton, and N. R. Franks. Collective memory and spatial sorting in animal groups. *J Theor Biol*, 218(1):1–11, 2002.

[55] R. P. Croll. Gastropod chemoreception. *Biol Rev*, 58(2):293–319, 1983.

[56] C. Damgaard. On the distribution of plant abundance data. *Ecol Inform*, 4(2):76–82, 2009.

[57] P. M. Davis. Statistics for describing populations. *Handbook of sampling methods for arthropods in agriculture*, pages 33–54, 1994.

[58] M. de Jager, F. Bartumeus, A. Kölzsch, F. J. Weissing, G. M. Hengeveld, B. A. Nolet, P. M. Herman, and J. van de Koppel. How superdiffusion gets arrested: ecological encounters explain shift from Lévy to Brownian movement. *Proc R Soc B*, 281(1774):20132605, 2014.

[59] D. L. DeAngelis and V. Grimm. Individual-based models in ecology after four decades. *F1000Prime Reports, 6:39*, 2014.

[60] DEFRA. *Drinking Water 2015; A summary of the Chief Inspectorate's report for drinking water in England. London: Drinking Water Inspectorate*, 2016.

[61] S. Dray, M. Royer-Carenzi, and C. Calenge. The exploratory analysis of autocorrelation in animal-movement studies. *Ecol Res*, 25(3):673–681, 2010.

[62] J. B. Dunning, D. J. Stewart, B. J. Danielson, B. R. Noon, T. L. Root, R. H. Lamberson, and E. E. Stevens. Spatially explicit population models: current forms and future uses. *Ecol Appl*, 5(1):3–11, 1995.

[63] D. Dunstan and D. Hodgson. Snails home. *Physica Scripta*, 89(6):068002, 2014.

[64] H. Edelhoff, J. Signer, and N. Balkenhol. Path segmentation for beginners: an overview of current methods for detecting changes in animal movement patterns. *Mov Ecol*, 4(1):21, 2016.

[65] H. Edelsbrunner, D. Kirkpatrick, and R. Seidel. On the shape of a set of points in the plane. *IEEE T Inform Theory*, 29(4):551–559, 1983.

[66] A. M. Edwards, R. A. Phillips, N. W. Watkins, M. P. Freeman, E. J. Murphy, V. Afanasyev, S. V. Buldyrev, M. G. da Luz, E. P. Raposo, H. E. Stanley, et al.

Revisiting Lévy flight search patterns of wandering albatrosses, bumblebees and deer. *Nature*, 449(7165):1044–1048, 2007.

[67] J. Ellis, N. Petrovskaya, E. Forbes, K. F. Walters, and S. Petrovskii. Movement patterns of the grey field slug (*Deroceras reticulatum*) in an arable field. *Sci Rep*, 10(1):1–16, 2020.

[68] J. Ellis, N. Petrovskaya, and S. Petrovskii. Effect of density-dependent individual movement on emerging spatial population distribution: Brownian motion vs Levy flights. *J Theor Biol*, 464:159–178, 2019.

[69] J. R. Ellis and N. B. Petrovskaya. A computational study of density-dependent individual movement and the formation of population clusters in two-dimensional spatial domains. *J Theor Biol*, 505:110421, 2020.

[70] P. E. Ellis. Learning and social aggregation in locust hoppers. *Anim Behav*, 7(1-2):91–IN4, 1959.

[71] J. T. Emlen. Flocking behavior in birds. *The Auk*, 69(2):160–170, 1952.

[72] M. Ester, H.-P. Kriegel, J. Sander, X. Xu, et al. A density-based algorithm for discovering clusters in large spatial databases with noise. In *Kdd*, volume 96, pages 226–231, 1996.

[73] B. Faugeras and O. Maury. Modeling fish population movements: from an individual-based representation to an advection-diffusion equation. *J Theor Biol. Aug 21;247(4):837-48.*, 2007.

[74] J. Felsenstein. A pain in the torus: some difficulties with models of isolation by distance. *Am Nat*, 109(967):359–368, 1975.

[75] R. A. Fisher. The wave of advance of advantageous genes. *Ann Eugenics*, 7:355–369, 1937.

[76] S. Fleischer, P. Blom, and R. Weisz. Sampling in precision IPM: when the objective is a map. *Phytopathology*, 89(11):1112–1118, 1999.

[77] E. Forbes. *Utilising the patchy distribution of slugs to optimise targeting of control; improved sustainability through precision application.* PhD thesis, Harper Adams University, 2019.

[78] E. Forbes, M. Back, A. Brooks, N. Petrovskaya, S. Petrovskii, T. Pope, and K. F. A. Walters. Sustainable management of slugs in commercial fields: Assessing the potential for targeting control measures. *Asp Appl Biol*, 134:89–96, 2017.

[79] E. Forbes, M. Back, A. Brooks, N. B. Petrovskaya, S. V. Petrovskii, T. Pope, and K. F. Walters. Stability of patches of higher population density within the heterogenous distribution of the gray field slug *Deroceras reticulatum* in arable fields in the UK. *Insects*, 12(1):9, 2021.

[80] E. Forbes, M. A. Back, A. Brooks, N. B. Petrovskaya, S. V. Petrovskii, T. W. Pope, and K. F. Walters. Locomotor behaviour promotes stability of the patchy distribution of slugs in arable fields: Tracking the movement of individual *Deroceras reticulatum*. *Pest Manag Sci*, 2020.

[81] M.-J. Fortin, M. R. Dale, and J. M. Ver Hoef. Spatial analysis in ecology. *Wiley StatsRef: Statistics Reference Online*, 4:2051–2058, 2002.

[82] J. M. Fryxell, M. Hazell, L. Börger, B. D. Dalziel, D. T. Haydon, J. M. Morales, T. McIntosh, and R. C. Rosatte. Multiple movement modes by large herbivores at multiple spatiotemporal scales. *P Nat Acad Sci*, 105(49):19114–19119, 2008.

[83] R. Garcia, F. Moss, A. Nihongi, J. R. Strickler, S. Göller, U. Erdmann, L. Schimansky-Geier, and I. M. Sokolov. Optimal foraging by zooplankton within patches: the case of daphnia. *Math Biosci*, 207(2):165–188, 2007.

[84] A. Gelperin. Olfactory basis of homing behavior in the giant garden slug, *Limax maximus*. *P Nat Acad Sci*, 71(3):966–970, 1974.

[85] B. Grimm, W. Paill, H. Kaiser, et al. Daily activity of the pest slug *Arion lusitanicus Mabille*. *J Mollus Stud*, 66(1):125–130, 2000.

[86] V. Grimm. Mathematical models and understanding in ecology. *Ecol Model*, 75:641–651, 1994.

[87] V. Grimm. Ten years of individual-based modelling in ecology: what have we learned and what could we learn in the future? *Ecol Model, 115, 129–148*, 1999.

[88] V. Grimm and S. F. Railsback. *Individual-based modeling and ecology*, volume 8. Princeton university press, 2013.

[89] D. Grünbaum and A. Okubo. Modelling social animal aggregations. In *Frontiers in mathematical biology*, pages 296–325. Springer, 1994.

[90] S. Gueron, S. A. Levin, and D. I. Rubenstein. The dynamics of herds: From individuals to aggregations. *J Theor Biol*, 182(1):85–98, 1996.

[91] T. Guilford, J. Meade, R. Freeman, D. Biro, T. Evans, F. Bonadonna, D. Boyle, S. Roberts, and C. Perrins. GPS tracking of the foraging movements of Manx Shearwaters *Puffinus puffinus* breeding on Skomer Island, Wales. *Ibis*, 150(3):462–473, 2008.

[92] W. S. C. Gurney and R. M. Nisbet. A note on nonlinear population transport. *J Theor Biol*, 56:249–251, 1976.

[93] A. Hastings, K. C. Abbott, K. Cuddington, T. Francis, G. Gellner, Y.-C. Lai, A. Morozov, S. Petrovskii, K. Scranton, and M. L. Zeeman. Transient phenomena in ecology. *Science*, 361(6406), 2018.

[94] D. M. Hawkins. The problem of overfitting. *J Chem Inf Comp Sci*, 44(1):1–12, 2004.

[95] J. Hayes and O. Castillo. A new approach for interpreting the morisita index of aggregation through quadrat size. *ISPRS Int Geo-Inf*, 6(10):296, 2017.

[96] J.-H. He. Variational iteration method–a kind of non-linear analytical technique: some examples. *Int J Nonlin Mech*, 34(4):699–708, 1999.

[97] E. Heinsalu, E. Hernández-García, and C. López. Spatial clustering of interacting bugs: Lévy flights versus Gaussian jumps. *EPL-Europhys Lett*, 92(4):40011, 2010.

[98] R. Henry and L. Disney. Assessments using invertebrates: posing the problem. In *Wildlife conservation evaluation*, pages 271–293. Springer, 1986.

[99] L. G. Higley and L. P. Pedigo. *Economic thresholds for integrated pest management*, volume 9. U of Nebraska Press, 1996.

[100] B. A. Huberman and N. S. Glance. Evolutionary games and computer simulations. *Proc Nat Acad Sci*, 90(16):7716–7718, 1993.

[101] C. Hui, R. Veldtman, and M. A. McGeoch. Measures, perceptions and scaling patterns of aggregated species distributions. *Ecography*, 33(1):95–102, 2010.

[102] S. H. Hurlbert. Spatial distribution of the montane unicorn. *Oikos*, 58(3):257–271, 1990.

[103] G. E. Hutchinson. The concept of pattern in ecology. *P Acad Nat Sci Phila*, 105:1–12, 1953.

[104] I. M. Ibrahim, L. Gilfoyle, R. Reynolds, and N. Voulvoulis. Integrated catchment management for reducing pesticide levels in water: engaging with stakeholders in East Anglia to tackle metaldehyde. *Sci Total Environ*, 656:1436–1447, 2019.

[105] R. A. Ims. Condition-dependent dispersal. *Dispersal*, 2001.

[106] A. James, J. W. Pitchford, and M. J. Plank. Efficient or inaccurate? analytical and numerical modelling of random search strategies. *Bull Math Biol*, 72(4):896–913, 2010.

[107] A. James, M. J. Plank, and A. M. Edwards. Assessing Lévy walks as models of animal foraging. *J Roy Soc Int*, 8(62):1233–1247, 2011.

[108] V. A. Jansen and A. L. Lloyd. Local stability analysis of spatially homogeneous solutions of multi-patch systems. *J Math Biol*, 41(3):232–252, 2000.

[109] V. A. Jansen, A. Mashanova, and S. Petrovskii. Comment on "Lévy walks evolve through interaction between movement and environmental complexity". *Science*, 335(6071):918–918, 2012.

[110] F. Jeltsch, K. Moloney, and S. J. Milton. Detecting process from snapshot pattern: lessons from tree spacing in the southern Kalahari. *Oikos*, 85(3):451–466, 1999.

[111] P. Jepson and J. Thacker. Analysis of the spatial component of pesticide side-effects on non-target invertebrate populations and its relevance to hazard analysis. *Funct Ecol*, 4(3):349–355, 1990.

[112] S. C. Johnson. Hierarchical clustering schemes. *Psychometrika*, 32(3):241–254, 1967.

[113] F. Jopp and H. Reuter. Dispersal of carabid beetles—emergence of distribution patterns. *Ecol Model*, 186(4):389–405, 2005.

[114] M. Kanevski, M. F. Kanevski, and M. Maignan. *Analysis and modelling of spatial environmental data*, volume 6501. EPFL press, 2004.

[115] P. Kareiva. Local movement in herbivorous insects: applying a passive diffusion model to mark-recapture field experiments. *Oecologia*, 57(3):322–327, 1983.

[116] P. Kareiva and N. Shigesada. Analyzing insect movement as a correlated random walk. *Oecologia*, 56(2-3):234–238, 1983.

[117] R. Kawai and S. Petrovskii. Multi-scale properties of random walk models of animal movement: lessons from statistical inference. *P Roy Soc A-Math Phy*, 468(2141):1428–1451, 2012.

[118] E. F. Keller and L. A. Segel. Initiation of slime mold aggregation viewed as an instability. *J Theor Biol*, 26(3):399–415, 1970.

[119] D. Kelly. The evolutionary ecology of mast seeding. *Trends Ecol Evol*, 9(12):465–470, 1994.

[120] A. J. King, A. M. Wilson, S. D. Wilshin, J. Lowe, H. Haddadi, S. Hailes, and A. J. Morton. Selfish-herd behaviour of sheep under threat. *Curr Biol*, 22(14):R561–R562, 2012.

[121] J. Klafter and I. M. Sokolov. Anomalous diffusion spreads its wings. *Phys World*, 18(8):29, 2005.

[122] C. A. Klausmeier. Regular and irregular patterns in semiarid vegetation. *Science*, 284(5421):1826–1828, 1999.

[123] M. Kogan. Integrated pest management: Historical perspectives and contemporary developments. *Annu Rev Entomol*, 43:243–270, 1998.

[124] A. N. Kolmogorov, I. G. Petrovsky, and N. S. Piskunov. Investigation of the equation of diffusion combined with increasing of the substance and its application to a biology problem. *Bull. Moscow State Univ. Ser. A: Math. and Mech.*, 1:1–25, 1937.

[125] T. Kolokolnikov, J. A. Carrillo, A. Bertozzi, R. Fetecau, and M. Lewis. Emergent behaviour in multi-particle systems with non-local interactions. *Physica D*, 260:1–4, 2013.

[126] A. Kölzsch, A. Alzate, F. Bartumeus, M. de Jager, E. J. Weerman, G. M. Hengeveld, M. Naguib, B. A. Nolet, and J. van de Koppel. Experimental evidence for inherent Lévy search behaviour in foraging animals. *Proc R Soc B*, 282(1807):20150424, 2015.

[127] M. Kot, M. A. Lewis, and P. van den Driessche. Dispersal data and the spread of invading organisms. *Ecology*, 77(7):2027–2042, 1996.

[128] R. Lefever and O. Lejeune. On the origin of tiger bush. *B Math Biol*, 59(2):263–294, 1997.

[129] D. Leitner. A dynamic model of nutrient uptake by root hairs. *New Phytol.*, 185:792–802, 2010.

[130] S. Levin. Patchiness in marine and terrestrial systems: from individuals to populations. *Philos T R Soc B*, 343(1303):99–103, 1994.

[131] S. A. Levin. The problem of pattern and scale in ecology: the Robert H. MacArthur award lecture. *Ecology*, 73(6):1943–1967, 1992.

[132] S. A. Levin, T. M. Powell, and J. H. Steele. Patch dynamics lecture notes in biomathematics, 1993.

[133] A. Liebhold, W. D. Koenig, and O. N. Bjørnstad. Spatial synchrony in population dynamics. *Annu Rev Ecol Evol Syst*, 35:467–490, 2004.

[134] M. Liebman and E. Dyck. Crop rotation and intercropping strategies for weed management. *Ecol Appl*, 3(1):92–122, 1993.

[135] Q.-X. Liu, A. Doelman, V. Rottschäfer, M. de Jager, P. M. Herman, M. Rietkerk, and J. van de Koppel. Phase separation explains a new class of self-organized spatial patterns in ecological systems. *P Natl Acad Sci*, 110(29):11905–11910, 2013.

[136] Q.-X. Liu, M. Rietkerk, P. M. Herman, T. Piersma, J. M. Fryxell, and J. van de Koppel. Phase separation driven by density-dependent movement: a novel mechanism for ecological patterns. *Phys Life Rev*, 19:107–121, 2016.

[137] M. Lloyd. Mean crowding. *J Anim Ecol*, 36(1):1–30, 1967.

[138] K. Lomax. Business failures: Another example of the analysis of failure data. *J Am Stat Assoc*, 49(268):847–852, 1954.

[139] A. J. Lotka. Elements of physical biology. *Science Progress in the Twentieth Century*, 21(82):341–343, 1926.

[140] D. Lyles, T. S. Rosenstock, A. Hastings, and P. H. Brown. The role of large environmental noise in masting: general model and example from pistachio trees. *J Theor Biol*, 259(4):701–713, 2009.

[141] R. MacArthur and E. Wilson. The theory of island biogeography the University of Chicago Press Princeton. *New Jersey*, 1967.

[142] P. K. Maini, K. J. Painter, and H. N. P. Chau. Spatial pattern formation in chemical and biological systems. *J Chem Soc, Faraday Trans*, 93:3601–3610, 1997.

[143] H. Malchow, S. Petrovskii, and E. Venturino. *Spatiotemporal Patterns in Ecology and Epidemiology: Theory, Models, and Simulations. 2008.* Chapman and Hall, CRC, London.

[144] A. Mashanova, T. H. Oliver, and V. A. Jansen. Evidence for intermittency and a truncated power law from highly resolved aphid movement data. *J Roy Soc Int*, 7(42):199–208, 2010.

[145] MATLAB. *9.4.0.813654 (R2018a)*. The MathWorks Inc., Natick, Massachusetts, 2018.

[146] G. A. Matthews. *Pesticide Application Methods 4th edition*. Wiley Blackwell, Oxford., 2014.

[147] G. A. Matthews. *Pesticides Health Safety and the Environment 2nd edition*. Wiley Blackwell, Oxford., 2016.

[148] A. L. McCarthy, S. Heppell, F. Royer, C. Freitas, and T. Dellinger. Identification of likely foraging habitat of pelagic loggerhead sea turtles (*Caretta caretta*) in the North Atlantic through analysis of telemetry track sinuosity. *Prog Oceanogr*, 86(1-2):224–231, 2010.

[149] E. J. McIntire and A. Fajardo. Beyond description: the active and effective way to infer processes from spatial patterns. *Ecology*, 90(1):46–56, 2009.

[150] E. Meron. *Nonlinear physics of ecosystems*. CRC Press, 2015.

[151] P. C. Miller. Patch spraying: future role of electronics in limiting pesticide use. *Pest Manag Sci*, 59(5):566–574, 2003.

[152] G. W. Milligan. Ultrametric hierarchical clustering algorithms. *Psychometrika*, 44(3):343–346, 1979.

[153] A. Mogilner and L. Edelstein-Keshet. A non-local model for a swarm. *J Math Biol*, 38(6):534–570, 1999.

[154] A. Mogilner, L. Edelstein-Keshet, L. Bent, and A. Spiros. Mutual interactions, potentials, and individual distance in a social aggregation. *J Math Biol*, 47(4):353–389, 2003.

[155] T. D. Montenegro-Johnson, P. Stamm, S. Strauss, A. T. Topham, M. Tsagris, A. T. Wood, R. S. Smith, and G. W. Bassel. Digital single-cell analysis of plant organ development using 3DCellAtlas. *Plant Cell*, 27(4):1018–1033, 2015.

[156] J. M. Morales, D. T. Haydon, J. Frair, K. E. Holsinger, and J. M. Fryxell. Extracting more out of relocation data: building movement models as mixtures of random walks. *Ecology*, 85(9):2436–2445, 2004.

[157] M. Morisita. Measuring of the dispersion of individuals and analysis of the distributional patterns. *Mem Fac Sci Kyushu Univ Ser E*, 2(21):5–23, 1959.

[158] A. Morozov and S. Petrovskii. Excitable population dynamics, biological control failure, and spatiotemporal pattern formation in a model ecosystem. *B Math Biol*, 71(4):863–887, 2009.

[159] G. Mueller-Warrant, N. Anderson, C. Sullivan, G. Whittaker, and K. Trippe. Can knowledge of spatial variability in slug populations help improve stand establishment? *Seed Prod Res Oregon State Univ*, 151:4–13, 2014.

[160] A. Murchie and A. Harrison. Mark-recapture of 'New Zealand flatworms' in grassland in Northern Ireland. *Proc Crop Protection in Northern Britain 2004*, 2526:63–67, 2004.

[161] J. D. Murray. How the leopard gets its spots. *Sci Am*, 258:80–87, 1988.

[162] J. D. Murray. *Mathematical biology: I. An introduction*, volume 17. Springer Science & Business Media, 2007.

[163] I. J. Myung. Tutorial on maximum likelihood estimation. *J Math Psychol*, 47(1):90–100, 2003.

[164] R. Nathan, W. M. Getz, E. Revilla, M. Holyoak, R. Kadmon, D. Saltz, and P. E. Smouse. A movement ecology paradigm for unifying organismal movement research. *Proc Natl A Sci*, 105(49):19052–19059, 2008.

[165] E. W. Neilson, T. Avgar, A. C. Burton, K. Broadley, and S. Boutin. Animal movement affects interpretation of occupancy models from camera-trap surveys of unmarked animals. *Ecosphere*, 9(1):e02092, 2018.

[166] C. Nicholls. Implications of not controlling slugs in oilseed rape and wheat in the UK. *HGCA Res Rev*, 79:1–9, 2014.

[167] J. D. Nichols. The role of abundance estimates in conservation decision-making. In *Applied Ecology and Human Dimensions in Biological Conservation*, pages 117–131. Springer, 2014.

[168] A. Okubo. Dynamical aspects of animal grouping: swarms, schools, flocks, and herds. *Adv Biophys*, 22:1–94, 1986.

[169] A. Okubo and S. A. Levin. A theoretical framework for data analysis of wind dispersal of seeds and pollen. *Ecology*, 70(2):329–338, 1989.

[170] H. G. Othmer, S. R. Dunbar, and W. Alt. Models of dispersal in biological systems. *J Math Biol*, 26(3):263–298, 1988.

[171] N. Owen-Smith, J. Fryxell, and E. Merrill. Foraging theory upscaled: the behavioural ecology of herbivore movement. *Philos T Roy Soc B*, 365(1550):2267–2278, 2010.

[172] V. Pareto and G. Busino. *La Courbe de la Repartition de la Richesse (Originally published in 1896)*. In: Busino G, editor. Oevres Completes de Vilfredo Pareto. Geneva: Librairie Droz., 1965.

[173] E. Parzen. On estimation of a probability density function and mode. *Ann Math Stat*, 33(3):1065–1076, 1962.

[174] N. Petrovskaya. 'Catch me if you can': Evaluating the population size in the presence of a spatial pattern. *Ecol Complex*, 34:100–110, 2018.

[175] N. Petrovskaya and N. Embleton. Evaluation of peak functions on ultra-coarse grids. *P Roy Soc A-Math Phy*, 469(2153):20120665, 2013.

[176] N. Petrovskaya and S. Petrovskii. Catching ghosts with a coarse net: use and abuse of spatial sampling data in detecting synchronization. *J R Soc Interface*, 14(127):20160855, 2017.

[177] N. Petrovskaya, S. Petrovskii, and A. K. Murchie. Challenges of ecological monitoring: estimating population abundance from sparse trap counts. *J R Soc Interface*, 9(68):420–435, 2012.

[178] N. Petrovskaya and W. Zhang. When seeing is not believing: Comparative study of various spatial distributions of invasive species. *J Theor Biol*, 488:110141, 2020.

[179] N. B. Petrovskaya, J. R. Ellis, E. Forbes, and K. F. Walters. Modelling a targeted use of pesticide procedure for pest populations with heterogeneous spatial distributions. *Ecol Model*, 427:109059, 2020.

[180] N. B. Petrovskaya, E. Forbes, S. V. Petrovskii, and K. F. Walters. Towards the development of a more accurate monitoring procedure for invertebrate populations, in the presence of an unknown spatial pattern of population distribution in the field. *Insects*, 9(1):29, 2018.

[181] S. Petrovskii, D. Bearup, D. A. Ahmed, and R. Blackshaw. Estimating insect population density from trap counts. *Ecol Complex*, 10:69–82, 2012.

[182] S. Petrovskii, B.-L. Li, and H. Malchow. Transition to spatiotemporal chaos can resolve the paradox of enrichment. *Ecol Complex*, 1(1):37–47, 2004.

[183] S. Petrovskii, A. Mashanova, and V. A. Jansen. Variation in individual walking behavior creates the impression of a Lévy flight. *Proc Nat Acad Sci*, 108(21):8704–8707, 2011.

[184] S. Petrovskii and N. Petrovskaya. Computational ecology as an emerging science. *Interface Foc*, 2:241–254, 2012.

[185] S. Petrovskii, N. Petrovskaya, and D. Bearup. Multiscale approach to pest insect monitoring: Random walks, pattern formation, synchronization, and networks. *Phys Life Rev*, 11:467–525, 2014.

[186] S. V. Petrovskii and B.-L. Li. *Exactly solvable models of biological invasion*. CRC Press, 2005.

[187] D. Pimentel. *Techniques for reducing pesticide use: economic and environmental benefits*. John Wiley and Sons, 1997.

[188] D. Pimentel. Pesticides and pest control. In *Integrated pest management: innovation-development process*, pages 83–87. Springer, 2009.

[189] D. Pimentel and A. Greiner. Environmental and socio-economic costs of pesticide use. In *Techniques for reducing pesticide use: Economic and environmental benefits*, pages 51–78. John Wiley & Sons Chichester UK, 1997.

[190] C. Piou, U. Berger, H. Hildenbrandt, V. Grimmb, K. Diele, and C. D'Lima. Simulating cryptic movements of a mangrove crab: Recovery phenomena after small scale fishery. *Ecol Model*, 205:110–122, 2007.

[191] T. J. Pitcher. Functions of shoaling behaviour in teleosts. In *The behaviour of teleost fishes*, pages 294–337. Springer, 1986.

[192] C. Port and G. Port. Biology and behavior of slugs in relation to crop damage and control. *Agric Zool Rev*, 1:255–299, 1986.

[193] J. R. Potts and S. V. Petrovskii. Fortune favours the brave: Movement responses shape demographic dynamics in strongly competing populations. *J Theor Biol*, 420:190–199, 2017.

[194] M. D. Preston, J. W. Pitchford, and A. J. Wood. Evolutionary optimality in stochastic search problems. *J Roy Soc Int*, 7(50):1301–1310, 2010.

[195] G. H. Pyke. Optimal foraging theory: a critical review. *Annu Rev Ecol Syst*, 15(1):523–575, 1984.

[196] G. H. Pyke. Understanding movements of organisms: it's time to abandon the Lévy foraging hypothesis. *Methods Ecol Evol*, 6(1):1–16, 2015.

[197] S. Raimondo, A. M. Liebhold, J. S. Strazanac, and L. Butler. Population synchrony within and among Lepidoptera species in relation to weather, phylogeny, and larval phenology. *Ecol Entomol*, 29(1):96–105, 2004.

[198] A. M. Reynolds. Mussels realize Weierstrassian Lévy walks as composite correlated random walks. *Sci Rep*, 4:4409, 2014.

[199] A. M. Reynolds. Current status and future directions of Lévy walk research. *Biology open*, 7(1):bio030106, 2018.

[200] A. M. Reynolds, L. Leprêtre, and D. A. Bohan. Movement patterns of Tenebrio beetles demonstrate empirically that correlated-random-walks have similitude with a Lévy walk. *Sci Rep*, 3(1):1–8, 2013.

[201] A. M. Reynolds, A. D. Smith, R. Menzel, U. Greggers, D. R. Reynolds, and J. R. Riley. Displaced honey bees perform optimal scale-free search flights. *Ecology*, 88(8):1955–1961, 2007.

[202] L. A. D. Rodrigues, D. C. Mistro, E. R. Cara, N. Petrovskaya, and S. Petrovskii. Patchy invasion of stage-structured alien species with short-distance and long-distance dispersal. *Bull Math Biol*, 77(8):1583–1619, 2015.

[203] C. D. Rollo and W. Wellington. Environmental orientation by terrestrial Mollusca with particular reference to homing behaviour. *Can J Zool*, 59(2):225–239, 1981.

[204] L. Roques, M.-A. Auger-Rozenberg, and A. Roques. Modelling the impact of an invasive insect via reaction-diffusion. *Math Biosci*, 216(1):47–55, 2008.

[205] M. Rosenblatt. Remarks on some nonparametric estimates of a density function. *Ann Math Stat*, 27(3):832–837, 1956.

[206] T. S. Rosenstock, A. Hastings, W. D. Koenig, D. J. Lyles, and P. H. Brown. Testing Moran's theorem in an agroecosystem. *Oikos*, 120(9):1434–1440, 2011.

[207] R. E. Rossi, D. J. Mulla, A. G. Journel, and E. H. Franz. Geostatistical tools for modeling and interpreting ecological spatial dependence. *Ecol Monogr*, 62(2):277–314, 1992.

[208] A. Sadighi and D. Ganji. Exact solutions of nonlinear diffusion equations by variational iteration method. *Comput Math Appl*, 54(7-8):1112–1121, 2007.

[209] P. J. Sammons, T. Furukawa, and A. Bulgin. Autonomous pesticide spraying robot for use in a greenhouse. In *Australian Conference on Robotics and Automation*, pages 1–9, 2005.

[210] A. Satake and Y. Iwasa. Pollen coupling of forest trees: Forming synchronized and periodic reproduction out of chaos. *J Theor Biol*, 203(2):63–84, 2000.

[211] O. J. Schmitz and G. Booth. Modelling food web complexity: The consequences of individual-based, spatially explicit behavioural ecology on trophic interactions. *Evol Ecol*, 11(4):379–398, 1997.

[212] G. Schofield, C. M. Bishop, G. MacLean, P. Brown, M. Baker, K. A. Katselidis, P. Dimopoulos, J. D. Pantis, and G. C. Hays. Novel GPS tracking of sea turtles as a tool for conservation management. *J Exp Mar Biol Ecol*, 347(1-2):58–68, 2007.

[213] U. Shankar and S. Raju. Integrated pest management in vegetable eco-system. *Ecologically Based Integrated Pest Management, Edition*, pages 619–650, 2012.

[214] A. Shelton and F. Badenes-Perez. Concepts and applications of trap cropping in pest management. *Annu Rev Entomol*, 51:285–308, 2006.

[215] E. L. Shepard, R. P. Wilson, W. G. Rees, E. Grundy, S. A. Lambertucci, and S. B. Vosper. Energy landscapes shape animal movement ecology. *Am Nat*, 182(3):298–312, 2013.

[216] D. W. Sims, N. E. Humphries, N. Hu, V. Medan, and J. Berni. Optimal searching behaviour generated intrinsically by the central pattern generator for locomotion. *Elife*, 8:e50316, 2019.

[217] D. W. Sims, E. J. Southall, N. E. Humphries, G. C. Hays, C. J. Bradshaw, J. W. Pitchford, A. James, M. Z. Ahmed, A. S. Brierley, M. A. Hindell, et al. Scaling laws of marine predator search behaviour. *Nature*, 451(7182):1098, 2008.

[218] J. G. Skellam. Random dispersal in theoretical populations. *Biometrika*, 38(1/2):196–218, 1951.

[219] G. W. Snedecor and W. G. Cochran. *Statistical methods*. Iowa state university press, 1967.

[220] F. Sohrabi, P. Shishehbor, M. Saber, and M. S. Mosaddegh. Lethal and sublethal effects of imidacloprid and buprofezin on the sweetpotato whitefly parasitoid *Eretmocerus mundus (Hymenoptera: Aphelinidae)*. *Crop Prot*, 45:98–103, 2013.

[221] N. W. Sotherton, P. A. Robertson, and S. D. Dowell. Manipulating pesticide use to increase the production of wild game birds in Britain. *Nat Quail Symp Proc*, 3(1):13, 1993.

[222] A. South. Terrestrial slugs: biology, ecology and control. *Chapman & Hall, London, United Kingdom*, 1992.

[223] D. W. Stephens, J. S. Brown, and R. C. Ydenberg. *Foraging: behavior and ecology*. University of Chicago Press, 2008.

[224] V. Stern, R. Smith, R. Van den Bosch, K. Hagen, et al. The integration of chemical and biological control of the spotted alfalfa aphid: the integrated control concept. *Hilgardia*, 29(2):81–101, 1959.

[225] J. Sun, S. P. Cornelius, J. Janssen, K. A. Gray, and A. E. Motter. Regularity underlies erratic population abundances in marine ecosystems. *J R Soc Interface*, 12(107):20150235, 2015.

[226] K. Sun, T. Zhang, and Y. Tianc. Dynamics analysis and control optimization of a pest management predator–prey model with an integrated control strategy. *Appl Math Comput*, 292:253–271, 2017.

[227] T. W. Swetnam and A. M. Lynch. Multicentury, regional-scale patterns of western spruce budworm outbreaks. *Ecol Monogr*, 63(4):399–424, 1993.

[228] B. E. Tabashnik. Evolution of pesticide resistance in predator/prey systems. *Bulletin of the ESA*, 32(3):156–161, 1986.

[229] Y. Tagawa, J. M. Mercado, V. N. Prakash, E. Calzavarini, C. Sun, and D. Lohse. Three-dimensional lagrangian voronoï analysis for clustering of particles and bubbles in turbulence. *J Fluid Mech*, 693:201–215, 2012.

[230] L. Taylor. Assessing and interpreting the spatial distributions of insect populations. *Annu Rev Entomol*, 29(1):321–357, 1984.

[231] P. F. Tilles, S. V. Petrovskii, and P. L. Natti. A random acceleration model of individual animal movement allowing for diffusive, superdiffusive and superballistic regimes. *Sci Rep*, 7(1):1–12, 2017.

[232] P. C. Tobin, L. M. Blackburn, R. H. Gray, C. T. Lettau, A. M. Liebhold, and K. F. Raffa. Using delimiting surveys to characterize the spatiotemporal dynamics facilitates the management of an invasive non-native insect. *Popul Ecol*, 55(4):545–555, 2013.

[233] M. Toger, I. Benenson, Y. Wang, D. Czamanski, and D. Malkinson. Pigs in space: An agent-based model of wild boar (*Sus scrofa*) movement into cities. *Landscape Urban Plan*, 173:70–80, 2018.

[234] C. M. Topaz, A. L. Bertozzi, and M. A. Lewis. A nonlocal continuum model for biological aggregation. *B Math Biol*, 68(7):1601, 2006.

[235] P. Turchin. *Quantitative analysis of movement*. Sinauer assoc. Sunderland (Mass.), 1998.

[236] A. M. Turing. The chemical basis of morphogenesis. *Philos T Roy Soc B*, 237:37–72, 1952.

[237] S. Twining, J. Clarke, S. Cook, S. Ellis, P. Gladders, F. Ritchie, and S. Wynn. Pesticide availability for potatoes following revision of directive 91/414/eec: Impact assessments and identification of research priorities. *Project Report*, 2, 2009.

[238] Y. Tyutyunov, I. Senina, and R. Arditi. Clustering due to acceleration in the response to population gradient: a simple self-organization model. *Am Nat*, 164(6):722–735, 2004.

[239] Y. V. Tyutyunov, A. Zagrebneva, F. Surkov, and A. Azovsky. Microscale patchiness of the distribution of copepods (*Harpacticoida*) as a result of trophotaxis. *Biophysics*, 54(3):355–360, 2009.

[240] T. Ueno, N. Masuda, S. Kume, and K. Kume. Dopamine modulates the rest period length without perturbation of its power law distribution in *Drosophila melanogaster*. *PLoS One*, 7(2):e32007, 2012.

[241] J. Van de Koppel, J. C. Gascoigne, G. Theraulaz, M. Rietkerk, W. M. Mooij, and P. M. Herman. Experimental evidence for spatial self-organization and its emergent effects in mussel bed ecosystems. *Science*, 322(5902):739–742, 2008.

[242] S. V. Viscido, M. Miller, and D. S. Wethey. The dilemma of the selfish herd: the search for a realistic movement rule. *J Theor Biol*, 217(2):183–194, 2002.

[243] G. Viswanathan, V. Afanasyev, S. V. Buldyrev, S. Havlin, M. Da Luz, E. Raposo, and H. E. Stanley. Lévy flights in random searches. *Physica A*, 282(1-2):1–12, 2000.

[244] G. M. Viswanathan, V. Afanasyev, S. Buldyrev, E. Murphy, P. Prince, and H. E. Stanley. Lévy flight search patterns of wandering albatrosses. *Nature*, 381(6581):413, 1996.

[245] G. M. Viswanathan, M. G. Da Luz, E. P. Raposo, and H. E. Stanley. *The physics of foraging: an introduction to random searches and biological encounters*. Cambridge University Press, 2011.

[246] S. C. Votier, W. J. Grecian, S. Patrick, and J. Newton. Inter-colony movements, at-sea behaviour and foraging in an immature seabird: results from GPS-PPT tracking, radio-tracking and stable isotope analysis. *Mar Biol*, 158(2):355–362, 2011.

[247] K. Vulinec and M. Miller. Aggregation and predator avoidance in whirligig beetles (*Coleoptera: Gyrinidae*). *J New York Entomol S*, 97(4):438–447, 1989.

[248] H. Wallin. The effects of spatial distribution on the development and reproduction of *Pterostichus cupreus L., P. melanarius Ill., P. niger Schall.* and *Harpalus rufipes DeGeer (Col., Carabidae)* on arable land. *J Appl Entomol*, 106(1-5):483–487, 1988.

[249] K. Walters. Personal communication, 2019.

[250] K. F. Walters, J. E. Young, B. Kromp, and P. D. Cox. Management of oilseed rape pests. In *Biological Control of Pests of Oilseed Rape; Alford, DV, Ed.; Blackwell Science: Oxford, UK*, pages 43–71. Wiley Online Library, 2003.

[251] M. P. Wand and M. C. Jones. *Kernel smoothing*. Chapman and Hall/CRC, 1994.

[252] D. R. Wareing. Directional trail following in *Deroceras reticulatum* (Müller). *J Mollus Stud*, 52(3):256–258, 1986.

[253] W. E. Waters. A quantitative measure of aggregation in insects. *J Econ Entomol*, 52(6):1180–1184, 1959.

[254] A. Watkins, J. Noble, R. Foster, B. Harmsen, and C. Doncaster. A spatially explicit agent-based model of the interactions between jaguar populations and their habitats. *Ecol Model*, 306:268–277, 2015.

[255] P. J. Watt, S. F. Nottingham, and S. Young. Toad tadpole aggregation behaviour: evidence for a predator avoidance function. *Anim Behav*, 54(4):865–872, 1997.

[256] J. C. Williams, C. S. ReVelle, and S. A. Levin. Spatial attributes and reserve design models: a review. *Environ Model Assess*, 10(3):163–181, 2005.

[257] R. Wilson, I. Griffiths, P. Legg, M. Friswell, O. Bidder, L. Halsey, S. A. Lambertucci, and E. Shepard. Turn costs change the value of animal search paths. *Ecol Lett*, 16(9):1145–1150, 2013.

[258] J. Wu and O. L. Loucks. From balance of nature to hierarchical patch dynamics: a paradigm shift in ecology. *Q Rev Biol*, 70(4):439–466, 1995.

[259] Z. Xie and J. Yan. Kernel density estimation of traffic accidents in a network space. *Comput Environ Urban*, 32(5):396–406, 2008.

[260] L. J. Young and J. Young. *Statistical ecology*. Springer Science & Business Media, 2013.

[261] W. R. Young, A. J. Roberts, and G. Stuhne. Reproductive pair correlations and the clustering of organisms. *Nature*, 412(6844):328–331, 2001.